Studies on some mono-, di- and tri-nuclear complexes of transition and non transition metals with N,O donor Schiff bases and their reduced analogues

Thesis submitted for the degree of

Doctor of Philosophy (Science)

Of

Jadavpur University

2024

By

Ipsita Mondal

Department of Chemistry

Jadavpur University

Kolkata-700032

India

CERTIFICATE FROM THE SUPERVISOR

This is to certify that the thesis entitled **"Studies on some mono-, di- and tri-nuclear complexes of transition and non transition metals with N,O donor Schiff bases and their reduced analogues"** submitted by Smt. Ipsita Mondal, who got her name registered on 8th February, 2022 for the award of Ph.D. (Science) degree of Jadavpur University, is absolutely based upon her own work under the supervision of Prof. Shouvik Chattopadhyay and that neither this thesis nor any part of it has been submitted for either any degree/diploma or any other academic award anywhere before.

Date: 16.02.2024

Shouvik Chattopadhyay

....

(Signature of the Supervisor(s) date with official seal)

Dr. Shouvik Chattopadhyay
Professor
Department of Chemistry
Jadavpur University
Kolkata-700032

JADAVPUR UNIVERSITY
KOLKATA-700 032
MARK SHEET

NO.: CW/19052/ 0988

(For Ph.D/M. Phil. Course Work)

Results of the   PH.D." COURSE WORK EXAMINATION, 2022

In   SCIENCE

Name   IPSITA MONDAL   Class Roll No.   202120104029

Examination Roll No.   PHDCHEM22229

held in   DECEMBER, 2022

Subject Code / Name	Credit Hr.(c_i)	Marks
COMPULSORY UNITS:: CHEM/PHD/CPE-RPE/A/B RESEARCH & PUBLICATION ETHICS,RESEARCH METHODOLOGY & REVIEW WORK	8	60
ELECTIVE UNITS :: CHEM/PHD/I-1 :: APPLICATION OF SPECTROSCOPIC STUDIES IN CHEMICAL RESEARCH CHEM/PHD/I-2 :: MATERIALS, CATELYSES & ELECTROCHEMICAL STUDIES CHEM/PHD/I-3 :: METALS IN LIFE & REACTION DYNAMICS CHEM/PHD/I-4 :: SINGLE CRYSTAL X-RAY STR. SUPRAMOLECULAR CHEM.& DFT COMPUTN.	8	79

Total Marks : 139   (out of   200   )

Remarks: P

Prepared by :   Checked by :

Controller of Examinations

Date of issue :   28 / 04 / 2023

DEDICATED TO MY

Family

"The only source of knowledge is experience"-

Albert Einstein

Preface

The work described in this thesis deals with synthesis and characterization of some transition and non-transition metal complexes. This thesis is divided into 6 chapters, the first of which is a review of the literature on the coordination chemistry of transition and non-transition metal complexes with N, O donor Schiff base ligands and reduced Schiff base ligands. The research works are presented in chapters II-V of the thesis. In Chapter VI, the noteworthy observations are emphasized.

The entire work was started in February 2022. The sources and formats of all the information in this document comply with academic regulations and ethical standards. I further declare that I have referenced and cited all materials and results that are not original to this work, as required by these rules and practices. I accept accountability for any inadvertent mistakes that may have occurred in spite of safeguards.

Dated: 16.02.2024

Ipsita Mondal

Department of Chemistry
Inorganic Section
Jadavpur University
Kolkata-700032

Acknowledgement

As I come to the end of my research project, I would like to express my sincere gratitude to all those who have supported me throughout the completion of this dissertation. First and foremost, I am highly indebted to my guide, **Prof. Shouvik Chattopadhyay**, Department of Chemistry, Jadavpur University for giving me an opportunity to be a part of his research group. I am grateful to him for his constant invaluable guidance, motivation, suggestions, patience and insightful feedback. His commitment to research and concern for students is astounding. His insightful feedback and unwavering support have been instrumental in shaping the direction of this research. It would not have been feasible to continue with this dissertation without his persistent help and brave remarks.

I extend my heartfelt appreciation to **Prof. Kajal Krishna Rajak**, the head of the department of chemistry, for facilities and assistance. Additionally, I owe a debt of gratitude to **Prof. Partha Roy** for his support, recommendations, and insightful counsel that have greatly enriched the content and quality of this work.

I am grateful to the Department of Chemistry, Jadavpur University, for providing the resources and environment conducive to academic excellence. The Department has been a nurturing academic home, and I am thankful for the opportunities it has afforded me.

The majority of the outcomes detailed in this thesis would not have been possible without collaboration with few laboratories. I owe a great deal of admiration and gratitude to **Dr. Antonio Bauza** and **Prof. Antonio Frontera**, Department de Química, Universitat de les Illes Balers, Spain; **Prof. Klaus Harms,** Fachbereich Chemie, Philipps-Universität Marburg, Marbur; **Dr. Snehasis Banerjee**, Govt. College of Engineering and Leather Technology, Salt Lake Sector-III, Block-LB, Kolkata 700106, India; **Dr. Sudipta Chatterjee,** Department of Chemistry, Serampore College, Serampore, Hooghly-712201, India.

I owe a debt of gratitude to my labmates for consistently creating a welcoming

environment and offering me moral support while I conducted my research. Special thanks to my labmates **Dr. Sourav Roy, Dr. Nandita Sarkar, Dr. Tanmoy Basak, Dr. Kousik Ghosh, Dr. Samim Khan, Dr. Snehasish Thakur, Dr. Abhisek Banerjee, Dr. Mainak Karmakar, Mr. Saikat Mirdya, Mr. Tamal Dutta, Mr. Sudip Bhunia, Mr. Rabi Shankar Sarkar, Mr. Susavan Bera, Mr. Puspendu Middha, Mrs. Sovana Maity, Mr. Mridul Karmakar, Mr. Sk. Wahedur, Mr. Biplab Halder, Mr. Md. Zishan.** My heartiest thank to my seniors **Dr. Prasanta Kumar Bhaumik**, **Dr. Subrata Jana**, **Dr. Mithun Das, Dr. Sumit Roy** and **Dr. Anik Bhattacharyya**.

My father, **Mr. Adhir Kumar Mondal**, my mother, **Mrs. Sushama Mondal**, and my brother, **Dr. Aritra Mondal**, have made the largest indirect contributions to my work. They have given up a great deal in order to help me realise my ambition and have always been there for me through all of life's highs and lows. I will be cordially grateful to my husband, **Dr. Bappaditya Naskar** for his moral and unwavering support in all circumstances. Last but not least my little son **Bihan**, who always give positive energy and unconditional love throughout my academic journey.

Last but not least, I acknowledge the participants of my study for their willingness to contribute to this research. Their involvement has been crucial to the success of this project.

In conclusion, I am grateful to all those who have played a role, big or small, in the completion of this thesis. Your support has been indispensable, and I am truly thankful for the collective effort that has gone into making this endeavour a reality.

Date: 16.02.2024   **Ipsita Mondal**
Kolkata, India   Department Of Chemistry
                                                                Jadavpur University

Table of Content

Chapter 1

General introduction, experimental section and summary of research work

Section: I.A

An overview on the coordination chemistry of transition and non- transition metal complexes

Transition elements have incomplete d-orbital, whereas in non-transition elements, d-orbital is absent or completely filled d orbital. In 1921, English chemist Charles Rugeley Bury (1890-1968) introduced the term "transition" for the first time.[1] Any element in groups 3 through 12 of the periodic table is referred to as a "transition metal" in the 2011 IUPAC Principles of Chemical Nomenclature. Many scientists accept this description since it matches the d-block parts exactly.[1a] Transition metals are shiny and have strong electrical and thermal conductivity. With the exception of groups 11 and 12, the most have high melting and boiling temperatures and are robust and hard. They also create a variety of useful alloys.[2] The majority of transition metals are ligand-compatible. Most of the transition metal forms coloured compounds. Due to their unpaired d electrons, the majority and many of their compounds are strongly paramagnetic. A crucial role for transition and non transition metals can be seen in contemporary inorganic chemistry.[2] They are widely distributed in nature and are becoming more and more important in catalysis for various reactions.[3] Transition and non transition metals are frequently used as catalysts in elemental form or in compounds like coordination complexes and oxides.[4]

We focus on a few particular transition and non-transition metals in this dissertation like Mn, Zn.

Both manganese and zinc have been known since very early times in history, yet very little is known about how they were discovered. **Manganese** is a chemical element with

the symbol Mn and atomic number 25. In 1774, manganese was first separated by Johan Gottlieb Gahn. Manganese may have originated from one of two sources: either from the Latin word "magnes," which means "magnet," or from the name "magnesia nigra," which is the black magnesium oxide.[5] It is well-known in the lab as potassium permanganate, or deep violet salt. In the periodic table it is placed in group 7 and period 4. Manganese is a transition metal, used in a wide range of industrial alloys, most notably stainless steels.[6] Manganese is commonly found in the oxidation states +2, +3, +4, +6, and +7. Manganese in aqueous solution is most frequently in the +2 oxidation state. Because of high pairing energy, manganese(II) often has a high spin, $S = 5/2$ ground state. It is colourless, which is due to the absence of spin-allowed d–d transitions. Manganese plays a crucial role in bone formation, the metabolism of macronutrients, and the body's defence mechanisms against free radicals.[7] It is an essential part of numerous proteins and enzymes.[8]

Table I.A.1: Important physical properties of **Manganese**

Physical State	Solid
Melting Point	1246 ° C
Boiling Point	2061 ° C
Density	7.21 g/cm^3
Appearence	Silvery metallic
Oxidation state	-3 to +7
Most Abundant Isotope	^{55}Mn

Zinc was most likely first recorded as "zincum" in the book "Liber Mineralium II" in the sixteenth century.[9] The chemical element zinc has the atomic number thirty and the

symbol Zn. It has an electron configuration of $[Ar]3d^{10}4s^2$. Zinc is not considered as a transition element. Zn(II) has no crystal field stabilisation energy (CFSE) due to its d^{10} electronic structure. Because of this, the polarising power of Zn(II) and the steric requirements of the ligands determine the stereochemistry of every zinc complex. Zinc, is the thirtieth element in the periodic table and the first member of the group 12. At room temperature, zinc is a little brittle metal that turns shiny-greyish after oxidation is removed. Zinc is an important trace element that is required for both prenatal and postnatal development in humans, animals, plants, and microbes.[10] After iron, it is the second most abundant trace metal in humans. Approximately two billion individuals in the poor world suffer from zinc deficiency, which is linked to numerous illnesses.[11] The main use of zinc is in hot-dip galvanising, which is a corrosion-resistant coating made from zinc applied to iron.[12] Additional uses include tiny, non-structural castings, electrical batteries, and alloys like brass.[13]

Table I.A.2: Important physical properties of **Zinc**

Physical State	Solid
Melting Point	419.53 $^\circ$ C
Boiling Point	907 $^\circ$ C
Density	7.14 g/cm^3
Appearence	Silver gray
Oxidation state	-2, 0, +1, +2
Most Abundant Isotope	^{64}Zn

The logical synthesis and design of manganese(III) and zinc(II) complexes are crucial nowadays because of their variety of structures and incredible supramolecular architectures.[14] A wide range of polydentate chelating ligands are utilised to design manganese(III) and zinc(II).[15] Schiff bases and reduced Schiff bases are the specific classes among them for their easy synthesis and easily adjustable steric and electrical characteristics.[16] It is also widely known that a variety of pseudohalides, like azide, thiocyanate etc, can be used to prepare different polynuclear complexes by utilising their distinct bridging modes.[17] In the current work, several mono-, di-, and poly-nuclear manganese(III) and zinc(II) complexes are prepared using such pseudohalide ligands.

The entire work of this thesis has essentially been designed with: (i) Manganese(III) complexes with tetradentate N_2O_2 donor Schiff bases and (ii) Zinc(II) complexes with N_2O_2 donor Schiff bases and reduced Schiff base ligand. A number of halides and pseudohalides have been utilised as co-ligands to aid in the production of complexes. A brief literature review of the synthesis, characterisation, and structural aspects of the aforementioned complexes is provided in the paragraphs that follow.

I.A.1. Manganese(III) complexes with tetradentate N_2O_2 donor Schiff bases

Tetradentate N_2O_2 donor Schiff base ligands are well-known as a unique class of significant chelating ligands.[16-20] These kinds of chelating ligands are highly intriguing to synthesis chemists because of their variable coordination behaviour.[18-20]

The 1:2 condensations of diamines and salicylaldehyde or substituted salicylaldehyde produces tetradentate N_2O_2 donor salen type Schiff bases. There are several literature reports of the synthesis and characterization of mononuclear manganese(III) complexes with this class of ligands. Structures of such selected complexes have been gathered in Scheme **I.A.1.**[18] These types of complexes may also have interesting application as biological activity.[18] Both

$[Mn(L^1)(H_2O)_2]^+$ and $[MnL^2(OOCH)(OH_2)]$ shows excellent catecholase-like activity using 3,5-di-tert-butylcatechol (3,5-DTBC) as the substrate with Kcat = 360 h^{-1} and 936.64 h^{-1} in acetonitrile medium.[18a,b] $[Mn(L^6)(NCS)(OH_2)]$ and $[Mn(L^7)(NCS)(OH_2)]$ $[MnL^7(OAc)(H_2O)]\cdot DMF$, $[MnL^7(N_3)(H_2O)]$ $[H_2L=N,N'-ethylenebis(3-ethoxysalicylaldimine)ethane-1,2-amine$ exhibit catecholase activity using the substrate 3,5-di-tert-butylcatechol.[18e,f]
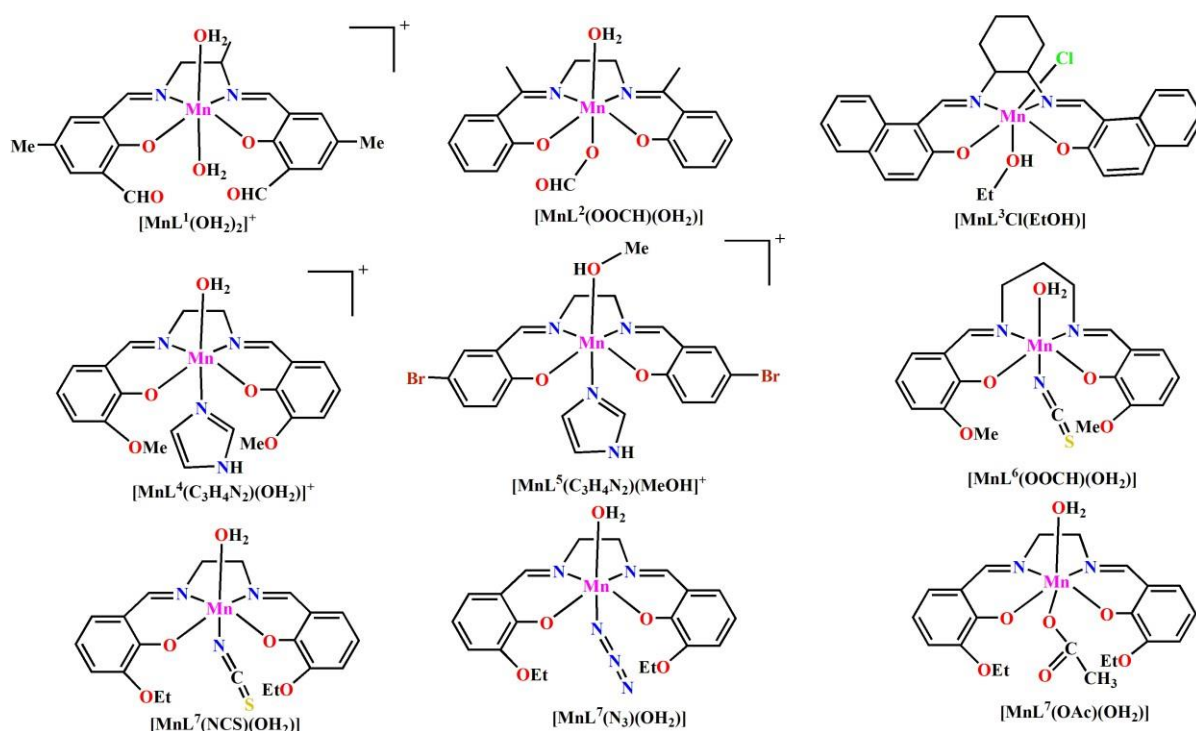
Scheme I.A.1: Schematic representation of $[MnL^1(OH_2)_2]^{+18a}$ {H$_2$L^1= N,N'-bis(3-formyl-5-methylsalicylidene)propane-1,2-diamine}; $[MnL^2(OOCH)(OH_2)]^+$ [18b] {H$_2$L^2= N,N'-bis(2-hydroxyacetophenone)-1,2-ethanediamine}; $[MnL^3Cl(EtOH)]$[18c] {H$_2$L^3= N,N'-bis[(2-hydroxy-1-naphthyl)methylidene)-cyclohexane-1,2-diamine}; $[MnL^4(C_3H_4N_2)(OH_2)]^{+18d}$ {H$_2$L^4= N,N'-bis(3-methoxysalicylidene)ethane-1,2-diamine}; $[MnL^5(C_3H_4N_2)(MeOH)]^{+18d}$ {H$_2$L^5= N,N'-bis(5-bromosalicylidene)ethane-1,2-diamine}; $[MnL^6(NCS)(OH_2)]$[18e]{H$_2$L^6= N,N'-bis(3-methoxysalicylidene)propane-1,3-diamine}; $[MnL^7(NCS)(OH_2)]$[18e], $[MnL^7(N_3)(OH_2)]$[18f] and $[MnL^7(OAc)(H_2O)]$[18f] {H$_2$L^7= N,N'-bis(3-ethoxysalicylidene)ethane-1,2-diamine}

A few selected pentacoordinated mononuclear manganese(III) complexes with N_2O_2 donor Schiff base ligands have been gathered in Scheme **I.A.2**. Here the four coordination sites were occupied by the N_2O_2 donor Schiff base ligand, and the halides, pseudohalides molecule occupied the remaining coordination position.[19] Some complexes might also be interestingly used to biological processes.[19] [MnL[8]Cl] exhibited considerable antiproliferative activity against both cell lines (IC50 = 13.62 μM (MCF-7) and 10.8 μM (Hep G2) comparable to cis-platin.[19a] The antibacterial activity of [MnL[10]Cl] has been tested against some Gram(+) and Gram(-) bacteria.[19c]
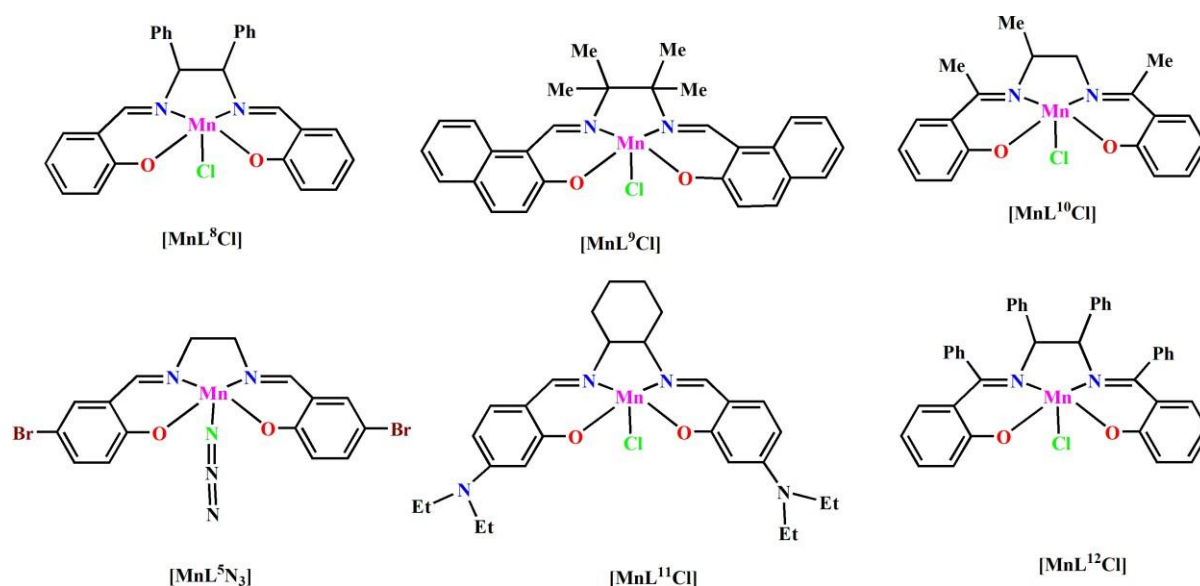
Scheme I.A.2: Schematic representation [MnL[8]Cl][19a] {H_2L^8= N,N'-bis(salicylidene)1,2-diphenylethylenediamine}; [MnL[9]Cl][19b] {H_2L^9=N,N'-(1,1,2,2-tetramethylethylene)bis(naphthylideneiminato)}; [MnL[10]Cl][19c] {H_2L^{10}= N,N'-bis(2-hydroxyacetophenon)propane-1,2-diamine}; [MnL[5]N$_3$][19d] {H_2L^5=N,N'-bis(5-bromosalicylidene)ethane-1,2-diamine}, [MnL[11]Cl][19e]{H_2L^{11}=N,N'-bis(4-(diethylamino)salicylaldimine)-cyclohexayl-1,2-diamine}, [MnL[12]Cl][19f]{ H_2L^{12}= N,N'-bis(2-hydroxybenzophenon)1,2-diphenylethylenediamine}

Dinuclear manganese(III) complexes with N_2O_2 donor Schiff base bridging ligands have been found in literature.[20, 21] Phenoxide, hydroxido and methoxido bridges are widely

known among them because of their significant roles in magnetism.[20, 21] A few selected phenoxido bridged dinuclear manganese(III) complexes with N_2O_2 donor Schiff base ligands have been displayed in Scheme **I.A.3**.[20] $[Mn(L^{11})(N_3)]_2$ and $[Mn(L^{13})(NCO)]_2$ show single-molecule magnet (SMM) behavior from 2 to 5 K.[20a,c] $[MnL^{12}(NCS)]_2$, $[Mn(L^{13})(NCO)]_2$ and $[MnL^{16}(ClO_4)]_2$ show ferromagnetic intra-dimer coupling between two Mn(III) centres.[20b, c, d] $[MnL^{14}(H_2O)]_2$ shows Inter-dimer antiferromagnetic interaction.[19b]

[MnL^{11}(N$_3$)]$_2$ [MnL^{12}(NCS)]$_2$ [MnL^{13}(NCO)]$_2$

[MnL^{14}(H$_2$O)]$_2$ [MnL^{15}(NO$_2$)]$_2$ [MnL^{16}(ClO$_4$)]$_2$
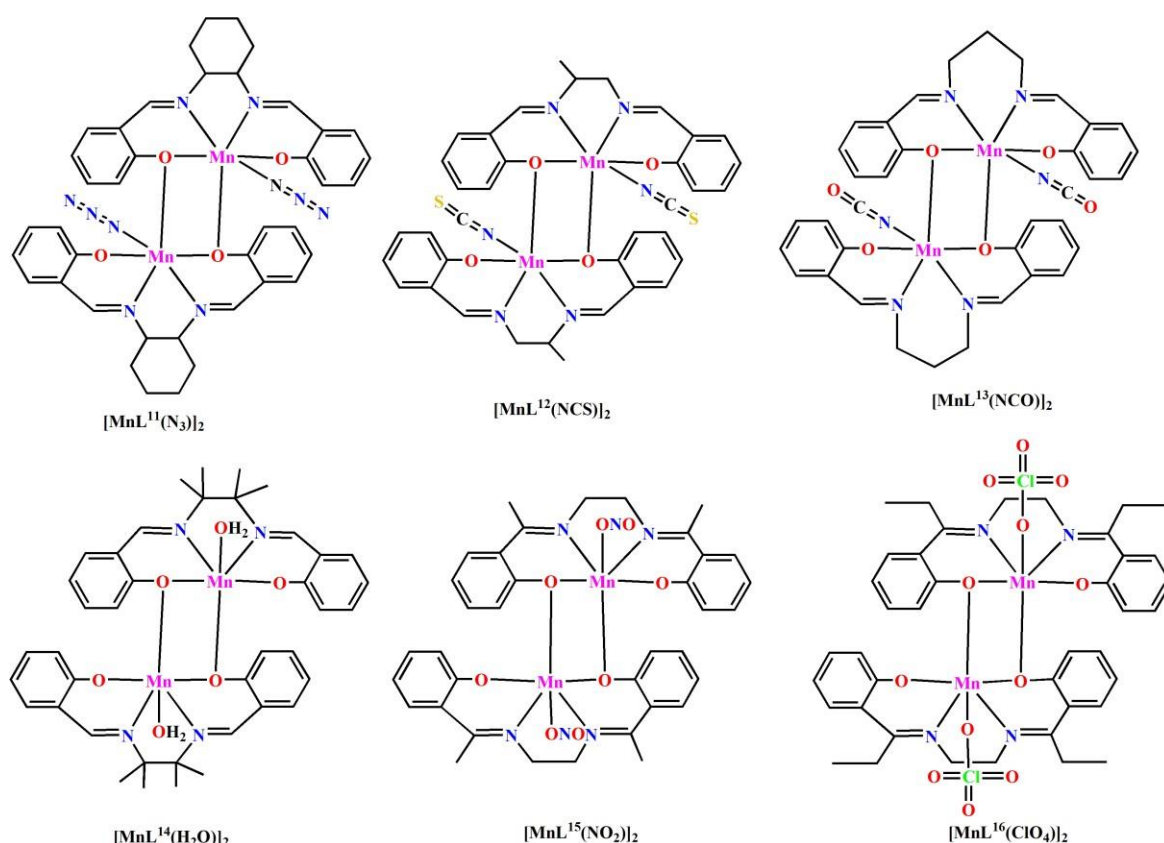
Scheme I.A.3: Schematic representation of $[MnL^{11}(N_3)]_2$[20a] {H_L^{11}= N,N'-bis(salicylidene)cyclohexanediamine}; $[MnL^{12}(NCS)]_2$[20b] {H$_2$L^{12}= N,N'-bis(salicylidene)propane-1,2-diamine}; $[Mn(L^{13})(NCO)]_2$[20c] {H$_2$L^{13}= N,N'-bis(salicylidene)propane-1,3-diamine}; $[MnL^{14}(H_2O)]_2$[19b] {H$_2$L^{14}= N,N'-(1,1,2,2-tetramethylethylene)bis(salicylideneiminato)}; $[MnL^{15}(NO_2)]_2$[18b] {H$_2$L^{15}= N,N'-bis(2-hydroxyacetophenone)-1,2-ethanediamine}; $[MnL^{16}(ClO_4)]_2$[20d] {H$_2$L^{16} = N,N''-bis(2-hydroxypropiophenone)-1,2-ethanediamine}

In addition to phenoxido bridged systems, there are published studies on dinuclear manganese(III) complexes with carboxylate, azido, and other bridging systems using N_2O_2 donor Schiff base ligands.[21] A few selected such dinuclear manganese(III) complexes with N_2O_2 donor Schiff base ligands have been gathered in Scheme **I.A.4**.[21] Antiferromagnetic exchange interaction was observed for $[(MnL^{17})_2(\mu\text{-}C_6H_5PO_2OH)]^+$, $[(MnL^{17})_2(OH_2)(OHCH_3)(\mu\text{-} phth)]$ and $[(MnL^{17})_2(\mu\text{-} OCOCH_2Ph)]^{+21b, c, f}$.

Schematic representation of complexes

$[(MnL^{17})_2(\mu\text{-}OAc)]^+$ $[(MnL^{17})_2(\mu\text{-} C_6H_5PO_2OH)]^+$ $[(MnL^{17})_2(H_2O)(CH_3OH)(\mu\text{-} phth)]$

$[(MnL^{17}(ClO_4)]_2(\mu\text{-} 4,4'\text{-bpy})$ $[\{MnL^{17}(OH_2)\}_2(\mu\text{-}_{1,3}\text{-}N_3)]^+$ $[(MnL^{17})_2(\mu\text{-}OCOCH_2Ph)]^+$
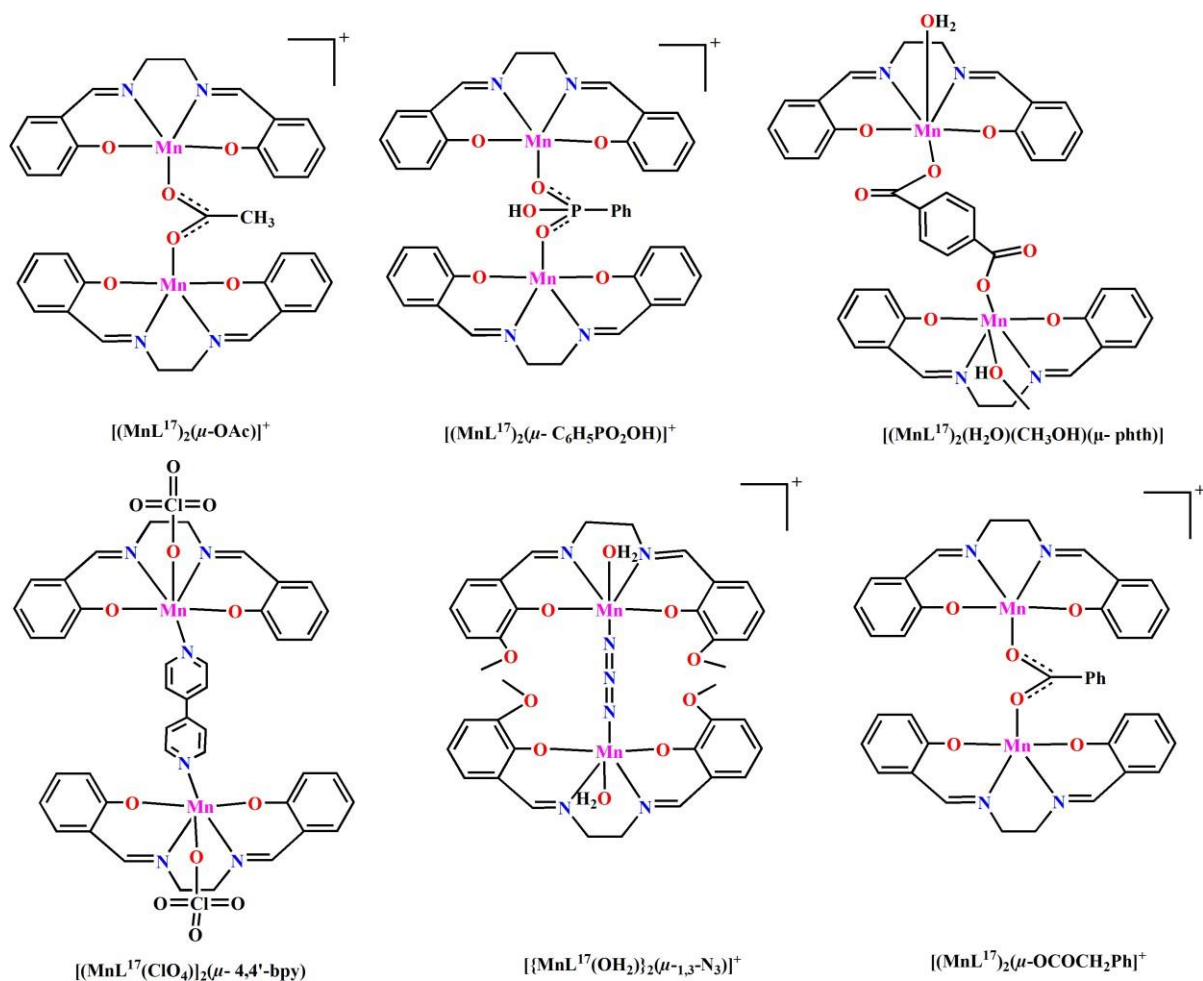
Scheme I.A.4: Schematic representation of $[(MnL^{17})_2(\mu\text{-}OAc)]^{+21a}$, $[(MnL^{17})_2(\mu\text{-}C_6H_5PO_2OH)]^{+21b}$, $[(MnL^{17})_2(OH_2)(OHCH_3)(\mu\text{-phth})]^{21c}$, $[(MnL^{17}(ClO_4)]_2(\mu\text{-}4,4''\text{-bpy})]^{21d}$, $[\{MnL^{17}(OH_2)\}_2(\mu\text{-}_{1,3}\text{-}N_3)]^{21e}$, $[(MnL^{17})_2(\mu\text{-}OCOCH_2Ph)]^{+21f}$, $[(MnL^{17})_2(\mu\text{-}OAc)]^{+21g}$ $\{H_2L^{17}= N,N'\text{-bis(salicylidene)-1,2-ethanediamine}\}$

Aziodo, thiocyanato, Phosphinato, dicyanamido bridged polynuclear Mn(III) complexes with N_2O_2 donor Schiff bases could also be found in literature.[22] Some polynuclear manganese(III) complexes with N_2O_2 donor Schiff base ligands have been gathered in Scheme **I.A.5**.[22] Thiocyanato bridged 1D polymeric complex, $[MnL^{13}(\mu_{1,3}\text{-}NCS)]_n$ exhibits weak ferromagnetic interaction with the coupling parameters (J) of -3.2 cm^{-1} whereas dicyanamido bridged 1D polymeric complex, $[MnL^{19}(\mu_{1,3}\text{-}N(CN)_2)]_n$ exhibits antiferromagnetic interaction with the coupling parameters (J) of -0.722 cm^{-1}.[22c, d]

$[MnL^{17}(HO_2PPh_2)]_n$

$[MnL^{18}(\mu_{1,1}\text{-}N_3)]_n$

$[MnL^{19}\{\mu_{1,3}\text{-}N(CN)_2\}]_n$

$[MnL^{13}(\mu_{1,3}\text{-}NCS)]_n$
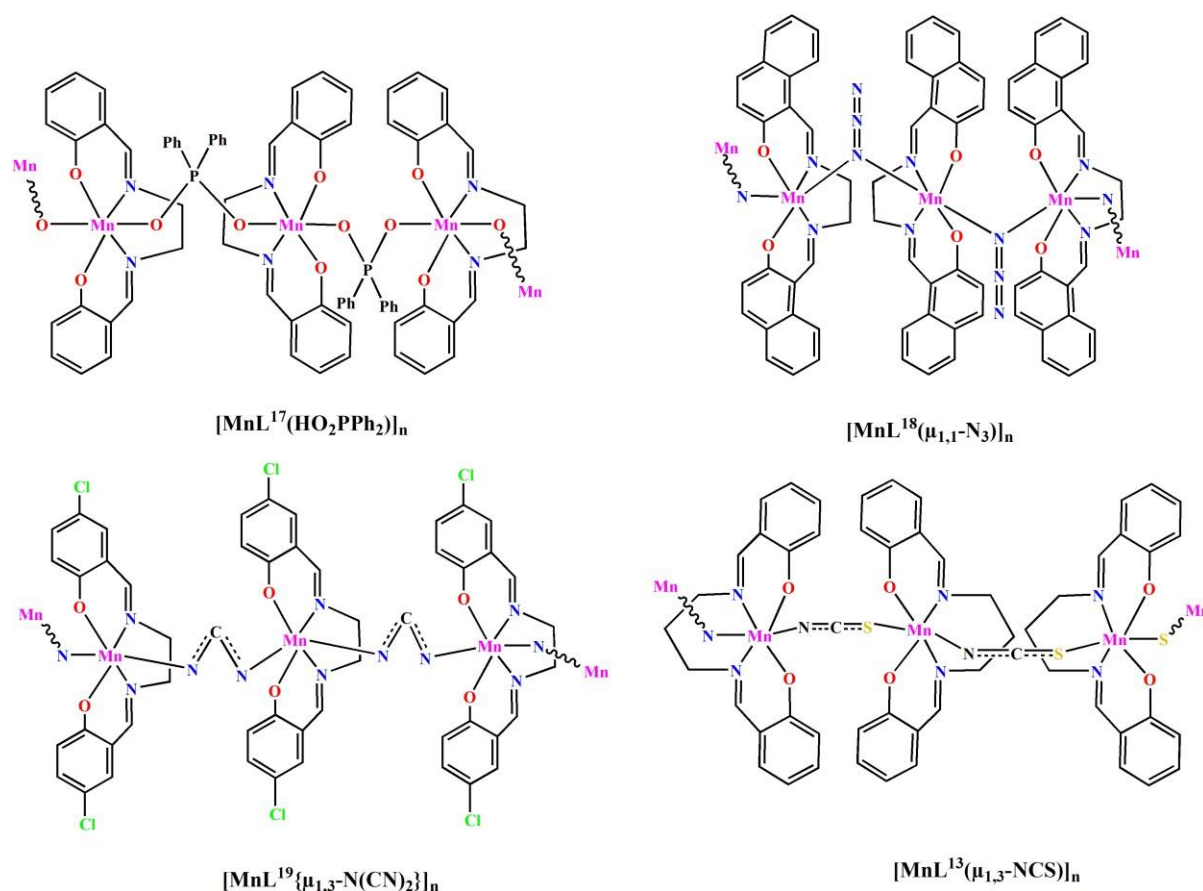
Scheme I.A.5: Schematic representation of $[MnL^{17}(HO_2PPh_2)]_n$[22a] {H_2L^{17}= N,N' bis(salicylidene)ethane-1,2-diamine}; $[MnL^{18}(\mu_{1,1}\text{-}N_3)]_n$ [22b] {H_2L^{18}= N,N'-bis[(2-hydroxy-1-naphthyl)methylidene)-ethane-1,2-diamine}; $[MnL^{19}(\mu_{1,3}\text{-}N(CN)_2)]_n$[22c] {$H_2L^{19}$= N,N' bis(5-chlorosalicylidene)ethane-1,2-diamine}; $[Mn(L^{13})(\mu_{1,3}\text{-}NCS)]_n$[22d] {$H_2L^{13}$= N,N' bis(salicylidene)propane-1,3-diamine}

I.A.2. Zinc complexes with tetradentate N_2O_2 donor Schiff bases

There are several mononuclear zinc(II) complexes with salen type ligands that have been synthesised and characterised in the presence of various halides, pseudohalides, or various other coligands.[23, 24] Some selected penta-nuclear complexes have been compiled in Scheme **I.A.6**.[23] N_2O_2 donor Schiff base ligand occupied four coordination sites, with solvent molecule occupying the remaining coordinating position. [ZnL^{1}Py] and [ZnL^{2}Py] used as electroluminescent materials.[23a] [ZnL^7(OH$_2$)] has strong activity against the bacteria for *B. subtilis* and *S. aureus*, and nearly equal activities against *E. coli*.[23c]
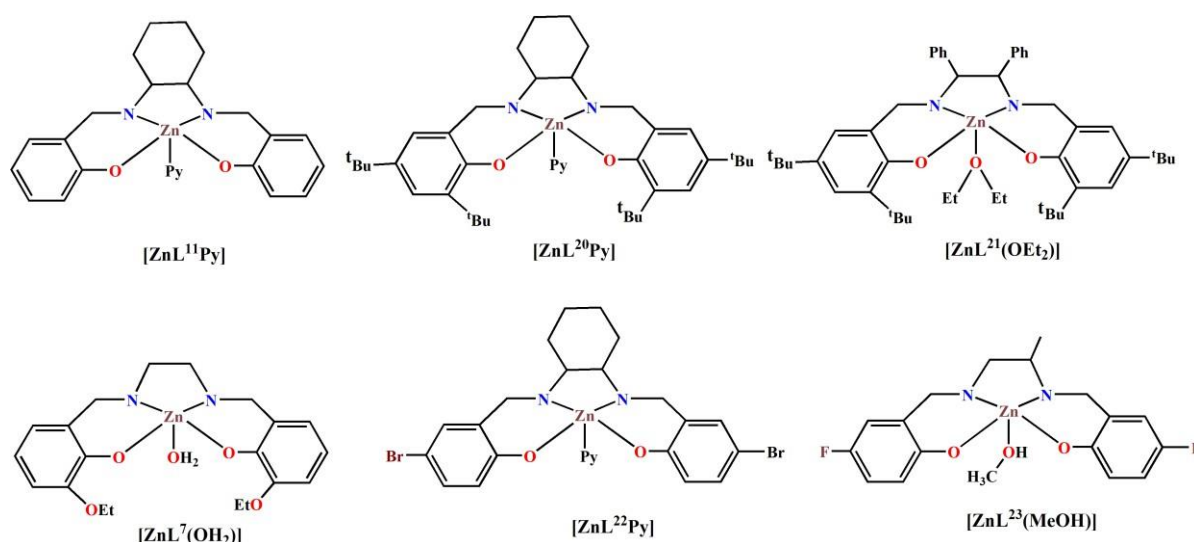
Scheme I.A.6. Schematic representation of [ZnL^{11}Py][23a] {H$_2$L^{11}= N,N' bis(salicylidene)cyclohexane-1,2-diamine}; [ZnL^{20}Py][23a] {H$_2$L^{20}= N,N'-bis(3,5-di-tert-butylsalicylidene)cyclohexane-1,2-diamine}; [ZnL^{21}(OEt$_2$)][23b] {H$_2$L^{21}= N,N'-bis(3,5-di-tert-butylsalicylidene)-1,2-diphenylethane-1,2-diamine}; [ZnL^7(OH$_2$)][23c] {H$_2$L^7= N,N'-bis(3-ethoysalicylidene)ethane-1,2-diamine}; [ZnL^{22}Py][23d] {H$_2$L^{22}=N,N'-bis(5-bromosalicylidene)cyclohexane-1,2-diamine}; [ZnL^{23}(MeOH)][23e] {H$_2$L^{23}= N,N'-bis(5-fluorosalicylidene)propane-1,2-diamine}.

One salient feature of salen type Schiff bases is the intriguing capacity of their phenoxo oxygen atoms to form μ2-bridges, providing high-nuclearity complexes.[24] Examples of such phenoxo bridged dinuclear zinc(II) complexes are shown in Scheme **I.A.7.**[24] [ZnL^{26}]$_2$ is chiral complex.[24d]

[ZnL^8]$_2$

[ZnL^{13}]$_2$

[ZnL^{24}]$_2$

[Zn$_2$L^{25}(OAc)$_2$(OH$_2$)]

[ZnL^{26}]$_2$
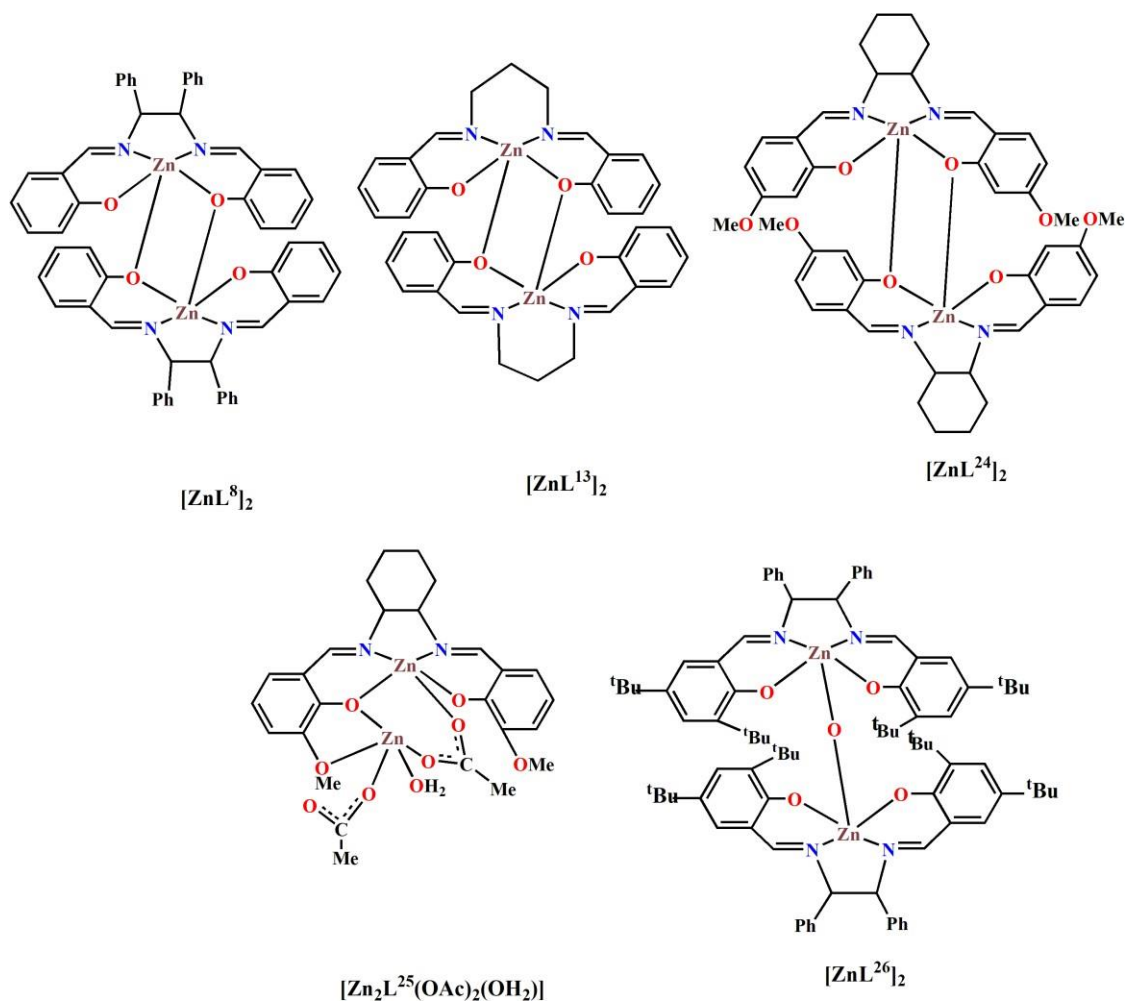
Scheme I.A.7. Schematic representation of [ZnL^8]$_2$[23b] {H$_2$L^8= N,N'-bis(salicylidene)-1,2-diphenylethane-1,2-diamine}; [ZnL^{13}]$_2$[24a] {H$_2$L^{13}= N,N'-bis(salicylidene)propane-1,3-diamine}; [ZnL^{24}]$_2$[24b] {H$_2$L^{24}= N,N'-bis(4-methoxysalicylidene)cyclohexane-1,2-diamine}; [Zn$_2$L^{25}(OAc)$_2$(OH$_2$)][24c] {H$_2$L^{25}= N,N'-bis(3-methoxysalicylidene)cyclohexane-1,2-diamine}; [ZnL^{26}]$_2$[24d] {H$_2$L^{26}= N,N'-bis(2,4-di-tertbutylsalicylidene)-1,2-diphenylethane-1,2-diamine}

Several research groups have prepared trinuclear zinc(II) Schiff base complexes **Scheme I.A.8.**[25] Cytotoxic effect of $[Zn_3L^7{}_2(OH_2)(\mu_1\text{-dca})(\mu_{1,5}\text{-dca})]$ against human breast cancer cell line (MCF7) revealed that it works as anti-cancerous agent in near future.[25]

$\{[ZnL^{27}]_2(OAc)_2Zn\}$ $[Zn_3(L^7)_2(OH_2)(\mu_1\text{-dca})(\mu_{1,5}\text{-dca})]$
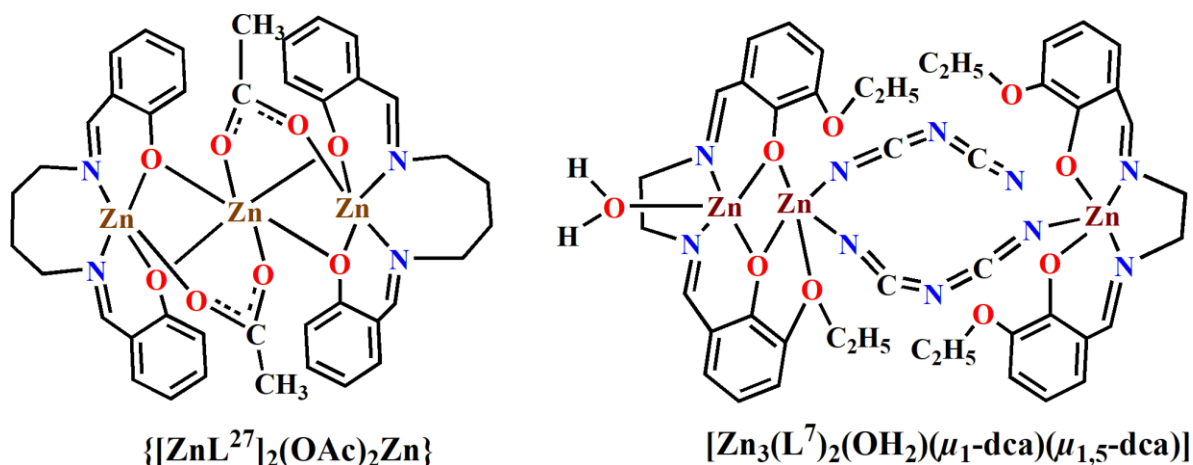
Scheme I.A.8. Schematic representation of $\{[ZnL^{27}]_2(OAc)_2Zn\}$[24a] [$H_2L^{27}=$ (N,N'-bis(salicylidene)butane-1,4-diamine]; $[Zn_3(L^7)_2(OH_2)(\mu_1\text{-dca})(\mu_{1,5}\text{-dca})]$[25] [$H_2L^7=$ (N,N'-bis(3-ethoysalicylidene)ethane-1,2-diamine].

Several coligands are used in conjunction with N_2O_2 donor Schiff base ligands to prepare high nuclearity complexes.[26] **Scheme I.A.9** contains a collection of pseudohalide bridged zinc(II) complex instances.[26] It's noteworthy to note that some complexes may also be applied to biological process.[26] Cytotoxic effect of $[Zn_4(L^{10})_2(\mu_1\text{-dca})_2(\mu_{1,5}\text{-dca})_2]$ against human breast cancer cell line (MCF7) revealed that it works as anti-cancerous agent in near future., Both complexes $[Zn_4(L^{28})_2(\mu_1\text{-dca})_2(\mu_{1,5}\text{-dca})_2]$ and $[Zn_4(L^{29})_2(\mu_1\text{-dca})_2(\mu_{1,5}\text{-dca})_2]$ exhibited *in vitro* antibacterial and anti-biofilm properties against some important Gram-positive and Gram–negative bacterial strains that strongly implying their prospective use as bacteriostatic or anti-biofilm agents.

[Zn$_4$(L^{28})$_2$(μ_1-dca)$_2$($\mu_{1,5}$-dca)$_2$]

[Zn$_4$(L^{29})$_2$(μ_1-dca)$_2$($\mu_{1,5}$-dca)$_2$]

[Zn$_4$(L^4)$_2$(μ_1-dca)$_2$($\mu_{1,5}$-dca)$_2$]

[Zn$_4$(L^{11})$_2$(OAc)$_3$(OH)]
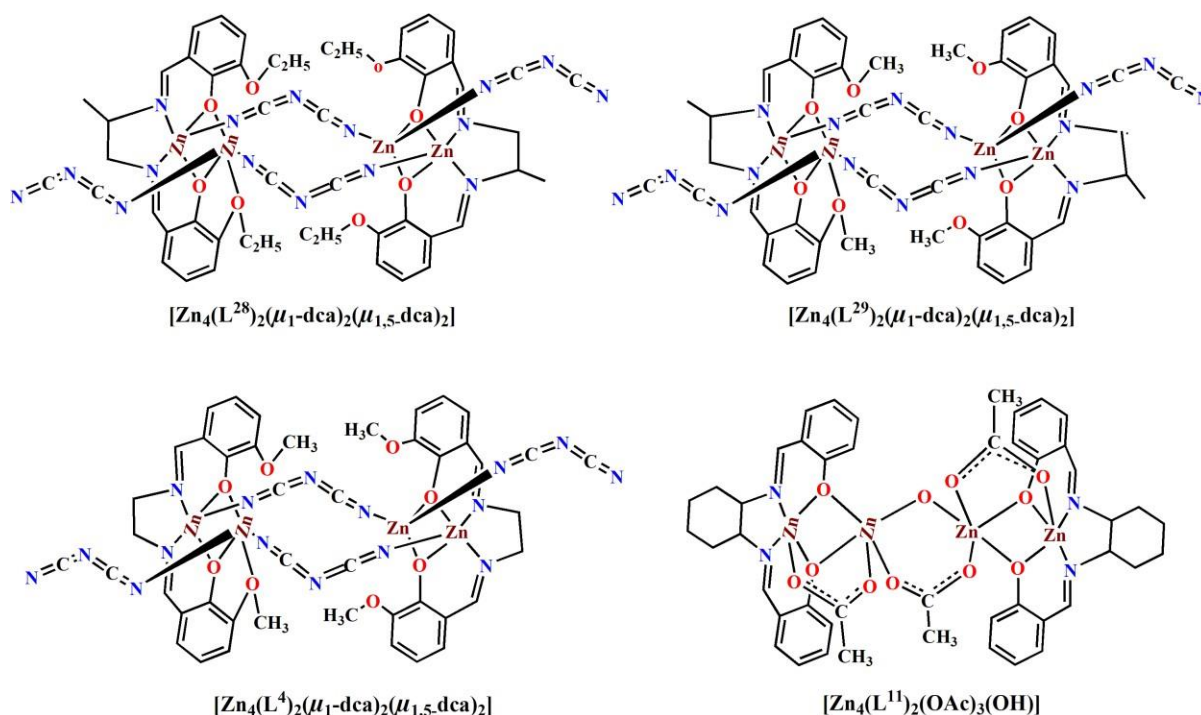
Scheme I.A.9. Schematic representation of [Zn$_4$(L^{28})$_2$(μ_1-dca)$_2$($\mu_{1,5}$-dca)$_2$][26a] [H$_2$L^{28}= N,N'-bis(3-ethoysalicylidene)propane-1,2-diamine], [Zn$_4$(L^{29})$_2$(μ_1-dca)$_2$($\mu_{1,5}$-dca)$_2$][26a] [H$_2$L^{29}= N,N'-bis(3-methoysalicylidene)propane-1,2-diamine]; [Zn$_4$(L^4)$_2$(μ_1-dca)$_2$($\mu_{1,5}$-dca)$_2$][26b] [H$_2$L^4= N,N'-bis(3-methoysalicylidene)ethane-1,2-diamine]; [Zn$_4$(L^{11})$_2$(OAc)$_3$(OH)][26c] [H$_2$L^{11}= N,N'-bis(salicylidene)cyclohexane-1,2-diamine]

M. Mahato *et al*. have synthesized a polynuclear complex [Zn$_2$(L^{19})(N$_3$)$_2$]$_n$ (Scheme **I.A.10)**. The optical properties of this complex have been investigated.[27]

I.A.3. Zinc complexes with reduced N$_2$O$_2$ donor ligands

In most cases, the 2:1 condensation reaction between a number of diamines and salicylaldehyde or modified salicylaldehyde is followed by reduction with NaBH$_4$ to produce reduced analogues of tetradentate N$_2$O$_2$ donor salicylidene type Schiff base ligands.[28] These kinds of chelating ligands are particularly fascinating to synthesis chemists because of the variable coordination behaviour. There are already a lot of zinc complexes with tetradentate ligands of the salen/salpn type in the literature.[25, 26a] Unfortunately, there is no evidence in the

literature for zinc complexes with their reduced equivalents. However, some evidence does exist for zinc complexes containing reduced N_2O_4 donor ligands.
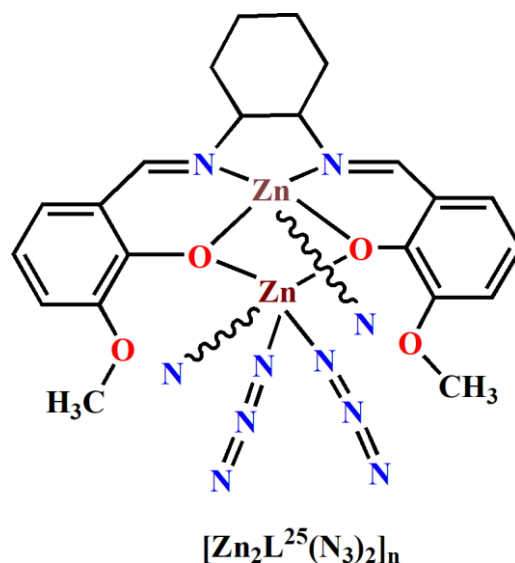
$[Zn_2L^{25}(N_3)_2]_n$

Scheme I.A.10. Schematic representation of $[Zn_2L^{25}(N_3)_2]_n{}^{27}$ $[H_2L^{25}=$ (1,2-cyclohexanediamino-N,N'-bis(3-methoxysalicylidene)]

I.A.4. Zinc complexes with reduced N_2O_4 donor ligands

The 2:1 condensation reaction between various diamines and 3-methoxy/3-ethoxy salicylaldehyde is usually followed by reduction with $NaBH_4$ to produce reduced analogues of N_2O_4 donor salicylidene type Schiff base ligands.[28]

There are various zinc complexes with these kinds of ligands in presence of several halides, pseudohalides or several other coligand have been synthesised and characterised in the literature.[28, 29] A few selected dinuclear complexes of have been gathered in Scheme **I.A.11**.[28]

M. Karmakar et al. have synthesised two dinuclear zinc(II) complexes$[ZnL^{30}(SCN)\mu_{1,3}$-OAc)Zn(DMSO)] and $[ZnL^{30}(dca)(\mu_{1,3}$-OAc)Zn(DMSO)]. Both complexes have also been found to be efficient photocatalyst for the degradation of methylene blue (MB).[28a] A. Thevenon et al. has synthesised another two dinuclear complexes $[ZnL^{31}]_2$.THF and $[ZnL^{31}]_2$.CH_3OH. Both the complexes are pheoxy bridged dinuclear

complexes where both zinc centers are in trigonal bipyramidal coordination environment. The complexes have been used catalysts for the ring opening copolymerization of epoxides.[28b]

[ZnL³⁰(SCN)(μ₁,₃-OAc)Zn(DMSO)]   [ZnL³⁰(dca)(μ₁,₃-OAc)Zn(DMSO)]   [ZnL³¹]₂
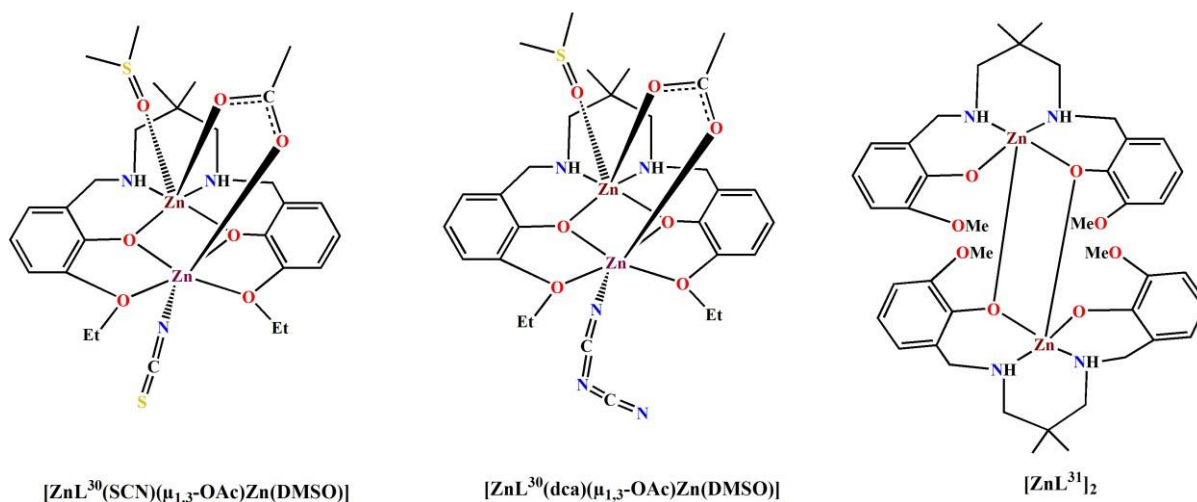
Scheme **I.A.11**.Schematic representation of [ZnL³⁰(SCN)(μ₁,₃-OAc)Zn(DMSO)][28a], [ZnL³⁰(dca)(μ₁,₃-OAc)Zn(DMSO)][28a], {H₂L³⁰ = 2,2' -[(2,2-dimethyl-1,3-propanediyl)bis(iminomethylene)]bis[6-ethoxy-phenol]} and [ZnL³¹]₂[28b], H₂L³¹ = 2,2' -[(2,2-dimethyl-1,3-propanediyl)bis(iminomethylene)]bis[6-methoxy-phenol]

Reports of trinuclear zinc(II) complexes having reduced N_2O_4 donor ligands have been found in literature.[29] Structures of few selected trinuclear complexes of have been gathered in Scheme **I.A.12**.[29] All complexes may be used as sensors for the detection of nitroaromatics in DMF via turn-off fluorescence response.[29]

M. Karmakar *et al*. have synthesized three tetranuclear zinc(II) dicyanamide complexes[30] (Scheme **I.A.13**.).

Structure of a unique penta-nuclear zinc(II) complex with N_2O_4 donor Schiff bases are shown in Scheme **I.A.14**.[31] The complex behaves as a sensor for the detection of nitroaromatics in DMF solution via turn-off fluorescence response.[31]
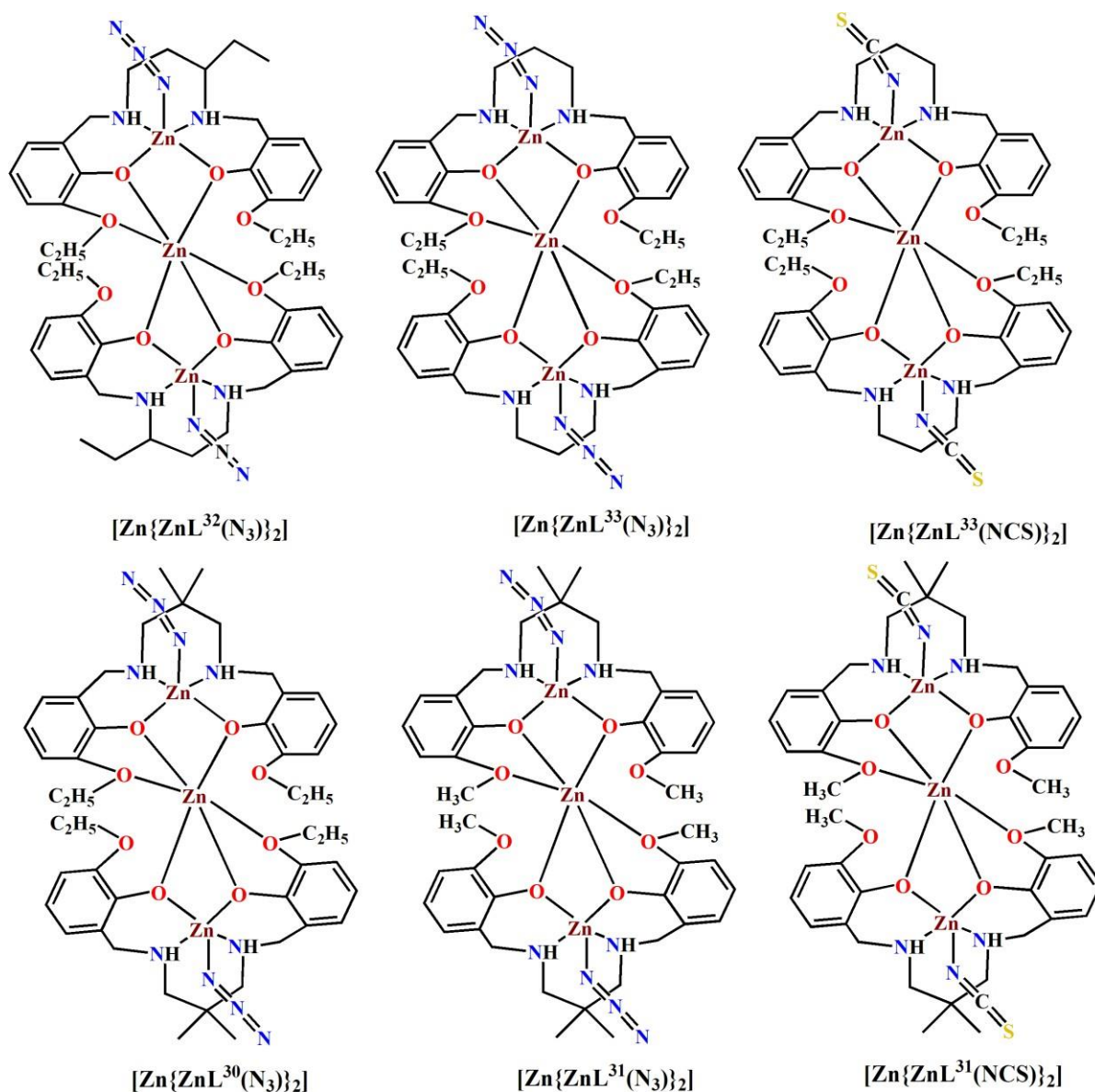
Scheme I.A.12. Schematic representation of [Zn{ZnL^{32}(N$_3$)}$_2$][29a] {H$_2$L^{32} = 2,2'-[(1-ethyl-1,3-propanediyl)bis(iminomethylene)]bis[6-ethoxyphenol]}; [Zn{ZnL^{33}(N$_3$)}$_2$][29b], [Zn{ZnL^{33}(NCS)}$_2$][29b], {H$_2$L^{33}=2,2'-[(1,3-propanediyl)bis(iminomethylene)]bis[6-ethoxyphenol]}, [Zn{ZnL^{30}(N$_3$)}$_2$][29b], {H$_2$L^{30} = 2,2' -[(2,2-dimethyl-1,3-propanediyl)bis(iminomethylene)]bis[6-ethoxy-phenol], [Zn{ZnL^{31}(N$_3$)}$_2$][29b], [Zn{ZnL^{31}(NCS)}$_2$][29b], H$_2$L^{31} = 2,2' -[(2,2-dimethyl-1,3-propanediyl)bis(iminomethylene)]bis[6-methoxy-phenol]
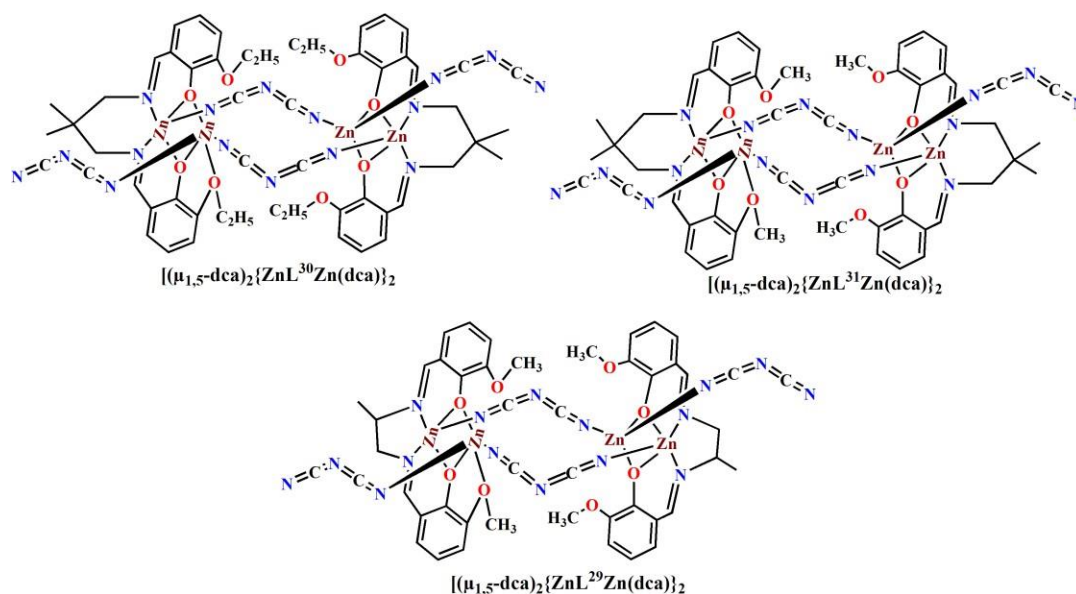
Scheme I.A.13. Schematic representation of $[(\mu_{1,5}\text{-dca})_2\{ZnL^{30}Zn(dca)\}_2]^{30}$ $[(\mu_{1,5}\text{-dca})_2\{ZnL^{31}Zn(dca)\}_2]^{30}$, $[(\mu_{1,5}\text{-dca})_2\{ZnL^{29}Zn(dca)\}_2]^{30}$ where $\{H_2L^{30}$ = 2,2' -[(2,2-dimethyl-1,3-propanediyl)bis(iminomethylene)]bis[6-ethoxy-phenol], H_2L^{31} = 2,2' -[(2,2-dimethyl-1,3-propanediyl)bis(iminomethylene)]bis[6-methoxy-phenol] and H_2L^{29} = 2,2' -[(1,2-propanediyl)bis(iminomethylene)]bis[6-methoxy-phenol]
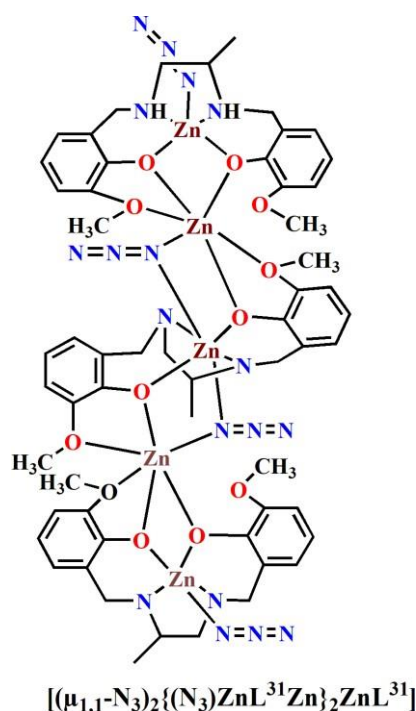
Scheme I.A.14. Schematic representation of $[(\mu_{1,1}\text{-N}_3)_2\{(N_3)ZnL^{31}Zn\}_2ZnL^{31}]$ $\{H_2L^{31}$= 2,2'-[(1-methyl-1,2-ethanediyl)bis(iminomethylene)]bis[6-methoxyphenol]\}

References

1 (a) M. Halka and B. Nordstrom, *Transition Metal,* 2nd Ed. 2019; (b) E. C. Constable, *Dalton Trans.*, 2019, **48**, 9408; (b) Weeks, Mary Elvira, *"Discovery of the Elements," Jour of Chem. Ed., Easton, P a.,* 6th Ed. 1960

2 (a) R. J. P. Williams, *R. Inst. Chem., Rev.*, 1968,**1**, 13; (c) Wolfgang Maret, Metallomics and the Cell, 2013, **12**, 479.

3 (a) K. Ghosh, A. Banerjee, A. Bauz´a, A. Frontera and S. Chattopadhyay, *RSC Adv.*, 2018, **8**, 28216; (b)N. Sarkar, K. Harms, S. Chattopadhyay, *Polyhedron*, 2018, **141**, 198; (c) T. Basak, A. Bhattacharyya, K. Harms and S. Chattopadhyay, *Polyhedron* 2019, **157**, 449.

4 (a) S. Dey, G. C. Dhal, D. Mohan and R. Prasad, *Advanced Composites and Hybrid Materials*, 2019, **2**, 626; (b) U. B. Kim, D, J, Jung, H. J. Jeon, K. Rathwell and S-gi Li, *Chemical Reviews*, 2020, **120**, 13382; (c) K. Ghosh, S. Roy, A. Ghosh, A. Banerjee, A. Bauzá, Antonio Frontera and S. Chattopadhyay, *Polyhedron,* 2016, **112,** 6.

5 (a) J. Emsley, "Manganese", Nature"s Building Blocks: An A-Z Guide to the Elements. Oxford, UK: Oxford University Press, 2001, p249; (b) P. D. Blanc, *NeuroToxicology*, 2018, **64**, 5; (c) V. N. Kuleshova , E. A. Zhegallob and E. L. Shkol"nik, *Dok. Earth Sci.*, 2011, **441**, 1611

6 (a) A. Kityk, M. Hnatko, V. Pavlik and M. Boˇca, *Mater. Res. Bull.*, 2021, **141**, 111348; (b) A. G. Tyurin, *Prot. Met.*, 2005, **41**, 74.

7 (a) D. S. Avila, R. L. Puntel and Michael Aschner, *Met. Ions Life Sci.*, 2013, **13**, 199; (b) M. Aschner, T. R. Guilarte, J. S. Schneider, W. Zheng, *Toxicol. Appl. Pharmacol*. 2007, **221**, 131.

8 (a) L. Li and X. Yang, *Oxid Med Cell Longev*, 2018, **11**, 1; (b) Schramm, V.L., Wedler, F.C. in *Manganese in Metabolism and Enzyme Function*, Academic Press, Orlando, FL, **1986**.

9 (a) J. Brugger,*Zinc. In: White W. (eds) Encyclopedia of Geochemistry. Encyclopedia of Earth Sciences Series*, Springer, 2016; b) P.T. Craddock, Endeavour, 2014, **28**, 357; (c)K. M. Hambidge, N. F. Krebs, 2007, **137**, 1101; c) Wolfgang Maret, Metallomics and the Cell, 2013, **12**, 479-501

10 (a) Wolfgang Maret, Met. Ions Life Sci., 2013, 13, 389-414; (b) C. T. Chasapis, A. C. Loutsidou, C, A. Spiliopoulou and M. E. Stefanidou, *Archives of Toxicology*, 2012, **86**, 521; (c) A. S Prasad., *Mol. Med.*, 2008, **14**, 353.

11 (a) A. S. Prasad, *Advances in Nutrition*, 2013, **4**,176; (b) F. M. G. Abregú, C. Caniffi, C. T Arranz and A. L Tomat, *Advances in Nutrition*, 2022, **13**, 833; (c) A. S. Prasad, *J Trace Elem Med Biol*, 2014, **28**, 357.

12 (a) A. Stwertka, *Guide to the Elements (Revised ed.), Oxford University Press,* 198O; (b) A. P. Yadav, A. Nishikata and T. Tsuru, *Corros. Eng., Sci. Technol.*, 2008, **43**, 23.

13 (a) C. J. Lan, T. S. Chin, P. H. Lin and T. P. Perng, *J. New Mat. Electrochem. Systems*, 2006, **9**, 27; (b) M. Fayette**,** H. J. Chang, X. Li and D. Reed, *ACS Energy Lett.*, 2022, **7**, 1888.

14 (a) L.-L. Qu, Y-L. Zhu, Y-Z. Li, H-B. Du and X-Z. You, *Cryst. Growth Des.*, 2011, **11**, 2444; (b) P. S. Mukherjee, K. S. Min, A. M. Arif and Peter J. Stang, *Inorg. Chem.* 2004, **43**, 6345; (c) O. A. Abbas, O. M. El-Roudi and S. A. Abdel-Latif, *Appl. Organomet. Chem.*, 2023, **37**, 7236.

15 (a) S. Jagannatha Swamy, E. R. Reddy, D. N. Raju and S. Jyothi, *Molecules*, 2006, **11,** 1000; (b) P. Cieslik, P. Comba, B. Dittmar, D. Ndiaye, É. Tóth, G. Velmurugan and H. Wadepohl, *Angew. Chem.*, 2022, **134**, 202115580.

16(a)T. Basak, S. Roy, S. Banerjee, R. M. Gomila, A. Frontera and S. Chattopadhyay, *Polyhedron*, 2022, **225,** 11604; (b) M. Karmakar, A. Frontera and S.Chattopadhyay, *CrystEngComm*, 2020,**22**, 6876; (c) S. Roy, M. GB. Drew and S. Chattopadhyay, 2018, **150**, 28.

17(a)K. Ghosh, K harms and S. Chattopadhyay, *Polyhedron*, 2017, **123,** 162; (b) T. Basak, M. GB Drew and S. Chattopadhyay, *Inorg. Chem. Comm.*, 2018, **98**, 92; (c) S. Roy, T. Dutta, M. GB. Drew, S. Chattopadhyay, *Polyhedron*, 2020, **178,** 114311.

18 (a) K. S. Banu, T. Chattopadhyay, A. Banerjee, M, Mukherjee, S. Bhattacharya, G. K. Patra, E. Zangrando and D. Das, *Dalton Trans.*, 2009, 8755; (b) P. Seth, M. GB. Drew and A. Ghosh, *J Mol Catal A Chem*, 2012, **365**, 154; (c) B-W. Wang, L. Jiang, S-Sheng. Shu, B-W. Li, Z. Dong, W. Gu, X. Liu, *Chirality*, 2015, **27**,142; (d) R. Li, J. Tian, H. Liu, S. Yan, S. Guo and J. Zhang, *Transition Met Chem*, 2011, **36**, 811; (e) M. Maiti, D. Sadhukhan,

S. Thakurta, E. Zangrando, G. Pilet, A. Bauzá, A. Frontera, B. Dede and S. Mitra, *Polyhedron*, 2014, **75**, 40; (f) P. Chakraborty, S. Majumder, A. Jana, S. Mohanta, *Inorg. Chim. Acta*, 2014, **410**, 65.

19 (a) M. Damercheli, D. Dayyani, M. Behzad, B. Mehravi and M. S. Ardestani, *J Coord Chem*, 2015, **68**, 1500; (b) H. Miyasaka, R. Clérac, T. Ishii, H-C. Chang, S. Kitagawa and M. Yamashita, *J. Chem. Soc.*, *Dalton Trans.*, 2002, 1528; (c) M. Fleck, M. Layek, R. saha, D. Bandyopadhyay, *Transition Met Chem***, 2013, **38**, 715; (d) Y. Liu, *Acta Cryst.*, 2011, **E67**, m322; (e) G. Lenoble, P. G. Lacroix, J. C. Daran, S. Di. Bella and K. Nakatani, *Inorg. Chem.*,

1998, **37**, 2158; (f) P. J. Pospisil, D. H. Carsten and E. N. Jacobsen, *Chem. Eur. J.*, 1996, **2**, 974.

20 (a) Q. Wu, Q. Pu, Y. Wu, H. Shi, Y. He, J. Li and Q. Fan, *J.coord. chem.*, 2015, **68**, 1010; (b) Y. Feng, C. Wanga, Y. Zhao, J. Li, D. Liao, S.Yan and Q. Wang, *Inorg. Chim. Acta*, 2009, **362**, 3563; (c) G. Bhargavi, M. V. Rajasekharan, J.-P. Costes and J.-P. Tuchagues, *Polyhedron*, 2009, **28**, 1253; (d) P. Seth, S. Giri and A. Ghosh, *Dalton Trans.*, 2015, **44**,12863.

21 (a) T-T. Wang, M. Ren,S-S. Bao, Z-S. Cai, B. Liu, Z-H. Zheng, Z-L. Xua and L-M. Zheng, *Dalton Trans.*, 2015, **44**, 4271; (b) C. Chen, D. Huang, X. Zhang, F. Chen, H. Zhu, Q. Liu, C. Zhang, D. Liao, L. Li and L. Sun, *Inorg. Chem.*, 2003, **42**, 3540; (c) Y. Deawati, D. Onggo, I. Mulyani, I. Hastiawan, D. Kurnia, P. Lönnecke, S. Schmorl, B. Kersting, E. H-Hawkins, *Inorg. Chim. Acta.*, 2018, **482**, 353; (d) T-T. Wang, M. Ren, S.-S. Bao and L-M. Zheng, *Eur. J. Inorg. Chem.*, 2014, 1042; (e) S. Nastase, F. Tuna, C. Maxim, C. A. Muryn, N. Avarvari, R. E. P. Winpenny, and M. Andruh, *Cryst. Growth Des.*, 2007, **7**, 1825; (f) P. Kar, P. M. Guha, M. G. B. Drew, T. Ishida and A. Ghosh, *Eur. J. Inorg. Chem.* 2011, 2075; (g) D. Mart´ınez, M. Motevalli and M. Watkinson, *Dalton Trans.*, 2010, **39**, 446.

22 (a) S. Richeter, J. Larionova, J. Long, A. V. Lee and D. Leclercq, *Eur. J. Inorg. Chem.* 2013, 3206; (b) R. Bikas, M. Emami, K. S´lepokurab and N. Noshiranzadeh, *New J. Chem.,* 2017, **41**, 9710; (c) X-Y. Liu, L-Q. Duan, Q. Wei and S-P. Chen, *Inorg. Chim. Acta.,* 2014, **423**, 462; (f) S. Sailaja, K. R. Reddy, M. V. Rajasekharan, Hureau, E. Rivie`re, J. Cano and J.-J. Girerd, *Inorg. Chem.* 2003, **42**, 180.

23 (a) D. Zhu , Z. Su , Z. Mu , Y. Qiu and Y. Wang, *J.Coord. Chem.*, 2006, **59**, 409; (b) N. Meyer and P. W. Roesky, *Z. Anorg. Allg. Chem.*, 2007, **633**, 2292; (c) H. Y. Liu, C. Li, and J. J. Ma, *Russ. J. Coord. Chem,* 2014, **4**0, 240; (d) E. Szłyk, A. Wojtczak, A. Surdykowski and

M. Goz´dzikiewicz, *Inorg. Chim. Acta*., 2005, **358**, 467; (e) L. F. Cai, *Russ. J. Coord. Chem,* 2017, **43**, 666.

24 (a) J. Reglinski, S. Morris and D. E. Stevenson, *Polyhedron*, 2002, **21**, 2175; (b) G. Consiglio, I. P. Oliveri, F. Punzo, A. L. Thompson, S. D. Bella and S. Failla, *Dalton Trans*., 2015, **44**, 13040; (c) L-y. Wu, D.-di Fan, X.-q. Lü and R. Lu, *Chinese. J. Polym. Sci., 2014, 32, 768; (d)* E. Martin, M. M. Belmonte, E. C. Escudero-Adán and A. W. Kleij, *Eur. J. Inorg. Chem*., 2014, 4632.

25 D. Majumdar, S. Das, R. Thomas, Z. Ullahe, S.S. Sreejithg, D. Dash, P. Shuklac, K. Bankuraa and D.Mishraa, *Inorg. Chim. Acta*., 2019, **492**, 221.

26 (a) D. Majumdar, D. Das, S. S. Sreejith, S. Das, J. K. Biswas, M. Mondal, D. Ghosh, K. Bankura, D. Mishra, *Inorg. Chim. Acta*., 2019, **489**, 244; (b) D. Majumdar, S. Das, R. Thomas, Z. Ullah, S. S. Sreejith, D. Das, P. Shukla, K. Bankura, D. Mishra, *Inorg. Chim. Acta*., 2019, **492**, 221; (c) Q. Shi, J. Yang, X. Lü, Inorg. Chem. Comm. 2015, **59**, 61.

27. M. Mahato, D. Dey, S. Pal, S. Saha, A. Ghosh, K. Harms and H. P. Nayek, *RSC Adv*., 2014, **4**, 64725.

28 (a) M. Karmakar and S. Chattopadhyay, *Polyhedron*, 2020, **184**, 114527, (b) A. Thevenon, J. A. Garden, A. J. P. White and Charlotte K. Williams, *Inorg. Chem*., 2015, **54**, 11906.

29 (a) M. Karmakar and S. Chattopadhyay, *Polyhedron*, 2020, **187**, 114639; (b) M. Karmakar, S. Roy and S. Chattopadhyay, *New J. Chem.,* 2019, **43**, 10093.

30 M. Karmakar, A. Frontera and S. Chattopadhyay, *CrystEngComm*, 2020,**22**, 6876.

31 M. Karmakar, T. Basak and S. Chattopadhyay, *New J. Chem.,* 2019,**43**, 4432.

Section: I.B

Materials and details of instrumentation

I.B.1. Materials

All chemicals were of AR grade and were used as purchased from Sigma-Aldrich, India (now Merck, India) without further purification. All syntheses and manipulations were carried out under aerobic conditions.

Caution!!! Metal complexes containing azide/perchloarte are potentially explosive, especially in the presence of organic ligands. Although no troubles were encountered in the entire research work using such complexes, only a small amount of such materials should be prepared and should be handled with great care.

I.B.2. Details of instrumentations

I.B.2.1. Elemental analyses

Elemental analyses (carbon, hydrogen and nitrogen) were performed using a PerkinElmer 240C elemental analyser.

I.B.2.2. Infrared spectra

Solid state IR spectra in KBr pellets (4000-450 cm^{-1}) were recorded using a PerkinElmer Spectrum Two FT-IR spectrophotometer. The concentration of samples in KBr was kept in the range of 0.2% to 1%. (Too high a concentration usually causes difficulties obtaining clear pellets).

I.B.2.3. Electronic spectra

Electronic spectra (200-1000 nm) in various solvents were recorded in a PerkinElmer Lambda 35 UV-visible spectrophotometer, Shimadzu UV-1700 UV-Vis spectrophotometer and „Duetta" fluorescence and absorbance Spectrometer were used to record electronic spectra (200-1000 nm) in various solvents of synthesized complexes.

I.B.2.4. Photophysical study

Steady-state fluorescence emission spectrum was recorded using Shimadzu RF-5301PC spectrofluorometer and „Duetta" fluorescence and absorbance Spectrometer at room temperature. Hamamatsu MCP photomultiplier (R3809) was used to record time dependent photoluminescence spectra and IBHDAS6 software was used to analyse the data. The emissions of the complexes were tentatively attributed to intra-ligand transitions modified by metal coordination. Intensity decay profiles were fitted to the sum of exponential series

$$I(t) = \sum_i \alpha_i \exp \frac{-t}{\tau_i}$$

where α_i was a factor representing the fractional contribution to the time resolved decay of the components with a lifetime of η_i. Mono/bi/tri-exponential functions were used to fit the decay profile of the complexes, with obtaining χ^2 close to 1. The intensity averaged lifetime (η_{av}) of the complexes were determined from the result of the exponential model using the following equation:

$$\tau_{av} = \frac{\sum \alpha_i \tau_i^2}{\sum \alpha_i \tau_i}$$

where, α_i and η_i are the pre-exponential factor and excited state luminescence decay time associated with the i-th component, respectively.

I.B.2.5. Powder X-ray diffraction

Powder X-ray diffraction was performed on a Bruker D8 instrument with Cu-K$_\alpha$ radiation (λ = 1.5418 Å) generated at 40 kV and 40 mA. The powder XRD spectrum was recorded in a 2θ range of 5–50° using a 1D Lynxeye detector under ambient conditions. In this process, samples were ground with a mortar and pestle to prepare fine powders. The powders were then dispersed with alcohol onto a zero background holder (ZBH). The alcohol was allowed to evaporate to provide a nice, even coating of powder adhered to the sample holder.

The experimental PXRD patterns of the bulk products were in good agreement with the simulated XRD patterns from single crystal X-ray diffraction results, indicating consistency of the bulk samples. The simulated patterns of the complexes were calculated from the single crystal structural data (cifs) using the CCDC Mercury software.

I.B.2.6. Hirshfeld Surface analyses

Hirshfeld surfaces[1] and associated 2D-fingerprint[2] plots were calculated using Crystal Explorer[3] which accepted a structure input file in CIF format. Bond lengths to hydrogen atoms were set to standard values. For each point on the Hirshfeld isosurface, two distances d_e, the distance from the point to the nearest nucleus external to the surface and d_i, the distance to the nearest nucleus internal to the surface, are defined. The normalized contact distance ($d$norm) based on d_e and d_i was given by

$$d_{norm} = \frac{(d_i - r_i^{vdw})}{r_i^{vdw}} + \frac{(d_e - r_e^{vdw})}{r_e^{vdw}}$$

where r_i^{vdw} and r_e^{vdw} were the van der Waals radii of the atoms. The value of d_{norm} was negative or positive depending on intermolecular contacts, being shorter or longer than the van der Waals separations. The parameter d_{norm} displayed a surface with a red-white-blue colour scheme, where bright red spots highlighted shorter contacts, white areas represented contacts around the van der Waals separation, and blue regions were devoid of close contacts. For a given crystal structure and set of spherical atomic electron densities, the Hirshfeld surface was unique[4] and it was this property that suggested the possibility of gaining additional insight into the intermolecular interaction of molecular crystals.

I.B.2.7. Crystal data collection and refinement details

Single crystals of complexes **1, 2, 3, 4, 6, 7, 8, 9** and **10** were used for data collection using a „Bruker D8 QUEST area detector" diffractometer equipped with graphite-monochromated Mo-K$_\alpha$ radiation (λ = 0.71073 Å) at 273 K. Molecular structures were solved by direct method and refined by full-matrix least squares on F^2 using the SHELX package[5] [SHELXL-18/1 was used for complexes **4, 6, 7, 8, 9, 10** and SHELX-14/7 was used for complexes **1, 2, 3**]. Non hydrogen atoms were refined with anisotropic thermal parameters. Hydrogen atoms, attached to nitrogen and oxygen, were located by difference Fourier maps and were kept at fixed positions. All other hydrogen atoms were placed in their geometrically idealized positions and constrained to ride on their parent atoms. Multi-scan empirical absorption corrections were applied to the data using the program SADABS[6].

In the unit cell of complex **1**, a highly disordered water molecule was present which could not be modeled as discrete atomic sites. We employed PLATON/SQUEEZE to calculate the diffraction contribution of the solvent molecules and thereby were able to produce a set of solvent-free diffraction intensities. Details about the SQUEEZE procedure are given in the respective CIF file.

A suitable single crystal of the complex **5** was picked, mounted on a glass fiber and diffraction intensities were measured with an STOE IPDS 2T diffractometer[7] equipped with Mo K$_\alpha$ radiation, a graphite monochromator (λ = 0.71073 Å) and an IMAGE PLATE detector[8] using an oil-coated shock-cooled crystal at 100(2) K. Absorption effects were corrected by a combination of empirical using crystal faces (STOE X-SHAPE & X-RED)[9] and semi-empirical using multiscanned reflexions (STOE LANA, absorption correction by scaling of reflection intensities)[10]. Cell constants were refined using 35228 of observed reflections of the data collection. The structure was solved by direct methods by using the program XT V2014/1 (Bruker AXS Inc., 2014) and refined by full matrix least squares procedures on F^2 using SHELXL-2018/3 (Sheldrick, 2018)[5]. The non-hydrogen atoms were refined anisotropically, carbon bonded hydrogen atoms were included at calculated positions and refined using the „riding model" with isotropic temperature factors at 1.2 times (for CH_3 groups 1.5 times) that of the preceding carbon atom[11].

I.B.2.8. Magnetic susceptibility measurements

The magnetic susceptibility measurements of complexes **1-4** were performed with a magnetic susceptibility balance, made by Sherwood Scientific, Cambridge, UK at room temperature (300 K). The corrected magnetic susceptibility, χ_m, was calculated using the relation: $\chi_{m} = \chi_{meas} - \chi_D$. Diamagnetic susceptibilities, χ_D were calculated using Pascal"s constants[12]. Effective magnetic moments were calculated using the formula, $\mu_{eff} = 2.828(\chi_m T)^{1/2}$, where χ_m was the corrected molar susceptibility. The instrument was calibrated using metallic nickel.

I.B.2.9. Computational details

The geometry optimizations of the complexes **7, 8** and **9** were carried out using the density functional theory method at the B3LYP level with the Gaussian 09 program package. Los

Alamos Effective Core Potentials lanL2DZ basis set was employed for the Zn atom. On the other hand, the split-valence 6-31G(d) basis set was applied for the other atoms. The starting structure of the investigated complex was used from its X-ray crystallographic data. The geometry optimization is performed without any constraint, and the nature of stationary points was confirmed by normal-mode analysis. The topological features derived from Bader''s theory of atoms in molecules (AIM) approach was applied to understand the electron-density features like charge density (ρ) and Laplacian of charge density ($\nabla^2\rho$) using ADF2014.10. The recently developed Reduced Density Gradient (RDG) based NCI (noncovalent interactions) index calculations were applied for real-space visualization of both attractive (van der Waals and hydrogen-bonding) and repulsive (steric) interactions based on properties of the electron density. Herein, the single-point calculations were based on the structure obtained from X-ray studies and in these structures, the hydrogen atom positions were normalized before computation. The interaction energies of dimers **(for complexes 7 and 8)** were calculated using basis set superposition error (BSSE) corrections by the following methods:

$$\Delta E(AB) = E(AB) - E(A) - E(B) + (\text{BSSE value of dimer})$$

In case of complex **4**, the geometries were computed at the M06-2X/def2-TZVP level of theory using the crystallographic coordinates. All calculations were performed with the GAUSSIAN-09 program[13]. The Grimme''s dispersion[14] correction was used as implemented in GAUSSIAN-09 program since it was adequate for the evaluation of noncovalent interactions where dispersion effects are relevant like ζ-hole interactions. The basis set superposition error for the calculation of interaction energies was corrected using the counterpoise method[15]. The NCI plot[16] isosurfaces was used to characterize noncovalent interactions. They correspond to both favorable and unfavorable interactions, as differentiated by the sign of the second density Hessian eigen value and defined by the isosurface color.

The color scheme is a red-yellow-green-blue scale with red for ρ^{+}_{cut} (repulsive) and blue for ρ^{-}_{cut} (attractive).

For complex **6**, desired calculations were performed with a Gaussian-16[17]at the PBE0[18]-D3/def2-TZVP[19] level of theory. The interaction energy of the tetrel bonding dimer was computed by calculating the difference between the energies of the isolated monomers and the one of their assembly. These energies were corrected using the Boys and Bernardi counterpoise method[20]. The Grimme"s D3 dispersion correction was used in the calculations[21]. To evaluate the interactions in the solid state, the crystallographic coordinates were used and only the position of the hydrogen bonds was optimized. This procedure and level of theory were used before to investigate non-covalent interactions in the solid state[22].The QTAIM analysis[23] and NCI plot index[23] calculations were computed at the same level of theory by means of the AIMAll program[24].The NBO version 3.1 program was used to evaluate donor-acceptor interactions[25] as implemented in Gaussian-16.

I.B.2.10. Figures and graphics

All the figures were plotted using DIAMOND[26], ORTEP-3[27], POV-Ray[28] and structures were analyzed with Mercury v 2.3[29], WinGX[30] softwares.

I.B.2.11. Catalase-like activity studies

Volumetric measurements of evolved dioxygen during the reactions of the manganese(III) complexes **1, 2, 3** and **4** with H_2O_2 were carried out as mentioned hereafter: a 50 cm^3 three-necked round-bottom flask containing a solution of the complex (10^{-3} M) in DMF (10 cm^3) was placed in a water bath at 25°C. One of the necks was connected to a burette and the others were stoppered by a rubber septum. While the solution was stirring, hydrogen peroxide (30% v/v) was injected into it through the rubber septum using a microsyringe. Volumes of evolved dioxygen were measured for 5 min time intervals volumetrically.

References

1 (a) M. A. Spackman and D. Jayatilaka, *CrystEngComm,* 2009, **11**, 19; (b) F. L. Hirshfeld, *Theor.Chim. Acta,* 1977, **44**, 129; (c) H. F. Clausen, M. S. Chevallier, M. A. Spackman and B. B. Iversen, *New J. Chem.*, 2010, **34**, 193.

2 (a) A. L. Rohl, M. Moret, W. Kaminsky, K. Claborn, J. J. McKinnon and B. Kahr, *Cryst. GrowthDes.*, 2008, **8**, 4517; (b) A. Parkin, G. Barr, W. Dong, C. J. Gilmore, D. Jayatilaka, J. J. McKinnon,M. A. Spackman and C. C. Wilson, *CrystEngComm*, 2007, **9**, 648; (c) M. A. Spackman and J. J. McKinnon, *CrystEngComm*, 2002, **4**, 378.

3 S. K. Wolff, D. J. Grimwood, J. J. McKinnon, D. Jayatilaka and M. A. Spackman, *Crystal Explorer2.0*, University of Western Australia, Perth, Australia, **2007**, http://hirshfeldsurfacenet.blogspot.com.

4 J. J. McKinnon, M. A. Spackman and A. S. Mitchell, *Acta Crystallogr., Sect. B: Struct. Crystallogr. Cryst. Chem.*, 2004, **60**, 627.

5 (a) G. M. Sheldrick, *Acta Cryst.,* 2015, **C71**, 3-8; (b) G. M. Sheldrick, *Acta Cryst.,* 2015, **A71**, 3-8.

6 G. M. Sheldrick, SADABS, V2014/5, Software for Empirical Absorption Correction, University of Göttingen, Institute fur Anorganische Chemieder Universitat, Gottingen, Germany, 1999–2003.

7 *X-Area*, STOE & Cie GmbH, Darmstadt, Germany, 2011.

8 (a) *X-Area Recipe*, STOE & Cie GmbH, Darmstadt, Germany, 2015; (b) *X-Area Integrate*, STOE & Cie GmbH, Darmstadt, Germany, 2016.

9 (a) *X-RED32*, STOE & Cie GmbH, Darmstadt, Germany, 2009; (b) *X-Shape*, STOE & Cie GmbH, Darmstadt, Germany, 2009.

10 *X-Area LANA*, STOE & Cie GmbH, Darmstadt, Germany, 2016.

11 K. Brandenburg, *Diamond - Crystal and Molecular Structure Visualization*, Crystal Impact - Dr. H. Putz & Dr. K. Brandenburg GbR, Bonn, Germany, 2014.

12 O. Kahn, Molecular magnetism, VCH, New York, 1993.

13 M. J. Frisch, G. W. Trucks, H. B. Schlegel, G. E. Scuseria, M. A. Robb, J. R. Cheeseman, G. Scalmani, V. Barone, B. Mennucci, G. A. Petersson, H. Nakatsuji, M. Caricato, X. Li, H. P. Hratchian, A. F. Izmaylov, J. Bloino, G. Zheng, J. L. Sonnenberg, M. Hada, M. Ehara, K. Toyota, R. Fukuda, J. Hasegawa, M. Ishida, T. Nakajima, Y. Honda, O. Kitao, H. Nakai, T. Vreven, J. A. Montgomery, Jr., J. E. Peralta, F. Ogliaro, M. Bearpark, J. J. Heyd, E. Brothers, K. N. Kudin, V. N. Staroverov, R. Kobayashi, J. Normand, K. Raghavachari, A. Rendell, J. C. Burant, S. S. Iyengar, J. Tomasi, M. Cossi, N. Rega, J. M. Millam, M. Klene, J. E. Knox, J. B. Cross, V. Bakken, C. Adamo, J. Jaramillo, R. Gomperts, R. E. Stratmann, O. Yazyev, A. J. Austin, R. Cammi, C. Pomelli, J. W. Ochterski, R. L. Martin, K. Morokuma, V. G. Zakrzewski, G. A. Voth, P. Salvador, J. J. Dannenberg, S. Dapprich, A. D. Daniels, Ö. Farkas, J. B. Foresman, J. V. Ortiz, J. Cioslowski, D. J. Fox, Gaussian 09 (Gaussian, Inc., Wallingford CT, 2009).

14 S. Grimme, J. Antony, S. Ehrlich and H. Krieg, *J. Chem. Phys.*, 2010, **132**, 154104.

15 S. F. Boys and F. Bernardi, *Mol. Phys.*, 1970, **19**, 553.

16 J. Contreras-García, E. R. Johnson, S. Keinan, R. Chaudret, J. -P. Piquemal, D. N. Beratan and W. Yang, *J. Chem. Theory Comput.*, 2011, **7**, 625.

17 M. J. Frisch, G.W. Trucks, H. B. Schlegel, G. E. Scuseria, M. A. Robb, J. R. Cheeseman, G. Scalmani, V. Barone, G. A. Petersson, H. Nakatsuji, X. Li, M. Caricato, A. Marenich, J. Bloino, B. G. Janesko, R. Gomperts, B. Mennucci, H. P. Hratchian, J. V. Ortiz, A. F. Izmaylov, J. L. Sonnenberg, D. Williams-Young, F. Ding, F. Lipparini, F. Egidi, J. Goings, B. Peng, A. Petrone, T. Henderson, D. Ranasinghe, V. G. Zakrzewski, J. Gao, N. Rega, G. Zheng, W. Liang, M. Hada, M. Ehara, K. Toyota, R. Fukuda, J. Hasegawa, M. Ishida, T. Nakajima, Y. Honda, O. Kitao, H. Nakai, T. Vreven, K. Throssell, J. A. Montgomery, Jr, J. E. Peralta, F. Ogliaro, M. Bearpark, J. J. Heyd, E. Brothers, K. N. Kudin, V. N. Staroverov, T. Keith, R. Kobayashi, J. Normand, K. Raghavachari, A. Rendell, J. C. Burant, S. S. Iyengar, J. Tomasi, M. Cossi, J. M. Millam, M. Klene, C. Adamo, R. Cammi, J. W. Ochterski, R. L. Martin, K. Morokuma, O. Farkas, J. B. Foresman and D. J. Fox, Gaussian 16 (Revision A.03), Gaussian Inc., Wallingford CT, 2016.

18 C. Adamo and V. Barone, *J. Chem. Phys.*, 1999, **110**, 6158.

19 F. Weigend and R. Ahlrichs, *Phys. Chem. Chem. Phys.*, 2005, **7**, 3297.

20 S. B. Boys and F. Bernardi, *Mol. Phys.*, 1970, **19**, 553.

21 S. Grimme, J. Antony, S. Ehrlich and H. Krieg, *J. Chem. Phys.*, 2010, **132**, 154104.

22 (a) P. Manna, S. K. Seth, M. Mitra, S. Ray Choudhury, A. Bauzá, A. Frontera and S. Mukhopadhyay, *Cryst. Growth Des.*, 2014, **14**, 5812; (b) M. Mirzaei, H. Eshtiagh-Hosseini, Z. Bolouri, Z. Rahmati, A. Esmaeilzadeh, A. Bauza, P. Ballester, M. Barceló-Oliver, J. T. Mague, B. Notash and A. Frontera, *Cryst. Growth Des.*, 2015, **15**, 1351.

23 (a) R. F. W. Bader, *J. Phys. Chem.*, 1998, **102**, 7314; (b) J. Contreras-Garcia, E. Johnson, S. Keinan, R. Chaudret, J.-P. Piquemal, D. Beratan and W. Yang, *J. Chem. Theor. Comp.*, 2011, **7**, 625.

24 T. A. Keith, AIMAll (Version 19.02.13), TK Gristmill Software, Overland Park KS, USA, 2019 (aim.tkgristmill.com).

25 A. E. Reed, L. A. Curtiss and F. Weinhold, *Chem. Rev.*, 1988, **88**, 899.

26 K. Diamond, *Crystal Impact GbR*, Germany, Bonn, 2007

27 M. N. Burnett and C. K. Johnson, *ORTEP-3: Oak Ridge Thermal Ellipsoid Plot Program for Crystal Structure Illustrations*, Report ORNL-6895, Oak Ridge National Laboratory, Oak Ridge, TN, USA, 1996.

28 Persistence of vision (TM) Raytracer, *Persistence of vision Pty. Ltd.*, Williamstown, Victoria, Australia, 2004.

29 C. F. Macrae, I. J. Bruno, J. A. Chisholm, P. R. Edgington, P. McCabe, E. Pidcock, L. R. Monge, R. Taylor, J. van de Streek and P. A. Wood, *J. Appl. Crystallogr.*, 2008, **41**, 466.

30 L. J. Farrugia, *J. Appl. Cryst.*, 1999, **32,** 837.

Section: I.C

Summary of research work

The thesis contains a total of nine chapters of which *Chapter I* deals with an overview on the coordination chemistry of manganese(III) and zinc(II) complexes with several Schiff base and reduced Schiff base ligands. The instrumental details are also included in this chapter. The whole research work has been gathered in *Chapters II-VI* of the thesis and finally the interesting observations are highlighted in *Chapter VII*. Summary of the research work is presented in this section.

Total six Schiff base ligands and two reduced Schiff base ligands have been used to synthesize a number of mono, di and trinuclear complexes of manganese(III) and zinc(II). **Scheme I.C.1** represents the tentative approach for the formation of reduced Schiff base derivatives from Schiff base ligands. IUPAC names and schematic representations of all eight ligands are gathered in **Scheme I.C.2.**

Synthesis of Schiff base and reduced Schiff base ligand

i) H_2L^1[N,N'-bis(3-methoxysalicylidene)1,2-ethanediamine]

The Schiff base ligand, H_2L^1, was synthesized by refluxing ethane-1,2-diamine (0.10 mL, ~1 mmol) with 3-methoxysalicylaldehyde (0.304 g, ~2 mmol) in methanol (20 mL) for ca. 1 h. The ligand was not purified and used directly for the synthesis of complex **1**.

ii) H_2L^2 [N,N'-bis(3-methoxysalicylidene)1,2-diamino-1-propene]

Another tetradentate, N_2O_2 donor Schiff base, H_2L^2, was synthesized following the similar method as that for H_2L^1 except propane-1,2-diamine (0.10 mL, ~1 mmol) was used

instead of ethane-1,2-diamine. The ligand was not purified and used directly for the synthesis of complex **2**.
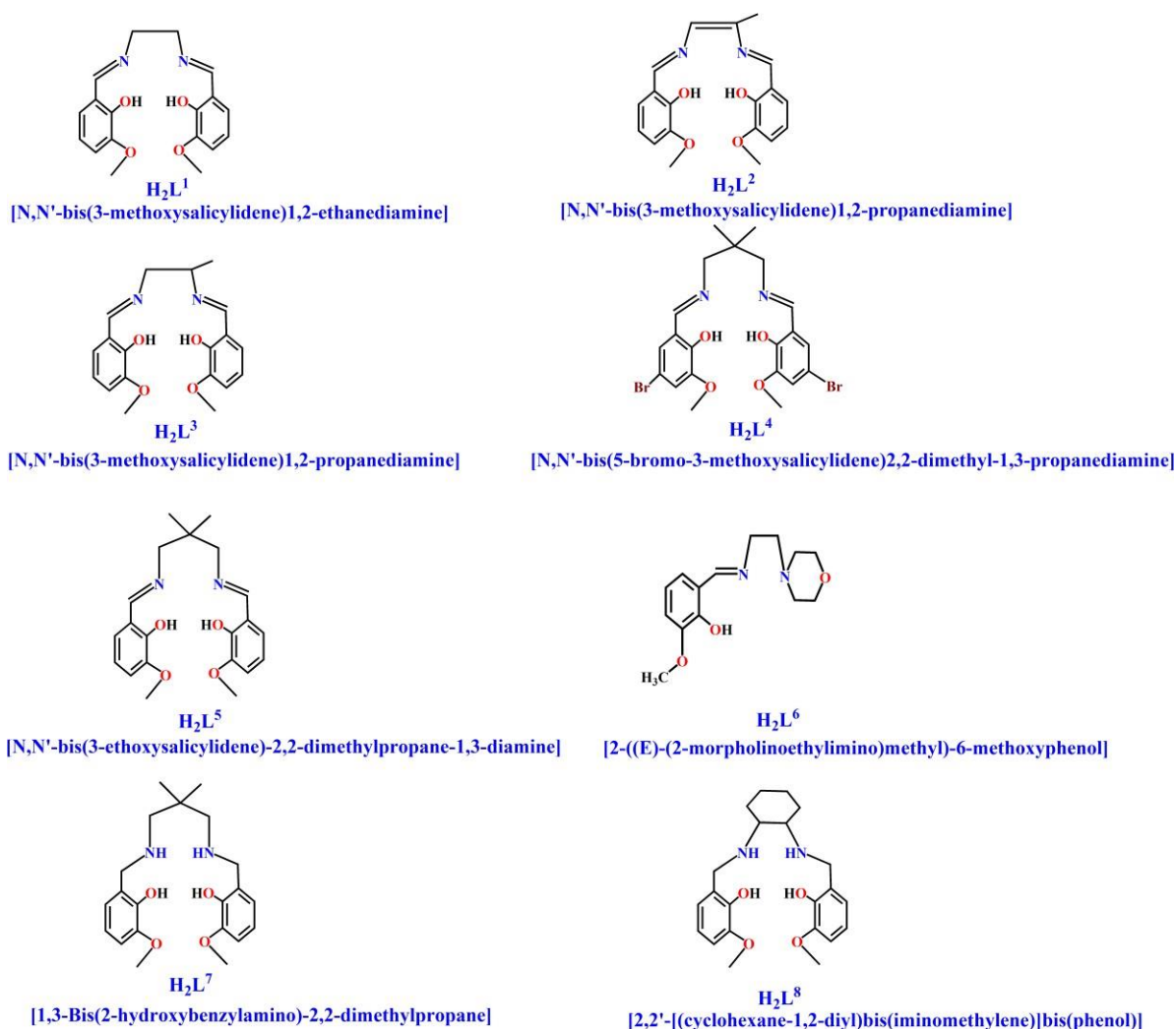
Scheme I.C.2: Schematic representations and IUPAC names of all the reduced Schiff base ligands used in the entire work.

iii) H_2L^3 [N,N'-bis(3-methoxysalicylidene)-1,2-propanediamine]

A methanol solution of propane-1,2-diamine (0.12 mL, ~1 mmol) and 3-methoxysalicylaldehyde (0.304 g, ~2 mmol) was refluxed for ca. 1 h to prepare the tetradentate Schiff base ligand H_2L^3. The ligand was not purified and methanol solution used directly for the synthesis of complex **3**.

iv) H_2L^4 [N,N'-bis(5-bromo-3-methoxysalicylidene)2,2-dimethyl-1,3-propanediamine]

The potentially tetradentate Schiff base ligand, H_2L^4, was prepared by facile condensation between 2,2-dimethylpropane-1,3-diammine and 5-bromo-2-hydroxy-3-methoxybenzaldehyde in 1:2 molar ratio in methanol following the similar method as that for H_2L^1 [29-31]. The ligand was not isolated and was directly used for synthesis of the complex **4**.

v) H_2L^5 [N,N'-bis(3-ethoxysalicylidene)-2,2-dimethylpropane-1,3-diamine]

A methanol solution (10 mL) of 3-ethoxysalicylaldehyde (332 mg, 2 mmol) and 2,2-dimethyl-1,3-diaminopropane (0.13 mL, 1 mmol) was refluxed for ca. 1 h to prepare a compartmental Schiff base ligand, H_2L^5. The ligand was not isolated but used directly for the synthesis of the complex **5**.

vi) HL^6 [2-((E)-(2-morpholinoethylimino)methyl)-6-methoxyphenol]

A clear yellow solution of Schiff base ligand, HL, was synthesized by refluxing 4-(2-aminoethyl)morpholine (0.13 mL, ~1 mmol) with 3-methoxysalicylaldehyde (0.152 g, ~1 mmol) in methanol (20 mL) for ca. 1 h. It was not isolated and used directly for the preparation of the complex **6**.

vii) H_2L^7 [1,3-Bis(2-hydroxybenzylamino)-2,2-dimethylpropane]

A Schiff base ligand, H_2L^a {H_2L^a= N,N'-bis(salicylidene)-2,2-dimethylpropane-1,3-diamine}, was synthesized by refluxing 2,2-dimethylpropane-1,3-diamine (1 mmol, 0.1 mL) with salicylaldehyde (2mmol, 0.2 mL) in methanol (20 mL) solution for ca. 2 h. The Schiff base ligand was not purified but used directly for the preparation of the reduced Schiff base ligand (H_2L^7). After that, the solution (10 mL) was cooled to 0°C and solid sodium borohydride (4 mmol, ~150 mg) was added to it with constant stirring. Then the resulting

solution was acidified with glacial acetic acid (2 mL) and stirred for 10 minutes. The methanol was evaporated to dryness under reduced pressure in a rotary evaporator (~60°C). The white residue was then dissolved in water (15 mL) and extracted with a mixture of dichloromethane (15 mL) and a saturated solution of sodium bicarbonate. The organic phase was dried over anhydrous sodium acetate and the solvent (i.e. dichloromethane) was evaporated under reduced pressure using a rotary evaporator to get the white color reduced Schiff base ligand (H_2L^7). The ligand was not purified and used directly for the synthesis of complexes **7**, **8**, **10**.

viii) H_2L^8 [2,2'-[(cyclohexane-1,2-diyl)bis(iminomethylene)]bis[phenol]]

A potential tetradentate, N_2O_2 donor Schiff base, H_2L^b { H_2L^b= N,N'-bis(salicylidene)-cyclohexane-1,2-diamine}, was synthesized following the similar method as that for H_2L^a except cyclohexane-1,2-diamine (mixture of *cis* and *trans*) (1 mmol, 0.1 mL) was used instead of 2,2-dimethylpropane-1,3-diamine. It was then reduced to prepare the desired reduced Schiff base ligand, H_2L^8. The ligand was not purified and used directly for the synthesis of complex **9**.

Chapter II

Section II.A

Three manganese(III) complexes, [Mn(L^1)(N$_3$)(H$_2$O)]·CH$_3$OH·H$_2$O (**1**), [Mn(L^2)(N$_3$)(H$_2$O)] (**2**) and [Mn(L^3)(H$_2$O)$_2$]ClO$_4$ (**3**) {where H_2L^1 = N,N'-bis(3-methoxysalicylidene)1,2-ethanediamine, H_2L^2 = N,N'-bis(3-methoxysalicylidene)1,2-diamino-1-propene and H_2L^3 = N,N'-bis(3-methoxysalicylidene)1,2-propanediamine}, have been synthesized and characterized by X-ray crystallography. Weak noncovalent interactions generate extended supra-molecular assemblies in all three complexes. Catalase mimicking

activities (catalytic decomposition of hydrogen peroxide into oxygen and water) of the complexes have been investigated. Complex **3** catalyzes the decomposition of hydrogen peroxide most effectively. The higher catalase mimicking efficiency of complex **3** has been related to its structure.

Section II.B

A mononuclear manganese(III) complex, [Mn*L*⁴(CH₃OH)(H₂O)]ClO₄, has been synthesized and structurally characterized {*H₂L*⁴ = N,N'-bis(5-bromo-3-methoxysalicylidene)2,2-dimethyl-1,3-propanediamine}. The energetic features of significant supramolecular interactions present in the complex, i.e. Br⋯Br, hydrogen bonding and π⋯π stacking interactions, have been calculated using DFT calculations and further corroborated with NCI plot index computational tool. Catalase mimicking activities (catalytic decomposition of hydrogen peroxide into oxygen and water) of the complex have been investigated. The complex catalyzes the decomposition of hydrogen peroxide effectively in solution. The efficiency of the complex towards catalytic decomposition of hydrogen peroxide has been related to its structure.

Chapter III

A hetero-trimetallic cadmium(II)/zinc(II) complex, [Cd{*L*⁵Zn(NCS)}₂] with a compartmental Schiff base ligand, N,N'-bis(3-ethoxysalicylidene)-2,2-dimethylpropane-1,3-diamine (*H₂L*⁵) has been synthesized and characterized by spectral and elemental analyses. Cadmium(II) is octa-coordinated and it shows trigonal dodecahedral geometry. The complex behaves as a sensor for the detection of various nitroaromatics via turn-off fluorescence response.

Chapter IV

The synthesis and X-ray characterization of a new dinuclear zinc(II) complex, $[(DMSO)_2ZnL^6(\mu_{1,1}\text{-}N_3)Zn(N_3)_2]$ using a tetradentate N_2O_2 donor Schiff base 2-((E)-(2-morpholinoethylimino)methyl)-6-methoxyphenol and azide as anionic co-ligand has been reported herein. This complex forms self-assembled dimers in the solid state governed by ζ-hole tetrel bonding interactions (C···N) involving the Zn-coordinated methoxy group. The interaction has been analysed energetically using DFT calculations and several computational tools (MEP surfaces, QTAIM and NCI plot analyses). Moreover, the interaction has been differentiated from a trifurcated CH_3···N H-bonding interaction using the NBO analysis and the inspection of the donor-acceptor orbital interactions.

Chapter V

Section V.A

Two zinc(II) complexes, $[Zn(H_2L^7)(OCOCH_3)(N_3)]$ and $[Zn(H_2L^7)(OCOCH_3)(NCS)]$, with a potential tetradentate reduced Schiff base ligand, 1,3-bis(2-hydroxybenzylamino)-2,2-dimethylpropane (H_2L^7) have been synthesized and characterized by X-ray crystallographic studies. In each complex, the ligand behaves as a bidentate ligand keeping the phenoxo arms pendant. The ability of the ligand to sense zinc(II) selectively has been assessed. Fluorescence titrations have also been done for the ligand and binding constant for ligand has been evaluated by Benesi−Hilderbrand equation. The electronic structures for the ground state and 1st excited state of both complexes were calculated. Based on optimized ground state geometry, the TDDFT/B3LYP method combined with SMD solvation model in methanol media was used to calculate the absorption properties of the investigated complexes. Investigation on the electronic structure of the excited states was also performed employing NTO representation. The calculation indicates that the fluorophore is originated

from the charge transfer from N_3/NCS to reduced Schiff base. On the other hand, Bader''s Quantum Theory of Atoms-in-Molecules (QTAIM) was used to obtain insight into the physical nature of weak non-covalent interactions in both complexes. Additionally, the Noncovalent Interactions Reduced Density Gradient (NCI-RDG) methods established nicely the presence of such noncovalent intermolecular interactions.
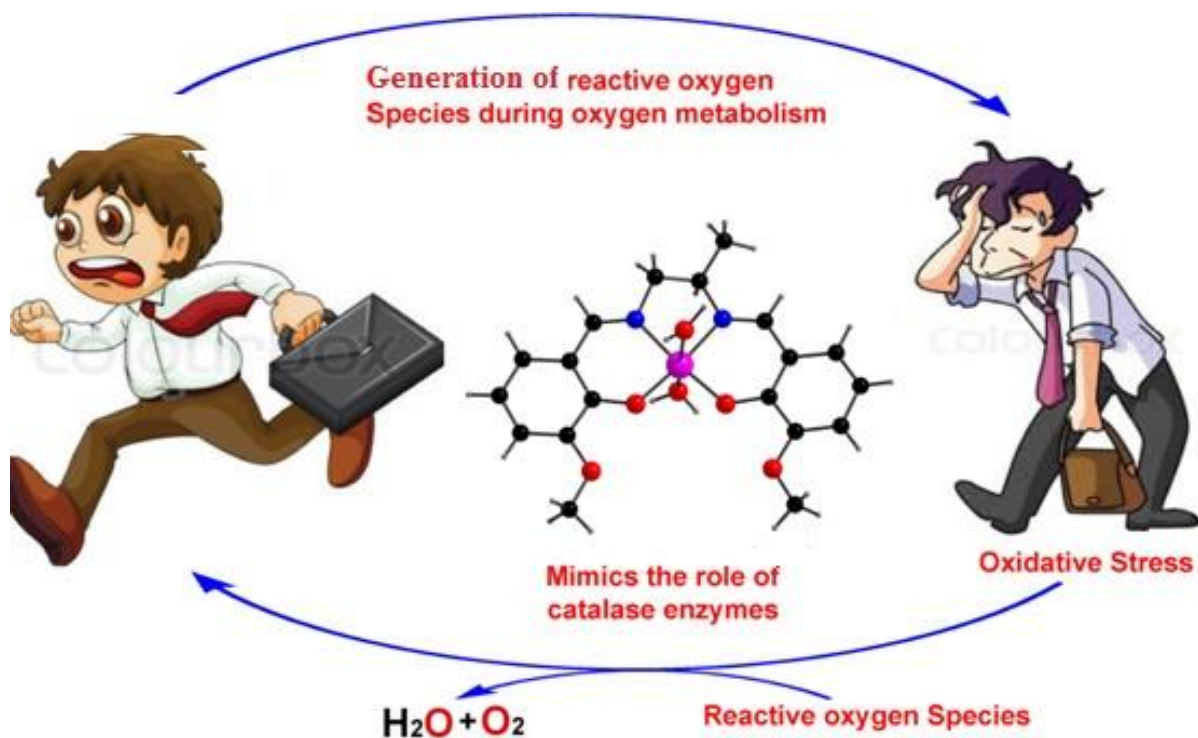
Section V.B

A zinc(II) complex, [Zn(H_2L^8)(OCOCH$_3$)$_2$] with a N_2O_2 donor reduced Schiff base ligand, 2,2'-[(cyclohexane-1,2-diyl)bis(iminomethylene)]bis[phenol] has been synthesized and its fluorescence property is explored. The hydrogen bonding environment in its solid state structure is well supported qualitatively and quantitatively with the help of Reduced Density Gradient (RDG) based NCI (non-covalent interactions) index calculation and AIM analyses. Also, the physical nature of other weak non-covalent interactions in the complex is examined. The absorption and emission properties of the complex are explained using density functional theory (DFT) calculations. Analysis of the natural transition orbitals (NTO) shows that the excited state can be mainly characterized by an intra-ligand charge transfer (ILCT) transition within a diamine from the highest-occupied NTO (hole) to the lowest-unoccupied NTO (electron).

Section V.C

A unique trinuclear centrosymmetric zinc(II) complex, [Zn$_3L^7{}_2$(CH$_3$CO$_2$)$_2$(DMSO)$_2$] has been synthesized and characterized by using a reduced schiff base ligand H_2L^7 {H_2L^7 = 1,3-bis(2-hydroxybenzylamino)2,2-dimethylpropane}. The complex has been characterized by spectral and elemental analysis. Single crystal X-ray diffraction analysis has confirmed the structure of the complex. The complex has showed strong fluorescence, which may be quenched in presence of different nitroaromatic substances. The complex thus used as a sensor for the detection of nitroaromatics in DMF via turn-off fluorescence response.

Chapter II

Synthesis, characterization of manganese(III) complexes with N_2O_2 donor tetradentate schiff base ligands: exploration of their catalase mimicking activity

Generation of reactive oxygen Species during oxygen metabolism

Mimics the role of catalase enzymes

Oxidative Stress

$H_2O + O_2$

Reactive oxygen Species

Section: II.A

Synthesis and structural characterization of three manganese(III) complexes with N_2O_2 donor tetradentate schiff base ligands: exploration of their catalase mimicking activity

II.A.1. Introduction

Manganese(III) complexes have attracted a lot of attention because of their interesting magnetic properties (with four unpaired electrons in high spin and two unpaired electrons in low spin complexes) and structural diversities.[1-5] SOD (superoxide dismutase) and catalase are two important enzymes that help to defend the cell structure against various reactive oxygen species, e.g. hydrogen peroxide, hydrogen superoxide etc[6-9] (capable of damaging different cellular components), produced naturally during oxygen metabolism.[10-12] If not destructed, these reactive oxygen species can cause oxidative stress leading to a number of human diseases.[13-15] SOD destroys hydrogen superoxide reducing it into hydrogen peroxide.[16,17] Catalase is responsible for the catalytic decomposition of hydrogen peroxide by means of its disproportionation reaction into nontoxic dioxygen and water.[18-20] Many manganese(III) complexes have also been used to mimic several enzymes, e. g. superoxide dismutase, catalase etc.[6-9] Signorella *et al.* reported a manganese(III) complex that can exhibit both superoxide dismutase and catalase-like activity.[21] Two manganese(II) complexes were also synthesised by the same group and both of these complexes show superoxide dismutase and catalase-like activity.[22] Britovsek *et al.* synthesized a bio-inspired manganese(II) complex with a linear pentadentate ligand framework containing soft sulfur donors and an

alternating NSNSN binding motif which can display excellent dual catalase/SOD-like antioxidant activity.[23] Párkányi *et al.* have reported a manganese(II) complex exhibiting similar type activity.[24] Synthesis, structural characterization and catalase-like activity of a number of manganese(II) complexes were reported by Devereux *et al.*[25] A novel single site manganese(II) complex was successfully synthesized and tested in the aqueous disproportionation of hydrogen peroxide by Barszcz *et al.*[26] Li *et al.* synthesized two new manganese(II) complexes which can decompose hydrogen peroxide catalytically, and possess the combined functions of SOD and catalase in basic or weakly basic solutions.[27]

With the specific aim to mimic catalase enzyme, we have synthesized and characterized three octahedral manganese complexes, each having [MnLXY] core, where H_2L is tetradentate Schiff base ligand occupying the equatorial positions; X and Y are monodentate ligands occupying the axial positions, as expected from considering the structures of similar Mn(III) complexes.[9,28] These monodentate ligands could be substituted by hydrogen peroxide to initiate catalase activity of the complexes (Manganese(III) is d^4 and labile). This special characteristic feature makes them good catalysts towards decomposition of hydrogen peroxide into dioxygen and water.

II.A.2. Experimental Section

II.A.2.1. Synthesis

II.A.2.1.1. Synthesis of *[Mn(L¹)(N₃)(H₂O)]·CH₃OH·H₂O (1) [H₂L¹ = N,N'-bis(3-methoxysalicylidene)-1,2-ethanediamine]*

The Schiff base ligand, H_2L^1, was synthesized by refluxing ethane-1,2-diamine (0.10 mL, ~1 mmol) with 3-methoxysalicylaldehyde (0.304 g, ~2 mmol) in methanol (20 mL) for ca. 1 h. The ligand was not isolated and a methanol solution (10 mL) of manganese(II)

perchlorate hexahydrate (370 mg, ~1 mmol) was then directly added to the methanolic solution of ligand under stirring condition. An aqueous methanol solution of sodium azide (0.065 g, ~1 mmol) was then added to it and stirring was continued for further ca. 2 h. The resulting solution was then filtered and kept for slow evaporation in open atmosphere. Dark brown coloured block shape single crystals, suitable for X-ray diffraction, were obtained after few days which were collected through filtration and then dried in aerobic condition.

Yield: 372 mg (~76 %); based on manganese(III). Anal. Calc. for $C_{19}H_{24}MnN_5O_7$ (FW = 489.37): C, 46.63; H, 4.94; N, 14.31 %. Found: C, 46.3; H, 5.0; N, 14.6 %. FT-IR (KBr, cm^{-1}): 1599, 1616, ($\upsilon_{C=N}$); 2035 (υ_{N_3}); 2833-2970 (υ_{C-H}); 3420 (υ_{O-H}). UV-Vis, λ_{max} (nm), [ε_{max} (L mol^{-1} cm^{-1})] (DMF), 272 (3.73 x 10^4), 327 (1.73 x 10^4), 426 (1.11 x 10^3), 501(3.75 x 10^2). Magnetic moment = 4.96 µB.

II.A.2.1.2. Synthesis of *[Mn(L²)(N₃)(H₂O)] (2) [H₂L² = N,N'-bis(3-methoxysalicylidene)-1,2-diamino-1-propene]*

In the preparation of complex **2**, propane-1,2-diamine (0.12 mL, ~1 mmol) was used instead of ethane-1,2-diamine. All other reagents were identical to that used in the preparation of complex **1**. Diffraction quality single crystals were obtained after a few days on slow evaporation of dark brown methanol solution of the complex in open atmosphere.

Yield: 326 mg (~72 %); based on manganese(III). Anal. Calc. for $C_{19}H_{20}MnN_5O_5$ (FW = 453.34): C, 50.34; H, 4.45; N, 15.45 %. Found: C, 50.5; H, 4.3; N, 15.6 %. FT-IR (KBr, cm^{-1}): 1600, 1619 ($\upsilon_{C=N}$); 2828-2955 (υ_{C-H}); 3435 (υ_{O-H}). UV-Vis, λ_{max} (nm), [ε_{max} (L mol^{-1} cm^{-1})] (DMF), 272 (3.98 × 10^4), 328 (5.26 × 10^3), 428 (1.94 × 10^3), 508 (4.88 x 10^2). Magnetic moment = 4.98µB.

II.A.2.1.3. Synthesis of [Mn(L³)(H₂O)₂]ClO₄ (3) [H₂L³ = N,N'-bis(3-methoxysalicylidene)-1,2-propanediamine]

A methanol solution of propane-1,2-diamine (0.12 mL, ~1 mmol) and 3-methoxysalicylaldehyde (0.304 g, ~2 mmol) was refluxed for ca. 1 h to prepare the tetradentate Schiff base ligand H_2L^3. A methanol (10 ml) solution of manganese(II) perchlorate hexahydrate (370 mg, ~1 mmol) was directly added into the methanol solution of the ligand H_2L^3 with constant stirring. The stirring was continued for an additional ca. 2 h to get a dark brown resulting solution. Deep brown blocked shaped single crystals of the complex, suitable for X-ray diffraction, were obtained after a few days by slow evaporation of resulting solution in open atmosphere.

Yield: 394 mg (~74 %); based on manganese(III). Anal. Calc. for $C_{19}H_{24}MnN_2O_{10}Cl$ (FW = 530.79): C, 42.99; H, 4.56; N, 5.28 %. Found: C, 42.8; H, 4.4; N, 5.4 %. FT-IR (KBr, cm^{-1}): 1601, 1616 ($\upsilon_{C=N}$); 2840-2965 (υ_{C-H}); 3430 (υ_{O-H}). UV-Vis, λ_{max} (nm), [ε_{max} (L mol^{-1} cm^{-1})] (DMF), 270 (3.68 × 10^4), 329 (4.04 × 10^3), 422 (1.71 × 10^3), 500 (2.81 x 10^2). Magnetic moment = 5.02μB

Table II.A.1: Crystal data and refinement details of complexes **1**, **2** and **3**.

Complex	**1**	**2**	**3**
Formula	$C_{19}H_{24}MnN_5O_7$	$C_{19}H_{20}MnN_5O_5$	$C_{19}H_{24}ClMnN_2O_{10}$
Formula Weight	489.37	453.34	530.79
Crystal System	Monoclinic	Monoclinic	Monoclinic
Space group	$P2_1/c$	$P2_1/c$	$P2_1/c$
a(Å)	11.7968(15)	13.281(5)	13.3432(13)
b(Å)	14.2327(18)	12.199(4)	13.3425(14)
c(Å)	13.9210(19)	14.327(5)	14.3907(15)
β(°)	113.999(4)	115.956(7)	117.519(3)
V(Å³)	2135.3(5)	2087.1(13)	2272.1(4)

Z	4	4	4
$d_{(calc)}$ [g/cm^3]	1.472	1.443	1.552
μ [mm^{-1}]	0.664	0.673	0.756
F(000)	984	936	1096
Total Reflections	12482	18726	14472
Unique Reflections	4007	3932	4098
Observed data [I > 2 ζ(I)]	3019	1771	3575
No. of parameters	290	273	318
R(int)	0.074	0.098	0.029
R1, wR2 (all data)	0.1164, 0.2984	0.1921, 0.2739	0.1042, 0.2474
R1, wR2 ([I > 2 ζ(I)]	0.0907, 0.2802	0.0928, 0.2091	0.0955, 0.2358

CCDC reference no 1871955-1871957 for complexes **1**, **2** and **3**, respectively.

II.A.3. Results and discussion

II.A.3.1. Synthesis

Schiff base ligands, H_2L^1 and H_2L^3, were synthesized by the 1:1 condensation of 3-methoxysalicyldehyde with ethane-1,2-diamine and propane-1,2-diamine respectively in methanol following the literature method[29,30] On the other hand, H_2L^2 was formed through oxidation of ligand, H_2L^3 in reaction environment. The ligands were not isolated and were used directly for the preparation of manganese(III) complexes.

Addition of the methanol solution of manganese(II) perchlorate hexahydrate in the methanol solution of the Schiff base, H_2L^1 followed by the addition of sodium azide produced a dark brown coloured complex, *[Mn(L^1)(N$_3$)(H$_2$O)]·CH$_3$OH·H$_2$O (**1**)*. Similarly, reaction of the methanol solution of manganese(II) perchlorate hexahydrate with methanol solution of Schiff base, H_2L^3, followed by the addition of sodium azide produced another dark brown coloured complex *[Mn(L^2)(N$_3$)(H$_2$O)] (**2**)*. It is very interesting to note that during the reaction 1,2-diaminopropane moiety of H$_2$L^3 is oxidized to 1,2-diamino-1-propene (1,2-pn) in

reaction environment and due to this oxidative dehydrogenation a new Schiff base ligand, H_2L^2 is formed. Oxidative dehydrogenation of diamine ligands coordinated to several transition metals is reported in the literature.[31,32] On the other hand, a methanol solution of manganese(II) perchlorate hexahydrate was made to react with methanolic solution of Schiff base, H_2L^3 under stirring condition to prepare mononuclear complex, *[Mn(L³)(H₂O)₂]ClO₄ (3)*. Synthetic route to all three complexes are shown in Scheme **II.A.1**. Manganese(II) was converted into manganese(III) by aerial oxidation, as was observed in many previous cases.[9,28]
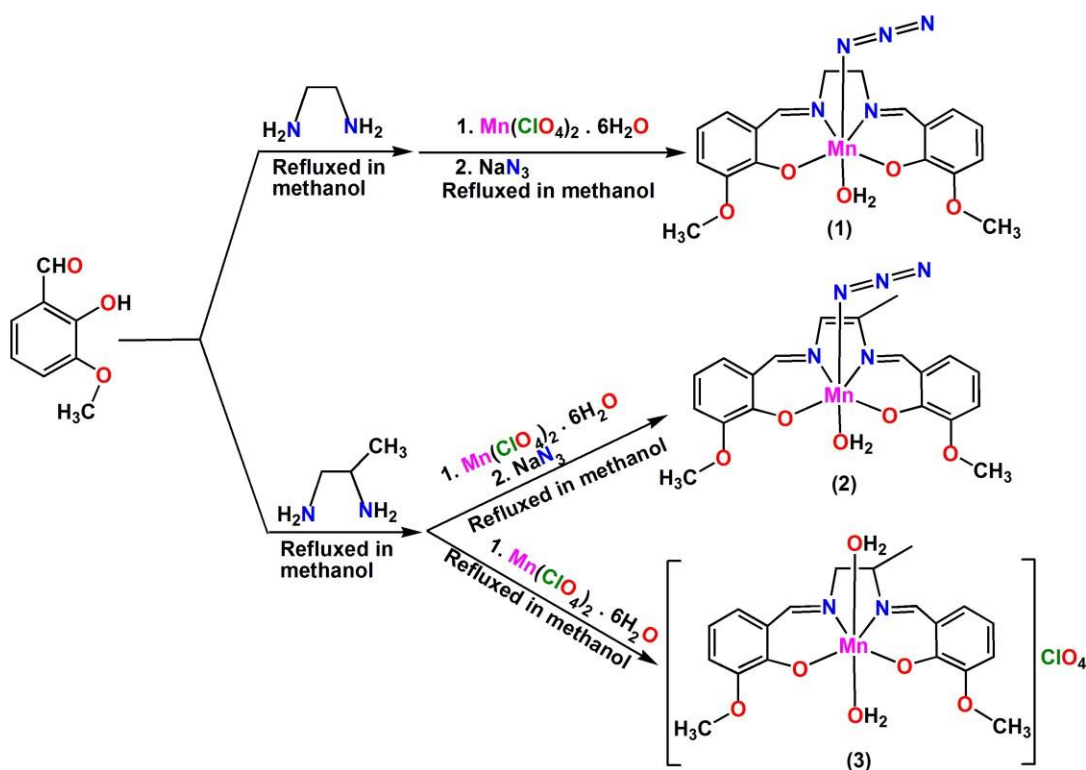
Scheme II.A.1: Synthetic route to the complexes.

II.A.3.2. Description of the structures

II.A.3.2.1. [Mn(L¹)(N₃)(H₂O)]·CH₃OH·H₂O (1)

The structure determination reveals that complex **1** consists of a discrete mononuclear unit *[Mn(L¹)(N₃)(H₂O)]*. A lattice methanol and water molecules are also present in the

asymmetric unit. Perspective view of the complex is given in Fig. **II.A.1**. A lattice water molecule was present which is squeezed in order to minimize the void space in the crystal structure. It crystallizes in monoclinic space group $P2_1/c$. The manganese(III) centre, Mn(1), has a six-coordinate pseudo-octahedral geometry in which two imine nitrogen atoms [N(1) and N(2)] and two phenoxo oxygen atoms [O(1) and O(2)] of the deprotonated di-Schiff base ligand $\{(L^1)^{2-}\}$ constitute the equatorial plane. The remaining two coordination sites of manganese(III) centre is occupied by one azide nitrogen atom [N(3)] and one water oxygen atom [O(5)] to constitute its axial plane. The axial Mn–O(5) and Mn–N(3) distances [2.367(6) and 2.244(6) Å, respectively] are much longer than the basal Mn–O(1), Mn–O(2), Mn–N(1) and Mn–N(2) distances [1.873(5), 1.873(5), 1.980(7) and 1.979(7) Å, respectively] (see Table **1**), which fall within the range observed for structurally characterized manganese(III) complexes.[33-40] The elongation of axial bonds indicates clear evidence of Jahn–Teller distortion, as expected for high-spin manganese(III) complexes.[28] The distortion from the perfect octahedral geometry can be easily observed from its coordinate bond angles, which deviate from the ideal values of 90° (for cis angles) or 180° (for trans angles). Mn(III)-N_{imine} and Mn(III)-$O_{phenoxo}$ bond lengths in the complex are comparable to previously reported similar type manganese(III)-Schiff base complexes.[33-40] The saturated five membered chelate ring, Cg(1) [Mn(1)–N(1)–C(9)–C(10)–N(2)] in this complex shows half chair conformation with puckering parameters[41] Q = 0.319(10) Å and ϕ = 91.2(11)°. The terminal azide is quasi-linear with the N-N-N angle being 178.6(10)°, as observed in similar complexes.[42,43]
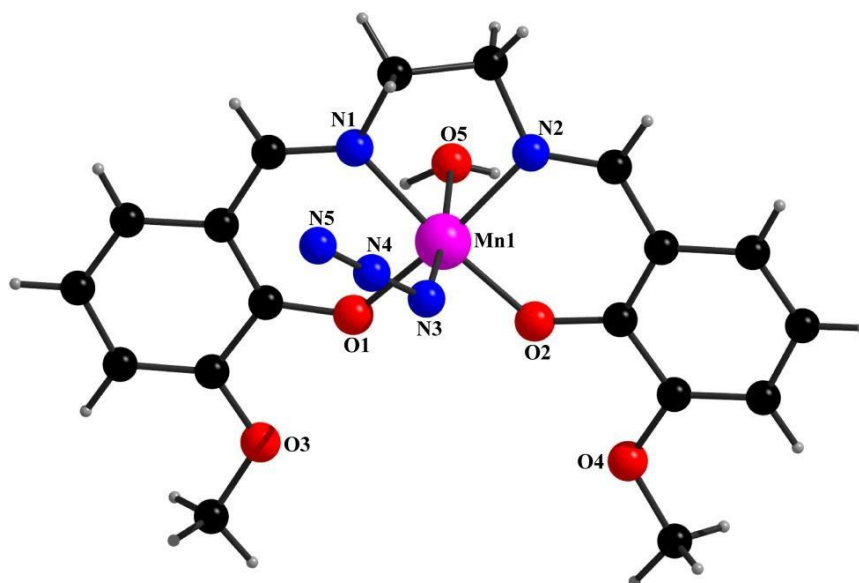
Fig. II.A.1: Perspective view of complex **1** with selective atom numbering scheme. Lattice methanol molecule has been omitted for clarity.

II.A.3.2.2. [Mn(L²)(N₃)(H₂O)] (2)

The X-ray crystal structure determination reveals that complex **2** crystallizes in the monoclinic space group, $P2_1/c$. Perspective view of the complex along with selective atom-numbering scheme is shown in Fig. **II.A.2**. The manganese(III) center is in a six-coordinate distorted octahedral environment, being bonded to two imine nitrogen atoms, N(1) and N(2), and two phenoxo oxygen atoms, O(1) and O(2), of a deprotonated Schiff base ligand, $(L^2)^-$. The remaining two axial coordination sites of manganese(III) centre is occupied by one azide nitrogen atom, N(3) and one water oxygen atom, O(5) to complete its octahedral geometry. The coordination geometry around the metal centre is highly distorted from ideal octahedral geometry as suggested by the coordinate bond angles. The axial Mn–O(5) and Mn–N(3) bond lengths are much longer than the equatorial Mn–O(1), Mn–O(2), Mn–N(1) and Mn–N(2) bond lengths (Table **II.A.2**), which clearly indicates Jahn–Teller distortion, as expected for high-spin manganese(III) complexes.[28] The terminal azide is quasi-linear as observed in previously reported similar type complexes with the N-N-N angle being 178.2(13)°.[42,43]

The most exciting observation is the oxidation of Schiff base ligand during the reaction procedure. The 1,2-diaminopropane moiety is oxidized to 1,2-diamino-1-propene (1,2-pn) via oxidative dehydrogenation reaction, which is probably catalyzed by manganese(III). The metal coordinated amine (or diamine) is oxidized by aerial oxygen to form α-imine (or α-di-imine).[32] In our case, 1,2-diaminopropane moiety of the Schiff base ligand, coordinated to manganese(III) is oxidized by aerial oxygen to an α-imine. The methyl group probably restricts the formation of an α-di-imine. This α-imine may easily then be rearranged to form the 1,2-diamino-1-propene. The C-C bond lengths of complexes **1**, **2** and **3** (oxidized part of salen-type ligands) are 1.484(13), 1.30(2) and 1.381(19), respectively. In case of complex **2**, much shorter C-C bond length confirms oxidation of Schiff base ligand.
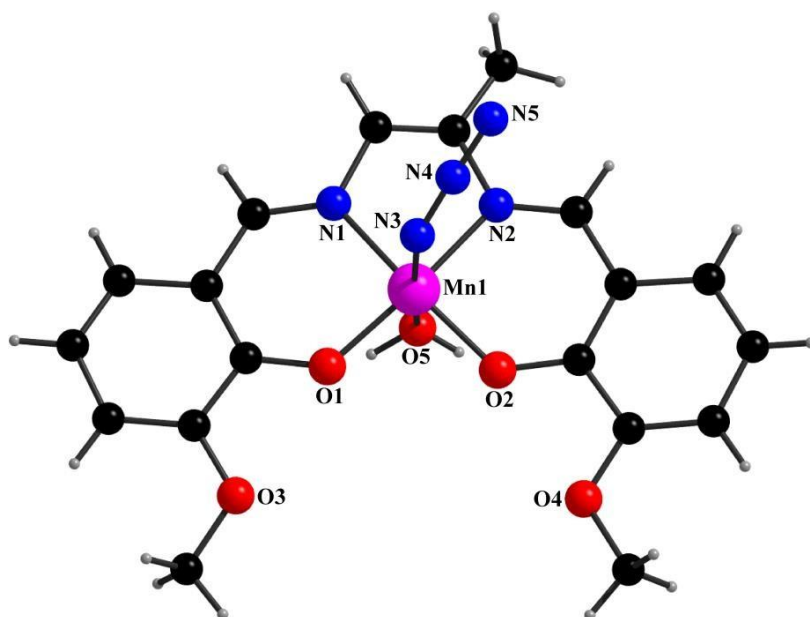

Fig. II.A.2: Perspective view of complex **2** with selective atom numbering scheme.

II.A.3.2.2. [Mn(L³)(H₂O)₂]ClO₄ (3)

Single crystal X-ray structure determination analysis reveals that the asymmetric unit of the complex consists of a mononuclear cation $[Mn(L^2)(H_2O)_2]^+$ together with a non-coordinating perchlorate anion. The complex crystallizes in the monoclinic space group

P2₁/c. A perspective view of the complex with selective atom-numbering scheme is shown in Fig. **II.A.3**. The central manganese(III) center, Mn(1), is in a six-coordinate octahedral environment, being bonded to two imines nitrogen atoms, N(1) and N(2) and two phenoxo oxygen atoms, O(1) and O(2), from a deprotonated Schiff base ligand (L^3)⁻. Other vacant sites are coordinated by two water oxygen atoms, O(5) and O(6), to complete its distorted octahedral geometry. The longer axial bonds compared to equatorial bonds (see Table **II.A.2**) are indicative of tetragonal elongations as a result of the Jahn–Teller distortion, expected for high-spin manganese(III) complexes with d^4 configuration.[9,28] The saturated five membered ring, [Mn(1)–N(1)–C(9)–C(10)–N(2)], has an half chair conformation, with puckering parameters $Q = 0.219(14)$ Å, $\phi = 100(2)°$.[41]
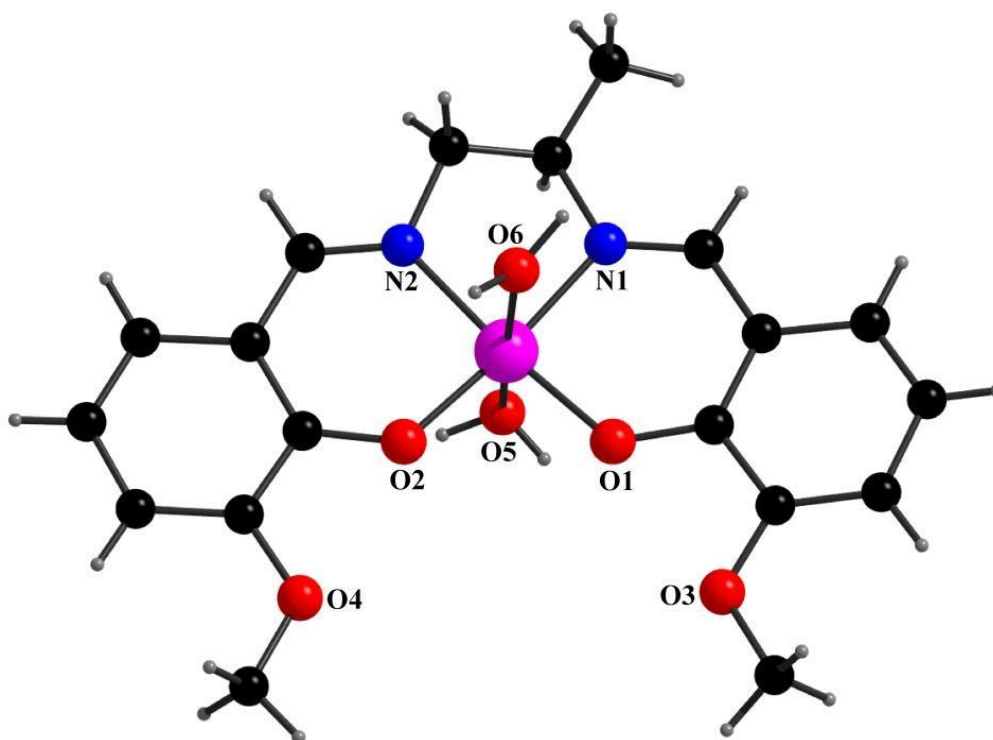

Fig. II.A.3: Perspective view of complex **3** with selective atom numbering scheme. Non-coordinated perchlorate anion has been omitted for clarity.

Table II.A.2: Selected Bond lengths (Å) of the complexes 1, 2 and **3.**

	1	2	3
Mn(1)-O(1)	1.873(5)	1.913(6)	1.867(6)
Mn(1)-O(2)	1.873(5)	1.895(6)	1.865(5)
Mn(1)-O(5)	2.367(6)	2.364(7)	2.221(5)
Mn(1)-O(6)	-	-	2.373(8)
Mn(1)-N(1)	1.980(7)	1.987(9)	1.968(7)
Mn(1)-N(2)	1.979(7)	2.004(9)	1.986(8)
Mn(1)-N(3)	2.244(6)	2.191(10)	-

Table II.A.3: Selected bond angles (°) of the complexes 1, 2 and **3.**

	1	2	3
O(1)-Mn(1)-O(2)	93.0(2)	92.2(2)	92.9(2)
O(1)-Mn(1)-O(5)	89.3(2)	88.2(3)	93.1(2)
O(1)-Mn(1)-O(6)	-	-	91.8(3)
O(1)-Mn(1)-N(1)	91.8(2)	92.5(3)	91.8(3)
O(1)-Mn(1)-N(2)	173.4(3)	171.1(3)	174.7(3)
O(1)-Mn(1)-N(3)	93.4(2)	95.3(3)	-
O(2)-Mn(1)-O(5)	92.9(2)	89.2(3)	91.4(2)
O(2)-Mn(1)-O(6)	-	-	90.8(3)
O(2)-Mn(1)-N(1)	174.6(3)	171.7(3)	175.0(3)
O(2)-Mn(1)-N(2)	91.6(3)	91.6(3)	92.2(3)

O(2)-Mn(1)-N(3)	94.2(2)	98.2(3)	-
O(5)-Mn(1)-N(1)	84.6(3)	84.1(3)	90.2(3)
O(5)-Mn(1)-N(2)	85.7(3)	83.7(3)	88.6(3)
O(5)-Mn(1)-N(3)	172.2(3)	171.7(4)	-
N(1)-Mn(1)-N(2)	83.4(3)	82.8(4)	83.1(3)
N(1)-Mn(1)-N(3)	88.0(3)	88.2(4)	-
N(2)-Mn(1)-N(3)	91.0(3)	92.3(4)	-
O(5)-Mn(1)-O(6)	-	-	174.5(3)
O(6)-Mn(1)-N(1)	-	-	87.2(4)
O(6)-Mn(1)-N(2)	-	-	86.3(3)

II.A.3.3. Supramolecular interactions

II.A.3.3.1 [Mn(L^1)(N$_3$)(H$_2$O)]·CH$_3$OH (1) and [Mn(L^2)(N$_3$)(H$_2$O)] (2)

Hydrogen atoms of coordinated water molecules in both complexes are involved in intermolecular hydrogen bonding interactions. The hydrogen atoms, H(5A) and H(5B), attached to water oxygen atom, O(5), participate in intermolecular hydrogen bonding interactions with the symmetry related phenoxo oxygen atoms, O(1)[a], O(2)[a] {for complex **1**} and O(1)[b], O(2)[b] {for complex **2**}, while at the same time they are hydrogen bonded with methoxy oxygen atoms O(3)[a], O(4)[a] {for complex **1**} and O(3)[b], O(4)[b] {for complex **2**}, {symmetry transformations [a] = 1-x,2-y,1-z and [b] = 1-x,1-y,1-z} of a neighbouring molecule. All donor-hydrogen···acceptor (Here, O-H···O) distances fall in the range of 2.81 to 3.10 Å, which indicate that both complexes exhibit strong hydrogen bonding interactions in solid state. In both complexes, supramolecular dimeric arrangements are formed due to this type of inter-molecular hydrogen bonding interactions. **Fig. II.A.4** illustrates the hydrogen bonded

dimeric arrangements of both complexes. Additionally in complex **1**, the hydrogen atom, H(6), attached to lattice methanolic oxygen atom, O(6), participate in hydrogen bonding interaction with the symmetry related azide nitrogen atom, N(5)[b] of a neighbouring molecule. All the hydrogen bonding interactions of complex **1** are shown in **Fig. II.A.5**. The geometric features of hydrogen bonding interactions are given in Table **II.A.4**.

A significant C-H⋯π interaction is present in complex **1**. The hydrogen atom, H(10B), attached to carbon atom, C(10), is involved in inter-molecular C-H⋯π interaction with symmetry related (x,3/2-y,1/2+z) phenyl ring, [C(2)–C(3)–C(4)–C(5)–C(6)–C(7)] of a neighbouring molecule, having a distance of 2.92 Å. Due to this C-H⋯π interaction a 1D supramolecular arrangement is formed (**Fig. II.A.6**).
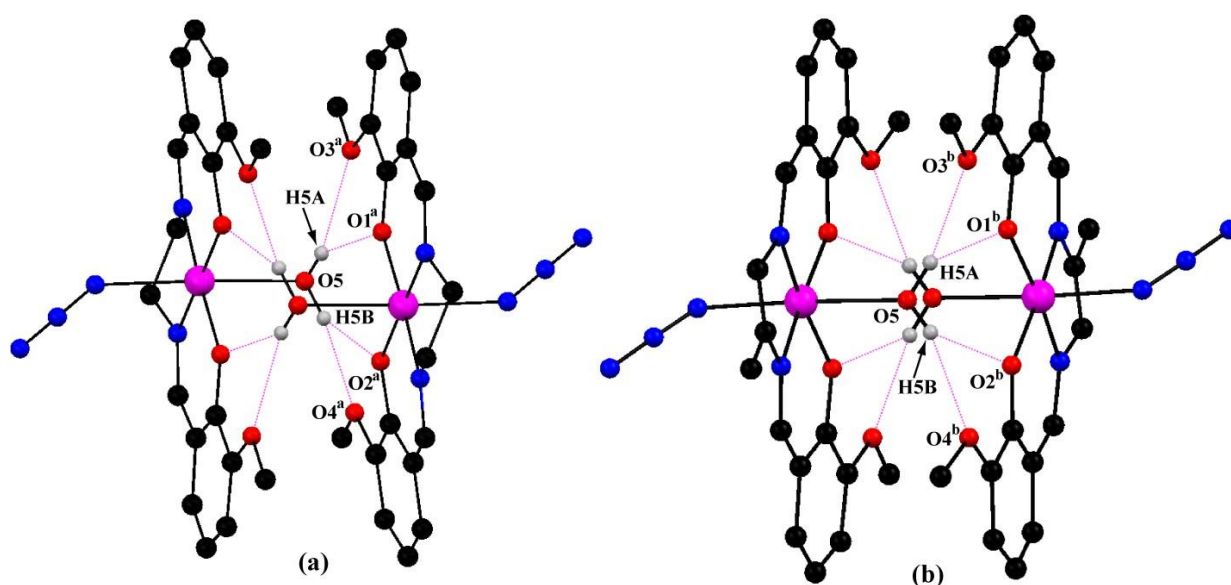

Fig. II.A.4.: Hydrogen bonded dimeric arrangements in complexes **1** (**a**) and **2** (**b**).

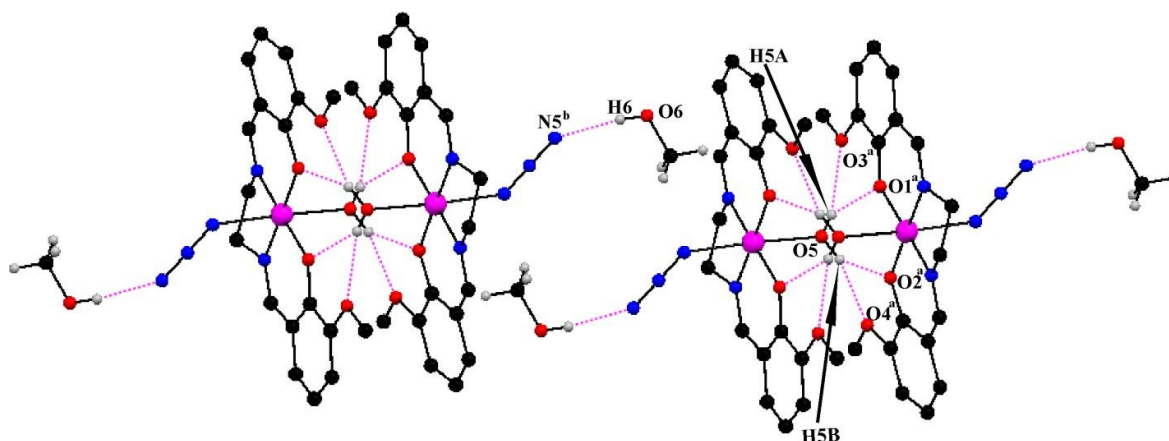Symmetry transformations [a] = 1-x,2-y,1-z and [b] = 1-x,1-y,1-z.

Fig. II.A.5: Hydrogen bonding interactions in complex **1**. Only relevant hydrogen atoms are shown for better clarity. Symmetry transformations [a] = 1-x,2-y,1-z and [b] = 1-x,1-y,1-z.
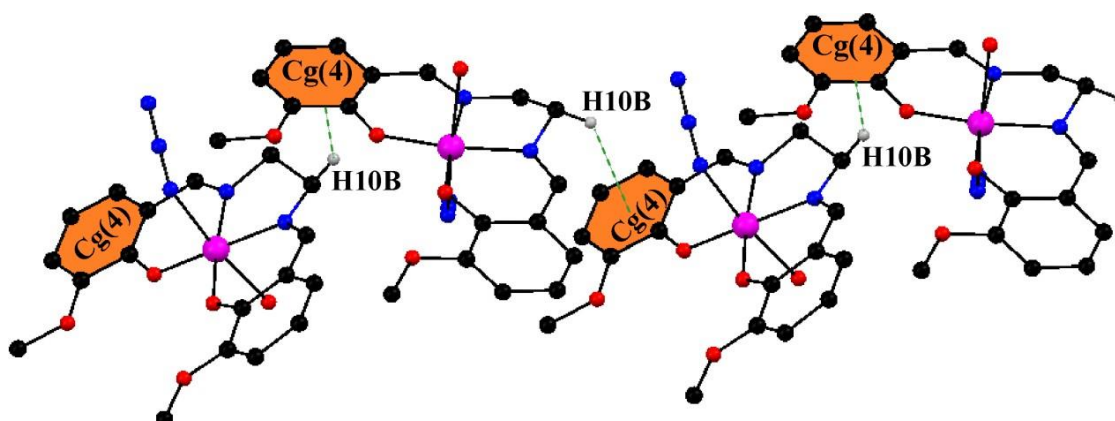

Fig. II.A.6: One-dimensional supramolecular arrangement via C-H···π interactions in complex **1**. Only the relevant hydrogen atoms are shown for clarity. Cg(4) denotes centre of gravity of the ring, [C(2)-C(3)-C(4)-C(5)-C(6)-C(7)].

Both complexes show important π···π stacking interactions. The centre of gravity of aromatic rings, [C(2)–C(3)–C(4)–C(5)–C(6)–C(7)] and [C(12)–C(13)–C(14)–C(15)–C(16)–C(17)], are stacked between symmetry related {1-x,2-y,1-z (for complex **1**) and 1-x,1-y,1-z (for complex **2**)} aromatic rings, [C(12)–C(13)–C(14)–C(15)–C(16)–C(17)] and [C(2)–C(3)–C(4)–C(5)–C(6)–C(7)], respectively from neighbouring molecules. All the Cg···Cg distances

are more or less comparable and are very close to 3.90 (Å). **Fig. II.A.7** illustrates the $\pi\cdots\pi$ stacking interactions of both complexes. Geometric features of C-H$\cdots\pi$ and $\pi\cdots\pi$ interactions are given in Tables **II.A.5** and **II.A.6**, respectively.

In complex **3**, hydrogen atoms, H(5A) and H(5B), attached to coordinated water oxygen atom, O(5), are engaged in hydrogen bond formation with symmetry related phenoxo oxygen atoms, O(1)[b] and O(2)[b], while at the same time they are hydrogen bonded with methoxy oxygen atoms O(3)[b] and O(4)[b], {symmetry transformation [b] = 1-x,1-y,1-z} of a neighbouring molecule to form a supramolecular dimer. Another hydrogen atom, H(6B), attached to water oxygen atom, O(6), is hydrogen bonded with symmetry related non-coordinated perchlorate oxygen atom, O(11)[c] {symmetry transformation [c] = -x,1-y, 1-z}. As the mean donor-acceptor distances fall within the range of 2.916 to 3.05 Å, the hydrogen bonding interactions are quite strong in solid state of the complex. All hydrogen bonding interactions are depicted in **Fig. II.A.8**.
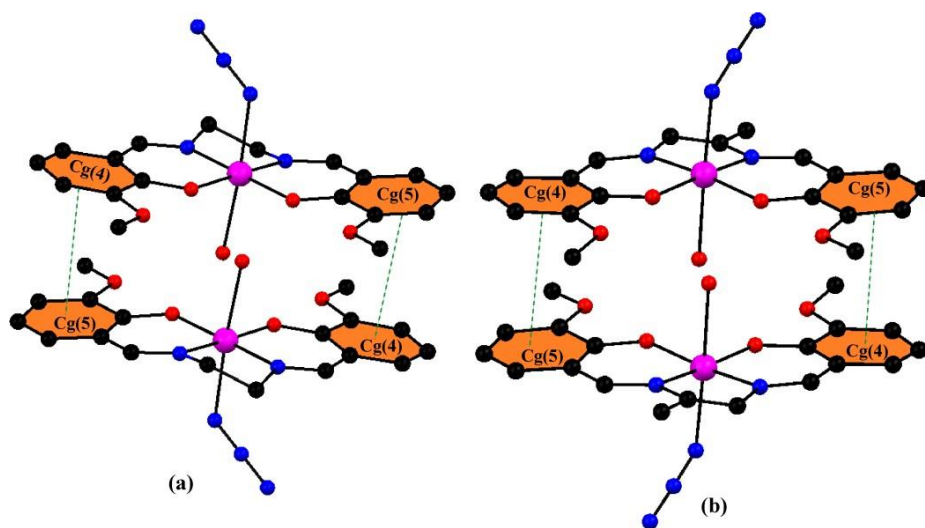

Fig. II.A.7: $\pi\cdots\pi$ stacking interactions in complexes **1** (**a**) and **2** (**b**). All hydrogen atoms are omitted for clarity. Cg(4) and Cg(5) denote centre of gravity of rings, [C(2)-C(3)-C(4)-C(5)-C(6)-C(7)] and [C(12)–C(13)–C(14)–C(15)–C(16)–C(17)], respectively.

The hydrogen atom, H(1B), attached to methoxy carbon atom, C(1), is involved in inter-molecular C-H⋯π interaction with symmetry related (1-x,1/2+y,1/2-z) phenyl ring, [C(13)-C(14)-C(15)-C(16)-C(17)-C(18)] of a neighbouring molecule, having a distance of 2.66 Å. A 1D supramolecular array is formed due to this C-H⋯π interaction (**Fig. II.A.9**).

The centre of gravity of phenyl rings, [C(2)–C(3)–C(4)–C(5)–C(6)–C(7)] and [C(13)–C(14)–C(15)–C(16)–C(17)–C(18)], are involved in face to face stacking interactions between symmetry related {1-x,1-y,1-z} phenyl rings, [C(13)–C(14)–C(15)–C(16)–C(17)–C(18)] and [C(2)–C(3)–C(4)–C(5)–C(6)–C(7)], respectively from a neighbouring molecule. The Cg⋯Cg distances are similar to each other and c.a. 3.89 (Å). **Fig. II.A.10**. illustrates the π⋯π stacking interactions of the complex. Geometric features of these supramolecular interactions i.e. H-bonding, C-H⋯π and π⋯π interactions are given in Tables **II.A.4**, **II.A.5** and **II.A.6**, respectively.

II.A.3.3. Hirshfeld surface analysis

Hirshfeld surfaces of all three complexes have been mapped over d_{norm}, shape index and curvedness (Fig. **II.A.11**). The surfaces are shown as transparent to allow visualization of the molecular moiety around which they are calculated. The dominant interactions between N⋯H/H⋯N for all complexes can be seen in the Hirshfeld surfaces as red spots on the d_{norm} surface in Fig. **II.A.11**. Additional visible spots in the Hirshfeld surfaces correspond to mainly C⋯H/H⋯C and H⋯H contacts. The tiny extent of area and light color on the Hirshfeld surfaces signify weaker and long range interactions other than hydrogen bonds.
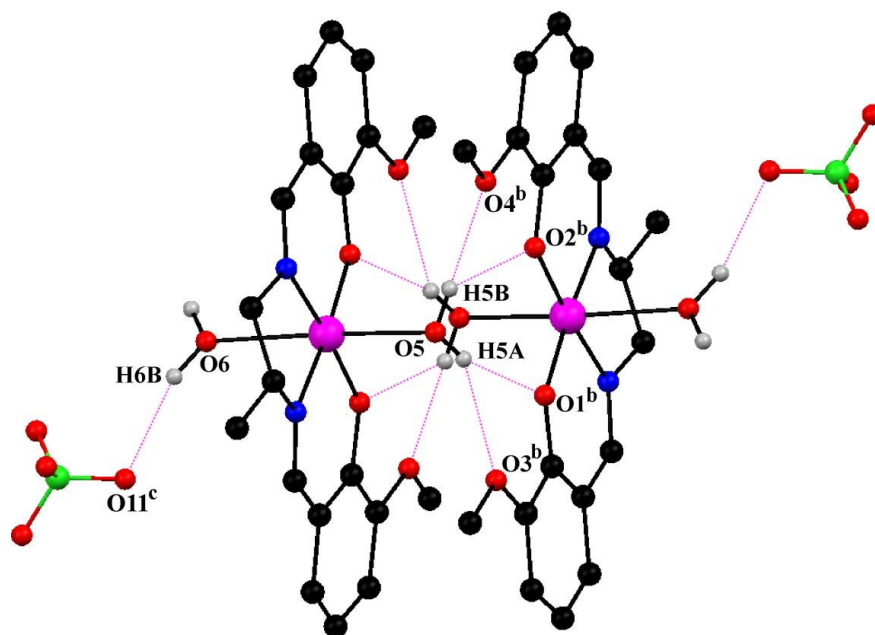
Fig. II.A.8.: Hydrogen bonding interactions in complex **3**. Only relevant hydrogen atoms are shown for better clarity. Symmetry transformations [b] = 1-x,1-y,1-z and [c] = -x,1-y, 1-z.

Table II.A.4: Hydrogen bond distances (Å) and angles (°) of complexes **1**, **2** and **3.**

Complex	D-H···A	D-H	H···A	D···A	∠D-H···A
	O(5)–H(5A)···O(1)[a]	0.74(8)	2.40(9)	2.911(9)	129(7)
	O(5)–H(5A)···O(3)[a]	0.74(8)	2.19(8)	2.898(9)	163(9)
1	O(5)–H(5B)···O(2)[a]	0.74(10)	2.32(11)	2.922(9)	140(10)
	O(5)–H(5B)···O(4)[a]	0.74(10)	2.30(10)	2.966(9)	151(11)
	O(6)–H(6)···N(5)[b]	0.8200	1.9900	2.810(13)	175.00
	O(5)–H(5A)···O(1)[b]	0.87(8)	2.19(8)	2.879(10)	136(6)
	O(5)–H(5A)···O(3)[b]	0.87(8)	2.31(8)	3.109(10)	154(8)
2	O(5)–H(5B)···O(2)[b]	0.70(12)	2.45(13)	2.894(9)	123(12)
	O(5)–H(5B)···O(4)[b]	0.70(12)	2.51(13)	3.068(9)	138(13)
	O(5)–H(5A)···O(1)[b]	0.74(10)	2.30(10)	2.958(8)	147(11)
	O(5)–H(5A)···O(3)[b]	0.74(10)	2.32(10)	2.916(8)	138(11)
3	O(5)–H(5B)···O(2)[b]	0.81(10)	2.31(12)	2.928(8)	133(8)
	O(5)–H(5B)···O(4)[b]	0.81(10)	2.18(8)	2.917(8)	153(10)
	O(6)–H(6B)···O(11)[c]	0.80(12)	2.27(14)	3.05(2)	165(14)

D = Donor; H= Hydrogen; A= Acceptor.

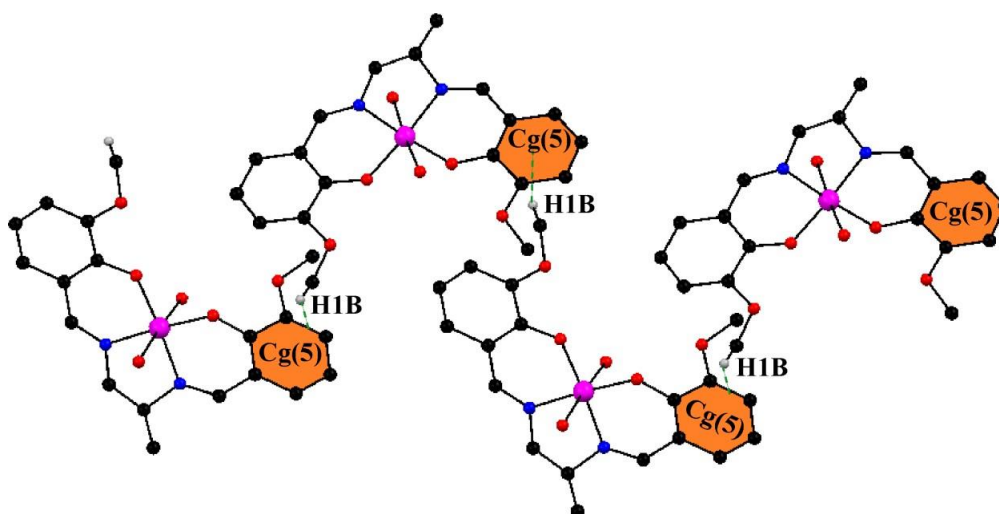Symmetry transformations [a] = 1-x, 2-y,1-z; [b] = 1-x,1-y,1-z;[c] = -x,1-y, 1-z

Fig. II.A.9.: One-dimensional supramolecular arrangement via C-H⋯π interactions in complex **3**. Only the relevant hydrogen atoms are shown for clarity. Cg(5) denotes centre of gravity of the ring, [C(13)-C(14)-C(15)-C(16)-C(17)-C(18)].

Table II.A.5: Geometric features (distances in Å and angles in °) of the C-H⋯π interactions obtained for complexes **1** and **3**.

Complex	X-H⋯Cg(Ring)	H⋯Cg (Å)	X-H⋯Cg (°)	X⋯Cg (Å)
1	C(10)-H(10B)⋯Cg(4)[d]	2.92	137	3.685(10)
3	C(1)-H(1B)⋯Cg(5)[e]	2.66	162	3.592(10)

Symmetry transformations: [d] = x,3/2-y,1/2+z; [e] = 1-x,1/2+y,1/2-z.

For complex **1,** Cg(4) = Centre of gravity of the ring [C(2)-C(3)-C(4)-C(5)-C(6)-C(7)].

For complex **3,** Cg(5) = Centre of gravity of the ring [C(13)-C(14)-C(15)-C(16)-C(17)-C(18)].
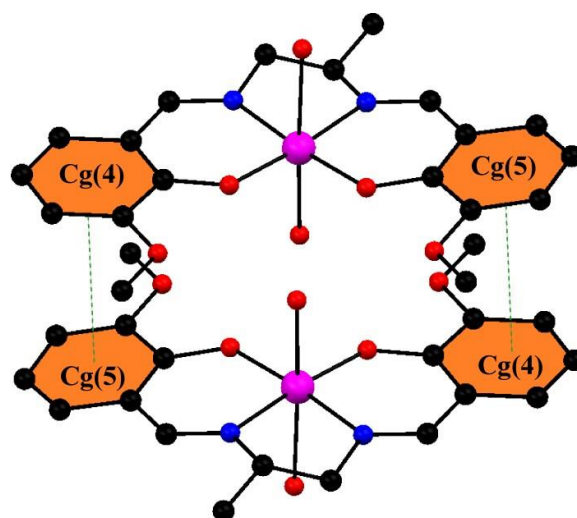
Fig. II.A.10.: $\pi\cdots\pi$ stacking interactions in complex **3**. All hydrogen atoms are omitted for clarity. Cg(4) and cg(5) denote centre of gravity of rings, [C(2)–C(3)–C(4)–C(5)–C(6)–C(7)] and [C(13)–C(14)–C(15)–C(16)–C(17)–C(18)], respectively.

Table II.A.6: Geometric features (distances in Å and angles in °) of the $\pi\cdots\pi$ stacking interactions obtained for the complexes **1**, **2** and **3**

Complex	Cg(Ring I)···Cg(Ring J)	Cg···Cg(Å)	α (°)	Cg(I)···Perp (Å)	Cg(J)···Perp (Å)
	Cg(4)···Cg(5)[a]	3.908(5)	10.0(4)	3.546(3)	3.625(4)
1	Cg(5)···Cg(4)[a]	3.908(5)	10.0(4)	3.625(4)	3.546(3)
	Cg(4)···Cg(5)[b]	3.885(7)	4.0(5)	3.717(4)	3.658(5)
2	Cg(5)···Cg(4)[b]	3.886(7)	4.0(5)	3.659(5)	3.717(4)
	Cg(4)···Cg(5)[b]	3.898(4)	8.1(4)	3.525(3)	3.546(3)
3	Cg(5)···Cg(4)[b]	3.897(4)	8.1(4)	3.546(3)	3.524(3)

Symmetry transformations [a] = 1-x, 2-y,1-z; [b] = 1-x,1-y,1-z.

For complex **1,** Cg(4) = Centre of gravity of the ring [C(2)-C(3)-C(4)-C(5)-C(6)-C(7)] and

Cg(5) = Centre of gravity of the ring [C(12)-C(13)-C(14)-C(15)-C(16)-C(17)].

For complex **2,** Cg(4) = Centre of gravity of the ring [C(2)-C(3)-C(4)-C(5)-C(6)-C(7)] and

Cg(5) = Centre of gravity of the ring [C(13)-C(14)-C(15)-C(16)-C(17)-C(18)].

For complex **3,** Cg(4) = Centre of gravity of the ring [C(2)-C(3)-C(4)-C(5)-C(6)-C(7)] and

Cg(5) = Centre of gravity of the ring [C(13)-C(14)-C(15)-C(16)-C(17)-C(18)].

Moreover, the two dimensional fingerprint plots (Fig. **II.A.12**) illustrate the difference between the intermolecular interaction patterns and the relative contributions (in percentage) for the major intermolecular interactions associated with the complex. In two dimensional fingerprint plots (Fig. **II.A.12**) intermolecular interactions appear as distinct spikes. Complementary regions are visible in the fingerprint plots where one molecule acts as a donor ($d_e > d_i$) and the other as an acceptor ($d_e < d_i$).
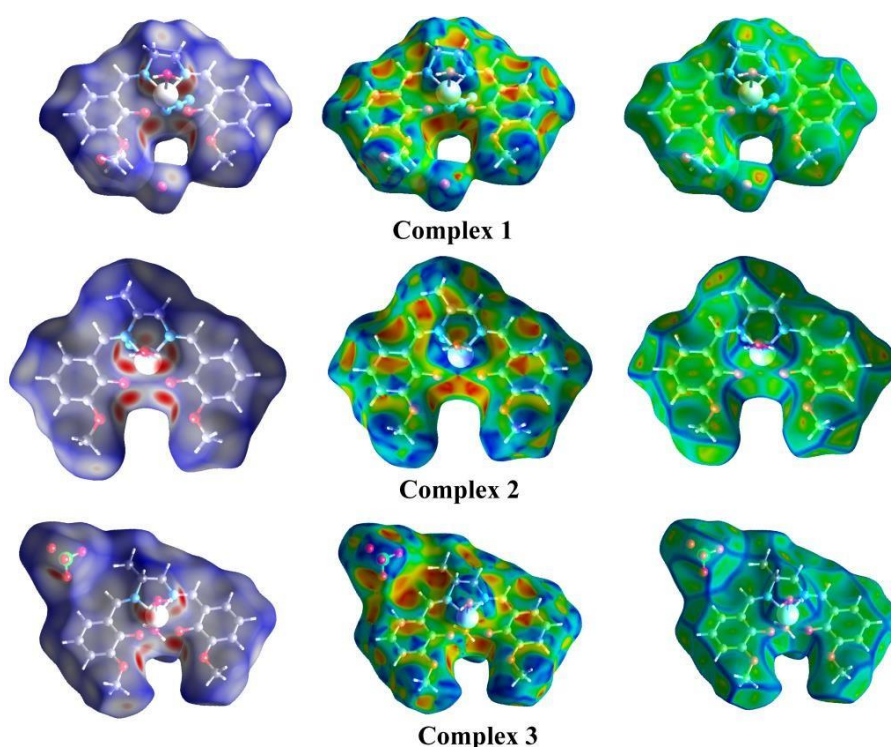

Complex 1

Complex 2

Complex 3

Fig. II.A.11: Hirshfeld surfaces mapped with d_{norm} (left-side), shape index (middle) and curvedness (right-side).

II.A.3.4. Spectral Analysis

Infrared spectra provide enough information to identify the way of bonding of the ligands to the metal centres. The most characteristic vibrations are selected by comparing the IR spectra of all complexes. In the IR spectra of all complexes, distinct bands as a result of the azomethine (C=N) groups around 1616 cm^{-1} are customarily noticed.[44] The appearances of strong bands around 2032 cm^{-1} indicate the presence of the monodentate azide coligands in complexes **1** and **2**, respectively.[42,43] Broad bands centered at around 3420 cm^{-1} due to O–H stretching vibrations are observed in IR spectra of all complexes.[45-47] Bands in the range of 2970–2830 cm^{-1} due to alkyl C–H bond stretching vibrations are usually noticed in IR spectra of all complexes.[48]

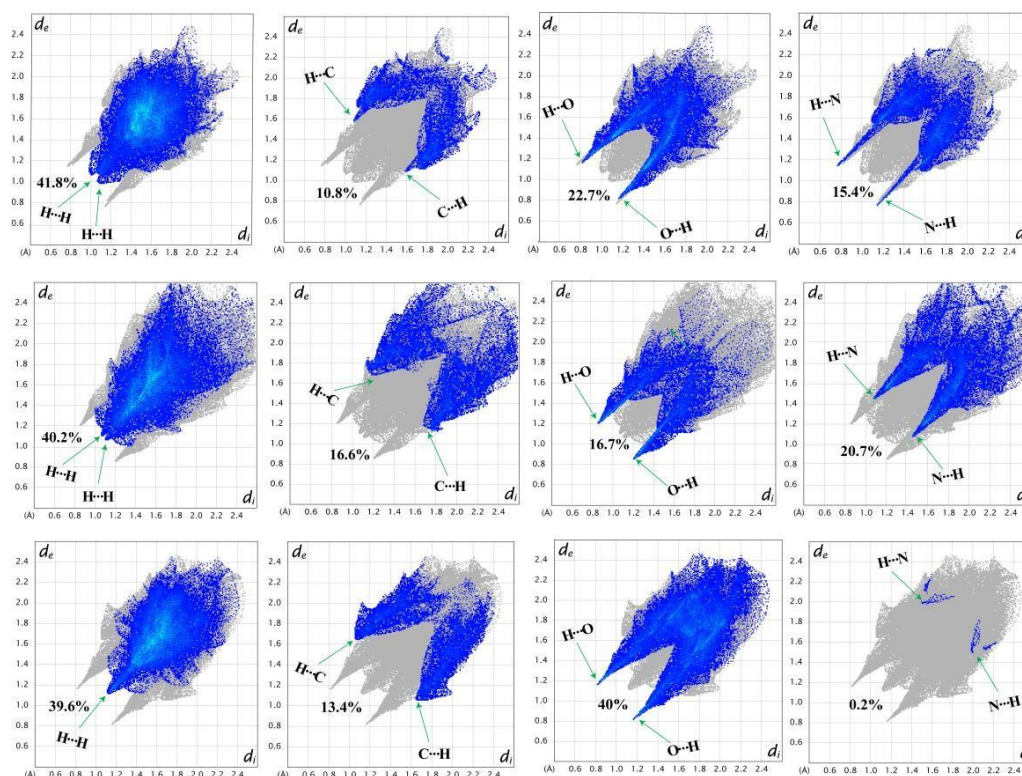**Fig. II.A.12**: Fingerprint plot: Resolved into H···H, C···H/H···C, O···H/H···O and N···H/H···N contact contributed to the total Hirshfeld Surface area of complex **1** (left), complex **2** (middle) and complex **3** (right).

The electronic spectra of the complexes are quite comparable to each other in DMF medium at room temperature. Intense absorption bands in the high energy region of 270 nm are assigned as intra-ligand $\pi \rightarrow \pi^*$ transitions involving the aromatic rings. Absorption bands around 325 nm are due to $n \rightarrow \pi^*$ transitions within the ligands. Strong absorption bands around 425 nm may be attributed to the ligand to metal charge transfer (LMCT) transitions.[49] Absorption bands with shoulders around 500 nm region are due to spin allowed d–d transitions.[50,51] Molar extinction coefficient value of d-d transition is very high may be due to the fact that LMCT band partly overlaps the d-d transition.

Formulations of all complexes as manganese(III) complexes are further supported by the room temperature solid state magnetic moment values in the region 4.96-5.02. These values are μB expected for discrete, high-spin (S = 2), magnetically non-coupled manganese(III) complexes having four unpaired electrons.[28,52]

II.A.3.5. Catalytic decomposition of hydrogen peroxide (Catalase mimicking activity) study

The catalytic activity of all three complexes towards decomposition of hydrogen peroxide has been investigated in DMF medium at 25°C temperature. In the beginning, solutions of the manganese(III) complexes were dark brown coloured but after addition of 30% (v/v) hydrogen peroxide they became fade yellow coloured or colorless and instantaneous evolution of a gas was observed for all three complexes. It can be easily understood that the evolved gas is oxygen and it comes from the catalytic decomposition of hydrogen peroxide solution. Volumetric measurements of this evolved oxygen confirmed that all three complexes are very much capable of catalytic decomposition of hydrogen peroxide into water and oxygen but the degree of decomposition is different i.e. complex **3** is the most efficient in hydrogen peroxide decomposition followed by other two complexes. Complexes

1 and **2** have comparable efficiency. To analyze the catalytic activity five set of experiments were carried out for each complexes with different initial amount of hydrogen peroxide (10, 20, 30, 40, 50 mL 30% v/v), and a constant catalyst concentration. The measurement of the volume of evolved oxygen indicates that for constant catalyst concentration the rate of decomposition increases with increase in the initial amount of hydrogen peroxide. The volume of oxygen evolved at different initial amount of 30% v/v hydrogen peroxide for most efficient complex i.e. complex **3** is shown in Fig. **II.A.13**. A blank experiment in presence of 30 mL hydrogen peroxide (30% v/v) has also been performed (Fig. **II.A. 13**). From Fig. **II.A. 13**, it can be clearly understood that at constant catalyst concentration, decomposition of H_2O_2 exhibits rate saturation kinetics. The efficiency of complex **3** at different initial amount of 30% v/v hydrogen peroxide is shown in the turnover number (TON) versus time plot in Fig. **II.A.14**. TON is defined as the number of moles of oxygen evolved per mole of the catalyst. Since two molecules of H_2O_2 on decomposition liberates one molecule of oxygen, if V_t and V_{inf} denote the volumes of oxygen given out at any time t and at the completion of reaction, then $(V_{inf}-V_t)$ is proportional to the amount of undecomposed H_2O_2 at time t. Now, rate constant of the reaction can be calculated from the equation: Rate constant, $k = 2.303/t$ $\log\{V_t/(V_{inf}-V_t)\}$, provided it follows first order kinetics. Substitution of experimental data (Table **3**) revealed constancy in the value of rate constant (k), confirming first order kinetics A plausible mechanistic pathway for the decomposition of hydrogen peroxide is also shown in Scheme **II.A.2**. In some previously published reports, similar type tentative catalytic cycles have been proposed.[9,53] It is clear from the catalytic cycle that during the catalytic cycle, manganese(III) is oxidised to manganese(IV) by replacing one axially coordinated ligand (water or azide) with concomitant reduction of H_2O_2 to H_2O. Subsequently, the oxidized form of catalyst goes back to its original form and reduces a second molecule of H_2O_2 producing O_2. Fig. **II.A.15** shows the comparison between turn over numbers of complexes **1**, **2** and **3**.

Complex **3** seems to be the most efficient catalyst as it contains two labile solvent molecules at the axial positions of its octahedral geometry. A few mononuclear manganese(III) complexes showing catalase mimicking activity already exist in literature. Some of these previously reported complexes exhibiting catalase mimicking activity are gathered in Table **II.A.4**.

Table II.A.3: Kinetic order for decomposition of H_2O_2 {50 mL 30% (v/v)} in presence of complex **3**.

Time (s)	$(V_t/V_{inf} - V_t)$	$\log(V_t/V_{inf} - V_t)$	K (s^{-1})
155	1.837209302	0.264158636	0.003924886
170	2.436619718	0.386787754	0.005239836
190	3.436363636	0.536099115	0.006498086
210	5.1	0.707570176	0.007759686

Table II.A.4: Maximal turnover number (TON) values for catalase mimicking activity of some reported mononuclear manganese(III) complexes.

Complex	Ligand donor Sites	TON	pH	Solvent	[Catalyst]	[H$_2$O$_2$]	References
MnL^4	N$_3$O$_3$	>300	-	CH$_3$CN	6×10^{-4} M	0.1 M	21
Mn(X-L^5)(OAc)	N$_2$O$_2$	2.5-8.4	8.1	H$_2$O	10×10^{-6} M	0.01 M	53
Mn(L^{6}R)(OAc)	N$_3$O$_2$	4–17	7.4	H$_2$O	10×10^{-6} M	0.05 M	54
Na[Mn(L^7)(H$_2$O)].5H$_2$	N$_2$O$_2$	178	8	H$_2$O	-	-	22

O

Complex	Donor			Solvent			Ref
Na[Mn(L^8)(MeOH)].4 H$_2$O	N$_2$O$_2$	25.2	8	H$_2$O	-	-	22
Mn(L^9)Y ; Y= N$_3$/SCN	N$_2$O$_3$	1200	-	DMF	-	0.0129 M	55
MnL^{10}(OTf)$_2$	N$_5$	7	8	CH$_3$CN/H$_2$O	60×10^{-6} M	0.033 M	23
MnL^{11}(OTf)$_2$	N$_3$O$_2$	17	8	CH$_3$CN/H$_2$O	60×10^{-6} M	0.033 M	23
MnL^{12}(OTf)$_2$	N$_3$S$_2$	39	8	CH$_3$CN/H$_2$O	60×10^{-6} M	0.033 M	23
MnL^{13}Cl$_2$	N$_4$	606	11.03	CH$_3$OH/H$_2$O	8.45 M	0.535 M	27
[MnL^{14}Cl]ClO$_4$·MeOH	N$_5$	609	11.03	CH$_3$OH/H$_2$O	8.50 M	0.535 M	27
[Mn(L^{16})Cl$_2$](CH$_3$OH)	N$_3$	75-83	9.6	H$_2$O	2.11×10^{-4} M	0.447 M	24
[Mn(L^{17})(SO$_4$)(H$_2$O)]$_n$	NO	320	7	H$_2$O	25×10^{-5} M	0.02 mol (30% w/w)	26
[Mn(L^{18})$_2$]$_n$	N$_2$O$_2$	918	>7	H$_2$O + imidazole	10.3 mg (solid)	0.114 mol (35% w/w)	25
[Mn(L^{19})(L^{20})$_2$]·4.5H$_2$O	NO$_2$, N$_4$	1110	>7	H$_2$O + imidazole	10 mg (solid)	0.114 mol	25

							(35% w/w)
$Mn(L^{20})(L^{21})(H_2O)$	NO_2, N_4	1374	>7	H_2O + imidazole	10.3 mg (solid)	0.114 mol	25
							(35% w/w)
$[Mn(L^{22})(CH_3OH)_2]Cl$ O_4	N_2O_2	29	-	CH_3CN	4×10^{-6} M	1.02 M	9

H_3^4 = 1-[N-(2-pyridylmethyl),N-(2-hydroxybenzyl)amino]-3-[N′-(2-hydroxybenzyl),N′-(4-methylbenzyl)amino]propan-2-ol; H_2L^5 = N,N'-bis(salicylidene)ethane-1,2-diamine; X = phenyl-ring substituent; R = cyclopentane-fused with ureido or acid–base catalyst auxiliary; H_2L^6 = N,N'-bis(3-methoxysalicylidene)ethane-1,2-diamine; H_2L^7 = 1,3-bis(5-sulphonatosalicylidenamino)propan-2-ol; H_2L^8 = 1,3-bis(5-sulphonatosalicylidenamino)propane; H_2L^9 = 1,4-bis(salicylidenamino)butan-2-ol; L^{10} = 2,6-bis[(N-methyl(2-pyridylmethyl)amino)methyl]pyridine; L^{11} = 2,6-bis[((2-pyridylmethyl)oxy)methyl]pyridine; L^{12} = 2,6-bis[((2-pyridylmethyl)sulpho)methyl]pyridine; L^{13} = 1-(benzimidazol-2-ylmethyl)-1,4,7-triazacyclononane; L^{14} = 1,4-bis(benzimidazol-2-ylmethyl)-1,4,7-triazacyclonone); HL^{15} = N-(2-hydroxybenzyl)-N,N′-bis[2-(Nmethylimidazolyl); L^{16} = 1,3-bis(2 -pyridylimino)-isoindolinemethyl]ethane-1,2-diamine; HL^{17} = 2-hydroxymethylpyridine; H_2L^{18} = 2-pyrazine carboxylic acid; L^{19} = 2,2,,-bipyridine; H_2L^{20} = 2,6-pyridinedicarboxylic acid; L^{21} = 4-hydroxypyridine-2,6-dicarboxylic acid; H_2L^{22} = N,N'-bis(1-(1'-hydroxy-2-naphthyl)ethylidene)propane-1,3-diamine.
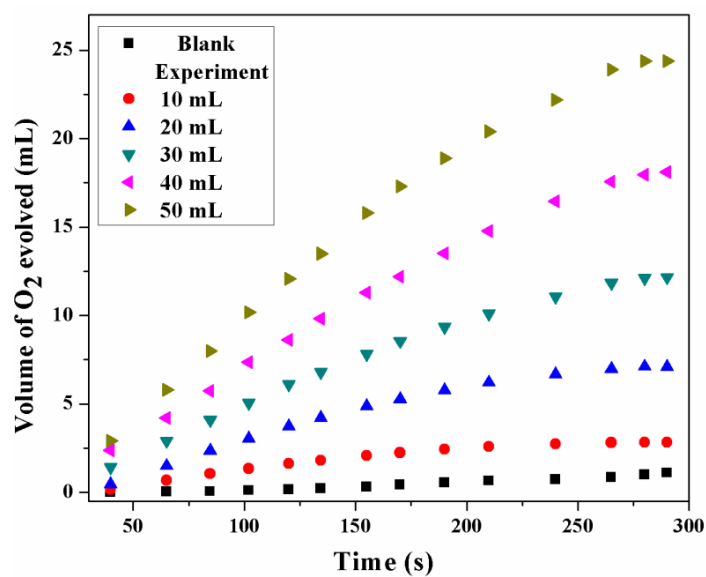
Fig. II.A.13: Time dependence of oxygen evolution upon reaction of complex **3** (10^{-3} M) with different initial amount of hydrogen peroxide at 25 °C. A blank experiment in presence of 30 mL H_2O_2 has also been included.
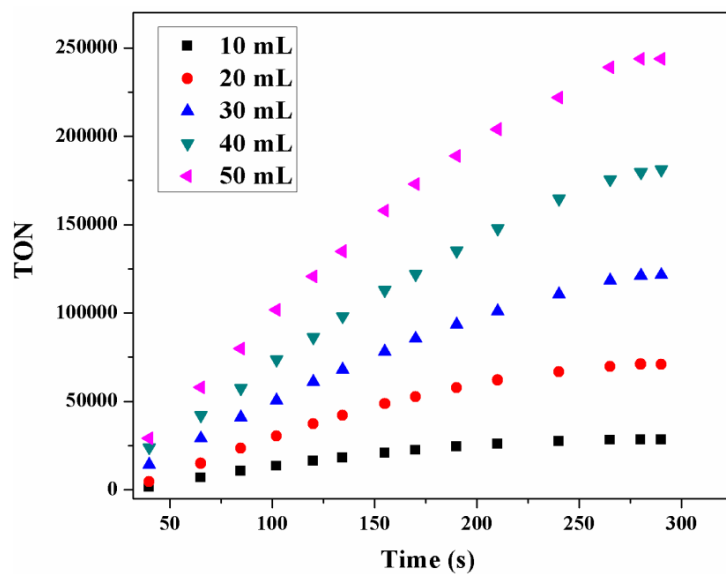

Fig. II.A.14: Turnover number {[Evolved oxygen]/[Catalyst]) vs time for complex **3** in the different initial amount of hydrogen peroxide at 25 °C.
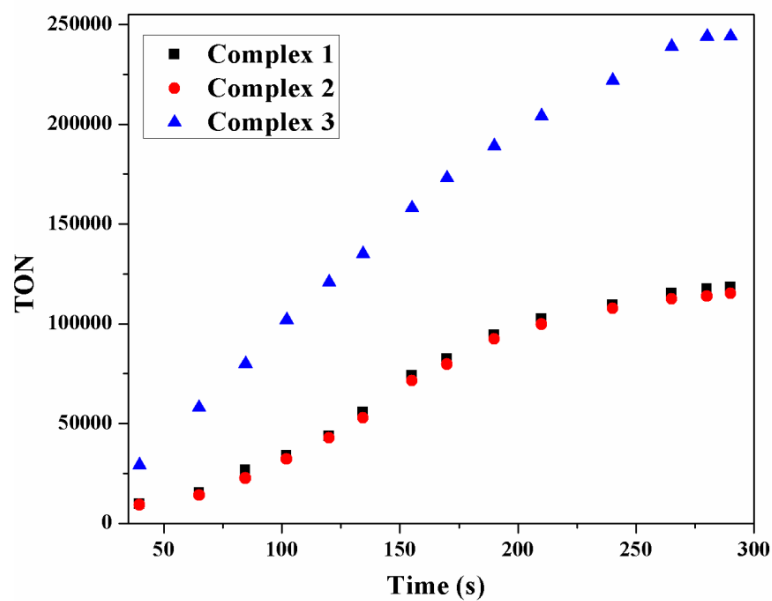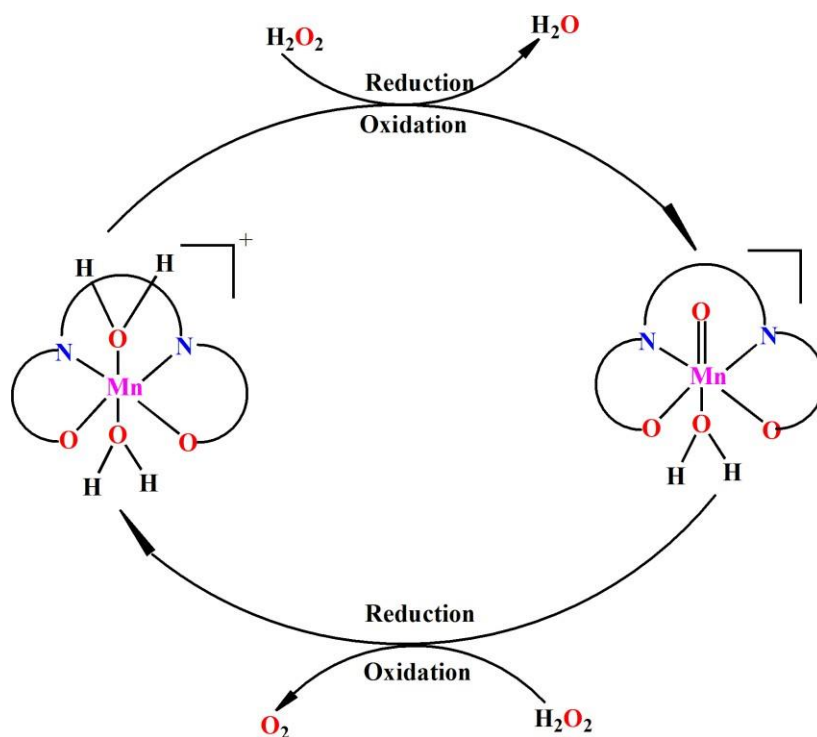
Fig. II.A.15: Comparison between turn over numbers of complexes **1**, **2** and **3** when 50 mL

30% (v/v) H_2O_2 is used in each case.

Scheme II.A.2: Plausible mechanistic pathway for the catalytic decomposition of hydrogen

peroxide into water and oxygen by complex **3**.

In order to verify whether these complexes is capable of maintaining its structural integrity after H_2O_2 decomposition process, IR spectrum of complex **3** was recorded before and after the decomposition reaction. The IR spectrum of complex **3** after decomposition reaction is in excellent agreement with the IR spectrum of pure complex, confirming the structural integrity of the complex after catalytic decomposition of H_2O_2. Alternatively, we can say that the complex is chemically intact during the decomposition reaction. Fig. **II.A.16** illustrates IR spectrum of complex **3** before and after the H_2O_2 decomposition reaction.

II.A.4. Conclusion

In the present work, three manganese(III) complexes derived from N_2O_2 donor tetradentate Schiff base ligands have been synthesized and the structures of these complexes have been confirmed by single crystal X-ray diffraction technique. The solid state structures
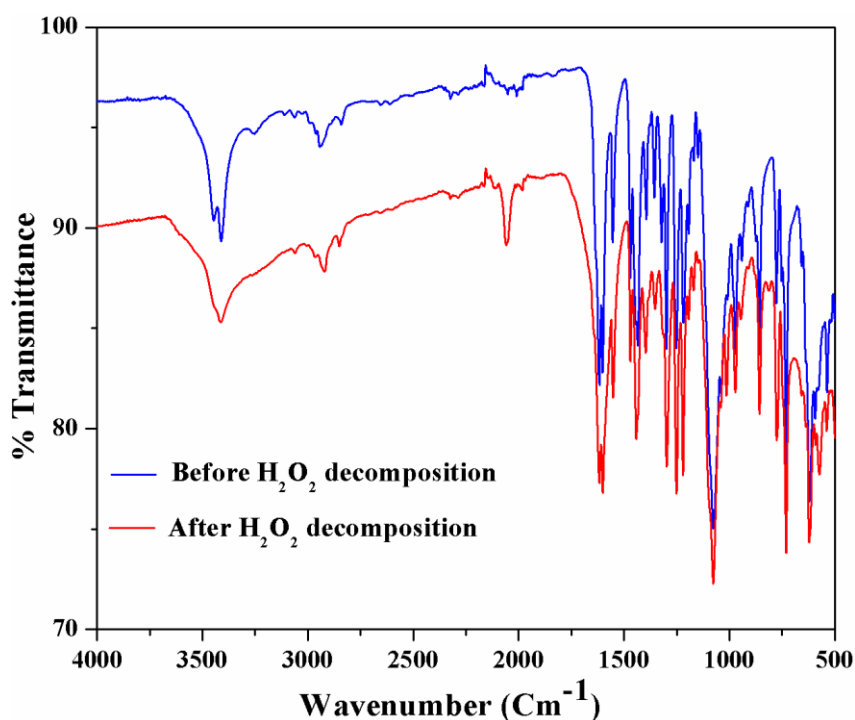

Fig. II.A.16: IR spectrum of complex **3** before (blue) and after (red) the H_2O_2 decomposition reaction.

of these complexes show the involvement of the organic ligands in several weak supramolecular interactions involving the alkoxy arms and the aromatic rings. All complexes are found to be active towards catalytic decomposition of hydrogen peroxide. Probable catalytic cycle showing the catalytic decomposition of hydrogen peroxide has also been projected. During the course of hydrogen peroxide decomposition, hydrogen peroxide molecule has to coordinate the manganese(III) center by replacing the axially coordinated ligands. Since water is a neutral molecule, it could easily be replaced by hydrogen peroxide. Alternatively, the replacement of azide coligand is probably somewhat difficult, as it is anionic in nature. The decomposition of hydrogen peroxide is, therefore, catalyzed more efficiently by complex **3** than other two complexes.

References

1 Q. Yue, X. Liu, W. -X. Guo, E. -Q. Gao, *CrystEngComm.*, 2018, **20**, 4258.

2 X. Dong, Y. Yao, Y. Li, Q. Wang, Y. Gou, *J. Mol. Struct.*, 2017, **1149**, 744.

3 M. Pait, M. Shatruk, D. Ray, *Dalton Trans.*, 2015, **44**, 11741.

4 S. Ganguly, P. Kar, M. Chakraborty, A. Ghosh, *New J. Chem.*, 2018, **42**, 9517.

5 G. E. Kostakis, A. M. Ako, A. K. Powell, *Chem. Soc. Rev.*, 2010, **39**, 2238.

6 M. Maneiro, M. R. Bermejo, A. Sousa, M. Fondo, A. M. Gonzalez, A. Sousa-Pedrares, C. A. McAuliffe, *Polyhedron*, 2000, **19**, 47.

7 M. Á. Vázquez-Fernández, M. R. Bermejo, M. I. Fernández-García, G. González-Riopedre, M. J. Rodríguez-Doutón, M. Maneiro, *J. Inorg. Biochem.*, 2011, **105**, 1538.

8 P. Kar, M. G. B. Drew, A. Ghosh, *Inorg. Chim. Acta.*, 2013, **405**, 349.

9 N. Sarkar, P. K. Bhaumik, S. Chattopadhyay, *Polyhedron*, 2016, **115**, 37.

10 R. Than, A. Schrodt, L. Westerheide, R. van Eldik, B. Krebs, *Eur. J. Inorg. Chem.*, 1999, 1537.

11 G.C. Dismukes, in: J. Reedijk, Bioinorganic catalysis (Ed.), Marcel Dekker, New York, 1993, p. 317.

12 E. Birben, U. M. Sahiner, C. Sackesen, S. Erzurum, O. Kalayci, *World Allergy Organ J.*, 2012, **5**, 9.

13 L. A. Pham-Huy, H. He, C. Pham-Huy, *Int. J. Biomed. Sci.*, 2008, **4**, 89.

14 D. Giustarini, I. Dalle-Donne, D. Tsikas, R. Rossi, *Crit. Rev. Clin. Lab. Sci.*, 2009, **46**, 241.

15 V. Kumar, A. A. Khan, A. Tripathi, P. K. Dixit, U. K. Bajaj, *The Journal of Phytopharmacology*., 2015, **4**, 126.

16 V. Gómez, M.Corbella, *Eur. J. Inorg. Chem*., 2012, 3147.

17 C. Palopoli, N. Bruzzo, C. Hureau, S. Ladeira, D. Murgida, S. Signorella, *Inorg. Chem*., 2011, **50**, 8973.

18 M. Grau, F. Rigodanza, A. J. P. White, A. Sorarú, M. Carraro, M. Bonchio, G. J. P. Britovsek, *Chem. Commun*., 2014, **50**, 4607.

19 B. Dede, I. Ozmen, F. Karipcin, *Polyhedron*, 2009, **28**, 3967.

20 B. Dede, F. Karipcin, M Cengiz, *J. Hazard. Mater.*, 2009, **163**, 1148.

21 G. N. Ledesma, H. Eury, E. Anxolabéhère-Mallart, C. Hureau, S. R. Signorella, *J. Inorg. Biochem*., 2015, **146**, 69.

22 D. Moreno, V. Daier, C. Palopoli, J.-P. Tuchagues, S. Signorella, *J. Inorg. Biochem*., 2010, **104**, 496.

23 M. Grau, F. Rigodanza, A.J.P. White, A. Soraru, M. Carraro, M. Bonchio, G. J. P. Britovsek, *Chem. Commun*., 2014, **50**, 4607.

24 J. Kaizer, T. Csay, P. Kovari, G. Speier, L. Parkanyi, *J. Mol. Catal. A Chem*., 2008, **280**, 203.

25 M. Devereux, M. McCann, V. Leon, V. McKee, R.J. Ball, *Polyhedron*, 2002, **21**, 1063.

26 M. Zienkiewicz, J. Szlachetko, C. Lothschütz, M. Hodorowicz, A. Jabłońska-Wawrzycka, J. Sá, B. Barszcz, *Dalton Trans*., 2013, *42*, 7761.

27 Q.X. Li, Q.-H. Luo, Y.Z. Li, Z.Q. Pan,M.C. Shen, *Eur. J. Inorg. Chem*., 2004, 4447.

28 N. Sarkar, M. G. B. Drew, K. Harms, A. Bauzá, A. Frontera, S Chattopadhyay, *CrystEngComm.*, 2018, **20**, 1077.

29 L. K. Das, R. M. Kadam, A. Bauzá, A. Frontera, A. Ghosh, *Inorg. Chem.*, 2012, **51**, 12407.

30 K. Ghosh, K. Harms, A. Bauzá, A. Frontera, S. Chattopadhyay, *Dalton Trans.*, 2018, **47**, 331.

31 F. R. Keene, *Coord. Chem. Rev.*, 1999, **187**, 121.

32 S. Jana, S. Chattopadhyay, *J. Coord. Chem.*, 2013, **66**, 3906.

33 M. Á. Vázquez-Fernández, M. I. Fernández-García, A. M. González-Noya, M. Maneiro, M. R. Bermejo, M. J. Rodríguez-Doutón, *Polyhedron.*, 2012, **31**, 379.

34 G. Assey, R. J. Butcher, Y. Gultneh, *Acta Cryst.*, 2010, **E66**, m851-m852.

35 C. -H. Li, K. -L. Huang, J. -M. Dou, Y.-N. Chi, Y. -Q. Xu, L. Shen, D. -Q. Wang, C. -W. Hu, *Cryst. Growth Des.*, 2008, **8**, 3141.

36 C. -G. Zhang, G. -H. Tian, Z. -F. Ma, D. -Y. Yan, *Transition Met. Chem.*, 2000, **25**, 270.

37 A. Gutiérrez, M. F. Perpiñán, A. E. Sánchez, M. C. Torralba, V. González, *Inorg. Chim. Acta.*, 2016, **453**, 169.

38 H. Kara, *Anal. Sci.*, 2008, **24**, 263.

39 S. Nastase, F. Tuna, C. Maxim, C. A. Muryn, N. Avarvari, R. E. P. Winpenny, M. Andruh, *Cryst. Growth Des.*, 2007, **7**, 1825.

40 M. R. Bermejo, M. I. Fernández, E. Gómez-Fórneas, A. González-Noya, M. Maneiro, R. Pedrido, M. J. Rodríguez, *Eur. J. Inorg. Chem.*, 2007, 3789.

41 D. Cremer, J. A. Pople, *J. Am. Chem. Soc.*, 1975, **97**, 1354.

42 K. Ghosh, S. Roy, A. Ghosh, A. Banerjee, A. Bauzá, A. Frontera, S. Chattopadhyay, *Polyhedron*, 2016, **112**, 6.

43 K. Ghosh, K Harms, S Chattopadhyay, *Polyhedron*, 2017, **123**, 162.

44 K. Nakamoto, Infrared Spectra of Inorganic and Coordination Compounds, Fourth ed., Wiley, New York, 1986.

45 M. Das, S. Chattopadhyay, *Polyhedron.*, 2013, **50**, 443.

46 A. Bhattacharyya, K. Harms, S. Chattopadhyay, *Inorg. Chem. Commun.*, 2014, **48**, 12.

47 J.-B. Brubach, A. Mermet, A. Filabozzi, A. Gerschel, P. Roy, *J. Chem. Phys.*, 2005, **122,** 184509.

48 K. Ghosh, K. Harms, S. Chattopadhyay, *ChemistrySelect.*, 2017, **2**, 8207.

49 A. Saha, P. Majumdar, S. Goswami, J. Chem. Soc. *Dalton Trans.*, 2000, 1703.

50 A. Bartyzel, A.A. Kaczor, *J. Coord. Chem.*, 2015, **68**, 3701.

51 P. Bhowmik, H.P. Nayek, M. Corbella, N´. Aliaga-Alcalde, S. Chattopadhyay, *Dalton Trans.*, 2011, **40**, 7916.

52 B. J. Kennedy, K. S. Murray, *Inorg. Chem.*, 1985, **24**, 1552.

53 S. R. Doctrow, K. Huffman, C. B. Marcus, G. Tocco, E. Malfroy, C. A. Adinolfi, H. Kruk, K. Baker, N. Lazarowych, J. Mascarenhas, B. Malfroy, *J. Med. Chem.*, 2002, **45**, 4549.

54 Y. Noritake, N. Umezawa, N. Kato, T. Higuchi, *Inorg. Chem.*, 2013, **52**, 3653.

55 V. Daier, D. Moreno, C. Duhayon, J.-P. Tuchagues, S. Signorella, *Eur. J. Inorg. Chem.*, 2010, 965.

Section: II.B

Synthesis and characterization of a manganese(III) Schiff base complex and exploration of Br⋯Br interaction in the solid state structure of the complex

II.B.1. Introduction

Noncovalent interactions are by far the most effective means for the formation of molecular aggregates and assemblies.[1-3] Among these interactions, conventional ones i.e. hydrogen bonding, C-H⋯π, π⋯π stacking etc are the most frequently observed and always have a superior feature compared to rest of the others.[4-6] On the contrary, uncommon halogen bonding interactions have emerged to one of the most attractive noncovalent interactions for last few decades.[7-10] These noncovalent interactions have been manipulated to determine the final structure of molecular solids.[11] The functional potential of halogen bonding interactions has been shown by a number of applications in the field of synthetic chemistry, crystal engineering, material science, and bioorganic chemistry.[12-14] Generally, halogen bonding interactions have two preferred geometries i.e. type I ($\theta_1=\theta_2$, symmetrical interactions) and type II ($\theta_1\approx180°$ & $\theta_2\approx90°$, bent interactions), where θ_1 and θ_2 are the two C-X⋯X angles (Scheme **II.B.1**).[15,16] There is a clear geometric and chemical distinction between these two types of halogen bonding interactions. According to IUPAC description, type I interaction is found for all halogens but type II interaction is the most favoured for heavier halogen derivatives i.e. bromine and iodine derivatives.[17,18] Both these two types of halogen bonding interactions constitute a topic of current interest and active research.
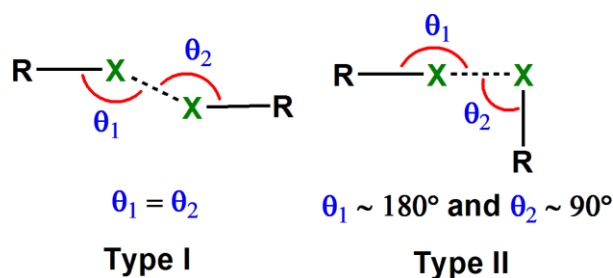
Scheme II.B.1: The two preferred geometries for halogen···halogen short contacts.

Previously, two manganese complexes have been synthesized and structurally characterized with brominated Schiff base ligands to analyze characteristic halogen bonding interactions.[19] In continuation of our comprehensive studies and with the aim to understand the type of halogen bonding which influence on structural features of metal complex, my concentration has been directed to analyse the energetic features of halogen bonding interactions along with several other more conventional interactions like hydrogen bonding and $\pi\cdots\pi$ stacking of a newly synthesized manganese(III) complex with brominated Schiff base ligand and several other coligands. The Br···Br interactions present in the complex shows type I geometry.

Several bio-relevant catalytic activities of various transition (e.g. manganese, iron, cobalt, copper, nickel etc) and non-transition (e.g. zinc) metal complexes have been designed, synthesised and explored for the last few years in our laboratory.[20-24] Several other groups are also working on these topics.[25-27] Catalase mimicking activities of few manganese(III) complexes have also been investigated.[28] In the present case, the synthesized manganese(II) complex has been found to have the ability to be used as catalyst in the decomposition of hydrogen peroxide (i.e. the ability to mimic catalase), monitored by measuring the volume of evolved oxygen in different catalyst concentration.

II.B.2. Experimental Section

II.B.2.1 Synthesis of [MnL⁴(CH₃OH)(H₂O)]ClO₄

A methanol solution (20 ml) of 2,2-dimethylpropane-1,3-diammine (0.12 mL, ~1 mmol) and 5-bromo-2-hydroxy-3-methoxybenzaldehyde (462 mg, ~2 mmol) was refluxed for ca. 1.5 h to prepare N_2O_2 donor tetradentate Schiff base ligand, H_2L^4. A methanol solution (10 mL) of manganese(II) perchlorate hexahydrate (740 mg, ~2 mmol) was then directly added to the methanol solution of H_2L^4 and the resulting solution was refluxed further for 1 h. After that the resulting mixture was cooled to room temperature and immediately a small amount of side product was separated, which was subsequently filtered off. Dark brown single crystals of the complex, suitable for X-ray diffraction, were obtained after few days by slow evaporation of the solution in open atmosphere.

Yield: 525 mg (~72 %); based on manganese(III). Anal. Calc. for $C_{22}H_{28}Br_2MnN_2O_{10}Cl$ (FW = 730.65): C, 36.17; H, 3.86; N, 3.83 %. Found: C, 36.3; H, 4.0; N, 3.7 %. FT-IR (KBr, cm⁻¹): 1090 (υ_{ClO4}); 1611, ($\upsilon_{C=N}$); 2830-2970 (υ_{C-H}); 3420 (υ_{O-H}). UV-Vis, λ_{max} (nm), [ε_{max} (L mol⁻¹ cm⁻¹)] (CH₃CN), 240 (3.39 x 10⁴), 294 (1.24 x 10⁴), 410 (5.03 x 10³), 540 (1.84 x 10²).
Magnetic moment = 4.98 μB

Table II.B.1: Crystal data and refinement details of the complex **4**

Formula	$C_{22}H_{27}Br_2MnN_2O_{10}Cl$
Formula Weight	730.65
Crystal System	Triclinic
Space group	$P\bar{1}$
a(Å)	12.6199(10)

b(Å)	14.1926(11)
c(Å)	17.6694(14)
α (°)	92.209(2)
β(°)	92.686(2)
γ(°)	115.688(2)
V(Å^3)	2842.7(4)
Z	4
$d_{(calc)}$ [g/cm^3]	1.707
μ [mm^{-1}]	3.424
F(000)	1464
Total Reflections	95687
Unique Reflections	12479
Observed data[I > 2 ζ(I)]	10292
R(int)	0.051
R1, wR2 (all data)	0.0606,0.1271
R1, wR2 ([I > 2 ζ(I)]	0.0479,0.1188
Residual Electron Density (eÅ^{-3})	1.246, -0.965

CCDC reference no 1882391

II.B.3. Results and discussions

II.B.3.1. Synthesis

The potentially tetradentate Schiff base ligand, H_2L^4, was prepared by facile condensation between 2,2-dimethylpropane-1,3-diammine and 5-bromo-2-hydroxy-3-methoxybenzaldehyde in 1:2 molar ratio in methanol following the literature method.[29-31] The ligand was not isolated and was directly used for synthesis of the manganese(III) complex. Addition of methanol solution of manganese(II) perchlorate hexahydrate in methanol solution of the Schiff base, H_2L^4, followed by refluxing for additional 1 h produced a dark brown coloured complex **4**, $[MnL^4(CH_3OH)(H_2O)]ClO_4$. Manganese(II) gets oxidized to manganese(III) by aerial oxygen under the reaction condition. Use of anaerobic condition prevents the formation of this complex which confirms the involvement of aerial oxygen in oxidation process. The formation of the complex is shown in Scheme **II.B.2**.
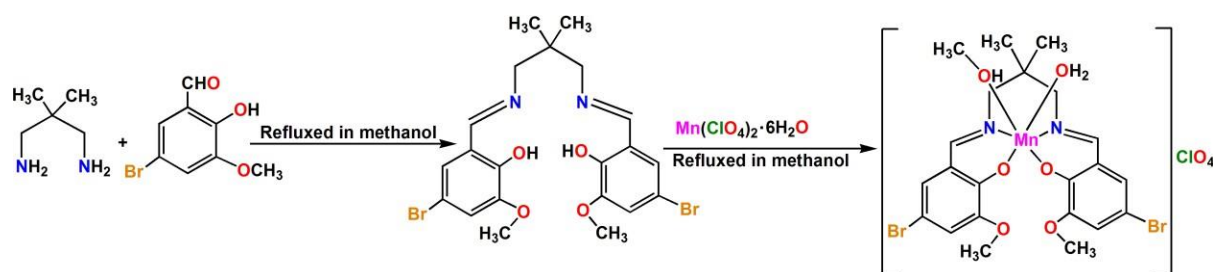
Scheme II.B.2: Synthetic route to the complex **4**.

II.B.3.2 Structure description of $[MnL^4(CH_3OH)(H_2O)]ClO_4$

Single crystal X-ray diffraction study reveals that the asymmetric unit of the complex consists of a mononuclear cation $[MnL^4(CH_3OH)(H_2O)]^+$ together with a non-coordinating perchlorate anion. The complex crystallizes in the triclinic space group $\bar{P}1$ There are two independent mononuclear subunits (A and B) with equivalent geometry. Perspective view of the complex (subunit A) along with selective atom-numbering scheme is shown in Fig.

II.B.1. Selected bond lengths and bond angles of subunit A are listed in Tables **II.B.2** and **II.B.3** respectively. The manganese(III) centre, Mn(1) has a six-coordinate distorted octahedral geometry in which two imine nitrogen atoms [N(1) and N(2)] and two phenoxo oxygen atoms [O(1) and O(2)] of a deprotonated Schiff base ligand, L^{2-}, constitute the equatorial plane. On the other hand, the axial positions are coordinated by a water oxygen atom, O(3) and a methanol oxygen atom, O(4), furnishing a distorted octahedral coordination sphere around itself. Both the axial bonds are much longer compared to the equatorial ones, as expected in similar type complexes. Bond lengths fall within the range observed for similar type mononuclear manganese(III) complexes.[32-34] The deviations of the coordinating oxygen atoms, O(1), O(2) and nitrogen atoms N(1), N(2) in the basal plane from the mean plane passing through them are –0.040(2), 0.051(2), 0.049(3) and –0.038(3) Å respectively. The deviation of manganese atom Mn(1) from the same plane is -0.0222(5) Å. The saturated six-membered chelate ring, R(1) [Mn(1)–N(1)–C(9)–C(10)–C(13)–N(2)] resembles a twist boat conformation with puckering parameters.[35,36] Q = 0.760(4) Å, θ= 90.1(3)°, φ = 281.2(3)°.
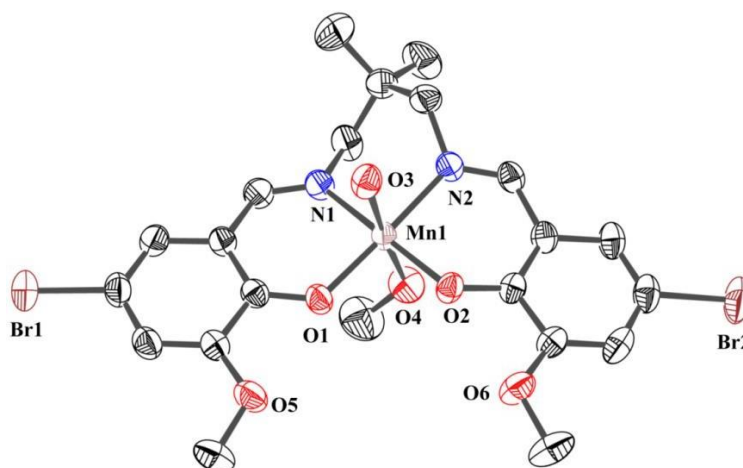

Fig. II.B.1: ORTEP view of subunit A of the complex (ellipsoids are drawn at the 50% probability level) with selected atom-numbering scheme. Hydrogen atoms have been omitted for clarity.

A perspective view of the complex (subunit B) along with selective atom-numbering scheme is shown in **Fig. II.B.2**. Single crystal X-ray diffraction experiments reveals that subunit B of the complex consists of a distinct mononuclear unit *[MnL^4(CH$_3$OH)(H$_2$O)]* together with a non-coordinated perchlorate anion. Selected bond lengths and bond angles of subunit B are listed in Tables **II.B.4** and **II.B.5** respectively. The manganese(III) centre, Mn(2) has a six-coordinate distorted octahedral geometry in which two imine nitrogen atoms [N(3) and N(4)] and two phenoxo oxygen atoms [O(7) and O(8)] of a deprotonated Schiff base ligand, *L^{2-}*, constitute the equatorial plane. On the other hand, the axial positions are coordinated by a water oxygen atom, O(9) and a methanol oxygen atom, O(10), furnishing a distorted octahedral coordination sphere around itself. The deviations of the coordinating oxygen atoms, O(7), O(8) and nitrogen atoms N(3), N(4) in the basal plane from the mean plane passing through them are 0.064(3), –0.076(2), –0.072(3) and 0.062(3) Å respectively. The deviation of manganese atom Mn(2) from the same plane is 0.0212(5) Å. The saturated six-membered chelate ring, R(2) [Mn(2)–N(3)–C(31)–C(32)–C(35)–N(4)] resembles a twist boat conformation with puckering parameters Q = 0.772(4) Å, θ = 89.4(3)°, ϕ = 278.2(3)°.

The complex **4** shows several hydrogen bonding interactions. Two hydrogen atoms, H(3A) and H(3B), of a water molecule attached with Mn(1) in subunit A form bifurcated hydrogen bonds with oxygen atoms of the Schiff base ligand. Hydrogen atom, H(3A), forms symmetry ([a] = -x,1-y,-z) related hydrogen bonds with a phenoxy oxygen, O(1) and a methoxy oxygen, O(5).
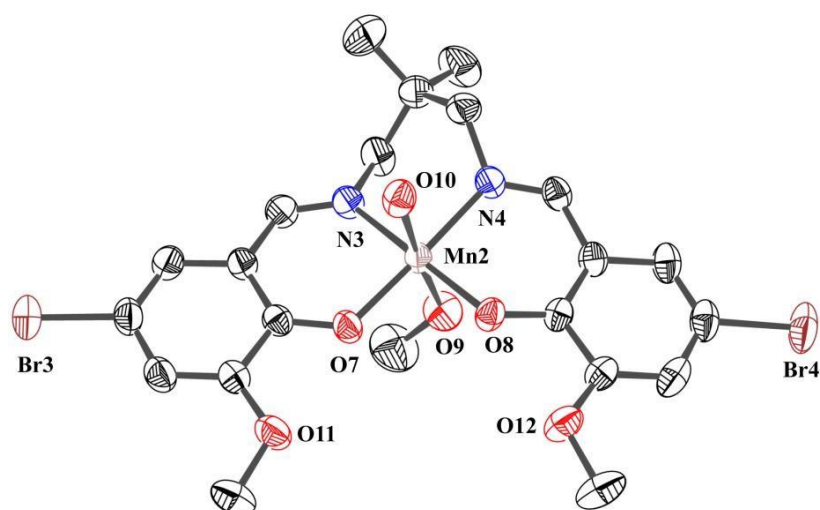
Fig. II.B.2.: ORTEP presentation of subunit B of the complex (ellipsoids are drawn at the 50% probability level) with selected atom-numbering scheme. Hydrogen atoms have been omitted for clarity.

Similarly hydrogen atom, H(3B), forms symmetry (^{a} = -x,1-y,-z) related hydrogen bonds with a phenoxy oxygen, O(2) and a methoxy oxygen, O(6). Hydrogen atom, H(4), attached with O(4) of a methanol forms another hydrogen bond with the oxygen atom, O(13), of a perchlorate ion. The hydrogen bonding interactions are shown in Fig. **II.B.3**. Details of geometric features of hydrogen bonding interactions are given in Table **II.B.6**.

Table II.B.2: Selected bond lengths (Å) of the complex **4** (subunit A)

Mn(1)-O(3)	2.230(2)
Mn(1)-O(4)	2.312(3)
Mn(1)-N(1)	1.996(3)
Mn(1)-N(2)	2.015(3)
Mn(1)-O(1)	1.882(3)
Mn(1)-O(2)	1.889(2)

Table II.B.3: Selected bond angles (°) of the complex **4** (subunit A)

O(1)-Mn(1)-O(2)	90.48(11)
O(1)-Mn(1)-O(3)	91.35(10)
O(1)-Mn(1)-O(4)	90.90(11)
O(1)-Mn(1)-N(1)	90.46(13)
O(1)-Mn(1)-N(2)	178.90(11)
O(2)-Mn(1)-O(3)	92.42(10)
O(2)-Mn(1)-O(4)	88.69(10)
O(2)-Mn(1)-N(1)	175.64(11)
O(2)-Mn(1)-N(2)	90.06(11)
O(3)-Mn(1)-O(4)	177.49(10)
O(3)-Mn(1)-N(1)	91.82(11)
O(3)-Mn(1)-N(2)	87.67(10)
O(4)-Mn(1)-N(1)	87.04(11)
O(4)-Mn(1)-N(2)	90.07(11)
N(1)-Mn(1)-N(2)	89.07(13)

Table II.B.4: Selected bond lengths (Å) of the complex **4** (subunit B)

Mn(2)-N(3)	2.013(3)
Mn(2)-O(7)	1.885(3)
Mn(2)-N(4)	1.998(3)
Mn(2)-O(10)	2.241(3)
Mn(2)-O(8)	1.887(3)
Mn(2)-O(9)	2.275(3)

Two hydrogen atoms, H(10A) and H(10B), of a water molecule attached with Mn(2) in subunit 2 form bifurcated hydrogen bonds with the oxygen atoms of Schiff base ligand. Hydrogen atom, H(10A), forms symmetry (^{b} = 1-x, 2-y,1-z) related hydrogen bonds with a phenoxy oxygen, O(7) and a methoxy oxygen, O(11). Similarly hydrogen atom, H(10B), form symmetry (^{b} = 1-x, 2-y,1-z) related hydrogen bonds with a phenoxy oxygen, O(8) and a methoxy oxygen, O(12). Hydrogen atom, H(9), attached with O(9) of a methanol forms symmetry (^{c} = 1-x, 1-y,1-z) related hydrogen bond with the oxygen atom, O(19), of a perchlorate ion. The hydrogen bonding interactions are shown in Fig. **II.B.4.**. Details of geometric features of hydrogen bonding interactions are given in Table **II.B.6**.

Table II.B.5: Selected bond angles (°) of the complex **4** (subunit B)

O(7)-Mn(2)-N(3)	90.65(13)
O(7)-Mn(2)-N(4)	177.34(12)
O(8)-Mn(2)-O(9)	89.51(12)
O(8)-Mn(2)-O(10)	89.67(10)
O(8)-Mn(2)-N(3)	174.22(11)
O(8)-Mn(2)-N(4)	90.15(12)
O(9)-Mn(2)-O(10)	176.78(12)
O(9)-Mn(2)-N(3)	84.90(12)
O(9)-Mn(2)-N(4)	91.06(12)
O(10)-Mn(2)-N(3)	95.84(11)
O(10)-Mn(2)-N(4)	85.83(10)
N(3)-Mn(2)-N(4)	88.52(14)
O(7)-Mn(2)-O(8)	90.92(11)
O(7)-Mn(2)-O(9)	91.39(12)
O(7)-Mn(2)-O(10)	91.74(11)

II.B.3.3. Theoretical calculations of solid state supramolecular interactions

Bromine atoms, present in the complex **4**, participate in bifurcated halogen bonding (Br···Br) interactions of type I. The theoretical study is basically devoted to analyse the energy associated to the halogen bonding interactions, along with other more conventional interactions and stronger interactions like hydrogen bonding and π···π stacking. Although the halogen bondings in interactions are weaker than hydrogen bonding, they are important fine-tuning the final geometry of the assemblies.
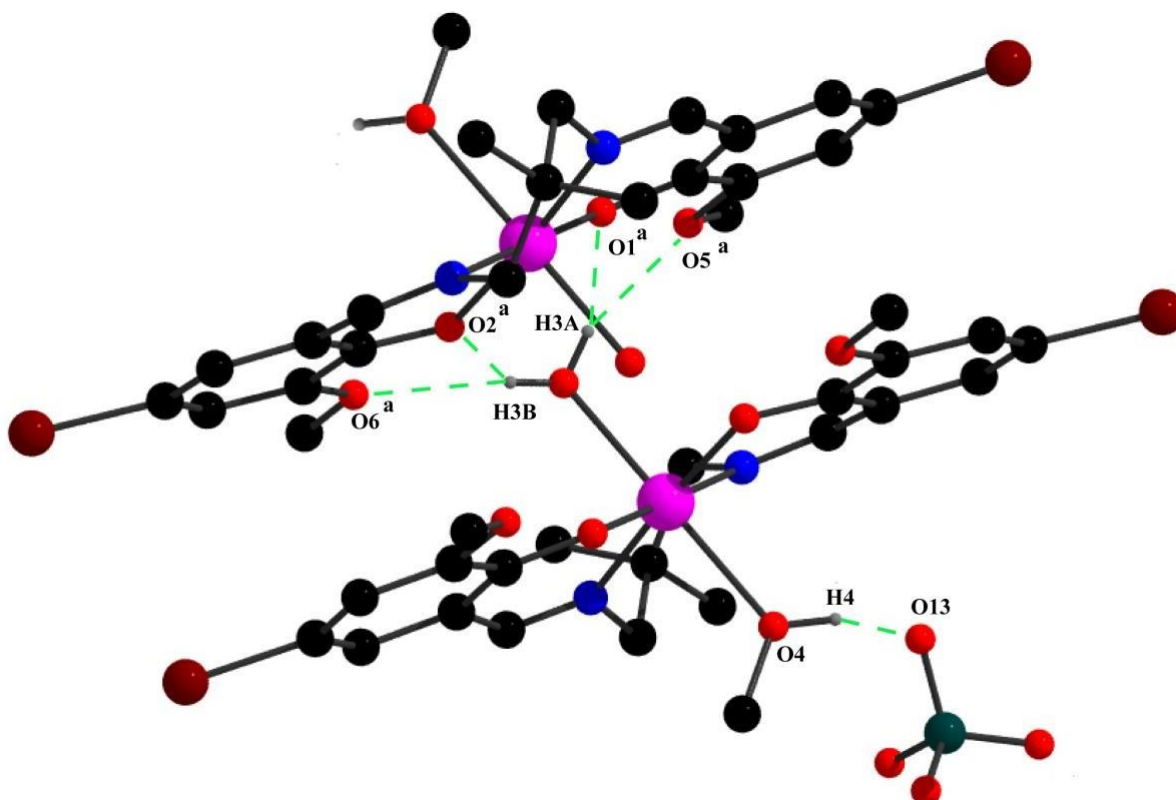
Fig. II.B.3: Hydrogen bonding interactions in the complex **4** (sub unit A). Only the relevant atoms have been shown for clarity.

Table II.B.6: Hydrogen bond distances (Å) and angles (∘) of the complex **4:**

D–H⋯A	D-H	H⋯A	D⋯A	∠D-H⋯A
O(3)-H(3A)⋯O(1) [a]	0.9000	2.3400	3.012(4)	131.00
O(3)-H(3A)⋯O(5) [a]	0.9000	2.0200	2.840(4)	152.00
O(3)-H(3B)⋯O(2) [a]	0.9500	2.1500	2.891(4)	134.00
O(3)-H(3B)⋯O(6) [a]	0.9500	2.0600	2.917(3)	149.00
O(10)-H(10A)⋯O(7) [b]	0.9000	2.3000	3.056(4)	141.00
O(10)-H(10A)⋯O(11) [b]	0.9000	2.1000	2.898(4)	146.00
O(10)-H(10B)⋯O(8) [b]	0.8000	2.2700	2.925(4)	138.00
O(10)-H(10B)⋯O(12) [b]	0.8000	2.0800	2.804(4)	149.00
O(4)-H(4)⋯O(13)	0.87(6)	2.10(6)	2.959(7)	170(5)
O(9)-H(9)⋯O(19) [c]	0.69(5)	2.09(5)	2.765(7)	166(6)

D = donor; H = hydrogen; A = acceptor Symmetry transformation: [a] = -x,1-y,-z, [b] = 1-x, 2-y,1-z, [c]= 1-x,1-y,1-z.

In Fig. **II.B.5a**, a partial view of the X-ray packing of the complex **4** has been represented where an infinite 1D supramolecular chain is represented. This 1D assembly is generated by the interaction of self-assembled π-stacked dimers, which are the monomeric units. Each monomeric unit establishes six halogen bonding interactions involving the bromine atoms at both ends of the complex **4** thus generating the polymeric chain. Curiously, the Br⋯Br interactions correspond halogen bonds of type I. That is, the geometry of the C–Br⋯Br–C contact in the solid state of the complex **4** exhibits similar C–Br⋯Br angles (Fig. **II.B.5a**)

instead of the most favoured combination (type II, one angle close to 180⁰ and the other close to 90⁰).
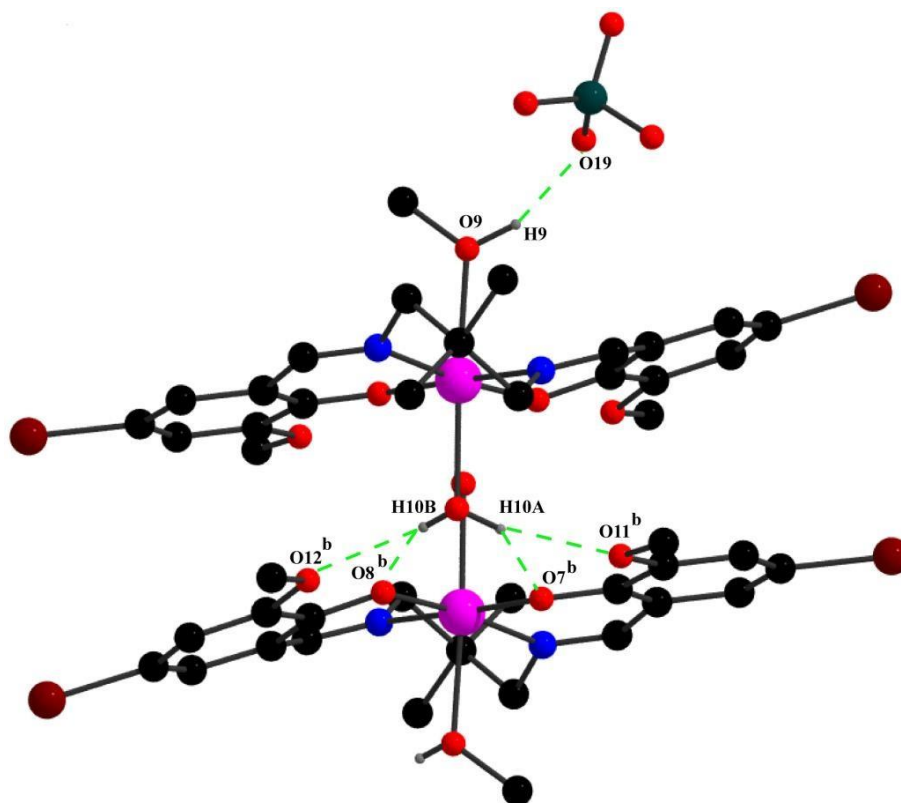

Fig. II.B.4.: Hydrogen bonding interactions in the complex **4** (sub unit B). Only the relevant atoms have been shown for clarity.

First the MEP surface of this complex has been computed in order to analyze the electron rich and electron poor parts of the molecule (Fig. **II.B.5b**). It is worth mentioning that the hydrogen atoms of the coordinated water molecule present large values of MEP due to the enhanced acidity of these protons as a consequence of the coordination to the Mn(III) metal center. As expected the most negative part corresponds to the perchlorate anion. In addition, there is another region of the surface where the MEP value is negative which corresponds to the cavity formed by the four oxygen atoms of the ligand. Therefore, the self–assembled dimer (Fig. **II.B.5c**) is stabilized by electrostatically enhanced hydrogen bonds that are established between the hydrogen atoms of water and the four oxygen atoms of the

organic ligand that is also facilitated by the geometric complementarities. Consequently, the interaction energy is very large and negative ($\Delta E_1 = -86.4$ kcal/mol) due to the simultaneous formation of eight strong hydrogen bonds and two additional π-stacking interactions, which further stabilize the assembly.
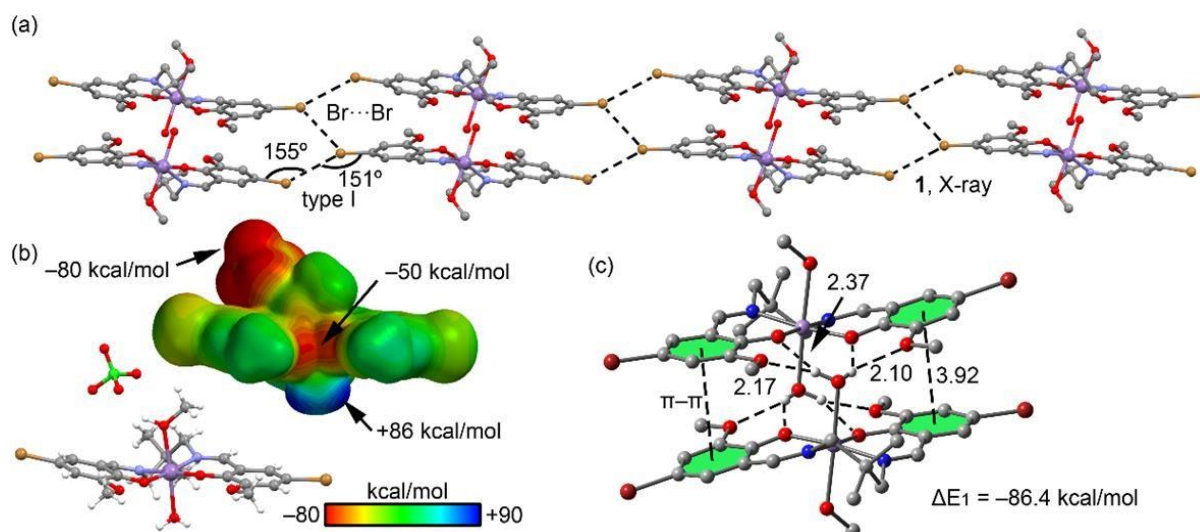
Fig. II.B.5: (a) 1D supramolecular chain observed in the X-ray solid state structure of the complex. H-atoms are omitted for clarity. (b) The MEP surface (isodensity = 0.001 a.u.) of the complex. The values are selected points of the surface are indicated. (c) Theoretical model used to evaluate the interaction energy.

The binding energy of the halogen bonding interaction has also been computed using a two monomeric retrieved from the infinite 1D chain. In Fig. **6a**, a representation of the MEP surface has been represented focused to the bromine atom and using a smaller energy range to finely differentiate the negative and positive regions. It can be appreciated that the distribution around the bromine atom is anisotropic, with a negative value at the location of the lone pairs and positive at the extension of the C–Br bond (ζ-hole). The interaction energy (computed as the interaction of two dimers) is very small $\Delta E_2 = -4.8$ kcal/mol, thus suggesting that each individual Br···Br interaction is very weak. This is common in type I

halogen bonding interactions, where the region with negligible MEP value of each Br atom interacts (weak van der Waals forces).

The "noncovalent Interaction plot" (NCI plot) index has also been computed in order to characterize the interactions in the Br···Br assembly of the complex. The NCI plot is an intuitive visualization index that enables the identification of non-covalent interactions easily and efficiently. The NCI plot is convenient to analyse host–guest interactions since it clearly shows which molecular regions interact. The colour scheme is a red-yellow-green-blue scale with red (repulsive) and blue (attractive). Yellow and green surfaces correspond to weak repulsive and weak attractive interactions, respectively. The representation of the NCI plot is shown in Fig. **II.B.6**. As noted, the halogen bonds are characterized by the presence of a small green isosurface that is located between the bromine atoms. The NCI plot shows the existence of a green and more extended isosurface between the π-systems of the ligands, confirming the existence of π-interactions that also contribute to the formation of the self-assembled dimers. Finally, this analysis also reveals a weak interaction (green isosurface) between the bromine atoms of the π-stacked dimers.
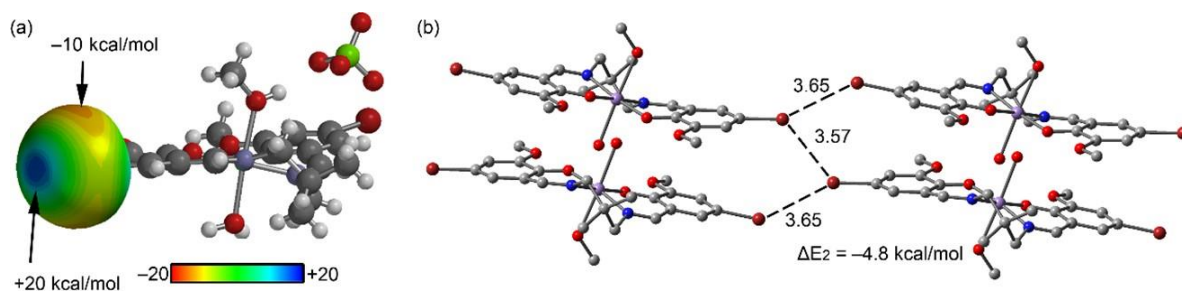
Fig. II.B.6: (a) Open MEP surface of the complex (isosurface 0.001 a.u.). (b) Theoretical model used to evaluate the Br···Br interactions. Hydrogen atoms are omitted for clarity.

II.B.3.4. Hirshfeld surface analysis

Hirshfeld surfaces of the complex **4**, mapped over d_{norm}, shape index and curvedness, have been illustrated in Fig. **II.B.7**.
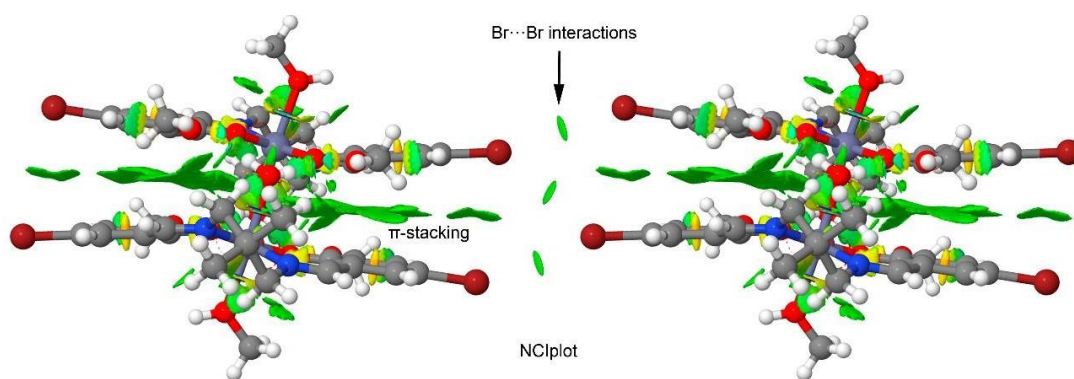

Fig. II.B.6: NCI surface of the assembly in the complex. The gradient cut-off is s = 0.35 au, and the color scale is −0.04 < ρ < 0.04 au.

Additional visible spots of light colour correspond to mainly C···H/H···C and H···H contacts have been also observed in the Hirshfeld surfaces signifying weaker and longer interaction. In addition, two dimensional fingerprint plots (Fig. **II.B.8**) represent the difference between the intermolecular interaction patterns and the relative contributions (in percentage) for the major intermolecular interactions associated with the complex **4**. The intermolecular interactions appear as distinct spikes in two dimensional fingerprint plots (Fig. **II.B.8**). In the 2D fingerprint plots, complementary regions are also visible where one molecule acts as a donor ($d_e > d_i$) and the other as an acceptor ($d_e < d_i$).

II.B.3.5. Spectral analysis of the complex 4

The IR and electronic spectra of the complex **4** are in well agreement with its crystal structure. The IR and electronic spectra of the complex are depicted in Figures **II.B.9** and **II.B.10**, respectively.
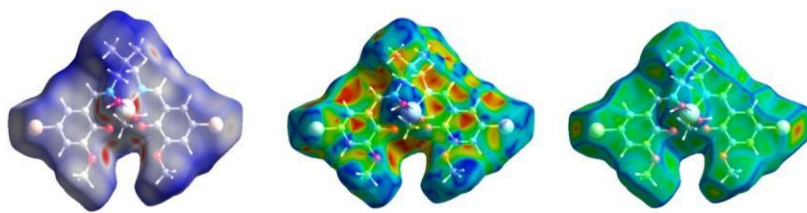
Fig. II.B.7: Hirshfeld surfaces mapped with d_{norm} (left), shape index (middle) and curvedness (right) of the complex **4**.

In the IR spectrum of the complex, distinct band due to the azomethine (C=N) group at 1611 cm^{-1} is customarily noticed.[37] Strong absorption band at c.a. 1090 cm^{-1} region indicates the presence of non-coordinated perchlorate anion in the complex.[38-39] Bands in the range of 2970–2830 cm^{-1} due to alkyl C–H bond stretching vibrations are typically noticed in IR spectra of the complex.[40-41] Broad absorption bands centered at around 3420 cm^{-1} due to O–H stretching vibrations of the coordinated water molecule, are observed in IR spectra of all complexes.[42-44]
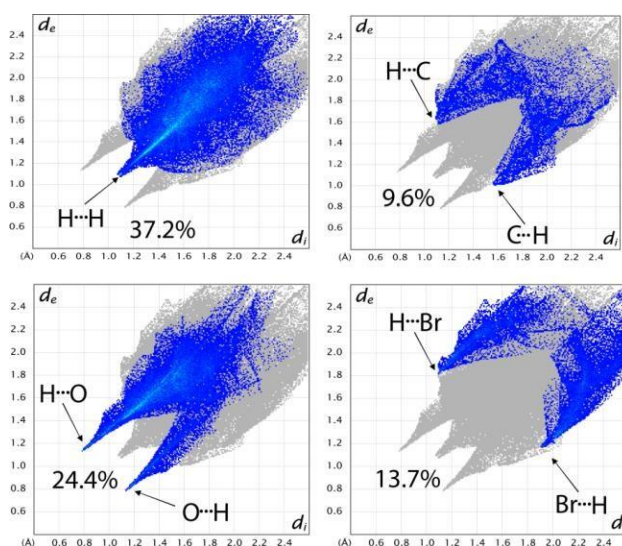
Fig. II.B.8: Two dimensional fingerprint plots of the complex: Resolved into H···H (top left), H···C/C···H (top right), H···O/O···H (bottom left) and H···Br/Br···H (bottom right) contacts contributed to the total Hirshfeld Surface area of the complex **4**.

Electronic spectrum of the complex consists of four major regions of absorptions. Intense absorption band in the high energy region of 240 and 294 nm may be assigned as intra-ligand n→π* and π→π* transitions, respectively involving the aromatic rings.[45-47] Strong and broad absorption band at 410 nm may be attributed to the ligand to metal charge transfer (LMCT) transitions from the phenolate oxygen $p_\pi \rightarrow d_{\pi*}$ of metal orbital.[45-47] The complex shows an absorption shoulder at 540 nm for the manganese(III) based d-d transition.[48-49]

The presence of a manganese(III) in complex **4** is supported by the room temperature solid state magnetic moments close to ~4.98 μB. This value is suggestive of magnetically non-coupled high spin manganese(III) complexes (d^4, $S = 2$).[45-47]
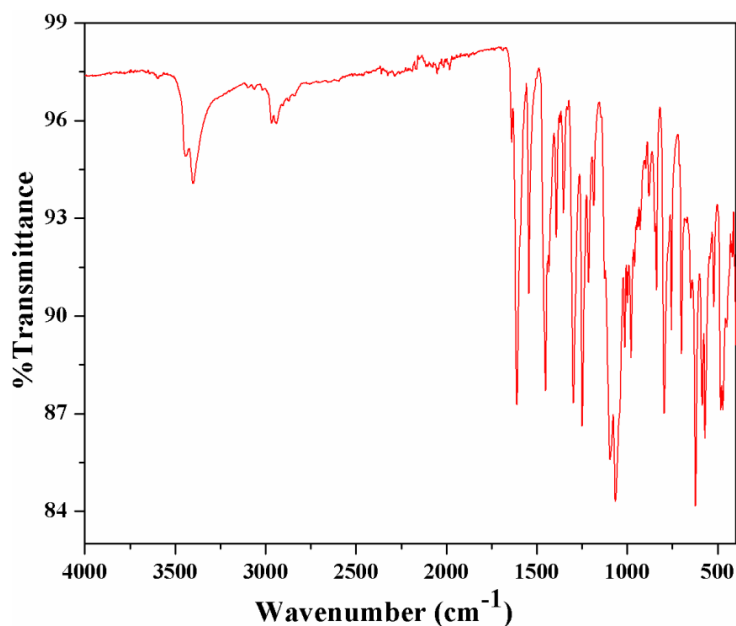
Fig. II.B.9: Infrared spectrum of the complex **4**.

II.B.3.6. Catalytic decomposition of hydrogen peroxide

The catalytic activity of the synthesized mononuclear manganese(III) complex towards disproportionation of hydrogen peroxide was investigated in DMF medium at 25°C.

The catalytic activity of the complex was tested by measuring the evolved dioxygen from a specific amount of 30% (v/v) hydrogen peroxide. Initially, colour of the complex solution
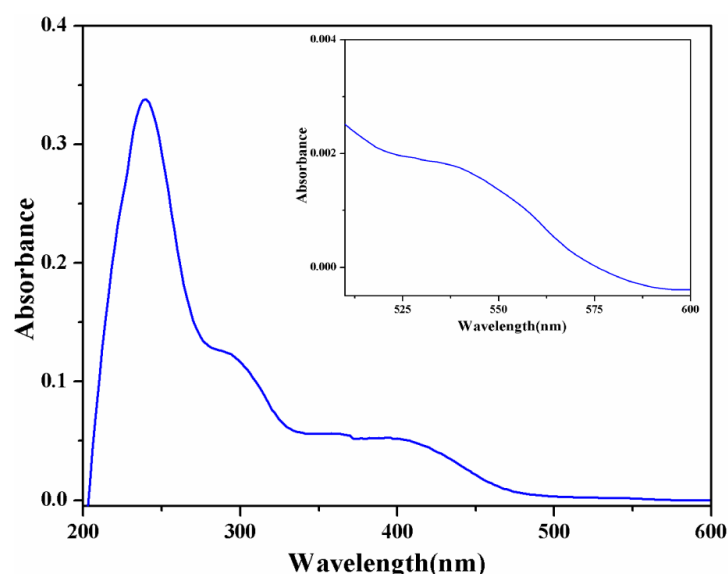

Fig. II.B.10: Electronic spectrum of the complex **4** in acetonitrile medium.

was dark brown but after addition of 30% (v/v) hydrogen peroxide, instantaneous evolution of a gas was observed followed by a change of solution colour from dark brown to fade yellow and after several hours the solution became colorless. It can be easily understand that the evolved gas is oxygen and it comes from the catalytic decomposition of hydrogen peroxide solution. Volumetric measurements of this evolved oxygen confirmed that the complex is sufficiently able to catalyzed disproportionation reaction of hydrogen peroxide. The course of oxygen evolution by the complex in DMF medium at room temperature is illustrate in Fig. **II.B.11**. To investigate the catalytic activity of the complex (5 mL 10^{-3} M) towards catalytic decomposition of H_2O_2, three sets of experiments were carried out with different initial amount of H_2O_2 solution (20, 30, 40 mL 30% v/v). The volume of evolved oxygen indicates that for constant complex concentration the rate of decomposition increases with increase in the initial amount of hydrogen peroxide. The evolution profile suggests the involvement of a fast catalytic process occurring at the initial stage. The rate of evolution of

oxygen becoms slower as the time progresses. Turnover number (TON) is defined as the number of moles of oxygen evolved per mole of the catalyst. Efficiency of the complex at different initial amount of hydrogen peroxide is shown in the turn over number (TON) versus time plot in Fig. **II.B.12**.

A probable mechanistic pathway for the catalytic decomposition of hydrogen peroxide has also been shown in Scheme **II.B.3**.
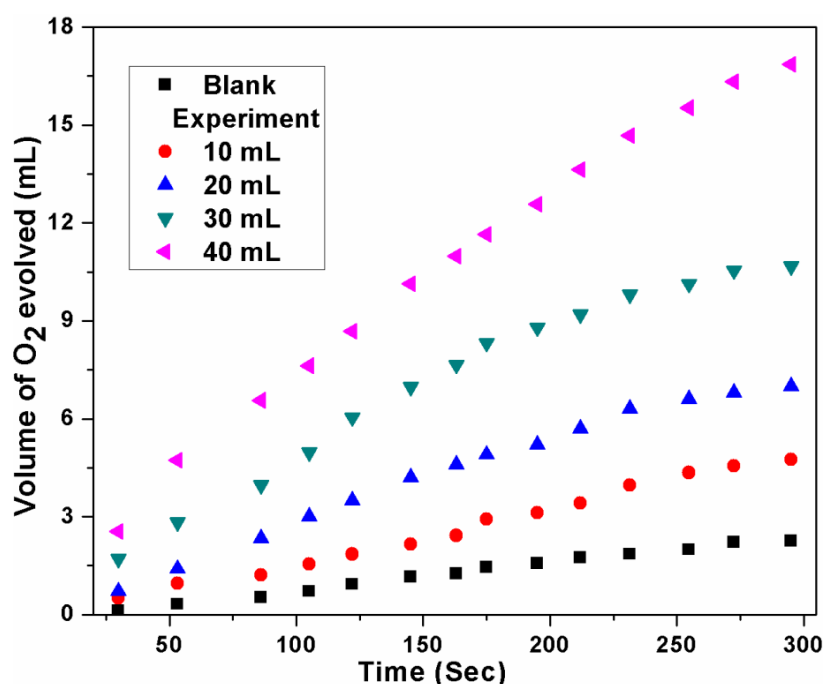

Fig. II.B.11: Time dependence of oxygen evolution upon reaction of the complex **4**(10^{-3} M) in DMF medium with different initial amount of 30 % (v/v) hydrogen peroxide at 25 °C. A blank experiment in presence of 30 mL H_2O_2 has also been included.

It is clear from the catalytic cycle that during the catalytic cycle, manganese(III) is oxidised to manganese(IV) by replacing one axially coordinated ligand simultaneously H_2O_2 is reduced to H_2O.

Subsequently, molecular oxygen is generated when the catalyst regenerates to its original form. Similar tentative catalytic cycles have also been proposed by several other groups.[22, 48,]

[49] Turn over numbers values for the catalytic decomposition of hydrogen peroxide using various amounts of 30% (v/v) H_2O_2 are gathered in **Table II.B.7**. Since two molecules of H_2O_2 on decomposition liberates one molecule of oxygen, if V_t and V_{inf} denote the volumes of oxygen given out at any time t and at the completion of reaction, then $(V_{inf}-V_t)$ is proportional to the amount of undecomposed H_2O_2 at time t.
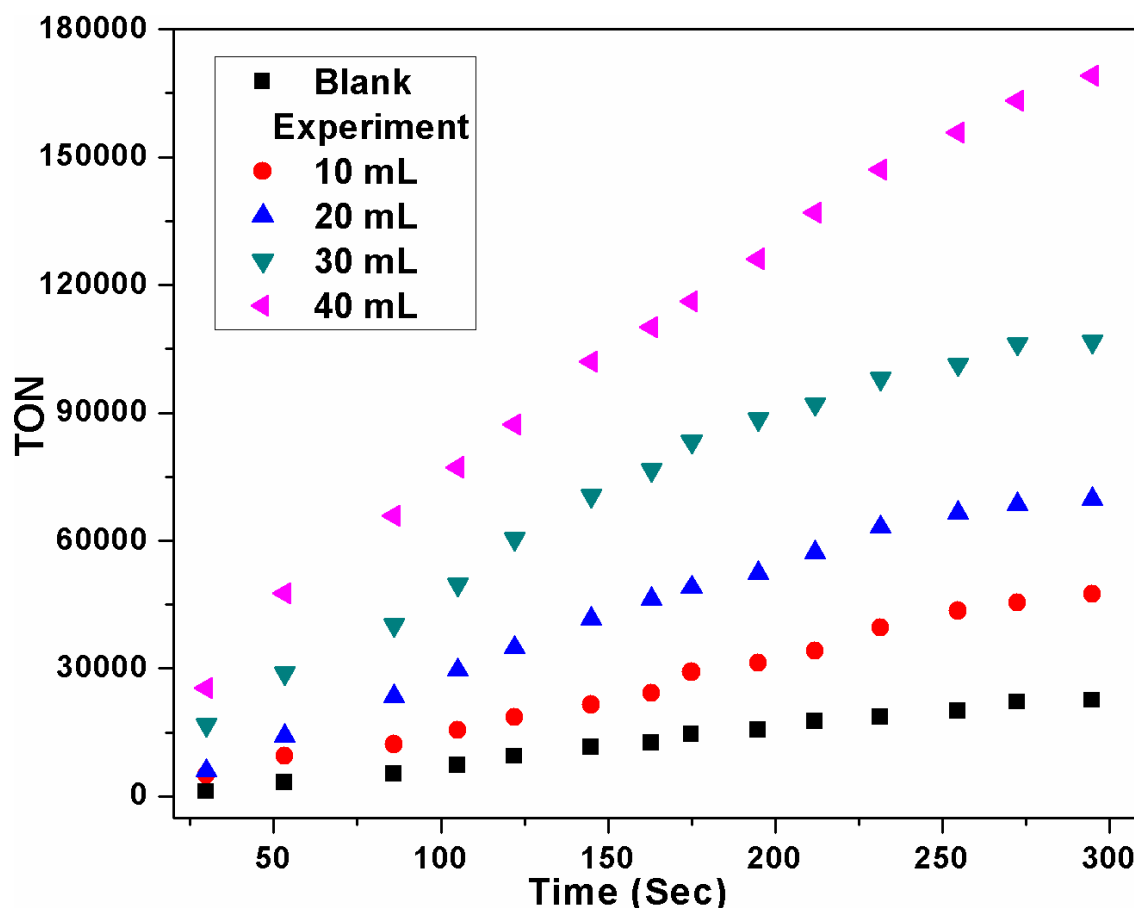

Fig. II.B.12: Turnover number {[Evolved O_2]/[Catalyst]) vs time plot in the different initial amount of H_2O_2 in DMF medium at 25 °C.

Substitution of experimental data (**Table II.B.8**) revealed constancy in the value of rate constant (k), confirming first order kinetics. From Figure **II.B.11**, it can also be clearly understood that at constant catalyst concentration, decomposition of H_2O_2 exhibits rate saturation kinetics. A few previously reported similar type mononuclear manganese(III)

complexes were found to be active towards catalytic decomposition of hydrogen peroxide. Some of these previously reported complexes are gathered in Table **Table II.B.9**.

II.B.3.7. Conclusions

In conclusion, one mononuclear Schiff base manganese(III) complex has been synthesized and structurally characterized. In solid state, the complex exhibits type I halogen bonding interactions along with conventional hydrogen bonding and $\pi\cdots\pi$ stacking interactions. Analysis of energies associated to these interactions has been conducted using DFT calculations, and further corroborated with NCI plot index computational tool. In addition, the catalytic activity of the complex toward the disproportionation of hydrogen peroxide has been investigated. The catalytic experiment results indicated that the complex has good catalase activity and may be used as suitable functional model for the pseudo-catalase enzyme.
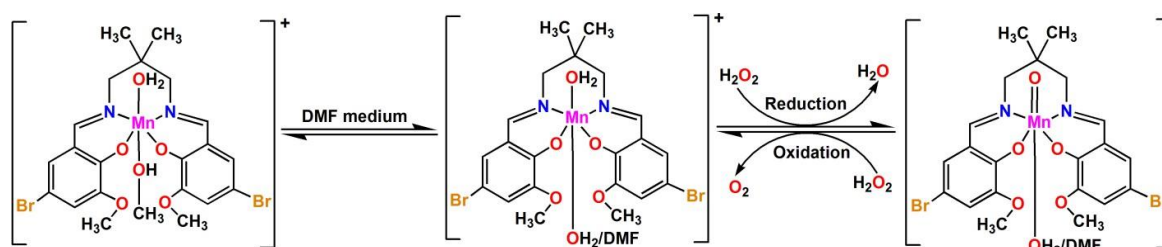
Scheme II.B.3: Possible mechanistic pathway for the catalytic disproportionation of hydrogen peroxide.

Table II.B.7: Turn over number values of the titled complex towards catalytic decomposition of hydrogen peroxide using various amounts of 30% (v/v) H_2O_2.

	Volume of H_2O_2 added		
Time (sec)	20 mL	30 mL	40 mL
	(TON X 10^3)	(TON X 10^3)	(TON X 10^3)
30	5949.07	16782.41	25509.26
53	14074.07	29571.76	48379.63
85	23402.77	40254.63	65833.33
104	30173.61	50335.65	77870.37
121	34837.96	61018.52	87951.39
145	42210.65	71099.53	102094.91
162	47025.46	76516.20	110069.44
175	49733.79	83287.04	116840.28
195	52291.66	88553.24	126921.29
212	57708.33	92013.88	137002.31
231	63726.85	98032.41	147685.18
255	67187.50	101342.59	156412.04
271	69143.52	106759.26	163784.722
295	69745.37	106759.26	169953.704

Table II.B.8: Kinetic order for decomposition of H_2O_2 {50 mL 30% (v/v)} in presence of the complex **4**.

Time (s)	$(V_t/V_{inf} - V_t)$	$\log(V_t/V_{inf} - V_t)$	K (s^{-1})
163	1.858350951	0.269127734	0.003802461
175	2.219047619	0.346166622	0.004555553
195	2.797752809	0.44680934	0.005276933
212	3.970588235	0.598854851	0.006505485

Table II.B.9: Maximal turnover number (TON) values for catalase mimicking activity of some previously reported mononuclear manganese(III) complexes.

Complex	Ligand donor Sites	TON	References
MnL^4	N$_3$O$_3$	>300	50
Mn(X-L^5)(OAc)	N$_2$O$_2$	2.5-8.4	51
Mn(L^{6}R)(OAc)	N$_3$O$_2$	4–17	52
Na[Mn(L^7)(H$_2$O)].5H$_2$O	N$_2$O$_2$	178	53
Na[Mn(L^8)(MeOH)].4H$_2$O	N$_2$O$_2$	25.2	53
Mn(L^9)Y ; Y= N$_3$/SCN	N$_2$O$_3$	1200	54
MnL^{10}(OTf)$_2$	N$_5$	7	55
MnL^{11}(OTf)$_2$	N$_3$O$_2$	55	55
MnL^{12}(OTf)$_2$	N$_3$S$_2$	39	55
MnL^{13}Cl$_2$	N$_4$	600	56
[MnL^{14}Cl]ClO$_4$·MeOH	N$_5$	600	56
Mn(L^{15})$^+$	N$_4$O	4	57

$[Mn(L^{16})Cl_2](CH_3OH)$	N_3	75-83	58
$[Mn(L^{17})(SO_4)(H_2O)]_n$	NO	320	59
$[Mn(L^{18})_2]_n$	N_2O_2	918	60
$[Mn(L^{19})(L^{20})_2].4.5H_2O$	NO_2, N_4	1110	60
$Mn(L^{20})(L^{21})(H_2O)$	NO_2, N_4	1374	60
$[Mn(L^{22})(CH_3OH)_2]ClO_4$	N_2O_2	29	28

[Catalyst]= 10 μM; $[H_2O_2]$ = 10 mM.

$H_3{}^4$ = 1-[N-(2-pyridylmethyl),N-(2-hydroxybenzyl)amino]-3-[N′-(2-hydroxybenzyl),N′-(4-methylbenzyl)amino]propan-2-ol; H_2L^5 = N,N'-bis(salicylidene)ethane-1,2-diamine; X = phenyl-ring substituent; R = cyclopentane-fused with ureido or acid–base catalyst auxiliary; H_2L^6 = N,N'-bis(3-methoxysalicylidene)ethane-1,2-diamine; H_2L^7 = 1,3-bis(5-sulphonatosalicylidenamino)propan-2-ol; H_2L^8 = 1,3-bis(5-sulphonatosalicylidenamino)propane; H_2L^9 = 1,4-bis(salicylidenamino)butan-2-ol; L^{10} = 2,6-bis[(N-methyl(2-pyridylmethyl)amino)methyl]pyridine; L^{11} = 2,6-bis[((2-pyridylmethyl)oxy)methyl]pyridine; L^{12} = 2,6-bis[((2-pyridylmethyl)sulpho)methyl]pyridine; L^{13} = 1-(benzimidazol-2-ylmethyl)-1,4,7-triazacyclononane; L^{14} = 1,4-bis(benzimidazol-2-ylmethyl)-1,4,7-triazacyclonone); HL^{15} = N-(2-hydroxybenzyl)-N,N′-bis[2-(Nmethylimidazolyl); L^{16} = 1,3-bis(2 -pyridylimino)-isoindolinemethyl]ethane-1,2-diamine; HL^{17} = 2-hydroxymethylpyridine; H_2L^{18} = 2-pyrazine carboxylic acid; L^{19} = 2,2,,-bipyridine; H_2L^{20} = 2,6-pyridinedicarboxylic acid; L^{21} = 4-hydroxypyridine-2,6-dicarboxylic acid; H_2L^{22} = N,N'-bis(1-(1'-hydroxy-2-naphthyl)ethylidene)propane-1,3-diamine.

References

1 P. Wei, X. Yan, F. Huang. *Chem. Soc. Rev*., 2015, **44,** 815.

2 A. Benrjee, A. Fontera, S. Chattopadhyay. *Dalton Trans*., 2019, **48**, 11433.

3 G. Mahmoudi, V. Stilinović, M. S. Gargari, A. Bauzá, G. Zaragoza, W. Kaminsky, V. Lynch, D. Choquesillo-Lazarte, K. Sivakumar, A. A. Khandari, A. Frontera. *CrystEngComm*, 2015, **17,** 3493.

4 H. W. Roesky, M. Andruh. *Coord. Chem. Rev*., 2003, **236,** 91.

5 S. Tsuzuki, A. Fujii. *Phys. Chem. Chem. Phys*., 2008, **10,** 2584.

6 T. R. Cook, Y. -R. Zheng, P. J. Stang. *Chem. Rev*., 2013, **113**, 734.

7 T. T. T. Bui, S. Dahaoui, C. Lecomte, G. R. Desiraju, E. Espinosa. *Angew. Chem. Int. Ed*., 2009, **48**, 3838.

8 L. C. Gilday, S. W. Robinson, T. A. Barendt, M. J. Langton, B. R. Mullaney, P. D. Beer. *Chem. Rev*., 2015, **115**, 7118.

9 M. Fourmigué, P. Batail. *Chem. Rev*., 2004, **104**, 5379.

10 G. Cavallo, P. Metrangolo, R. Milani, T. Pilati, A. Priimagi, G. Resnati, G. Terraneo. *Chem. Rev*., 2016, **116**, 2478.

11 B. Moulton, M. J. Zaworotko. *Chem. Rev*., 2001, **101**, 1629.

12 P. Metrangolo, H. Neukirch, T Pilati, G. Resnati. *Acc. Chem. Res*., 2005, **38**, 386.

13 P. Metrangolo, F. Meyer, T. Pilati, G. Resnati, G. Terraneo. *Angew. Chem. Int. Ed*., 2008, **47**, 6114.

14 F. Meyer, P. Dubois. *CrystEngComm*, 2013, **15**, 3058.

15 G. R. Desiraju, R. Parthasarathy. *J. Am. Chem. Soc.*, 1989, **111**, 8725.

16 D. A. Safin, M. G. Babashkina, K. Robeyns, Y. Garcia. *RSC Adv.*, 2016, **6**, 53669.

17 P. Metrangolo, G. Resnati. *Chem. Commun.*, 2013, **49**, 1783

18 A. Mukherjee, S. Tothadi, G. R. Desiraju. *Acc. Chem. Res.*, 2014, **47**, 2514.

19 N. Sarkar, K. Harms, A. Bauzá. A. Frontera, S. Chattopadhyay. *ChemistrySelect*, 2017, **2**, 2975.

20 K. Ghosh, S. Roy, A. Ghosh, A. Banerjee, A. Bauzá, A. Frontera, S. Chattopadhyay. *Polyhedron*, 2016, **112**, 6.

21 K. Ghosh, K Harms, S Chattopadhyay. *Polyhedron*, 2017, **123**, 162.

22 T. Basak, A. Bhattacharyya, K. Harms, S. Chattopadhyay. *Polyhedron*, 2019, **157**, 449.

23 T. Basak, A. Bhattacharyya, M. Das, K. Harms, A. Bauzá, A. Frontera, S. Chattopadhyay. *ChemistrySelect*, 2017, **2**, 6286.

24 S. Roy, M. G. B. Drew, S. Chattopadhyay. *Polyhedron*, 2018, **150**, 28.

25 J. Zhou, Y. Chen, L. Lan, C. Zhang, M. Pan, Y. Wang, B. Han, Z. Wang, J. Jiao, Q. Chen. *Anal. Biochem.*, 2019, **567**, 51.

26 Á. Dancs, N. V. May, K. Selmeczi, Z. Darula, A. Szorcsik, F. Matyuska, T. Páli, T. Gajda. *New J. Chem.*, 2017, **41**, 808.

27 S. Das, A. Sahu, M. Joshi, S. Paul, M. Shit, A. R. Choudhury, B. Biswas. *ChemistrySelect*, 2018, **3**, 10774.

28 N. Sarkar, P. K. Bhaumik, S. Chattopadhyay. *Polyhedron*, 2016, **115**, 37.

[50] 29 K. Ghosh, K. Harms, A. Bauzá, A. Frontera, S. Chattopadhyay. *Dalton Trans*., 2018, **47**, 331.

[51] 30 L. M. Manus, R. J. Holbrook, T. A. Atesin, M. C. Heffern, A. S. Harney, A. L. Eckermann, T. J. Meade. *Inorg. Chem*., 2013, **52**, 1069.

[52] 31 A. Hazari, L. K. Das, Ramakant M. Kadam, A. Bauzá, A. Frontera, A. Ghosh. *Dalton Trans*., 2015, **44**, 3862.

[53] 32 N. Sarkar, M. G. B. Drew, K. Harms, A. Bauzá, A. Frontera, S. Chattopadhyay. *CrystEngComm*, 2018, **20**, 1077.

[54] 33 N. Sarkar, M. Das, S. Chattopadhyay. *Inorg. Chim. Acta*, 2017, **457**, 19.

[55] 34 N. Sarkar, K. Harms, A. Frontera, S. Chattopadhyay. *New J. Chem*., 2017, **41**, 8053.

[56] 35 D. Cremer, J. A. Pople. *J. Am. Chem. Soc*., 1975, **97**, 1354.

[57] 36 D. G. Evans, J. C. A. Boeyens. *Acta Cryst*., 1989, **B45**, 581.

[58] 37 K. Nakamoto, Infrared Spectra of Inorganic and Coordination Compounds, Fourth ed., Wiley, New York, 1986.

[59] 38 R. P. Scholer, A. E. Merbach. *Inorg. Chim. Acta*, 1975, **15**, 15.

[60] 39 R. Salmasi, A. Salimi, M. Gholizadeh, M. Rahmani, J. C. Garrison. *J. Mol. Struct*., 2019, **1179**, 549.

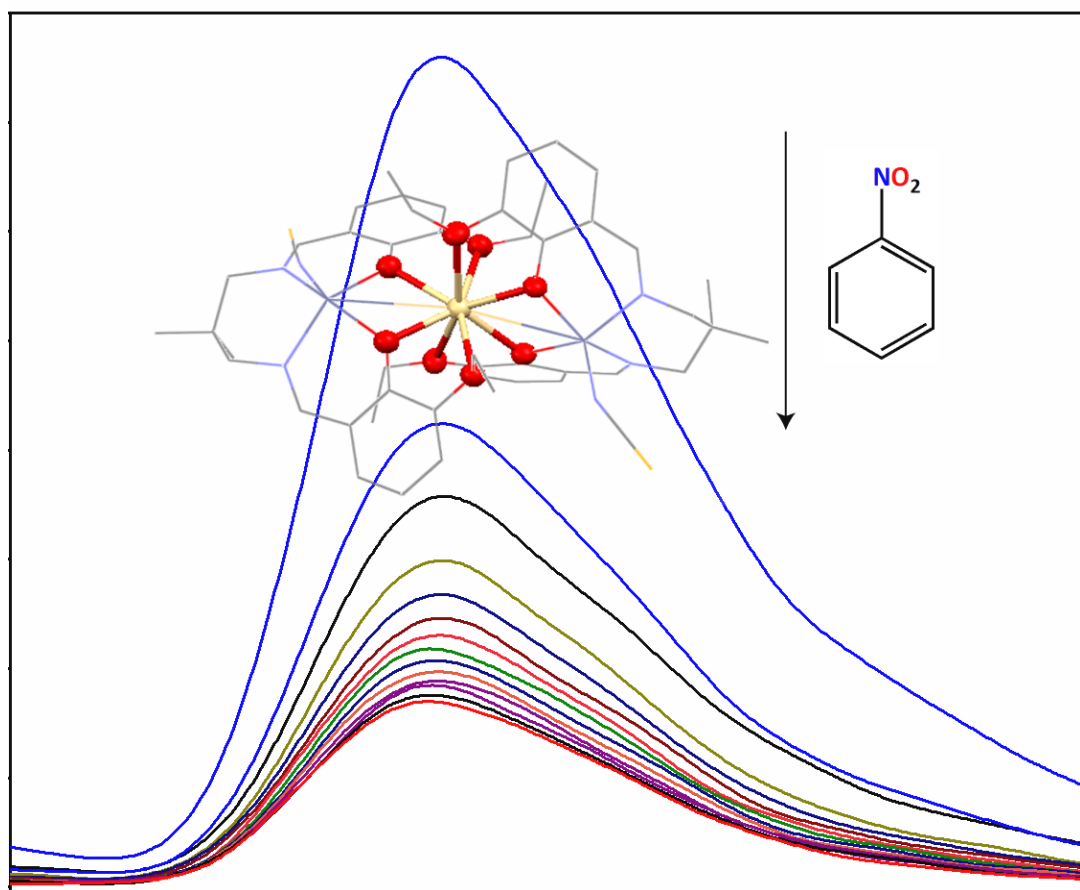[61] 40 K. Ghosh, K. Harms, A. Bauzá, A. Frontera, S. Chattopadhyay. *Dalton Trans*., 2018, **47**, 331.

[62] 41 K. Ghosh, K. Harms, S. Chattopadhyay. *ChemistrySelect*, 2017, **2**, 8207.

[63] 42 M. Das, S. Chattopadhyay. *Polyhedron*, 2013, **50**, 443.

[64] 43 A. Bhattacharyya, K. Harms, S. Chattopadhyay. *Inorg. Chem. Commun.*, 2014, **48**, 12.

[65] 44 J.-B. Brubach, A. Mermet, A. Filabozzi, A. Gerschel, P. Roy. *J. Chem. Phys.*, 2005, **122**, 184509.

[66] 45 N. Sarkar, M. G. B. Drew, K. Harms, A. Bauzá, A. Frontera, S. Chattopadhyay. *CrystEngComm*, 2018, **20**, 1077.

[67] 46 N. Sarkar, M. Das, S. Chattopadhyay. *Inorg. Chim. Acta*, 2017, **457**, 19.

[68] 47 N. Sarkar, K. Harms, A. Frontera, S. Chattopadhyay. *New J. Chem.*, 2017, **41**, 8053.

[69] 48 A. Rey, J.A. Zazo, J.A. Casas, A. Bahamonde, J.J. Rodriguez. *Appl. Catal., A, General*, 2011, **402**, 146.

[70] 49 K. C. Gupta, A. K. Sutar. Coord. *Chem. Rev.*, 2008, **252**, 1420.

[39] 50 G. N. Ledesma, H. Eury, E. A. Mallart, C. Hureau, S. R. Signorella. *J. Inorg. Biochem.*, 2010, **104**, 496.

[40] 51 S. R. Doctrow, K. Huffman, C. Bucay Marcus, G. Tocco, E. Malfroy, C.A. Adinolfi, H. Kruk, K. Baker, N. Lazarowych, J. Mascarenhas, B. Malfroy. *J. Med. Chem.*, 2002, **45**, 4549.

[41] 52 Y. Noritake, N. Umezawa, N. Kato, T. Higuchi. *Inorg. Chem.*, 2013, **52**, 3653.

[42] 53 D. Moreno, V. Daier, C. Palopoli, J.-P. Tuchagues, S. Signorella. *J. Inorg. Biochem.*, 2010, **104**, 496.

[43] 54 V. Daier, D. Moreno, C. Duhayon, J.-P. Tuchagues, S. Signorella. *Eur. J. Inorg. Chem.*, 2010, 965.

[44] 55 M. Grau, F. Rigodanza, A.J.P. White, A. Soraru, M. Carraro, M. Bonchio, G. J. P. Britovsek. *Chem. Commun.*, 2014, **50**, 4607.

[45] 56 Q. X. Li, Q.-H. Luo, Y.Z. Li, Z.Q. Pan, M.C. Shen. *Eur. J. Inorg. Chem.*, 2004, 4447

[46] 57 A.S. Bernard, C. Giroud, H.Y.V. Ching, A. Meunier, V. Ambike, C. Amatore, M.G. Collignon, F. Lemaître, C. Policar. *Dalton Trans.*, 2012, **41,** 6399.

[47] 58 J. Kaizer, T. Csay, P. Kovari, G. Speier, L. Parkanyi. *J. Mol. Catal. A Chem.*, 2008, **280**, 203.

[48] 59 M. Zienkiewicz, J. Szlachetko, C. Lothschütz, M. Hodorowicz, A. Jabłońska-Wawrzycka, J. Sá, B. Barszcz. *Dalton Trans.*, 2013, **42**, 7761.

[49] 60 M. Devereux, M. McCann, V. Leon, V. McKee, R.J. Ball. *Polyhedron*, 2002, **21**, 1063.

Chapter III

Trigonal dodecahedral cadmium(II) complex with zinc(II)-salen type metalloligand: Synthesis, structure, self-assembly and application in sensing of nitroaromatics.

III.1. Introduction

Although crown ethers, cryptands and related ligands are particularly good classes of complexing agents for alkali and 3d metal ions,[1] there are many other simpler and certainly more affordable ligands that are also extremely effective in this respect.[2] One such ligand is N,N'-bis(3-methoxysalicylidene)propane-1,3-diamine,[3] produced by the condensation of 3-methoxysalicaldehyde and 1,3-diaminopropane. This compartmental Schiff base has already been used exhaustively to prepare varieties of hetero-bimetallic 3d/4f complexes.[4] Structure determination showed that the 3d metals were placed in the N_2O_2 compartment of the ligand whereas lanthanide ions were placed in the O_4 compartment in all the complexes without exception.[5] The metal centres in many such complexes were found to be ferromagnetically coupled.[6] The ligand has also been used to prepare linear trinuclear complexes.[7] Many such complexes were found to show SMM behavior.[8] Many other compartmental Schiff bases, e.g. N,N'-bis(3-ethoxysalicylidene)propane-1,3-diamine, N,N'-bis(3-methoxysalicylidene)ethane-1,2-diamine, N,N'-bis(3-methoxysalicylidene)-2,2-dimethylpropane-1,3-diamine etc have also been used to prepare many such homo and heteronuclear complexes.[9] Nitroaromatic compounds are potential explosive, highly toxic in nature and are serious pollution sources of environment.[10] So, the detection of nitroaromatic compounds is an important area of current research. Moreover, fluorescence based detection has recently been considered as one of the most promising techniques for explosive detection.[11]

In the present work, a compartmental Schiff base ligand, N,N'-bis(3-ethoxysalicylidene)-2,2-dimethylpropane-1,3-diamine (H_2L^5) has been used to prepare a hetero-trimetallic complex, Cd{L^5Zn(NCS)}$_2$ **(5)**, where cadmium(II) is exhibiting octa-coordinate trigonal dodecahedral geometry. Although several trinuclear cadmium(II) complexes having similar formula were reported in literature,[12] there is only two crystal structures reported of any trinuclear zinc(II)-cadmium(II)-zinc(II) complex with

compartmental Schiff bases.[13] The complex acts as turn-off fluorescence chemosensor for detection of various nitroaromatics.

III.2. Experimental Section

III.2.1 Synthesis

III.2.1.1. Synthesis of H$_2$L^5 [N,N'-bis(3-ethoxysalicylidene)-2,2-dimethylpropane-1,3-diamine]

A methanol solution (10 mL) of 3-ethoxysalicylaldehyde (332 mg, 2 mmol) and 2,2-dimethyl-1,3-diaminopropane (0.13 mL, 1 mmol) was refluxed for ca. 1 h. The ligand was not isolated but used directly for the synthesis of the complex **5**.

III.2.1.2. Synthesis of Cd{LZn(NCS)}$_2$ (5)

A methanol (10 mL) solution of zinc(II) acetate dihydrate (219 mg, 1 mmol) was added to the methanol solution (20 mL) of H$_2$L^5 and the resulting solution was stirred for 15 min. After that a methanol (10 mL) solution of cadmium(II) acetate dihydrate (266 mg, 1 mmol) was added to it and stirred for another 15 min. Finally a methanol solution of sodium thiocyanate (81 mg, 1 mmol) was added and the solution was stirred for about 2 h. Few drops of DMF was added and the resulting solution was kept for crystallization. Single crystals, suitable for X-ray diffraction, were obtained after 3-4 days on slow evaporation of the filtrate in open atmosphere.

Yield: 432.09 mg, 75% [based on zinc(II)]. Anal. Calc. for C$_{48}$H$_{56}$CdN$_6$O$_8$Zn$_2$S$_2$ (FW = 1152.24): C, 50.03; H, 4.90; N, 7.29%. Found: C, 50.1; H, 4.8; N, 7.3%. FT-IR (KBr, cm^{-1}): 1634 (C=N); 2079(NCS); 2900 (C-H). UV-Vis [λ_{max} (nm)] [ε_{max} (L mol^{-1} cm^{-1})] (DMF): 274 (4.12×10^4); 364 (1.71×10^4).

III.3. Results and Discussion

III.3.1. Synthesis

2,2-dimethyl-1,3-diaminopropane was refluxed with 3-ethoxysalicylaldehyde in 1:2 ratio to form a N_2O_4 donor Schiff base ligand (H_2L^5) following the literature method.[14] The Schiff base (H_2L^5) on reaction with zinc(II) acetate dehydrate, cadmium(II) acetate dihydrate followed by the addition of sodium thiocyanate and few drops of DMF produced the complex. Formation of the complex has been shown in Scheme **III.1**.
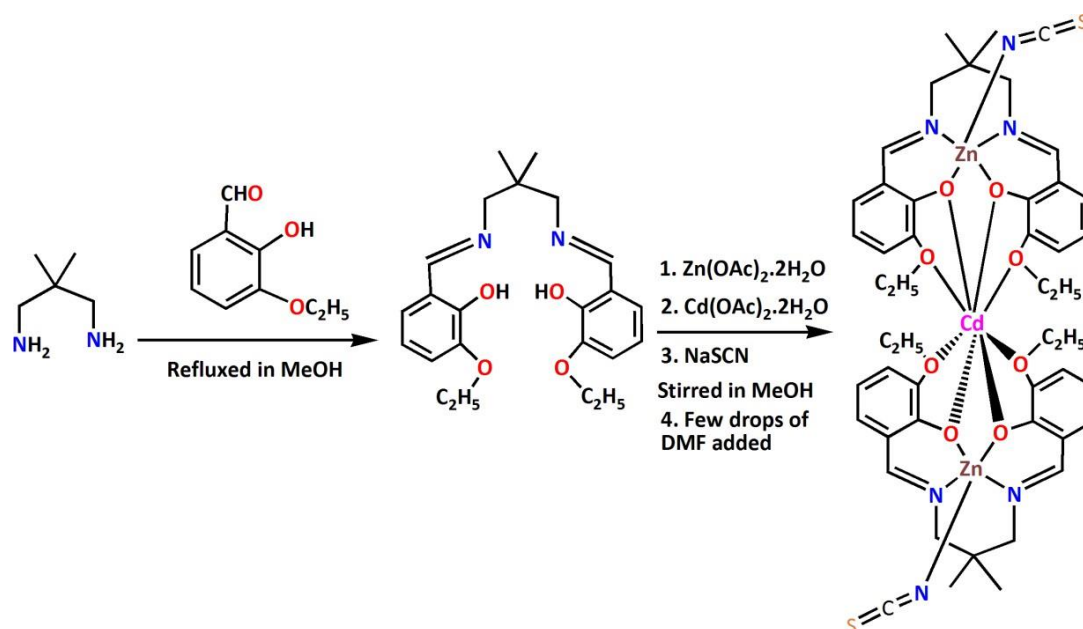
Scheme III.1: Preparation of the ligand and the complex.

III.3.2. Structure description

The X-ray crystal structure determination revealed that the complex **5** crystallizes in monoclinic space group $P2_1/c$. Crystallographic data and refinement details are given in Table **III.1**. The molecular structure of the complex is built from isolated hetero-trinuclear molecules of $Cd\{L^5Zn(NCS)\}_2$. The complex consists of two terminal „metalloligands" (ZnL), one central cadmium and two thiocyanate co-ligands as shown in **Fig. III.1**. Important bond lengths and bond angles have been gathered in Tables **III.2** and **III.3** respectively.

H_2L^5 is a N_2O_4 donor compartmental Schiff base with inner N_2O_2 and outer O_4 compartments with zinc(II) centres occupying the inner N_2O_2 cavity and keeping the outer O_4 cavity vacant. Thiocyanate coordinates with zinc(II) of ZnL^5 moiety to produce $(SCN)ZnL^5$. Two such $(SCN)ZnL^5$ moieties, in turn, coordinate one cadmium(II) centre through eight oxygen atoms of two outer O_4 compartments of the ligand. $(SCN)ZnL^5$ moieties may, therefore, be considered as metalloligand. Zinc(II) and cadmium(II) centres assume square pyramidal and trigonal dodecahedral geometries respectively.

Table III.1: Crystal data and refinement details of the complex **5**.

Formula	$C_{48}H_{56}CdN_6O_8Zn_2S_2$
Formula Weight	1152.24
Temperature(K)	100
Crystal system	Monoclinic
Space group	$P2_1/c$
a (Å)	12.4207(3)
b (Å)	26.1757(8)
c (Å)	15.9278(4)
β (°)	108.520(2)
Z	4
d_{calc}(g cm^{-3})	1.559
μ (mm^{-1})	1.542
F (000)	2360
Total Reflections	44065
Unique Reflections	9116
Observed data [I > 2 ζ (I)]	6659
No. of parameters	632
R (int)	0.072

R1, wR2 (all data)	0.0647, 0.1356
R1, wR2 [I > 2 ζ (I)]	0.0467, 0.1293

CCDC reference no 1852257

Table III.2: Selected bond lengths (Å) of the complex **5**.

Cd(1)-O(1)	2.268(4)	Zn(1)-O(2)	2.082(4)
Cd(1)-O(2)	2.312(3)	Zn(1)-N(1)	2.093(5)
Cd(1)-O(3)	2.528(3)	Zn(1)-N(2)	2.071(4)
Cd(1)-O(4)	2.443(3)	Zn(1)-N(3)	1.987(5)
Cd(1)-O(5)	2.280(3)	Zn(2)-O(5)	2.033(3)
Cd(1)-O(6)	2.313(3)	Zn(2)-O(6)	2.064(3)
Cd(1)-O(7)	2.488(3)	Zn(2)-N(4)	2.104(4)
Cd(1)-O(8)	2.612(3)	Zn(2)-N(5)	2.103(4)
Zn(1)-O(1)	2.036(3)	Zn(2)-N(6)	1.987(4)

Table III.3: Selected bond angles (°) of the complex **5**

O(1)-Cd(1)-O(2)	67.90(12)	O(5)-Cd(1)-O(8)	132.40(12)
O(1)-Cd(1)-O(3)	66.99(12)	O(6)-Cd(1)-O(7)	134.48(12)
O(1)-Cd(1)-O(4)	134.24(12)	O(6)-Cd(1)-O(8)	63.81(11)
O(1)-Cd(1)-O(5)	135.22(12)	O(7)-Cd(1)-O(8)	155.32(11)
O(1)-Cd(1)-O(6)	124.67(12)	O(1)-Zn(1)-O(2)	76.78(14)
O(1)-Cd(1)-O(7)	93.97(12)	O(1)-Zn(1)-N(1)	87.42(16)
O(1)-Cd(1)-O(8)	81.75(12)	O(1)-Zn(1)-N(2)	152.57(17)
O(2)-Cd(1)-O(3)	134.50(13)	O(1)-Zn(1)-N(3)	105.94(17)
O(2)-Cd(1)-O(4)	66.90(13)	O(2)-Zn(1)-N(1)	140.97(16)
O(2)-Cd(1)-O(5)	137.83(11)	O(2)-Zn(1)-N(2)	87.12(17)
O(2)-Cd(1)-O(6)	133.29(11)	O(2)-Zn(1)-N(3)	117.99(17)
O(2)-Cd(1)-O(7)	79.83(11)	N(1)-Zn(1)-N(2)	91.57(18)
O(2)-Cd(1)-O(8)	76.04(11)	N(1)-Zn(1)-N(3)	100.5(2)
O(3)-Cd(1)-O(4)	158.60(12)	N(2)-Zn(1)-N(3)	101.19(19)

O(3)-Cd(1)-O(5)	76.23(12)	O(5)-Zn(2)-O(6)	79.35(13)
O(3)-Cd(1)-O(6)	79.60(11)	O(5)-Zn(2)-N(4)	87.22(15)
O(3)-Cd(1)-O(7)	97.60(11)	O(5)-Zn(2)-N(5)	145.30(15)
O(3)-Cd(1)-O(8)	102.91(10)	O(5)-Zn(2)-N(6)	116.21(17)
O(4)-Cd(1)-O(5)	85.60(12)	O(6)-Zn(2)-N(4)	151.68(14)
O(4)-Cd(1)-O(6)	83.52(11)	O(6)-Zn(2)-N(5)	87.66(15)
O(4)-Cd(1)-O(7)	84.91(11)	O(6)-Zn(2)-N(6)	110.64(16)
O(4)-Cd(1)-O(8)	81.00(11)	N(4)-Zn(2)-N(5)	89.51(17)
O(5)-Cd(1)-O(6)	69.43(11)	N(4)-Zn(2)-N(6)	97.65(17)
O(5)-Cd(1)-O(7)	65.89(12)	N(5)-Zn(2)-N(6)	98.46(18)

They [Zn(1) and Zn(2)] are coordinated with two imine nitrogen atoms [N(1), N(2) for Zn(1) and N(4), N(5) for Zn(2)] and two phenoxo oxygen atoms [O(1), O(2) for Zn(1) and O(5), O(6) for Zn(2)] of the deprotonated Schiff bases. The fifth site is coordinated by a nitrogen atom, [N(3) for Zn(1) and N(6) for Zn(2)] from thiocyanate co-ligand. The distortions of these geometries [around both zinc(II) centres] from square pyramid to trigonal bipyramid have been calculated by the Addison parameter (η).[15] The value of η is defined as the difference between the two largest donor metal-donor angles divided by 60, η is 0 for the ideal square pyramid and 1 for the trigonal bipyramid. The η values of Zn(1) and Zn(2) are 0.193 and 0.106 respectively, indicating that the geometries around zinc(II) centres are slightly distorted from their ideal square pyramidal geometry. The trans angles, N(1)-Zn(1)-O(2), N(2)-Zn(1)-O(1) [around Zn(1)] and N(5)-Zn(2)-O(5), N(4)-Zn(2)-O(6) [around Zn(2)] are found to be 141.0(2), 152.6(2), 145.3(1) and 151.7(1) respectively. For Zn(1) centre, the deviation of the coordinating atoms, O(1), O(2), N(1) and N(2) in the basal plane from the mean plane passing through them are -0.009(3), 0.224(3), 0.223(5), 0.222(5) Å respectively. The deviation of Zn(1) from the same plane is -0.459(6) Å. For Zn(2) centre, the deviation of the coordinating atoms O(5), O(6), N(4) and N(5) in the basal plane from the mean plane

passing through them are 0.166(3), 0.050(3), 0.063(4), 0.165(4) Å respectively. The deviation of Zn(2) from the same plane is -0.444(5) Å.

The saturated six membered chelate rings [Zn(1)–N(1)–C(10)–C(11)–C(14)–N(2)] and [Zn(2)–N(4)–C(34)–C(35)–C(38)–N(5)] have half chair conformations with puckering parameters q = 0.596(6) Å; θ = 6.8(5)°; ϕ = 211(4)° and q = 0.606(5) Å; θ = 8.8(4)°; ϕ = 151(3)° respectively.[16]
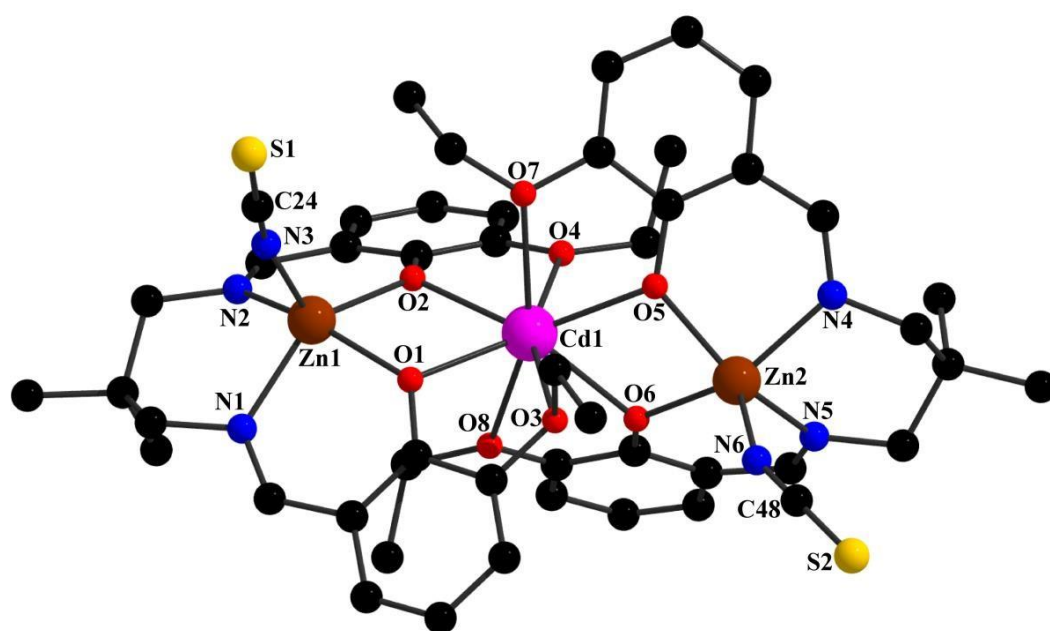
Fig. III.1: Perspective view of the complex with selective atom numbering scheme. Hydrogen atoms have been omitted for clarity.

The central cadmium is octa-coordinated by four phenoxy oxygen atoms and four ethoxy oxygen atoms of two deprotonated Schiff base ligands assuming a trigonal-dodecahedron geometry (Fig. **III.2**). The Cd-O(phenoxy) distances are larger [2.268(4)-2.313(4) Å] compared to the Cd-O(methoxy) distances [2.443(3)-2.612(3) Å]. The dihedral angle between the mean planes passing through [O(1)-O(2)-O(3)-O(4)] and [O(5)-O(6)-O(7)-O(8)] is 89.88°, suggesting that the Schiff base ligands are almost orthogonal to each other.
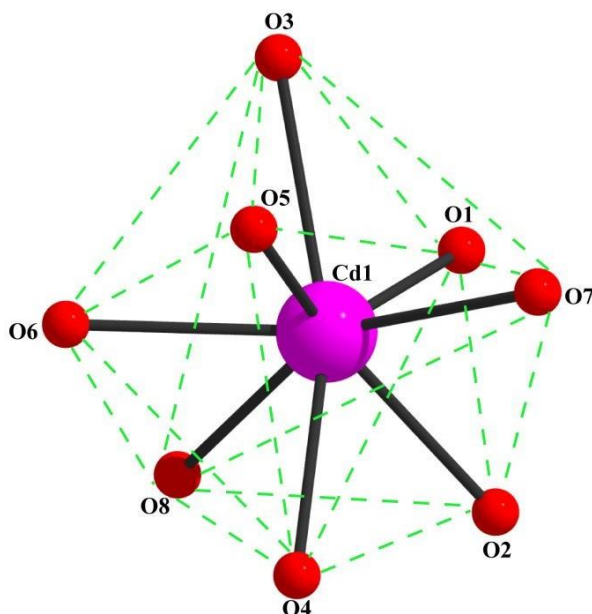
Fig. III.2: Trigonal dodecahedral geometry of cadmium(II) in the complex.

The distances between the metal centres are 3.507(8) Å for Cd(1)···Zn(1) and 3.432(8) Å for Cd(1)···Zn(2). The angles, Zn(1)-O(1)-Cd(1), Zn(1)-O(2)-Cd(1), Zn(2)-O(6)-Cd(1) and Zn(1)-O(5)-Cd(1) are 109.1(1), 105.8(1), 103.1(1) and 105.3(1) respectively.

The complex **5** shows two inter-molecular and one intra-molecular C-H···π interactions. The hydrogen atom, H(37A), attached to carbon atom, C(37), is involved in inter-molecular C-H···π interactions with the phenyl ring [C(3)–C(4)–C(5)–C(6)–C(7)–C(8)] forming a 1D structure (Fig. **III.3**). Similarly the hydrogen atom, H(42), attached to carbon atom, C(42), is involved in another inter-molecular C-H···π interactions with the phenyl ring [C(16)–C(17)–C(18)–C(19)–C(20)–C(21)] forming a zigzag structure (Fig. **III.4**). The hydrogen atom, H(23B), attached to carbon atom, C(23), shows a intra-molecular C-H···π interaction with the phenyl ring [C(27)–C(28)–C(29)–C(30)–C(31)–C(32)] as shown in **Fig. III.5**. The details of the geometric features of the C-H···π interactions are given in **Table III.4.**

Table III.4: Geometric features (distances in Å and angles in°) of the C-H⋯π interactions obtained for the complex 5.

X-H⋯Cg(Ring)	H⋯Cg	C-H⋯Cg	C⋯Cg
C(37)-	2.78	166	3.733(6)
C(42)-	2.86	143	3.668(5)
C(23)-	2.93	154	3.835(6)

Symmetry transformations: [a] = x,3/2-y,1/2+z; [b] = -1+x,y,z. Cg(7) = Centre of gravity of the ring, C(3)–C(4)–C(5)–C(6)–C(7)–C(8); Cg(8) = Centre of gravity of the ring, C(16)–C(17)–C(18)–C(19)–C(20)–C(21); Cg(9) = Centre of gravity of the ring, C(27)–C(28)–C(29)–C(30)–C(31)–C(32).
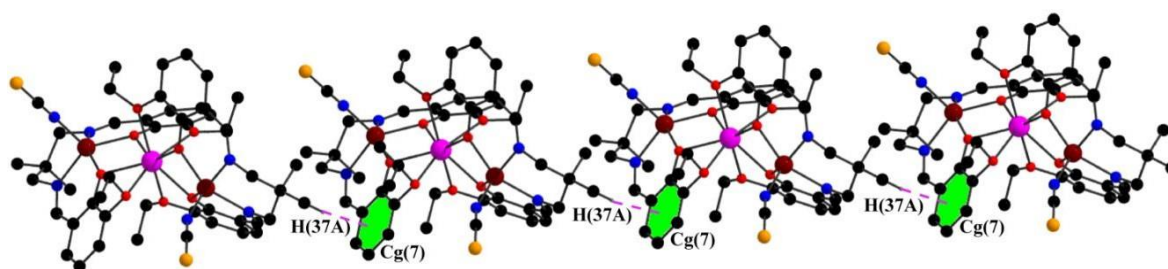
Fig. III.3: Perspective view of inter-molecular C-H⋯π interactions forming a 1D structure with selective atom numbering scheme. Only relevant atoms have been shown for clarity.

III.3.3. IR, UV-Vis and Fluorescence spectra

A sharp band around 1634 cm^{-1} due to azomethine (C=N) group has been routinely noticed in the IR spectrum of the complex.[17] A strong band at 2079 cm^{-1} in IR spectrum of the complex indicates the presence of thiocyanate.[18] Band around 2900 cm^{-1} in the IR spectrum of the complex has been observed due to alkyl C-H bond stretching.[19]
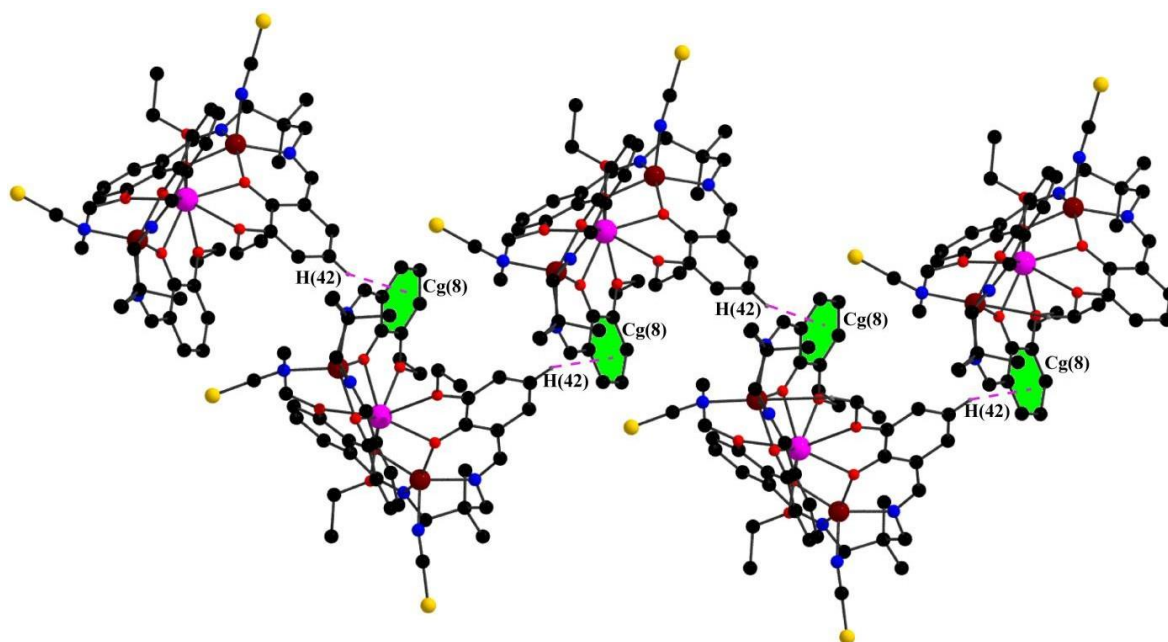
Fig. III.4: Perspective view of inter-molecular C-H···π interactions forming a zigzag structure with selective atom numbering scheme. Only relavant atoms have been shown for clarity.
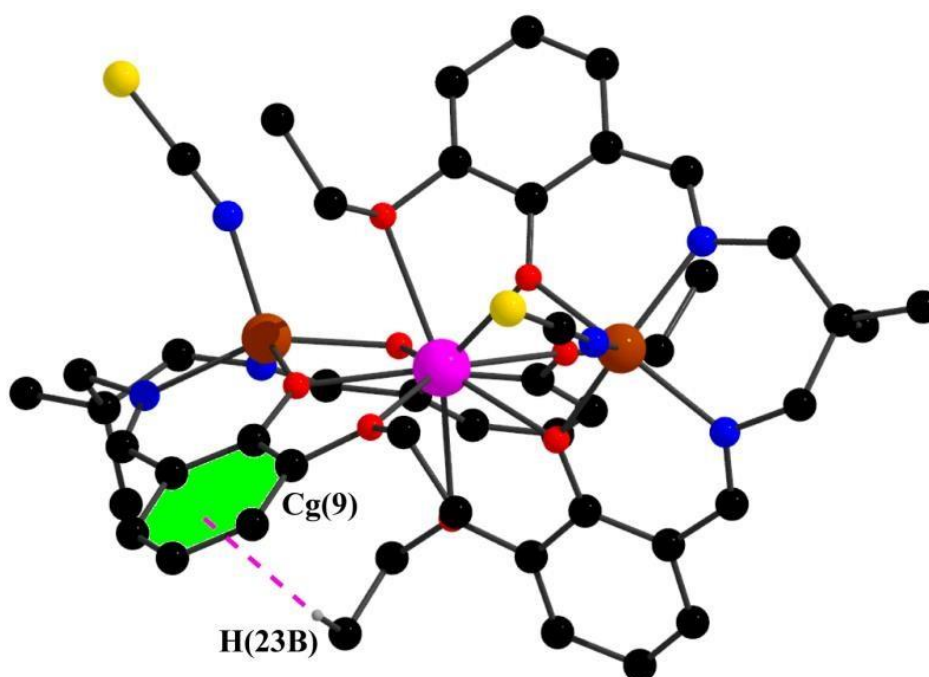
Fig. III.5: Perspective view of intra-molecular C-H···π interactions with selective atom numbering scheme. Only relavant atoms have been shown for clarity.

Electronic spectrum of the complex consists of two bands at 274 nm and 364 nmrespectively. The absorption band at 364 nm may be assigned as $\pi^* \leftarrow n$ transition.[20] Band at 274 nm may be assigned as $\pi^* \leftarrow \pi$ transitions respectively.[21]

The complex exhibits fluorescence in DMF. The fluorescence data have been listed in **Table III.5** (without solvent correction). These are assigned as intra-ligand ($\pi^* \leftarrow \pi$) fluorescence.[21] The mean lifetime (Γ_{avg}) of the exited state is 16 ns at room temperature. The fluorescence spectra of the complex along with the ligand has been shown in **Fig. III.6**.

Table III.5: Photophysical data for ligand and the complex.

	Absorption (nm)	Emission (nm)
Complex 1	270	460
Ligand (H_2L)	270	460
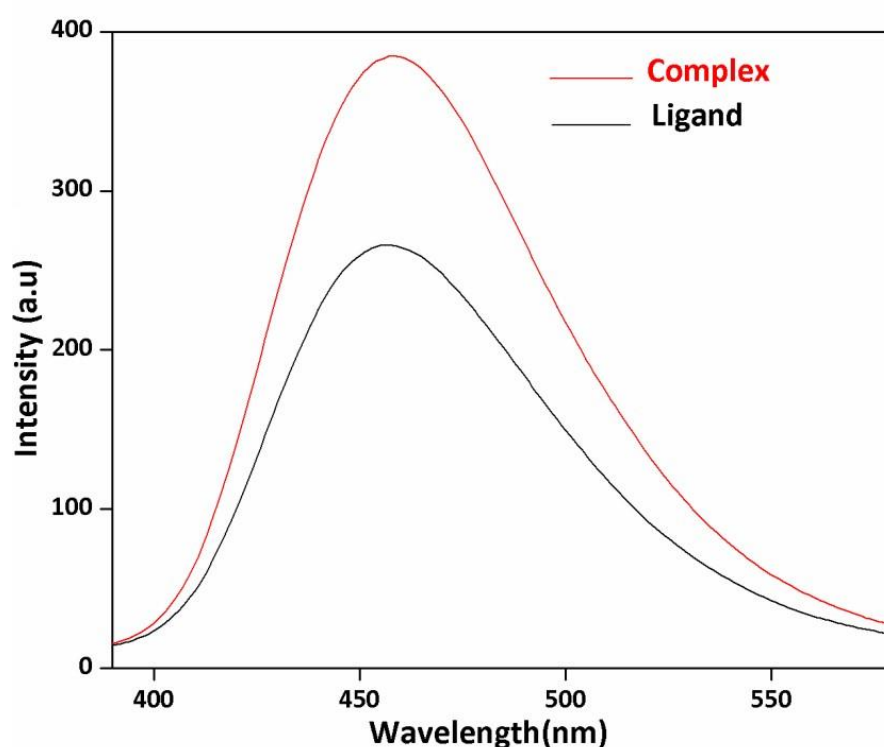
Fig. III.6: Fluorescence spectra of the ligand and the complex **5** in DMF (excitation wavelength 270 nm and conc. 10^{-5} M).

III.3.4. Nitro Sensing

The complex **5** has been found to be applicable as sensors for perilous organic analytes.

To find its applicability fluorescence spectra of the complex have been recorded in presence of organic analytes such as benzene, toluene and different nitroaromatics (3-nitrobenzoic acid, 3-methyl-4-nitrobenzoic acid, nitrobenzene and 1,3-dinitrobenzene). Although no quenching of fluorescence intensity has been observed upon addition of benzene and toluene, significant quenching of fluorescence intensity has been observed upon addition of different nitroaromatics (**Fig. III.7**). These observations tell that the complex can be used for the detection of nitroaromatics. The quenching of fluorescence intensity by nitroaromatics compared to other aromatics may be related with their more electron deficient nature.
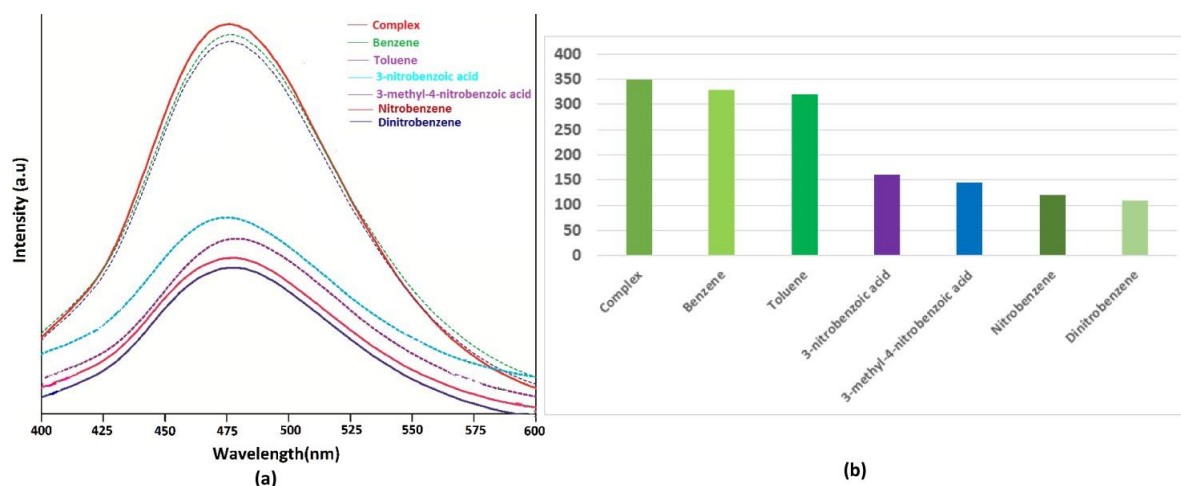
Fig. III.7: (a) Fluorescence spectra of the complex **5** in DMF (excitation wavelength 270 nm and conc. 10^{-5} M) upon the addition of various organic analytes. (b) Relative changes in fluorescent intensity of the complex in presence of various organic analytes.

The fluorescence titrations of the complex **5** by adding different nitroaromatics (3-nitrobenzoic acid, 3-methyl-4-nitrobenzoic acid, nitrobenzene and 1,3-dinitrobenzene) separately have been done in DMF solutions. In order to check these, fluorescence titrations of the complex (10^{-5} M) in DMF are performed by gradually adding (10 µL) nitroaromatics

(10^{-2} M) separately. The fluorescence intensity of the complex kept on decreasing with an increase in the concentration of nitroaromatics. The quenching of the fluorescence intensity of the complex in DMF with an increase in the concentration of nitroaromatics has been shown in **Fig. III.8**.
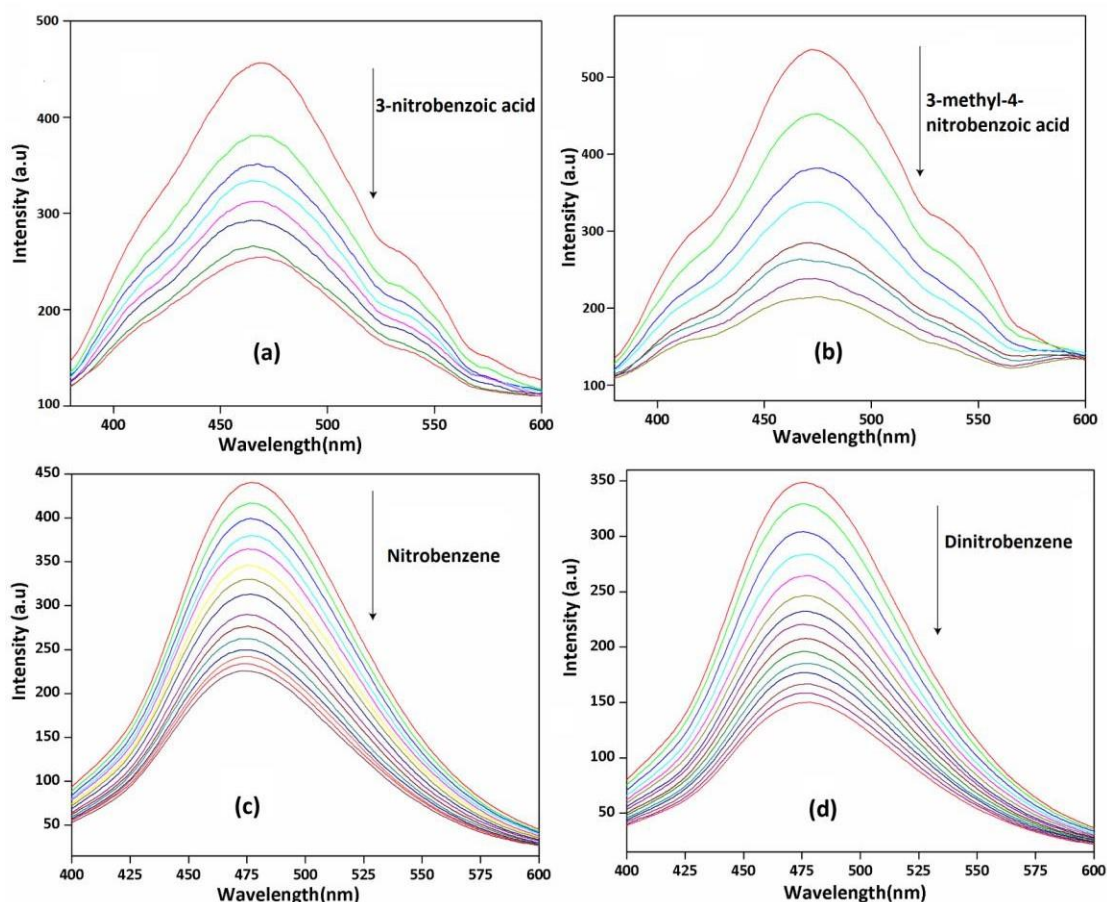

Fig. III.8: Fluorescence spectra of the complex **5** in DMF (excitation wavelength 270 nm and conc. 10^{-5} M) upon increasing concentration of 3-nitrobenzoic acid (a), 3-methyl-4-nitrobenzoic acid (b), nitrobenzene (c) and 1,3-dinitrobenzene nitrobenzene (d).

The efficient quenching by nitroaromatics can be explained considering the possibility of $\pi \cdots \pi$ interactions between nitroaromatics and the Schiff base complex, inducing electron transfer from the excited state of metal complex to the ground state of electron-deficient nitroaromatics. A schematic representation of electron transfer from the complex to nitrobenzene has been shown in **Fig. III.9**. The nitroaromatics with electron-deficient

property can obtain an electron from excited ligand,[22] which can be confirmed by molecular orbital theory.[22]
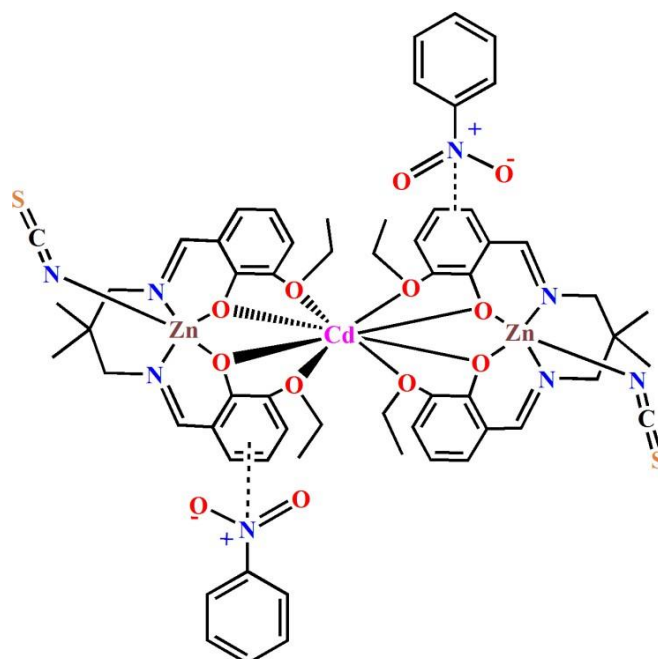
Fig. III.9: Schematic representation of electron transfer from the complex to nitrobenzene.

The quenching efficiency of nitroaromatics is quantitatively determined by the Stern-Volmer equation given below,

$$\frac{I_0}{I} = 1 + K_{sv}\,[Q]$$

Where, K_{SV} is the quenching constant (M^{-1}), $[Q]$ is the molar concentration of the quencher, I_0 and I are luminescence intensities before and after adding the quencher, respectively. At low concentrations, the Stern-Volmer plot of nitroaromatics is linear whereas at higher concentrations, consequently deviate from linearity and turn upward (Fig. 10), which may be due to self-absorption.[23] The Stern-Volmer quenching constants (K_{sv}) have been calculated from the slope of the linearly fitted curves (insets in **Fig. III.10**) and gathered in **Table III.6**.

The fluorescence titrations of the complex **5** by adding nitroaromatics have also been checked in different solvents (DMSO, CH$_3$CN, MeOH). For that nitrobenzene and dinitrobenzene

have been choosen arbitrarily and the plots have been shown in the Fig. **III.11**- **III.13**. The stern-Volmer plots of the complex with nitrobenzene and dinitrobenzene in different solvents have been given in the **Fig. III.14**- **III.16**. The Stern-Volmer quenching constants (K_{sv}) in different solvents have been gathered in Table **III.6**.
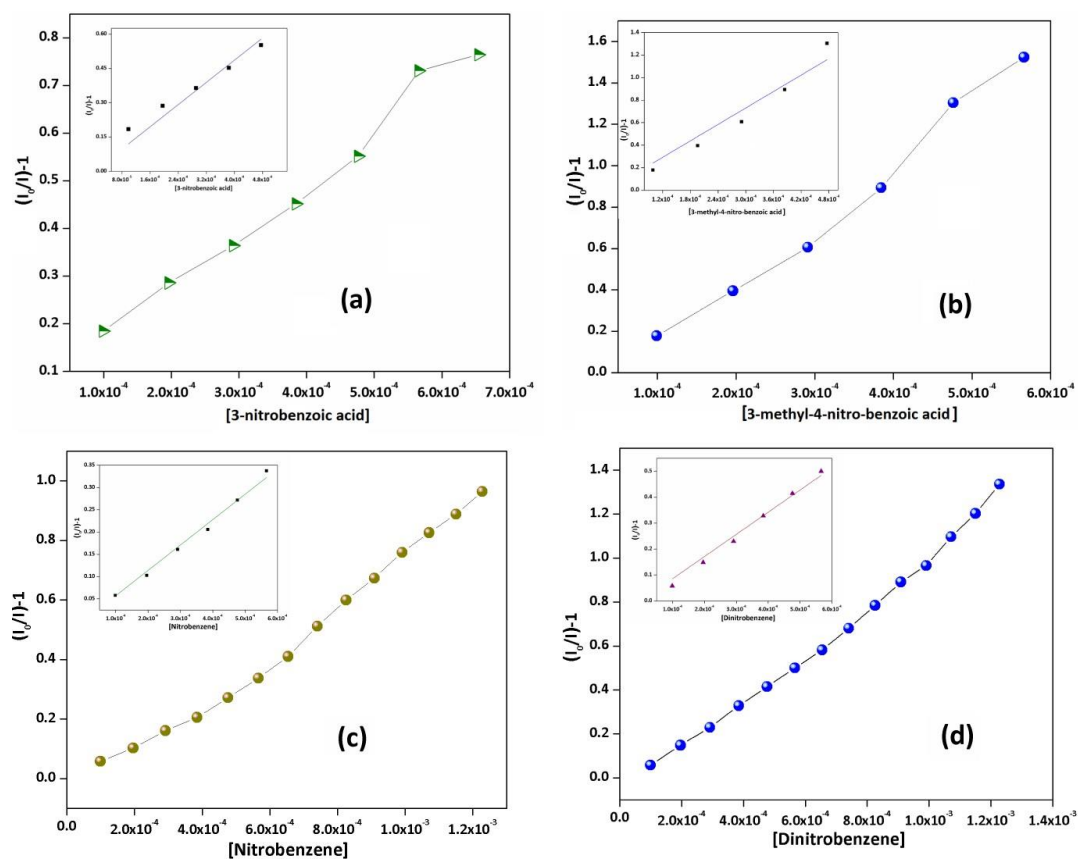

Fig. III.10: Stern-Volmer plot of the complex **5** with 3-nitrobenzoic acid (a), 3-methyl-4-nitrobenzoic acid (b), nitrobenzene (c) and 1,3-dinitrobenzene (d) in DMF.

Table III.6: Stern-Volmer constants of the complex **5** (K_{sv}) with different nitroaromatics in DMF.

3-nitrobenzoic acid	3-methyl-4-nitrobenzoic acid	Nitrobenzene	Dinitrobenzene
5.8×10^2	9.1×10^2	5.7×10^2	8.6×10^2

Relative fluorescence quantum yields for the complex have been measured in DMF using quinine sulfate (in 0.5 (M) H_2SO_4/ = 0.54) as the quantum yield standard.[24] The fluorescence quantum yield of the complex is 0.324. The quantum yield of the complex decreases after adding nitrobenzene and dinitrobenzene separately and the values are 0.136 and 0.094 respectively. Quantum yields have been calculated following the literature method.[25]
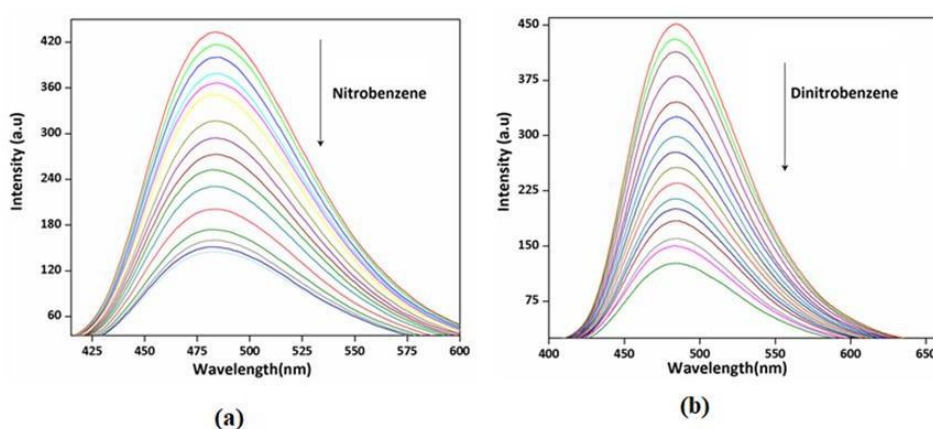
Fig. III.11: Fluorescence spectra of the complex in DMSO (excitation wavelength 270 nm and conc. 10^{-5} M) upon increasing concentration of nitrobenzene (a) and dinitrobenzene (b).
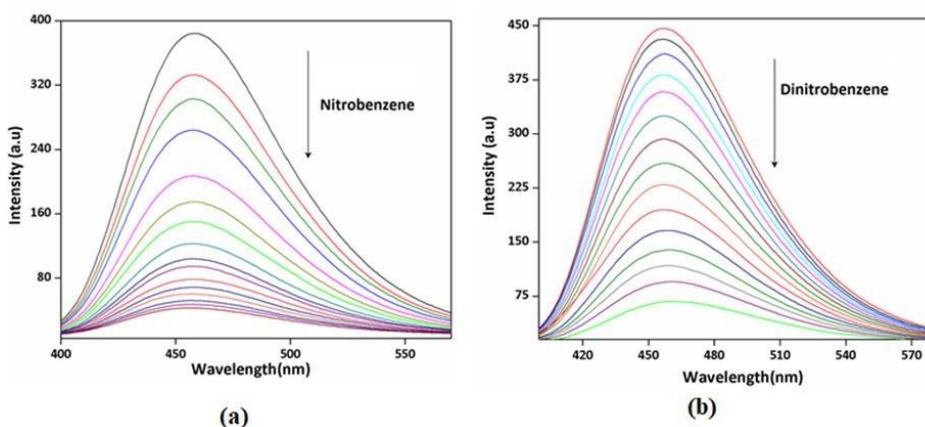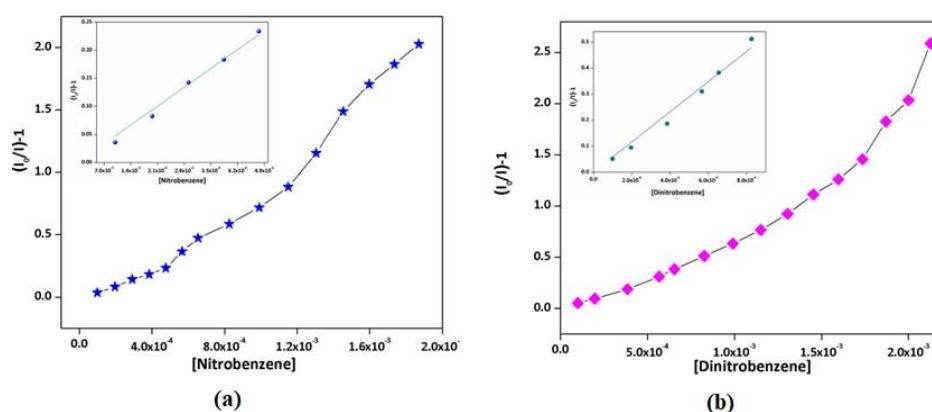

Fig. III.12: Fluorescence spectra of the complex in CH_3CN (excitation wavelength 270 nm and conc. 10^{-5} M) upon increasing concentration of nitrobenzene (a) and dinitrobenzene (b).
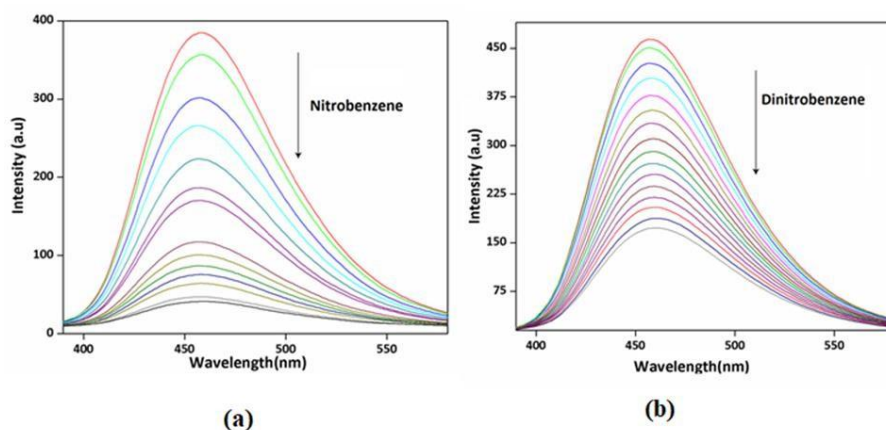
Fig. III.13: Fluorescence spectra of the complex in MeOH (excitation wavelength 270 nm and conc. 10^{-5} M) upon increasing concentration of nitrobenzene (a) and dinitrobenzene (b).

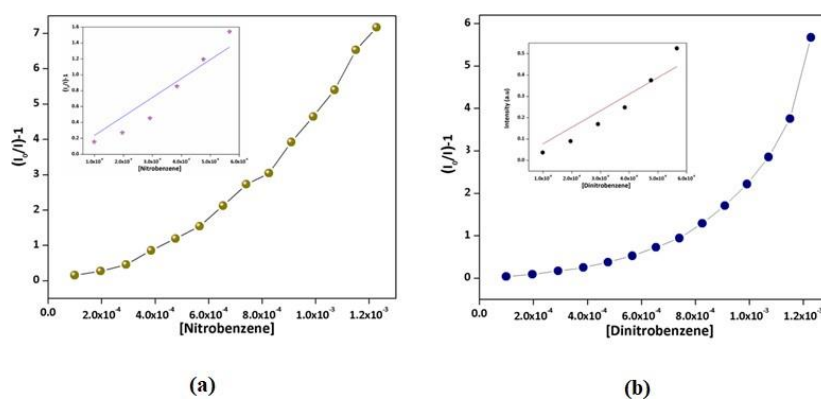**Fig. III.14:** Stern-Volmer plot of the complex with nitrobenzene (a) and dinitrobenzene (b) in DMSO.

Fig. III.15: Stern-Volmer plot of the complex with nitrobenzene (a) and dinitrobenzene (b) in CH_3CN.
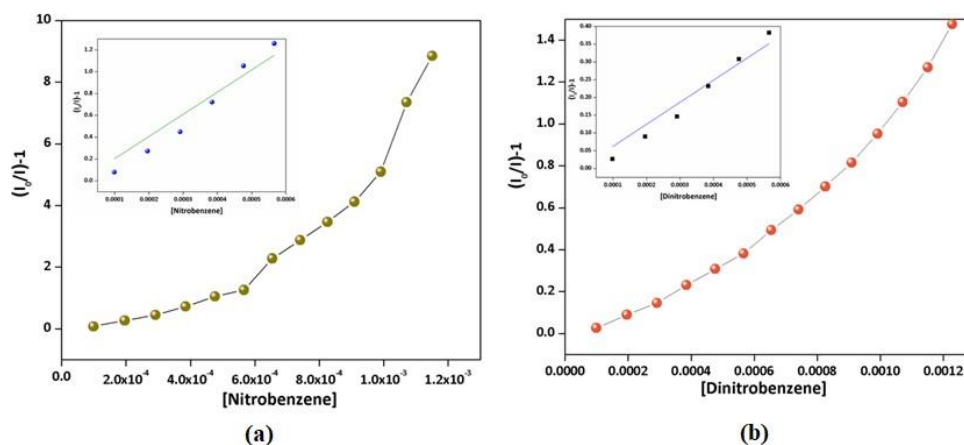
Fig. III.16: Stern-Volmer plot of the complex with nitrobenzene (a) and dinitrobenzene (b) in MeOH.
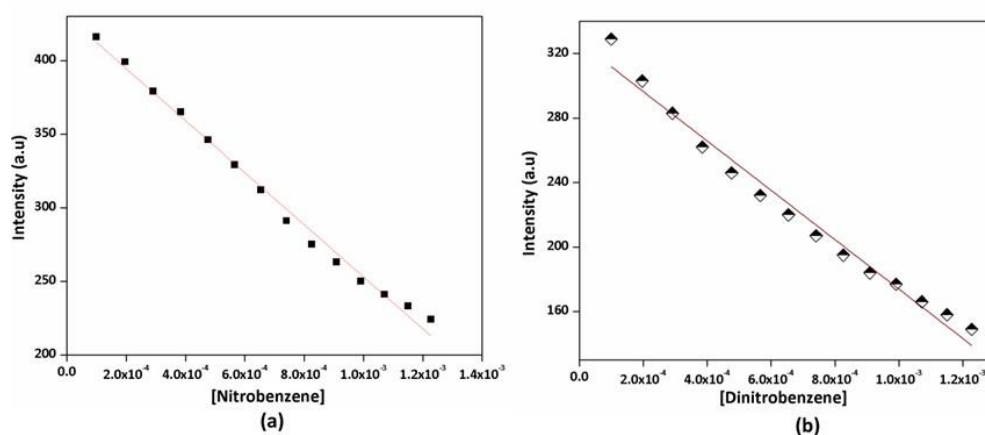

Fig. III.17: Plot of limit of detection of the complex towards nitrobenzene (a) and dinitrobenzene (b) in DMF
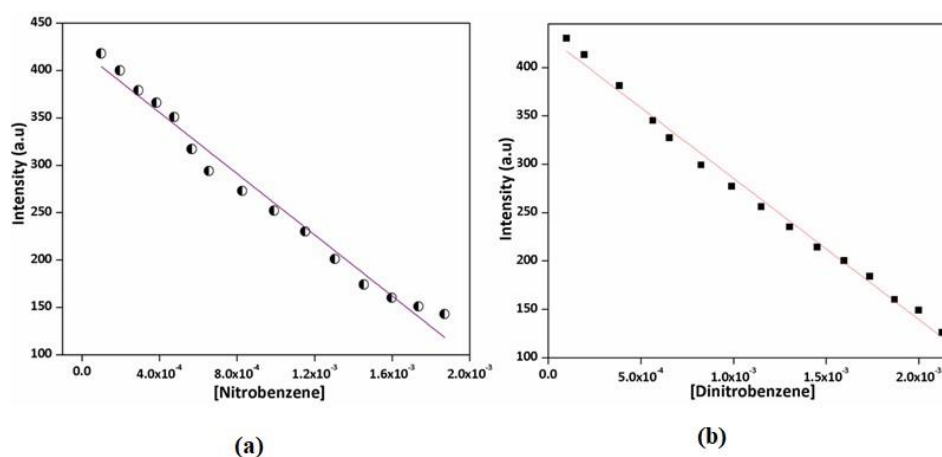

Fig. III.18: Plot of limit of detection of the complex towards nitrobenzene (a) and dinitrobenzene (b) in DMSO.
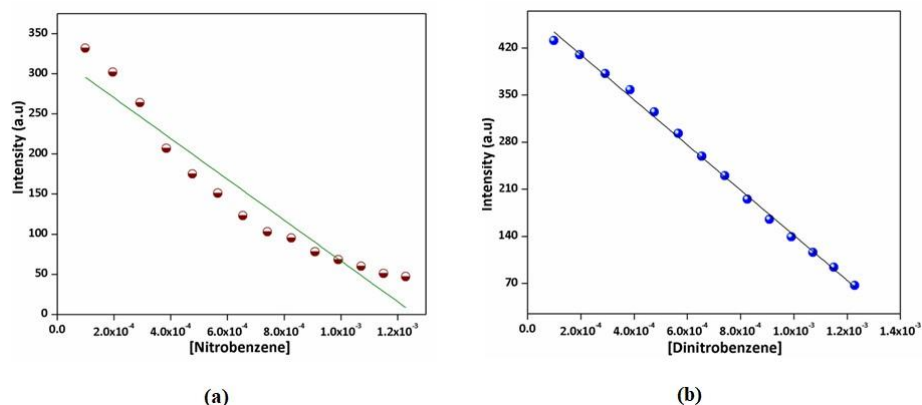
Fig. III.19: Plot of limit of detection of the complex towards nitrobenzene (a) and dinitrobenzene (b) in CH_3CN.
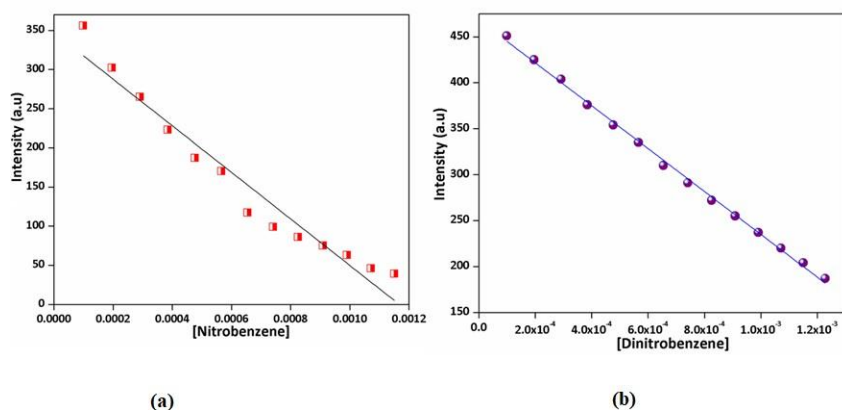

Fig. III.20: Plot of limit of detection of the complex towards nitrobenzene (a) and dinitrobenzene (b) in MeOH.

Table III.6: Stern-Volmer constants of the complex (K_{sv}) with nitroaromatics (nitrobenzene and dinitrobenzene) in different solvents.

	DMF	**DMSO**	**CH₃CN**	**MeOH**
Nitrobenzene	$5.7x10^2$	$4.7x10^2$	$2.03x10^2$	$7.76x10^2$
Dinitrobenzene	8.6 $x10^2$	$5.8x10^2$	$6.21x10^2$	$2.3x10^2$

The limit of detection (LOD) for nitrobenzene and dinitrobenzene of the complex in different solvents have also been gathered in **Table III.7**. The limit of detection of

nitrobenzene and dinitrobenzene of the complex in different solvents have been shown in **Figs. III.17**- **III.20**.

Table III.7: LOD values for nitrobenzene and dinitrobenzene of the complex **5** in different solvents.

	DMF	DMSO	CH$_3$CN	MeOH
Nitrobenzene	1.76×10^{-6}	1.93×10^{-6}	1.23×10^{-6}	1.05×10^{-6}
Dinitrobenzene	2.03×10^{-6}	2.13×10^{-6}	9.28×10^{-7}	1.34×10^{-6}

III.3.5. X-ray diffraction of powdered sample

The experimental X-ray diffraction pattern of the powdered sample of the complex is in good agreement with the simulated XRD pattern from single crystal X-ray diffraction results. This indicates the uniformity of the bulk material. The simulated pattern of the complex has been calculated from the single crystal structural data (cif) using the CCDC Mercury software.

III.3.6. Hirshfeld surface analysis

Hirshfeld surfaces of the complex, mapped over d$_{norm}$ (range of -0.1 to 1.5 Å), shape index and curvedness, have been illustrated in **Fig. III.21**. Red spots on the d$_{norm}$ surface (Fig. 12) indicate the interaction between sulphur and hydrogen atoms. O···H and N···H contacts are also observed in the Hirshfeld surfaces as smaller visible spots of light colour indicating weaker and longer contact. The intermolecular interactions appear as distinct spikes in the 2D fingerprint plot have been shown in **Fig. III.22**.
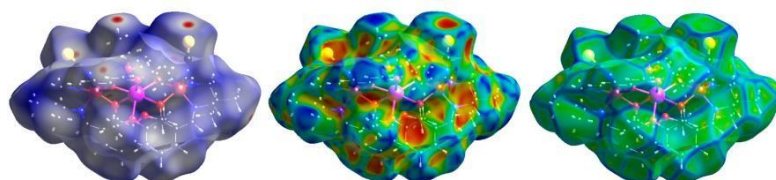

Fig. III.21: Hirshfeld surfaces mapped with d$_{norm}$ (left), shape index (middle) and curvedness (right) of the complex.
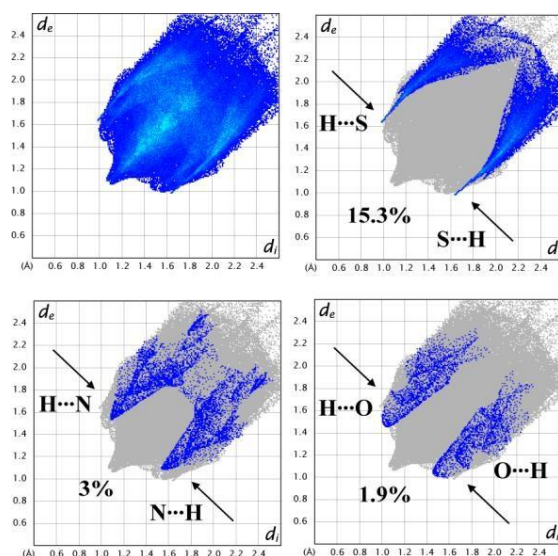
Fig. III.22: Fingerprint plot: Full (top left), resolved into H···S/S···H (top right), H···O/O···H (bottom left) and H···N/N···H (bottom right) contacts contributed to the total Hirshfeld Surface area of the complex.

III.4. Conclusion

A zinc-salen type complex is used as a ligand to synthesize a heterotrinuclear zinc(II)-cdmium(II)-zinc(II) complex, Cd{L^{5}Zn(NCS)}$_2$ **(5)**. The cadmium(II) is exhibiting octa-coordinated trigonal dodecahedral geometry, as confirmed by X-ray crystallographic analysis. Zinc(II) centres are penta-coordinated and show square pyramidal geometries. The complex shows strong luminescence property and can behave as a turn-off fluorosensor for the detection of various nitroaromatics.

References

1 (a) E. Campazzi, E. Solari, R. Scopelliti, C. Floriani, *Chem. Commun.*, 1999, 1617; (b) S. T. Liddle, K. Izod, *Organometallics*, 2004, **23**, 5550; (c) L. M. Engelhardt, W.-P. Leung, C. L. Raston, A. H. White, J. Chem. Soc., *Chem. Commun.*, 1983, 386; (d) G. Weber, G. M. Sheldrick, T. Burgemeister, F. Dietl, A. Mannschreck, A. Merz, *Tetrahedron*, 1984, **40**, 855; (e) D. R. Turner, S. N. Pek, S. R. Batten, *New J. Chem.*, 2008, **32**, 719; (f) H. Plenio, *Inorg. Chem.*, 1994, **33**, 6123.

2 A. Ray, G. M. Rosair, R. Rajeev, R. B. Sunoj, E. Rentschler, S. Mitra, *Dalton Trans.*, 2009, 9510.

3 (a) S. Bhattacharya, S. Mohanta, *Inorg. Chim. Acta*, 2015, **432**, 169; (b) A. Jana, S. Mohanta, *CrystEngComm*, 2014, **16**, 5494; (c) S. Roy, M. G. B. Drew, A. Bauzá, A. Frontera, S. Chattopadhyay, *CrystEngComm*, 2018, 20, 1679.

4 (a) V. Vieru, T. D. Pasatoiu, L. Ungur, E. Suturina, A. M. Madalan, C. Duhayon, J.-P. Sutter, M. Andruh and L. F. Chibotaru, *Inorg. Chem.*, 2016, **55**, 12158; (b) M.-J. Liu, K.-Q. Hu, C.-M. Liu, A.-L. Cui and H.-Z. Kou, *New J. Chem.*, 2016, **40**, 8643; (c) T. D. Pasatoiu, C. Tiseanu, A. M. Madalan, B. Jurca, C. Duhayon, J. P. Sutter and M. Andruh, *Inorg. Chem.*, 2011, **50**, 5879; (d) J. H. Lee, S. Y. Im, S. W. Lee, *Polyhedron*, 2016, **118**, 125.

5 (a) H. J. Im, S. W. Lee, *Polyhedron*, 2016, **110**, 24; (b) D. Visinescu, M.-G. Alexandru, A. M. Madalan, C. Pichon, C. Duhayon, J.-P. Sutter, M. Andruh, *Dalton Trans.*, 2015, **44**, 16713; (c) M.-G. Alexandru, D. Visinescu, M. Andruh, N. Marino, D. Armentano, J. Cano, F. Lloret and M. Julve, *Chem. Eur. J.*, 2015, 21, 5429; (d) N. Bridonneau, G. Gontard, V. Marvaud, *Dalton Trans.*, 2015, **44**, 5170.
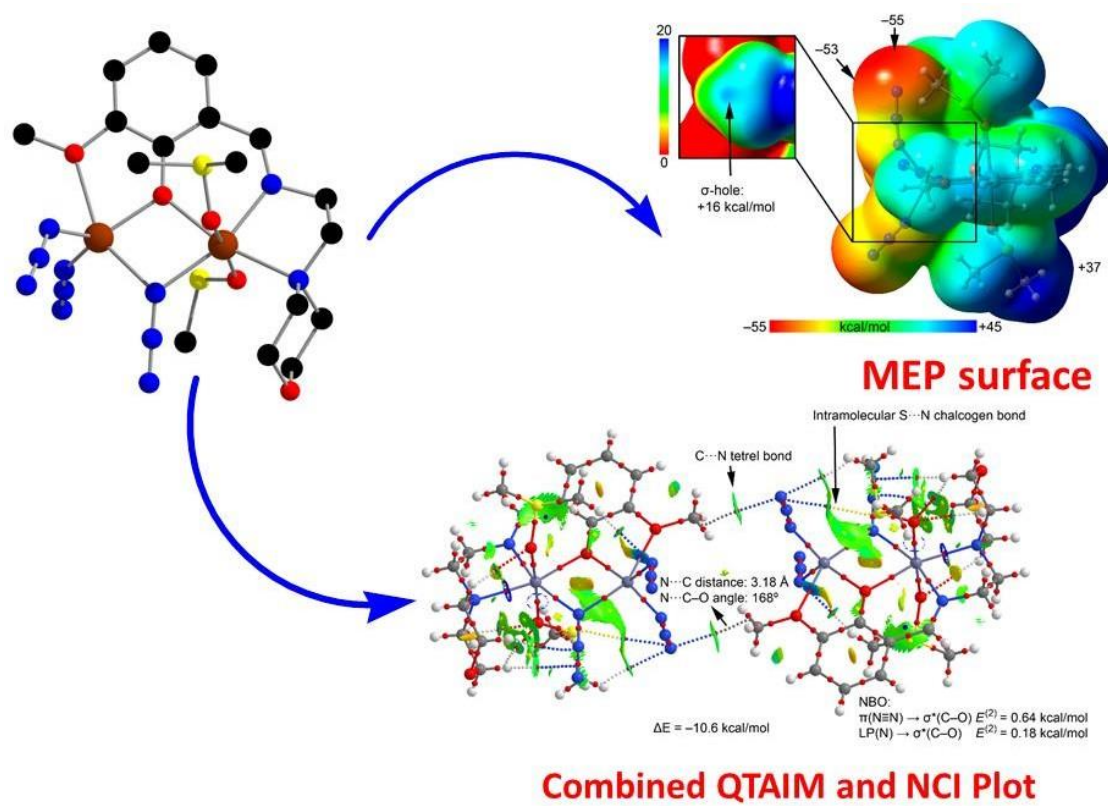
6 (a) G. Novitchi, J.-P. Costes, B. Donnadieu, *Eur. J. Inorg. Chem.,* 2004, 1808; (b) J.-P. Costes, F. Dahan, J. Garcia-Tojal, *Chem. Eur. J.*, 2002, **8**, 5430.

7 (a) D. Majumdar, S. Das, J. K. Biswas, M. Mondal, *J. Mol. Struct.*, 2017, **1134**, 617; (b) S. Banerjee, A. Bauza, A. Frontera, A. Saha, *RSC Adv.*, 2016, **6**, 39376; (c) H. Wang, D. Zhang, Z.-H. Ni, X. Li, L. Tian, J. Jiang, *Inorg. Chem.*, 2009, **48**, 5946.

8 (a) M. Andruh, *Chem. Commun.*, 2011, **47**, 3025; (b) T. D. Pasatoiu, J.-P. Sutter, A. M. Madalan, F. Z. C. Fellah, C. Duhayon, M. Andruh, *Inorg. Chem.*, 2011, **50**, 5890;
(c) K. Liua, W. Shi, P. Cheng, Coord. *Chem. Rev.*, 2015, **290**, 74.

9 (a) S. Handa, V. Gnanadesikan, S. Matsunaga, M. Shibasak, *J. Am. Chem. Soc.*, 2007, **129**, 4900; (b) W.-K. Wong, X. Yang, R. A. Jones, J. H. Rivers, V. Lynch, W.-K. Lo, D. Xiao, M. M. Oye, A. L. Holmes, *Inorg. Chem.*, 2006, **45**, 4340; (c) M. Nayak, R. Koner, H.-H. Lin, U. Florke, H.-H. Wei, S. Mohanta, *Inorg. Chem.*, 2006, **45**, 10764; (d) M. Sakamoto, K. Manseki, H. Okawa, *Coord. Chem. Rev.*, 2001, **221**, 379; (e) M. Andruh, D. G. Branzea, R. Gheorghe, A. M. Madalan, *CrystEngComm*, 2009, **11**, 2571.

10 (a) W. Wang, J. Yang, R. Wang, L. Zhang, J. Yu, D. Sun, *Cryst. Growth Des.*, 2015, **15**, 2589; (b) Y. Salinas, R. M. Martinez-Manez, M. D. Marcos, F. L. Sancenon, A. M. Costero, M. Parra, S. Gil, *Chem. Soc. Rev.*, 2012, **41**, 1261; (c) Y. Fu, H.-H. Han, J. Zhang, X.-P. He, B. L. Feringa, H. Tian, *J. Am. Chem. Soc.*, 2018, **140**, 8671; (d) D.-K. Ji, Y. Zhang, Y. Zang, J. Li, G.-R. Chen, X.-P. He, H. Tian, *Adv. Mater.*, 2016, **28**, 9356; (e) J. Zhang, Y. Fu, H.-H. Han, Y. Zang, J. Li, X.-P. He, B. L. Feringa, H. Tian, *Nat. Commun.*, 2017, **8**, 987; (f) X.-P. He, Y.-L. Zeng, X.-Y. Tang, N. Li, D.-M. Zhou, G.-R. Chen, H. Tian, *Angew. Chem. Int. Ed.*, 2016, **55**, 13995.

11 (a) A. Chowdhury, P. S. Mukherjee, *ChemPlusChem*, 2016, **81**, 1360; (b) S. J. Toal, W. C. Trogler, *J. Mater. Chem.*, 2006, **16**, 2871; (c) D. Banerjee, Z. Hu, S. Pramanik, X. Zhang, H. Wang, J. Li, *CrystEngComm*, 2013, **15**, 9745; (d) A. Das, S. Jana and A. Ghosh, *Cryst. Growth Des.*, 2018, **18**, 2335.

12 (a) B. Naskar, R. Modak, D. K. Maiti, M. G. B. Drew, A. Bauzá, A. Frontera, C. D. Mukhopadhyay, S. Mishra, K. D. Saha and S. Goswami, *Dalton Trans.*, 2017, **46**, 9498; (b) S. Banerjee, A. Bauz´a, A. Frontera and A. Saha, *RSC Adv.*, 2016, **6**, 39376; (c) L. Jiang, D.-Y. Zhang, J.-J. Suo, W. Gu, J.-L.Tian, X. Liu and S.-P. Yana, *Dalton Trans.*, 2016, **45**, 10233; (d) D. Majumdar, S. Das, J. K. Biswas, M. Mondal, *J. Mol. Struct.*, 2017, **1134**, 617.

13 H. Wang, D. Zhang, Z.-H. Ni, X. Li, L. Tian and J. Jiang, *Inorg. Chem.*, 2009, **48**, 5946.

14 (a) J.-P. Costes, F. Dahan, A. Dupuis, J.-P. Laurent, *Inorg. Chem.*, 1996, **35**, 2400; (b) S. Roy, M. G. B. Drew, A. Frontera and S. Chattopadhyay, *ChemistrySelect*, 2017, **2**, 7880.

15 (a) A.W. Addition, T.N. Rao, J. Reedjik, J. van Rinj, C.G. Verscholar, *J. Chem. Soc., Dalton Trans.*, 1984, 1349; (b) S. Khan, A. A. Masum, Md. M. Islam, M. G. B. Drew, A. Bauzá, A. Frontera, S. Chattopadhyay, *Polyhedron*, 2017, **123**, 334.

16 D. Cremer, J. A. Pople, *J. Am. Chem. Soc.*, 1975, **97**, 1354; (b) D. Cremer, *Acta Crystallogr. Sect. B: Struct. Sci.*, 1984, **40**, 498; (c) J. C. A. Boeyens, *J. Cryst. Mol. Struct.*, 1978, **8**, 317.

17 (a) V. P. Singh, P. Singh, A. K. Singh, *Inorg. Chim. Acta*, 2011, **379**, 56; (b) P. K. Bhaumik, S. Roy, K. Harms, S. Chattopadhyay, *Polyhedron*, 2014, 81, 168; (c) S. Roy, P. K. Bhaumik, K. Harms, S. Chattopadhyay, *Polyhedron*, 2014, **75**, 57; (d) A. Bhattacharyya, S. Sen, K. Harms, S. Chattopadhyay, *Polyhedron*, 2015, **88**, 156.

18 (a) S. Roy, A. Dey, P. P. Ray, J. Ortega-Castro, A. Frontera, S. Chattopadhyay*, Chem. Commun.*, 2015, **51**, 12974; (b) A. Bhattacharyya, S. Roy, J. Chakraborty, S.Chattopadhyay, *Polyhedron*, 2016, **112**, 109; (c) S. Roy, M. G. B. Drew, S. Chattopadhyay, *Polyhedron*, 2018, **150**, 28.

19 (a) S. Roy, M. G. B. Drew, A. Bauza, A. Frontera, S. Chattopadhyay, *Dalton Trans.*, 2017, **46**, 5384; (b) S. Roy, M. G. B. Drew, A. Bauza, A. Frontera, S. Chattopadhyay, *ChemistrySelect*, 2017, **2**, 10586.

20 A. Majumder, G. M. Rosair, A. Mallick, N. Chattopadhyay, S. Mitra, *Polyhedron*, 2006, **25**, 1753.

21 T. Basak, A. Bhattacharyya, M. Das, K. Harms, A. Bauza´, A. Frontera, S. Chattopadhyay, *ChemistrySelect*, 2017, **2**, 6286.

22 (a) H. Wang, W. Yang, Z.-M. Sun, *Chem.-Asian J.*, 2013, **8**, 982; (b) D. Ma, B. Li, X. Zhou, Q. Zhou, K. Liu, G. Zeng, G. Li, Z. Shi, S. Feng, *Chem. Commun.*, 2013, **49**, 8964; (c) B. Gole, A. K. Bar, P. S. Mukherjee, *Chem. Commun.*, 2011, **47**, 12137; (d) D. Tian, Y. Li, R.-Y. Chen, Z. Chang, G.-Y. Wang, X.-H. Bu, *J. Mater. Chem. A*, 2014, **2**, 1465; (e) G.-Y. Wang, C. Song, D.-M. Kong, W.-J. Ruan, Z. Chang, Y. Li, *J. Mater. Chem. A*, 2014, **2**, 2213; (f) Y.-C. He, H.-M. Zhang, Y.-Y. Liu, Q.-Y. Zhai, Q.-T. Shen, S.-Y. Song, J.-F. Ma, *Cryst. Growth Des.*, 2014, **14**, 3174.

23 Z.-J. Wang, L. Qin, J.-X. Chen, H.-G. Zheng, *Inorg. Chem.*, 2016, **55**, 10999.

24 R. A. Velapoldi, K. D. Mielenz, Standard Reference Materials: A Fluorescence Standard Reference Material: Quinine Sulfate Dihydrate, National Bureau of Standards Special Publication 260-64, National Bureau of Standards, Washington, DC, 1980.

25 J. R. Lakowicz, Principles of Fluorescence Spectroscopy, third ed., Springer-Verlag, New York, 2006.

Chapter IV

RH₃C···N tetrel bonding interactions in the solid state of a dinuclear zinc complex

MEP surface

σ-hole:
+16 kcal/mol

−55 kcal/mol +45

C···N tetrel bond

Intramolecular S···N chalcogen bond

N···C distance: 3.18 Å
N···C–O angle: 168°

NBO:
$\pi(N≡N) \rightarrow \sigma^*(C–O)$ $E^{(2)}$ = 0.64 kcal/mol
$LP(N) \rightarrow \sigma^*(C–O)$ $E^{(2)}$ = 0.18 kcal/mol

ΔE = −10.6 kcal/mol

Combined QTAIM and NCI Plot

IV.1. Introduction

Over the last five years, ζ-hole interactions,[1] involving elements of groups 12–18 of the Periodic Table[2] have emerged as key players in supramolecular chemistry. For instance, they have been used in substitution of the ubiquitous H-bonding in several fields like molecular recognition, catalysis and crystal engineering.[2b] The position, size and number of the depleted areas of electron density on the surface of covalently bonded atoms depend on the type (single or double/delocalized bonds) and number of covalent bonds formed by the atom. In particular, ζ-holes are located approximately along the vector of a single ζ-bond. In case of group 14, the ζ-holes are large and accessible for interacting with electron rich atoms in the heavier tetrel atoms (Ge, Sn and Pb).[3] For Si and specially C, the ζ-hole is usually very small, thus leading to ζ-hole interactions with a marked directionality. The linearity of this type of bonding, has been confirmed by multitude CSD analyses[4] combined with computational studies.[5] It is well known that the ζ-hole intensity increases as the electron withdrawing ability of its substituents increases. Therefore, the ζ-hole opposite to C–Y bonds where Y = fluorine, cyano, or nitro or a charged atom/group is favoured over other substituents.[6]

2:1 condensation of salicylalaldehyde and ethylenediamine produces a N_2O_2 donor tetradentate Schiff base, which is commonly known as „salen" [sal (from salicylaldehyde) + en (ethylenediamine) = salen]. Use or other diamines and different salicyalaldehyde derivatives produced many other „salen type" Schiff bases. These salen type N_2O_2 donor Schiff bases have been widely used to synthesize many di and polynuclear zinc complexes exploiting the bridging ability of phenoxo oxygen atoms.[7] Tridentate N_2O donor Schiff bases have also been used by many research groups to prepare such complexes.[8] In the present work, we have used a tetradentate N_2O_2 donor Schiff base to prepare a new dinuclear zinc complex. It forms in the solid state self-assembled supramolecular dimers where the

coordinated methoxy group of one monomer interacts via tetrel bonding interaction with the azido group of the other monomer and vice versa. Although other interactions like π-stacking are also important governing the solid state architecture of the dinuclear Zn-complex reported herein, we have focused our work mainly on the more unconventional tetrel bonding interactions, which have been investigated using DFT calculations combined with molecular electrostatic potential (MEP) surfaces, the quantum theory of "atoms-in-molecules" and the non-covalent interaction index (NCI plot). The ζ-hole nature of the interaction has been confirmed by using the natural bond orbital (NBO) method.

IV.2. Experimental Section

IV.2.1. Synthesis

IV.2.1.1. Synthesis of ligand 2-((E)-(2-morpholinoethylimino)methyl)-6-methoxyphenol (*HL⁶*)

A clear yellow solution of Schiff base ligand, HL^6, was synthesized by refluxing 4-(2-aminoethyl)morpholine (0.13 mL,~1 mmol) with 3-methoxysalicylaldehyde (0.152 g, ~1 mmol) in methanol (20 mL) for ca. 1 h. It was not isolated and used directly for the preparation of the complex **6**.

IV.2.1.2. Synthesis of complex [(DMSO)₂ZnL(μ₁,₁-N₃)Zn(N₃)₂] (6)

Methanol solution (10 mL) containing zinc perchlorate hexahydrate (744 mg, 2 mmol) was added to the yellow solution of Schiff base ligand, HL^6 (1 mmol) and the resulting solution was stirred for 1 hour. Then the methanol-water (2:1) solution of sodium azide (180 mg, 2 mmol) was added to it and stirred for an additional 1 h. Few drops of DMSO was added to the mixture as solvent and then filtered. Single crystals, suitable for X-

ray diffraction, were obtained after one week by slow evaporation of the filtrate in open atmosphere.

Yield: 251 mg (~80%).Anal. Calc. for $C_{18}H_{31}N_{11}O_5S_2Zn_2$ (FW = 676.44): C, 31.96; H, 4.62; N, 22.78 %. Found: C, 31.83; H, 4.51; N, 22.89%. FT-IR (KBr, cm-1): 2999-2862 (ν_{C-H}), 1647 ($\nu_{C=N}$), 2057(ν_{N3}). Magnetic moment: 0.01 BM (~Diamagnetic).

IV.3. Results and discussion

IV.3.1. Synthesis

The Schiff base ligand, HL^6 was synthesized by the condensation of 4-(2-aminoethyl)morpholine with 3-methoxysalicylaldehyde following the literature method.[9] The ligand was not isolated and was used directly for the preparation of zinc complex. Addition of the methanol solution of zinc perchlorate hexahydrate in the methanol solution of the Schiff base, HL^6 followed by the addition of sodium azide produced dinuclear complex, *[(DMSO)₂ZnL(µ₁,₁-N₃)Zn(N₃)₂]* (**6**).
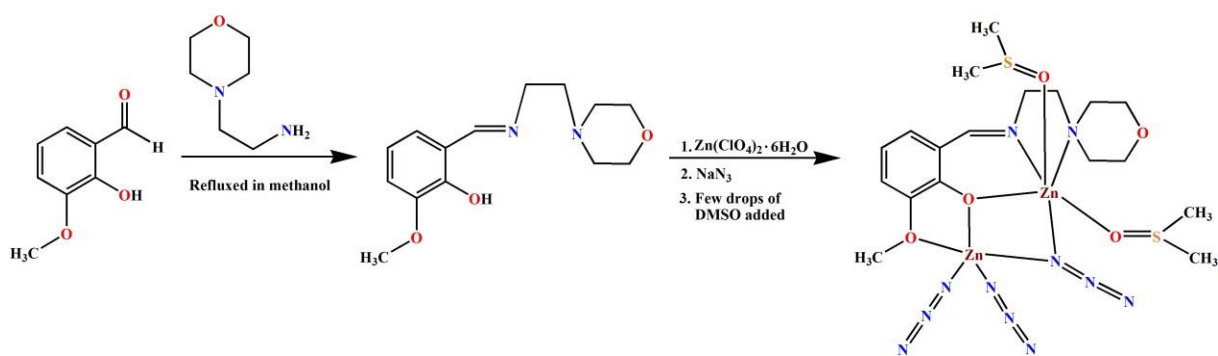
Scheme IV.1: Synthetic route to complex **6**.

IV.3.2. Description of the structure of *[(DMSO)₂ZnL(µ₁,₁-N₃)Zn(N₃)₂] (6)*

Single crystal X-ray diffraction analysis reveals that the complex **6** crystallizes in the triclinic space group, *P-1*. It features dual end-to-end azide bridged dinuclear structure. Perspective view of the complex is given in **Fig. IV.1**.
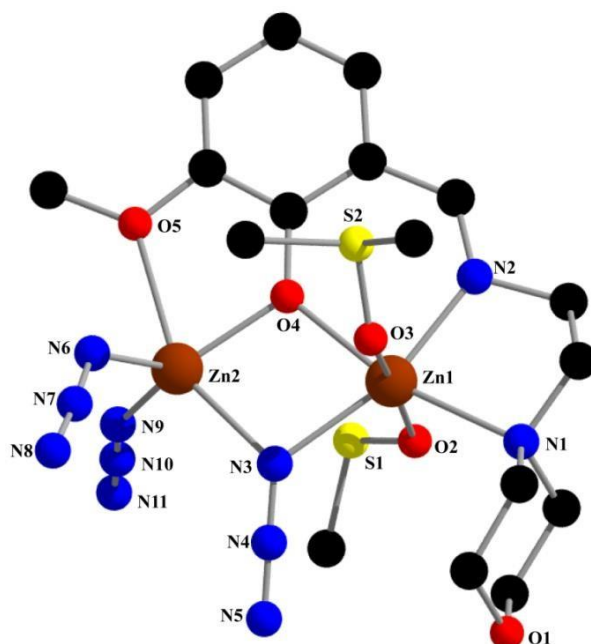

Fig. IV.1: Perspective view of complex **6** with selective atom numbering scheme. Hydrogen atoms have been omitted for clarity.

The coordination polyhedra around both metal centers are different, Zn(1) is hexa-coordinated, while Zn(2) is penta-coordinated. Zn(1) exhibits distorted octahedral coordination sphere, being coordinated by N(1) and N(2) and O(4) of the Schiff base ligand, O(2) and O(3) of two DMSO molecules and N(3) of a bridging azide. Zn(2) is coordinated by two terminal azide nitrogen atoms, N(6) and N(9), one phenoxo oxygen atom, O(4) and one methoxy oxygen atom, O(5), of one Schiff base ligand, and a nitrogen atom, N(3), from a bridging azide. The geometry of a penta-coordinated metal complex may conveniently be measured by the Addison parameter (η) that is ideally zero for a square-pyramidal complex and is one for a trigonal bipyramidal complex [$\eta = (x−y)/60$, where x and y are the two largest

ligand–metal–ligand angles in the coordination sphere].[10] Addison parameter (η) value of the complex is 0.48. This η value indicates that the geometry around the zinc center, Zn(2), lies in between the square pyramidal and trigonal bipyramidal geometry. Important bond lengths and bond angles are given in Table **IV.2** and **IV.3** respectively.

Notable feature in the crystal packing of this complex is that, this complex shows one significant π⋯π stacking interaction (Fig. **IV.2**) between the phenyl ring, R(6) [C(8)-C(9)-C(10)-C(11)-C(12)-C(13)] and its symmetry related counterpart, R(6)[a], of a neighbour molecule ([a] = symmetry transformation = 1-x,1-y,-z). Perpendicular distance from Cg(6) [Cg(6) is the centre of gravity of the ring R(6)] to the symmetry related (1-x,1-y,-z) phenyl ring R(6)[a] of neighbouring molecule is 3.4707(12) Å. Both rings, R(6) and R(6)[a] are more or less parallel and therefore, the perpendicular distance from Cg(6)[a] of a symmetry related ([a] = 1-x,1-y,-z) neighbouring molecule to the phenyl ring R(6) is also 3.4707(12) Å. The center-to-center separation [Cg(6)⋯Cg(6)[a]] of R(6) and R(6)[a] rings is 3.7821(17) Å. Details of geometric features of π⋯π stacking interaction is given in Table **IV.4**. Moreover, we have also evaluated the interaction energy of the dimer, which is very large (–19.0 kcal/mol) at the PBE0/def2-TZVP, in line with similar complexes previously analysed in the literature.[11] The antiparallel arrangement of the rings in combination to the large dipole of the monomer (μ_D = 20.5 D), due to the metal coordination, enhances the antiparallel dipole⋯dipole attraction. A careful inspection of the dimer reveals the existence of two symmetrically equivalent C–H⋯N H-bonds that are established between one aromatic C–H bond and one N-atom of the azido ligand. These interactions also contribute to the large interaction energy obtained for the π-stacked dimer. Fig. **IV.2b** also shows the tetrel bonding dimer for comparison purposes. In this dimer, the aromatic rings are separated more than 10 Å and do not participate in the dimerization process (lack of π-interactions). In contrast the dimer is exclusively stabilized by C⋯N tetrel bonds as further analysed below.

Table IV.1: Crystal data and refinement details of the complex **6**

Formula	$C_{18}H_{31}N_{11}O_5S_2Zn_2$
Formula Weight	676.44
Temperature (K)	273
Crystal System	Triclinic
Space group	*P-1*
a (Å)	9.2129(9)
b (Å)	9.9156(10)
c (Å)	17.7795(18)
α (°)	80.589(3)
β (°)	77.092(3)
γ (°)	64.355(3)
V(Å^3)	1423.1(2)
Z	2
d_{cal} (g cm^{-3})	1.579
μ(mm^{-1})	1.882
F(000)	696
Total reflection	39040
Unique Reflections	5066
Observe data[I>2ζ(I)]	4579
R(int)	0.0409
R1, *w*R2 (all data)	0.0322, 0.0751
R1, *w*R2 [I>2σ(I)]	0.0280,0.0718
Residual Electron Density (eÅ^{-3})	0.0373, -0.508

CCDC reference no 2022312.

Table IV.2: Selected bond lengths (Å) of the complex

Zn(1)-O(2)	2.1460(18)
Zn(1)-O(3)	2.1173(17)
Zn(1)-O(4)	2.1160(18)
Zn(1)-N(1)	2.266(2)
Zn(1)-N(2)	2.071(2)
Zn(1)-N(3)	2.146(2)
Zn(2)-O(4)	1.979(2)
Zn(2)-O(5)	2.361(2)
Zn(2)-N(3)	2.153(2)
Zn(2)-N(6)	1.955(5)
Zn(2)-N(9)	1.966(3)

Table IV.3: Selected bond angles (°) of the complex.

O(2)-Zn(1)-O(3)	172.38(7)	N(1)-Zn(1)-N(3)	115.90(8)
O(2)-Zn(1)-O(4)	95.31(7)	N(2)-Zn(1)-N(3)	161.39(8)
O(2)-Zn(1)-N(1)	88.84(7)	O(4)-Zn(2)-O(5)	72.21(8)
O(2)-Zn(1)-N(2)	89.23(8)	O(4)-Zn(2)-N(3)	79.81(8)
O(2)-Zn(1)-N(3)	88.45(8)	O(4)-Zn(2)-N(6)	123.01(16)
O(3)-Zn(1)-O(4)	90.52(7)	O(4)-Zn(2)-N(9)	122.34(10)
O(3)-Zn(1)-N(1)	86.57(7)	O(5)-Zn(2)-N(3)	151.74(8)
O(3)-Zn(1)-N(2)	96.20(8)	O(5)-Zn(2)-N(6)	92.34(16)
O(3)-Zn(1)-N(3)	88.09(8)	O(5)-Zn(2)-N(9)	86.45(10)
O(4)-Zn(1)-N(1)	166.59(7)	N(3)-Zn(2)-N(6)	106.41(15)
O(4)-Zn(1)-N(2)	84.81(8)	N(3)-Zn(2)-N(9)	105.77(10)
O(4)-Zn(1)-N(3)	77.04(8)	N(6)-Zn(2)-N(9)	110.42(17)
N(1)-Zn(1)-N(2)	82.50(8)		

Table IV.4: Geometric features (distances in Å and angles in °) of the π···π stacking

Cg(Ring I)···Cg(Ring J)	Cg···Cg(Å)	α (°)	Cg(I)···Perp (Å)	Cg(J)···Perp (Å)
Cg(6)···Cg(6)[a]	3.7821(17)	0	3.4707(12)	3.4706(12)

Cg(6) is the centre of gravity of the ring, R(6) [C(8)-C(9)-C(10)-C(11)-C(12)-C(13)]; α is dihedral angle between ring I and ring J; Cg(I)···Perp is the perpendicular distance from Cg(I) to ring J; Cg(J)···Perp is the perpendicular distance from Cg(J) to ring I; Symmetry transformation: ^{a} = 1-x, 1-y, -z
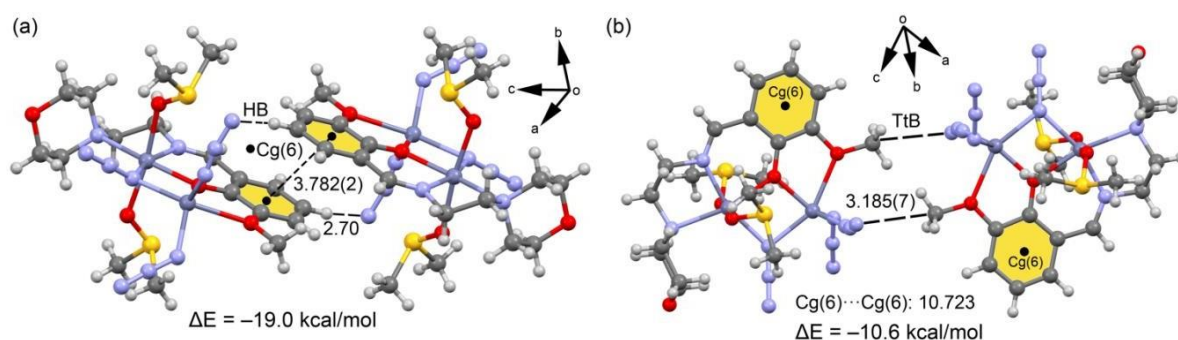

Fig. IV.2: (a) Perspective view of π···π interaction and the dimerization energy. (b) Tetrel bonding dimer showing the large separation of the aromatic rings. Distances in Å. Cg(6) is the centre of gravity of the ring, R(6) [C(8)-C(9)-C(10)-C(11)-C(12)-C(13)]

IV.3.3. Spectral and magnetic properties

In the IR spectra of complex (Fig. **IV.3**), distinct band as a result of the azomethine(>C=N) group around 1647 cm^{-1} are customarily noticed.[12] One intense peak at 2057 cm^{-1} indicates the presence of azide.[13,14] Broad band within the range from 2999–2862 cm^{-1} due to alkyl C–H stretching vibrations are observed in the IR spectra of the complex.[15] The electronic spectrum shows bands at 260 and 370 nm, which may be assigned as π→π* and n→π* transitions, respectively. The absence of any d-d transition is in accordance with the presence of d^{10} configuration of zinc. Room temperature magnetic susceptibility measurement shows that the complex is diamagnetic, as expected for zinc complexes with d^{10} electronic configuration.
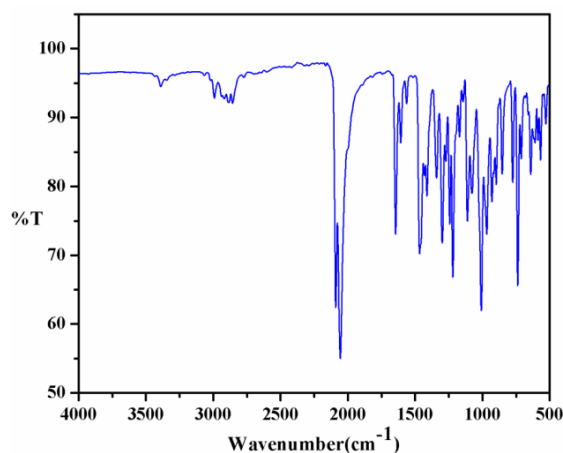
Fig. IV.3: IR spectrum of the complex.

IV.3.4. Theoretical study

In addition to the conventional π-π interaction described above (section **IV.3.3**, Fig. **IV.2a**), complex [(DMSO)$_2$ZnL(μ$_{1,1}$-N$_3$)Zn(N$_3$)$_2$] also forms self-assembled dimers in the solid state governed by more unconventional ζ-hole tetrel bonding (TtB) interactions (see Fig. **IV.2b** and Fig. **IV.4**). The N···C distances are 3.185(7) and 3.286(8), which are similar to the sum of C and N van der Waals radii (3.25 Å). The energetic features and physical nature of these interactions are analysed in this section where we intend to differentiate two possible situations: O–C···N ζ-hole tetrel bonding from C–H···N H-bonding.
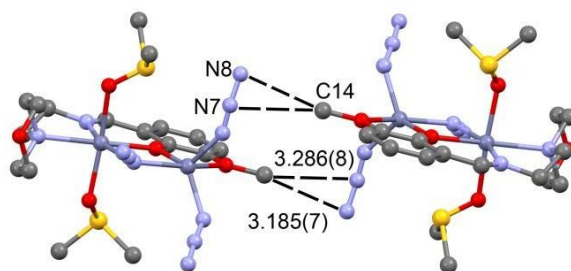
Fig. **IV.4**. Partial view of the X-ray structure with indication of the self-assemble dimer and the tetrel bonding interactions as dashed lines. Distances in Å.

At first the molecular electrostatic energy (MEP) surface of the complex has been computed to rationalize the TtB interactions from an electrostatic point of view (Fig. **IV.5**). The most negative region corresponds to the terminal N-atoms of the azido groups (–55 kcal/mol) and the most positive at the C–H groups of the coordinated DMSO molecules. More interestingly, this complex exhibits a ζ-hole at the carbon atom of the methoxy group of the ligand, which can be better appreciated if a reduced MEP scale is used for the plot (see top left part of Fig. 5). The MEP value at the ζ-hole is moderately strong (+16 kcal/mol) due to the coordination of the methoxy group to the zinc ion that intensifies the ζ-hole at the carbon atom. Similar values of ζ-holes have been reported in similar cadmium complexes.[16]
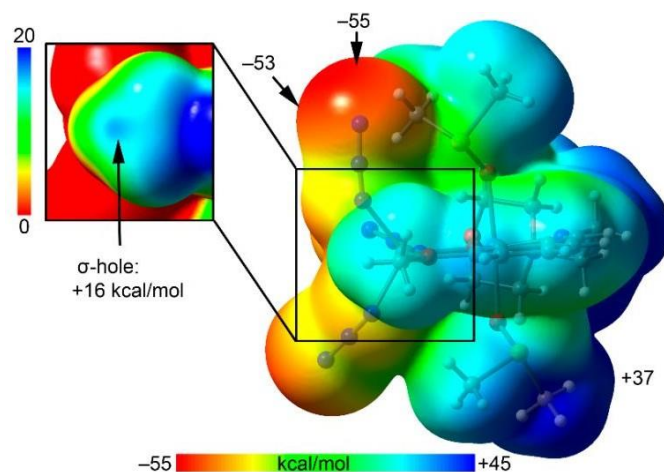

Fig. IV.5: Molecular electrostatic potential (MEP) surfaced of complexes $[(DMSO)_2ZnL(\mu_{1,1}\text{-}N_3)Zn(N_3)_2]$ at the PBE0-D3/def2-TZVP level of theory (isosurface value 0.001 a.u.). The MEP energies at selected points are given in kcal/mol.

Fig. **IV.6** shows the QTAIM distribution of critical points (CPs) overlapped with the NCI index plot (0.4 a.u. isosurface) computed for the self-assembled centrosymmetric dimer retrieved from the solid state X-ray structure of $[(DMSO)_2ZnL^6(\mu_{1,1}\text{-}N_3)Zn(N_3)_2]$. The dimer contains two symmetrically equivalent non-covalent carbon bonding interactions involving the methyl groups and azido ligands. The C$\cdots$N distance (3.185 Å) is shorter than the sum of

van der Waals radii and the three N···H distances are longer than the sum of van der Waals radii (2.86 – 3.19 Å), thus suggesting the formation of a TtB instead of a trifurcated H-bond. The N···C–O angle is large (168º) thus indicating a quite directional interaction, in agreement with the MEP surface that shows a small area at the methyl group where the ζ-hole is located (blue isocontour, +16 kcal/mol in Fig. 6). It should be emphasized that the MEP minimum is located at the interacting N-atom, thus indicating that this TtB is electrostatically very favoured. Consequently, the dimerization energy is large ΔE = –10.6 kcal/mol confirming the attractive and strong nature of the ζ-hole TtB interaction (–5.3 kcal/mol each TtB). The QTAIM analysis evidences that the terminal N-atom of the azido ligand is indeed connected to the carbon atom by a bond CP (red sphere) and bond path, thus supporting the formation of the TtBs. The NCI plot also shows a green isosurface located between the N-atom and mostly the C-atom of the methyl group, thus further characterizing the TtB interaction. The green colour of the isosurface is a further confirmation of the attractive nature of the interaction. Moreover, Natural Bond Orbital (NBO) analysis has been performed since it is a convenient tool to differentiate the carbon bonding from the trifurcated hydrogen bonding in the ROCH$_3$···N TtB interaction described above. That is, a C–H···N hydrogen bonding interaction implies an electron donation from a lone pair (LP) or π orbital of the azido group to an empty anti-bonding (BD*) C–H ζ–orbital. The alternative O–C···N TtB (ζ-hole) interaction implies an electron donation from an LP or π orbital of the azido group to an empty anti-bonding C–O ζ–orbital. Consequently, to shed light into in this dimer, NBO calculations have been performed focusing on the second order perturbation analysis since it is very convenient to analyze donor-acceptor orbital interactions.

The results gathered in Fig. **IV.5** (lower-right side) reveal the existence of two donor-acceptor orbital interactions, one between the nitrogen (LP) orbital and the empty (BD*) C–O

orbital ($E^{(2)}$ = 0.64 kcal/mol) and other between the N≡N (π) orbital and the empty (BD*) C–O orbital (E$^{(2)}$ = 0.18 kcal/mol).
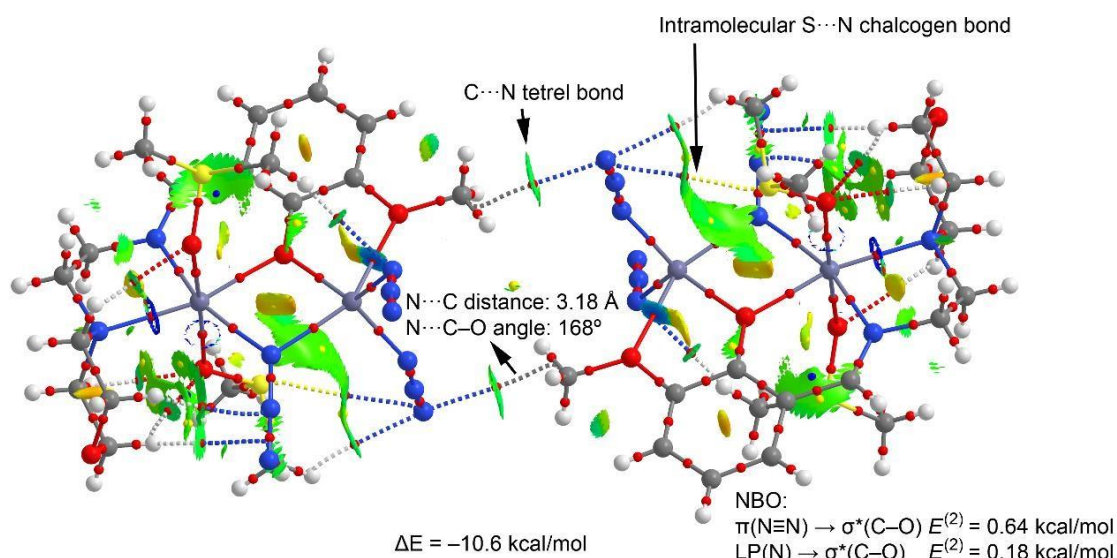

Fig. IV.5: Combined QTAIM (bond, ring and cage critical points represented in red, yellow and blue spheres, respectively) and NCI plot (isosurface = 0.4 a.u., gradient cut-off = 0.004 a.u., color range –0.04 ≤ sign(λ_2)*ρ ≤ 0.04 a.u.) for the centrosymmetric dimer of [(DMSO)$_2$ZnL($\mu_{1,1}$-N$_3$)Zn(N$_3$)$_2$] at the PBE0-D3/def2-TZVP level of theory

Remarkably, no other orbital donor-acceptor interaction has been found involving the azido and the H-atoms of the methyl group. Similar results have been described before in tetrel bonds involving the methyl group of DMF and also in a bis-Schiff base of N-allyl isatin. Therefore, from an orbital point of view, the non-covalent interaction can be clearly defined as a TtB interaction. Finally, it should be emphasized that the orbital contributions are very small compared to the total interaction energy (–10.6 kcal/mol) thus indicating that orbital effects are negligible and the interaction is dominated by electrostatic effects, in line with the MEP surface analysis.

IV. 4. Concluding Remarks

In the present study, a new dinuclear zinc Schiff-base complex has been synthesized and X-ray characterized. The importance of non-covalent ζ-hole TtB interactions in the solid state has been described and studied focusing on the energetic features and characterized using QTAIM and NCI Plot. The existence of ζ-hole N(azide)⋯C TtB interaction instead of three C–H⋯N(azide) H-bonds has been confirmed by NBO analysis. Keeping in mind the current interest in the exploration of ζ-hole interactions, the present work may shed light on such non-covalent forces in coordination complexes and its importance in crystal engineering.

References

1 (a) P. Politzer, J. S. Murray, Crystals., 2019, **9**, 165; (b) P. Politzer, J. S. Murray, T. Clark, G. Resnati, *Phys. Chem. Chem. Phys*., 2017, **19**, 32166.

2 (a) A. Bauzá, I. Alkorta, J. Elguero, T. J. Mooibroek, A. Frontera, *Angew. Chem. Int. Ed*., 2020, **59**, 17482; (b) I. Alkorta, J. Elguero, A. Frontera, *Crystals*, 2020, **10**, 180; (c) A. Frontera, *Molecules*, 2020, **25**, 3419; (c) R. M. Gomila, A. Frontera, *Front. Chem*., 2020, **8**, 395; (d) A. Bauzá, A. Frontera, *Coord. Chem. Rev*., 2020, **404**, 213112; (e) G. Cavallo, P. Metrangolo, T. Pilati, G. Resnati, G. Terraneo, *Cryst. Growth Des*., 2014, **14**, 2697; (f) G. Terraneo, G. Resnati, Bonding Matters. *Cryst. Growth Des*., 2017, **17**, 1439; (g) A. Frontera, A. Bauzà, *Chem. Eur. J*., 2018, **24**, 7228–7234; (h) A. A. Eliseeva, D. M. Ivanov, A. V. Rozhkov, I. V. Ananyev, A. Frontera and V. Yu. Kukushkin, *JACS Au*, 2021, **1**, 10.1021/jacsau.1c00012; (i) S. Yu, P. Kumar, J. S.Ward, A. Frontera and K. Rissanen, *Chem*, 10.1016/j.chempr.2021.01.003.

3 A. Frontera, *C*, 2020, **6**, 60.

4 (a) P. Scilabra, G. Terraneo, G. Resnati, *Acc. Chem. Res*., 2019, **52**, 1313; (b) P. Scilabra, G. Terraneo, G. J. Resnati, *Fluor. Chem*., 2017, **203**, 62.

5 (a) V. R. Mundlapati, D. K. Sahoo, S. Bhaumik, S. Jena, A. Chandrakar and H. S. Biswal, *Angew. Chem. Int. Ed.*, 2018, **57**, 16496; (b) T. J. Mooibroek, *Molecules*, 2019, **24**, 3370.

6 (a) A. Bauzá, T. J. Mooibroek and A. Frontera, *Chem. Phys. Chem*., 2015, **16**, 2496; (b) A. Bauzá, T. J. Mooibroek and A. Frontera, *Chem Eur. J*., 2014, **20**, 10245; (c) A. Bauzá, T. J. Mooibroek and A. Frontera, *Chem. Commun*., 2014, **50**, 12626; (d) A. Bauzá and A. Frontera, *Crystals*, 2016, **6**, 26.
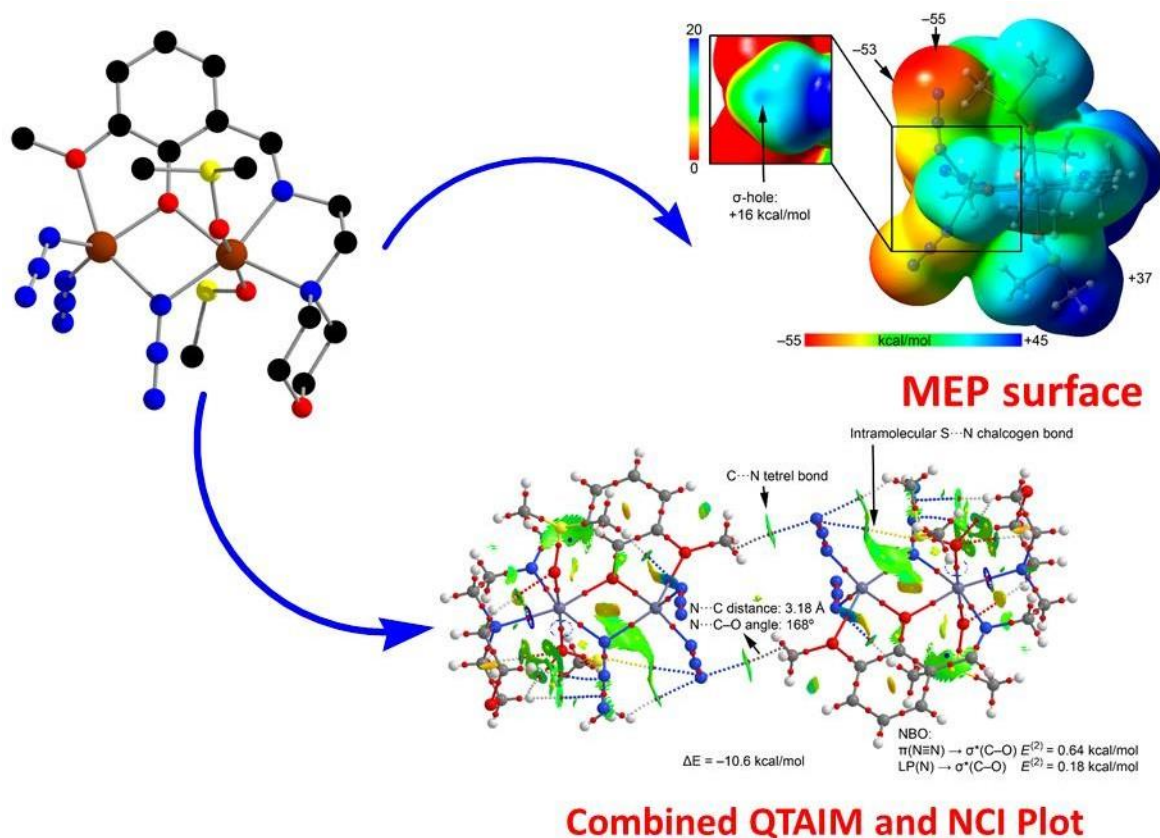
7 (a) M. Karmakar, T. Basak, S. Chattopadhyay, *New J. Chem.*, 2019, **43**, 4432; (b) M. Karmakara, A. Frontera, S. Chattopadhyay, *CrystEngComm*, 2020, **22**, 6876.

8 (a) T. Basak, A. Bhattacharyya, K. Harms, S. Chattopadhyay, *Polyhedron*, 2019, **157**, 449; (b) T. Basak, M. G. B. Drew, S. Chattopadhyay, *Inorg. Chem. Comm.*, 2018, 98, 92.

9 S. Roy, I. Mondal, K. Harms, S. Chattopadhyay, *Polyhedron*, 2019, **159**, 265.

10 I. Mondal, T. Basak, S. Banerjee, S. Chattopadhyay, *CrystEngComm.*, 2020, **22**, 3005.

11 (a) P. Sharma, A. Gogoi, A. K. Verma, A. Frontera and M. K. Bhattacharyya, *New J. Chem.*, 2020, **44**, 5473; (b) A. Das, P. Sharma, A. Frontera, A. K. Verma, M. Barcelo-Oliver, S. Hussain and M. K. Bhattacharyya, *J. Mol. Struct.*, 2020, **1223**, 129246; (c) S. M. N. Islam, D. Dutta, P. Sharma, A. K. Verma, A. Frontera and M. K. Bhattacharyya, *Inorg. Chim. Acta*, 2019, **498**, 119108; (d) U. Saha, D. Dutta, A. Bauzá, A. Frontera, B. Sarma and M. K. Bhattacharyya, *Polyhedron*, 2019, **159**, 387; (e) A. Gogoi, A. Das, A. Frontera, A. K. Verma and M. K. Bhattacharyya, *Inorg. Chim. Acta*, 2019, **493**, 1; (f) M. K. Bhattacharyya, D. Dutta, S. M. N. Islam, A. Frontera, P. Sharma, A. K. Verma and A. Das, *Inorg. Chim. Acta*, 2020, **501**, 119233; (g) U. Saha, D. Dutta, H. Nath, A. Franconetti, A. Frontera and M. K. Bhattacharyya, *Inorg. Chim. Acta*, 2019, **488**, 159.

12 (a) V. P. Singh, P. Singh and A. K. Singh, *Inorg. Chim. Acta.*, 2011, **379**, 56; (b) A. Bhattacharyya, S. Sen, K. Harms and S. Chattopadhyay, *Polyhedron*, 2015, **88**, 156.

13 P. K. Bhaumik, A. Banerjee, T. Dutta, S. Chatterjee, A. Frontera, S. Chattopadhyay, *CrystEngComm*, 2020, **22**, 5263.

14 S. Roy, M. G. B. Drew, A. Bauzá, A. Frontera, S. Chattopadhyay, *Dalton Trans.*, 2017, **46**, 5384.

15 S. Roy, M. G. B. Drew, A. Bauzá, A. Frontera, S. Chattopadhyay, *Chemistry Select*, 2017, **2**, 10586.

16 P. Pal, S. Konar, P. Lama, K. Das, A. Bauzá, A. Frontera and S. Mukhopadhyay, *J. Phys. Chem. B*, 2016, **120**, 6803.

Chapter V

Some zinc(II) complexes with tetradentate reduced Schiff base ligands: luminescence property and application in sensing of nitroaromatics

σ-hole: +16 kcal/mol

MEP surface

Intramolecular S···N chalcogen bond

C···N tetrel bond

N···C distance: 3.18 Å
N···C–O angle: 168°

ΔE = −10.6 kcal/mol

NBO:
$\pi(N \equiv N) \rightarrow \sigma^*(C-O)$ $E^{(2)}$ = 0.64 kcal/mol
$LP(N) \rightarrow \sigma^*(C-O)$ $E^{(2)}$ = 0.18 kcal/mol

Combined QTAIM and NCI Plot

Section: V.A

A theoretical insight on the rigid hydrogen-bonded network in the solid state structure of two zinc(II) complexes and their strong fluorescence behaviors

V.A.1. Introduction

The easy synthetic route, stability and complexing ability are mainly responsible for the enduring recognition of salen type Schiff base ligand for long. They have widely been used to prepare several of transition and non-transition metal complexes for long.[1] Many such complexes were found to have interesting applications in material science.[2] Sodium borohydride is a mild reducing agent and it could easily be used to reduce these salen type N_2O_2 donor Schiff bases.[3] These reduced Schiff bases may also be used to form transition and non- transition metal complexes.[4] Due to more flexibility (as a result of reduction of imine linkage) of these reduced Schiff bases, the molecular architectures of their complexes are more versatile.[5] They have also been shown to have different applications in catalysis and magnetism.[5a, 6] However, compared with the huge reports on the complexes of salen type Schiff bases, their reduced counterparts are relatively less explored. In the present work, a reduced Schiff base ligand has been synthesized and used to act as a chemosensor for the detection of zinc(II) via turn-on fluorescence response. The reduced Schiff base was also used to prepare two zinc(II) complexes.

Non-covalent interactions in the supramolecular assembly of the complex were studied energetically using theoretical DFT calculations to understand clearly the intermolecular hydrogen bonding in the dimeric form of the complex. These interactions have also been analyzed using several computational tools, including Bader's "atoms-in-

molecules" (AIM) and MEP analyses and Reduced Density Gradient (NCI-RDG) methods established nicely the presence of such noncovalent intermolecular interactions.

In this work, we would like to report the synthesis, structure, characterization of two zinc(II) complexes, *[Zn(H₂L)(OCOCH₃)(N₃)] (7) and [Zn(H₂L)(OCOCH₃)(NCS)] (8),* with a potential tetradentate reduced Schiff base ligand, *1,3-bis(2-hydroxybenzylamino)-2,2-dimethylpropane (H_2L^7).* In each complex, the ligand behaves as a bidentate ligand keeping the phenoxo arms pendant. The ability of the ligand to sense zinc(II) selectively has been assessed. Fluorescence titrations have also been done for the ligand and binding constant for ligand has been evaluated by Benesi−Hilderbrand equation. The electronic structures for the ground state and 1st excited state of both complexes were calculated. Based on optimized ground state geometry, the TDDFT/B3LYP method combined with SMD solvation model in methanol media was used to calculate the absorption properties of the investigated complexes. Investigation on the electronic structure of the excited states was also performed employing NTO representation. The calculation indicates that the fluorophore is originated from the charge transfer from N_3/NCS to reduced Schiff base. On the other hand, Bader"s Quantum Theory of Atoms-in-Molecules (QTAIM) was used to obtain insight into the physical nature of weak non-covalent interactions in both complexes. Additionally, the Noncovalent Interactions Reduced Density Gradient (NCI-RDG) methods established nicely the presence of such noncovalent intermolecular interactions.

V.A.2. Experimental

V.A.2.2. Synthesis

V.A.2.2.1. Synthesis of the ligand, 1,3-Bis(2-hydroxybenzylamino)-2,2-dimethylpropane (H_2L^7)

A Schiff base ligand, *{N,N'-bis(salicylidene)-2,2-dimethylpropane-1,3-diamine}*, was synthesized by refluxing 2,2-dimethylpropane-1,3-diamine (1 mmol, 0.1 mL) with salicylaldehyde (2mmol, 0.2 mL) in methanol (20 mL) solution for ca. 2 h. The Schiff base ligand was not purified but used directly for the preparation of the reduced Schiff base ligand (H_2L^7). After that, the solution (10 mL) was cooled to 0°C and solid sodium borohydride (4 mmol, ~150 mg) was added to it with constant stirring. Then the resulting solution was acidified with glacial acetic acid (2 mL) and stirred for 10 minutes. The methanol was evaporated to dryness under reduced pressure in a rotary evaporator (~60°C). The white residue was then dissolved in water (15 mL) and extracted with a mixture of dichloromethane (15 mL) and a saturated solution of sodium bicarbonate. The organic phase was dried over anhydrous sodium acetate and the solvent (i.e. dichloromethane) was evaporated under reduced pressure using a rotary evaporator to get the white color reduced Schiff base ligand (H_2L^7).

Yield: 0.251g (~80%). Anal. Calc. for $C_{19}H_{26}N_2O_2$ (FW= 314.19): C, 72.58; H, 8.33; N, 8.91 %. Found: C, 72.4; H, 8.2; N, 9.0%. FT-IR (KBr, cm^{-1}): 3304 (ν_{O-H}), 3046 (ν_{N-H}), 2955-2850 (ν_{C-H}). UV-Vis, λ_{max} (nm), [ε_{max} (dm^3 mol^{-1} cm^{-1})] (CH$_3$OH), 275 (~10^2).^{1}H NMR (CD$_3$CN) (ppm) δ: 7.11, 7.13 and 7.11 (t, *J* = 7.7 Hz, 2H, aromatic CH), 7.04 and 7.06 (d, *J* = 7.1 Hz, 2H, aromatic CH), 6.74-6.80 (m, 4H, aromatic CH), 5.5 (b, 2H, phenolic OH),3.92 (s, 4H, benzyl CH$_2$), 2.48 (s, 4H, methylene CH$_2$), 2.04 (m, 1H, amine NH),0.95 (s, 6H, methyl CH$_3$).

V.A.2.2.2. Synthesis of complexes

[Zn(H$_2$L^7)(OCOCH$_3$)(N$_3$)](7)

The methanol solution (10 mL) of zinc(II) acetate dihydrate (1 mmol, 0.300 g) was added to the methanol solution (20 mL) of the reduced Schiff base ligand, *H$_2$L^7* and the

resulting solution was stirred. After 15 min of stirring, methanol-water (2:1) solution of sodium azide (90 mg, 1 mmol) was added to it. The mixture was stirred for 2 h and then filtered. It was kept in open air at room temperature for 3 days. White crystalline product was collected by filtration. X-ray quality single crystals were collected from this crystalline product.

Yield: 340 g, 71% (based on zinc). Anal. Calc. for $C_{21}H_{29}N_5O_4Zn$(F.W. 480.88): C, 52.45; H, 6.08; N, 14.56 %. Found: C, 52.3; H, 5.9; N, 14.6 %. FT-IR (KBr, cm^{-1}): 3255 (ν_{N-H}); 2945-2835(ν_{C-H}); 2058 (ν_{N3}). λ_{max} (nm) [ε_{max}(lit mol^{-1} cm^{-1})] (CH$_3$OH): 284 (5.2 x10^3), 234 (1.09x10^4).^{1}H NMR (CD$_3$CN) (ppm) δ: 7.14, 7.11 and 7.09 (t, J = 7.7 Hz, 2H, aromatic CH), 7.05 and 7.03 (d, J = 7.1 Hz, 2H, aromatic CH), 6.76 (bs, 4H, aromatic CH), 5.5 (b, 2H, phenolic OH), 3.92 (s, 4H, benzyl CH$_2$), 2.11 (s, 4H, methylene CH$_2$), 1.86 (s, 1H, amine NH), 0.96 (s, 6H, methyl CH$_3$).

[Zn(H$_2$L^7)(OCOCH$_3$)(NCS)] (8)

Complex **8** was prepared in a similar method as that of complex **7** except that sodium thiocyanate was used instead of sodium azide. The solution was filtered and kept in the open air at room temperature for 2 days. The white coloured X-ray quality single crystals suitable for X-ray diffraction were obtained by filtration.

Yield: ~360 g, 72% (based on zinc). Anal. Calc. for $C_{22}H_{29}N_3O_4SZn$(F.W. 496.93): C, 53.17; H, 5.88; N, 8.46%. Found: C, 53.0; H, 5.7; N, 8.5 %. FT-IR (KBr, cm^{-1}): 3255 (ν_{N-H}); 2945-2835(ν_{C-H}); 2086 (ν_{NCS}). λ_{max} (nm) [ε_{max}(lit mol^{-1} cm^{-1})] (CH$_3$OH): 284 (5.6x10^3), 234 (1.33x10^4).^{1}H NMR (CD$_3$CN) (ppm) δ: 7.14, 7.11 and 7.09 (t, J = 7.7 Hz, 2H, aromatic CH), 7.05 and 7.03 (d, J = 7.1 Hz, 2H, aromatic CH), 6.76 (bs, 4H, aromatic CH), 5.5 (b, 2H, phenolic OH), 3.92 (s, 4H, benzyl CH$_2$), 2.11 (s, 4H, methylene CH$_2$), 1.86 (s, 1H, amine NH),0.96 (s, 6H, methyl CH$_3$).

V.A.2.5. Binding stoichiometry (Job's plot)

Job's continuation method was employed to find out the binding stoichiometry of the

Table V.A.1. Crystal data and refinement details of complexes **7** and **8**.

Complex	7	8
Formula	$C_{21}H_{29}N_5O_4Zn$	$C_{22}H_{29}N_3O_4SZn$
Formula Weight	480.88	496.93
Temperature (K)	273	273
Crystal System	Monoclinic	Monoclinic
Space group	$P2_1/n$	$P2_1/n$
a (Å)	11.3910(8)	11.3882(12)
b (Å)	18.0035(13)	17.9996(19)
c (Å)	11.849(1)	11.8463(15)
β (°)	108.327(4)	108.327(4)
V(Å^3)	2306.7(3)	2305.1(5)
Z	4	4
d_{cal} (g cm^{-3})	1.385	1.432
μ(mm^{-1})	1.101	1.189
F(000)	1008.0	1040.0
Total reflection	34581	36474
Unique Reflections	4717	5089
Observe data[I>2ζ(I)]	3947	4157
R(int)	0.032	0.033
R1, wR2 (all data)	0.0481, 0.1200	0.0692, 0.1805
R1, wR2 [I>2σ(I)]	0.0327, 0.1000	0.0520, 0.1605
Residual Electron Density (eÅ^{-3})	0.757, −0.758	0.880, −0.989

CCDC reference nos 1970023 and 1970024 for complexes **7** and **8** respectively.

chemosensor with that of Zn^{2+} ions using emission spectroscopy. At room temperature (25 °C), the fluorescence was noted for solutions where the concentrations of Zn^{2+} ions, as well as the ligand concentration, were varied with respect to one another, but the sum of their concentrations was kept constant at 1×10^{-4} M. Relative change in fluorescence ($\Delta I/I_0$) were plotted as a function of mole fraction of Zn^{2+}. From the break point the stoichiometry was estimated.

V.A.3. Results and discussion

V.A.3.1. Synthesis

A N_2O_2 donor Schiff base ligand was synthesized by refluxing salicylaldehyde and 2,2-dimethyl-1,3-diaminopropane in methanol. The resulting Schiff base solutions were reduced with sodium borohydride in methanol to obtain the corresponding reduced Schiff base ligand, H_2L^7, following the literature method.[9] After reduction the white residue was extracted in organic layer from the mixture of dichloromethane and saturated solution of sodium bicarbonate. The solvent (i.e. dichloromethane) was evaporated under the reduced pressure to obtain the pure reduced Schiff base ligand.

V.A.3.2. IR, electronic and NMR Spectra

The most important observation in the IR spectrum of the ligand is the absence of any band around 1600 cm^{-1} (characteristic of azomethine (>C=N) stretching vibrations) and this confirms the reduction of the Schiff base moiety. In the electronic spectrum of the ligand, two absorption bands are observed around 229 nm and 275 nm, which may be attributed as the π→π* and n→π* electron transfer transitions, respectively.[10] Both UV-Vis and IR spectra are shown in Fig. **V.A.1.** and **V.A.2.** respectively.
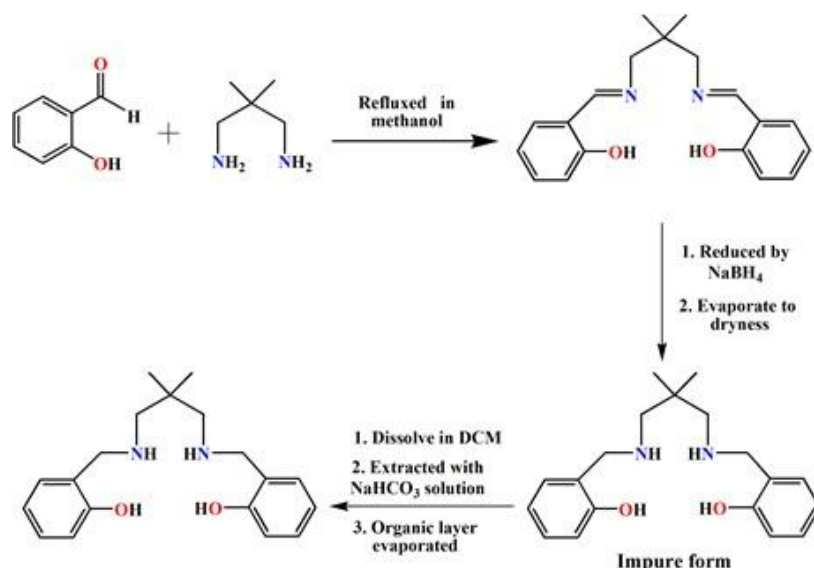
Scheme V.A.1.: Synthetic route to the „reduced Schiff base" ligand.

In the NMR spectrum of the ligand, the aromatic protons of reduced Schiff base are noticed in the range of 6.80-7.11 ppm. The methylene and benzyl protons appear as singlet at 2.48 ppm and 3.92 ppm, respectively. Methyl protons of 2,2-dimethyl-1,3-diaminopropane appear as singlet at 0.95 ppm. Amine protons are observed as multiplet at 2.04 ppm. The phenolic hydrogen is observed as a broad singlet around ~5.5 ppm. ^{1}H NMR spectrum of the ligand is shown in Fig. **V.A.3.**
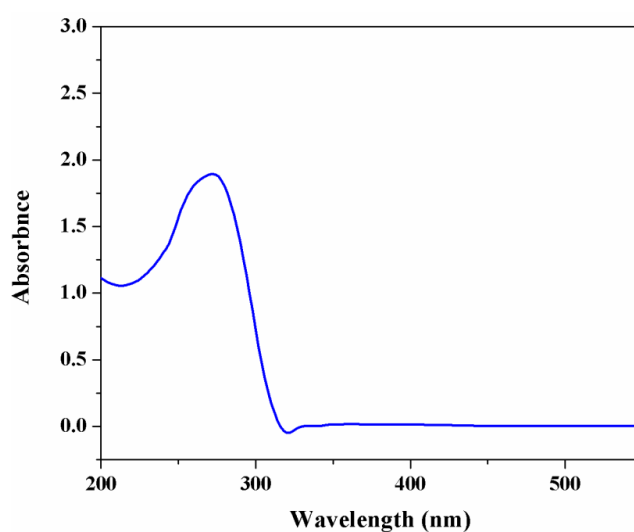
Fig. V.A.1. UV-Vis spectrum of ligand (**H₂L⁷**).
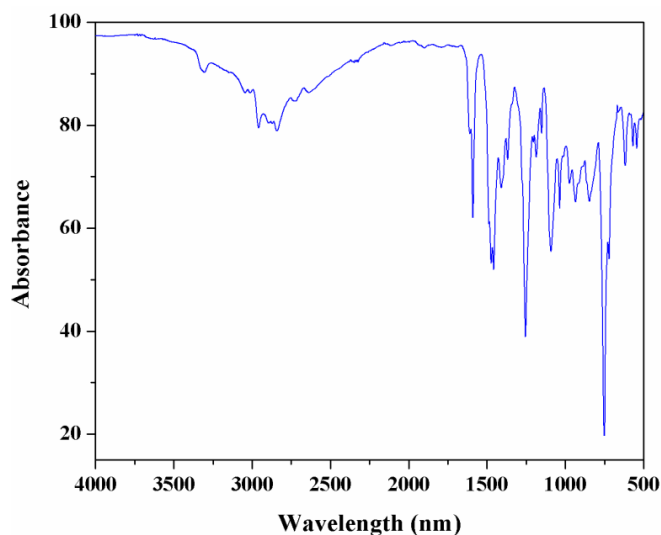
Fig. V.A.2. IR spectrum of ligand (**H₂L⁷**)

V.A.3.3. Fluorescence Properties

Upon excitation at 275 nm in methanol solution, the emission occurs at 311 nm. The fluorescence intensity of the ligand is enormously enhanced upon addition of zinc(II) salt

 (Fig. **V.A.4**).
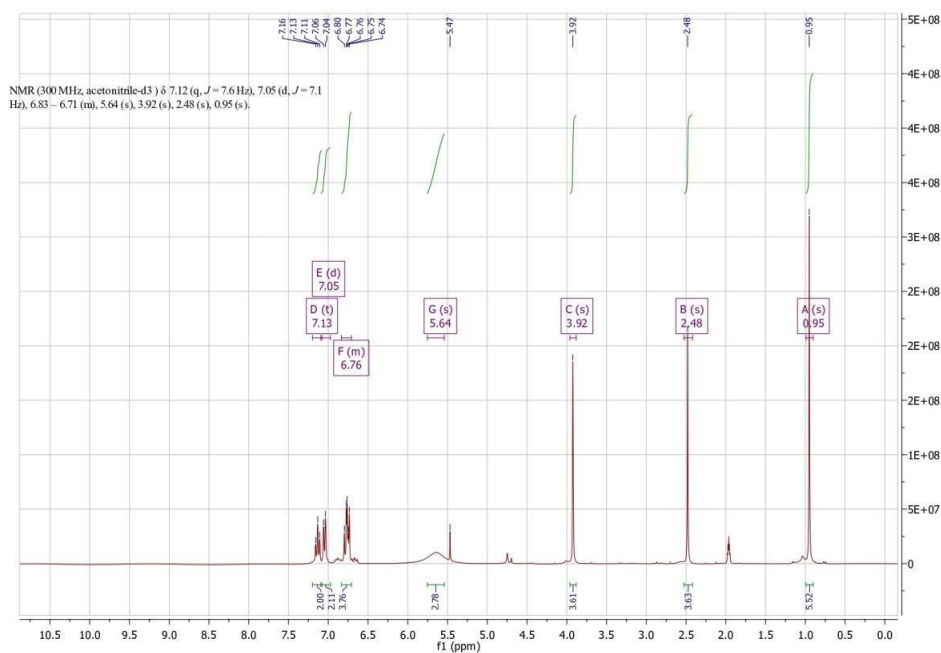
Fig. V.A.3. NMR spectrum of ligand (**H₂L⁷**)
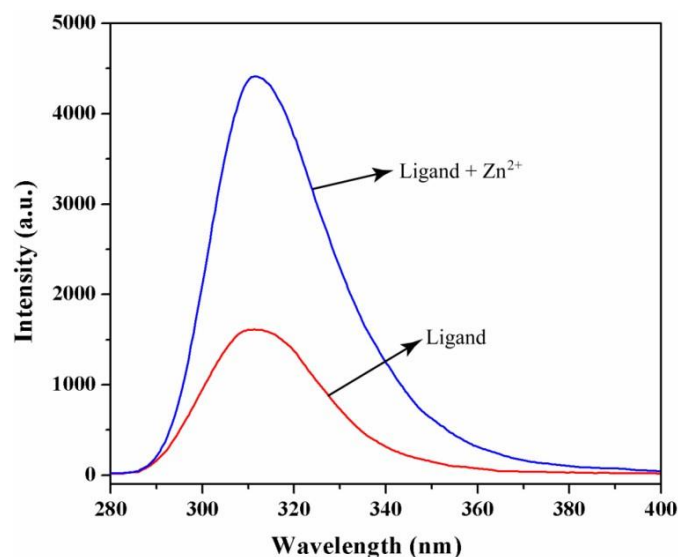
Fig. V.A.4. Fluorescent spectra of ligand in absence (red) and in presence (blue) of of zinc(II) salt (900µL).

Emission for the reduced Schiff base ligand is tentatively attributed to the intra-ligand electronic transitions. Fluorescence lifetime of the ligand is investigated at room temperature and found 3.3 ns. Decay profile (Fig. **V.A.5.**) is fitted to a multi-exponential model:

$$I(t) = \sum_i a_i \exp \frac{-t}{c_i}$$

Where, mono-exponential functions are used to fit the emission of the ligand and obtaining χ^2 close to 1.

In order to evaluate the sensing behavior of H_2L^7, different solutions containing 1:1 mixture of the ligand (H_2L^7) and various metal ions have been prepared using acetate salts of different bivalent metal ions, e.g., Mn^{2+}, Co^{2+}, Ni^{2+}, Cu^{2+}, Cd^{2+}, Pb^{2+}, and Zn^{2+}. Fluorescence intensities of these solutions were measured. In case of $Zn(OAc)_2$ and $Cd(OAc)_2$, a significant change in fluorescence intensity is observed on addition of the metal ions as shown in **Fig. V.A.6.** However, maximum fluorescence intensity is observed for $Zn(OAc)_2$.
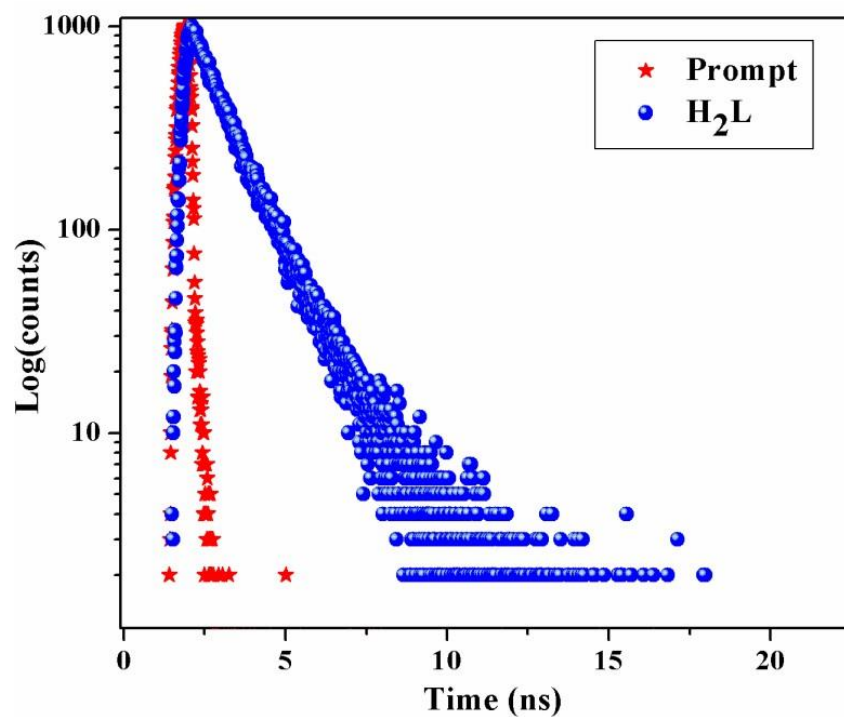
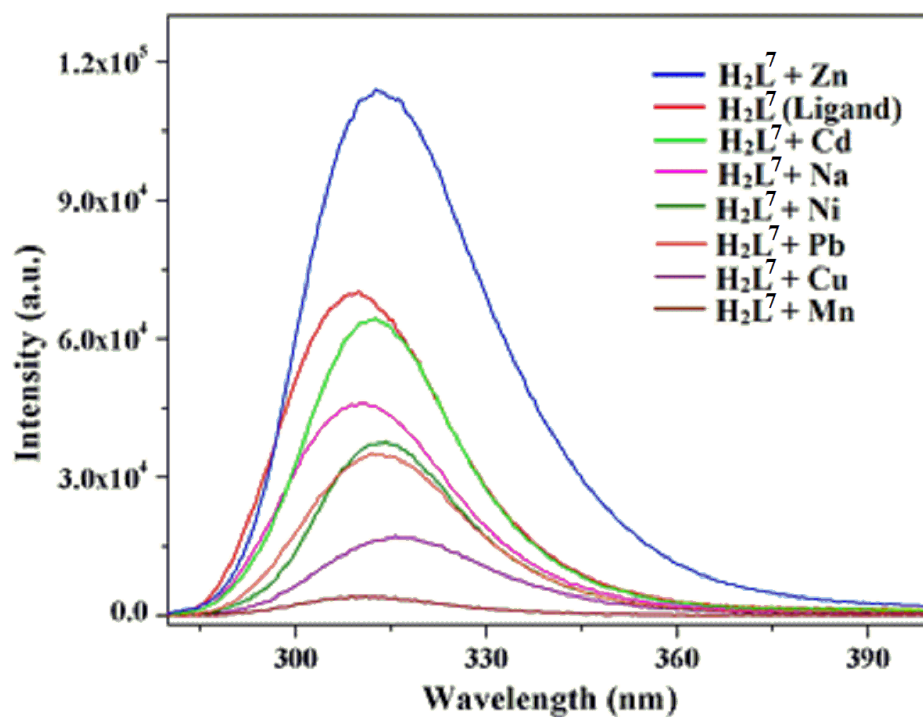**Fig. V.A.5.** The excited-state decay profiles for ligand following pulsed excitation at 275 nm in methanol.

Fig. V.A.6. Fluorescence spectra of the mixture of ligand H_2L^7 in the presence of various metal ions.

V.A.3.4. Fluorescence titration

Job"s plot may be used to define the binding stoichiometry of ligand with Zn^{2+}. It is derived using fluorescence titration experiment, and maximum fluorescence intensity is observed when the mole fraction of the Zn^{2+} ions is about 0.45, which indicates the formation of about 1:1 complex between H_2L and Zn^{2+}. The plot has been shown in **Fig. V.A.7**.
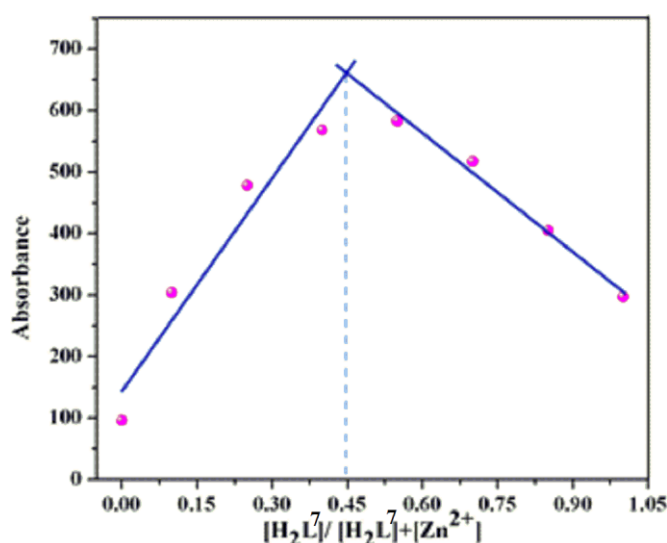
Fig. V.A.7. Job"s plot for determining the stoichiometry of H_2L^7 and Zn^{2+}.

The fluorescence titration of the ligand (H_2L^7) is carried out by the gradual addition of Zn^{2+} [using $Zn(OAc)_2$]. The fluorescence intensity increases linearly, indicating that Zn^{2+} is quantitatively bound to ligand H_2L^7 and shows excellent sensitivity. The plot of fluorescence intensity change ($I-I_0$) with the addition of Zn^{2+} shows a polynomial curve (Fig. **V.A.8**). This suggests that the fluorescence intensity increases linearly at the lower concentration of Zn^{2+} and becomes parallel to x-axis, when Zn^{2+} addition is higher. Now the binding constant between ligand H_2L^7 and Zn^{2+} is calculated for a 1:1 stoichiometry using the Benesi-Hilderbrand equation, where I_0= emission intensities in the absence of quencher, I= intermediate intensities and I_a= intensity at an infinite concentration of the Zn^{2+} ion.

$$\frac{1}{I - I_0} = \frac{1}{K(I_\infty - I_0)[Q]^n} + \frac{1}{I_\infty - I_0}$$

From the Benesi−Hilderbrand plot, the binding constant K can easily been obtained from the slope and the value of K is 1.056×10^6 M^{-1}. Here the n=1 and the plot has been shown in Fig. **V.A.9**.
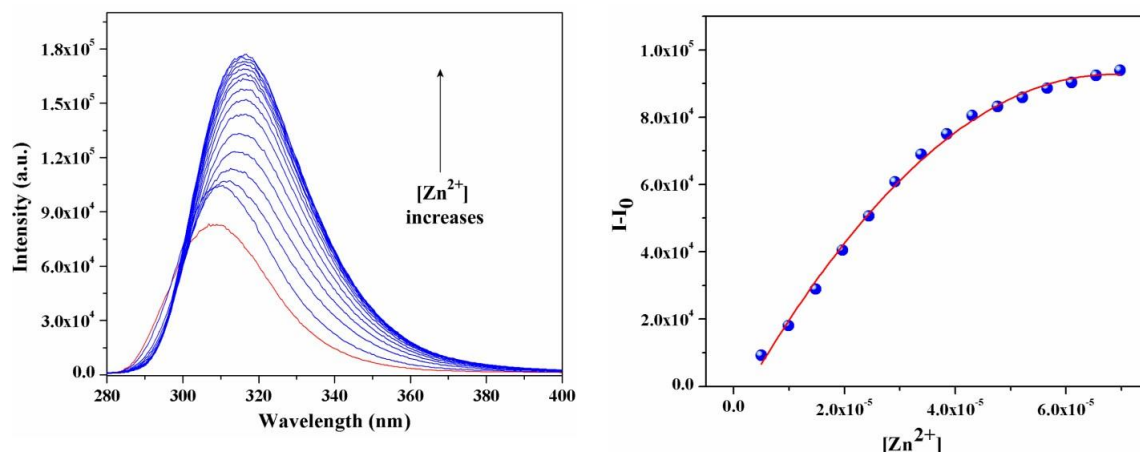

Fig. V.A.8. Fluorescence titration curve of ligand H$_2$L^7 with Zn^{2+} ion in methanol at room temperature(left) and change in fluorescence intensity (I-I$_0$) with the equivalent of Zn^{2+} ion added (right).
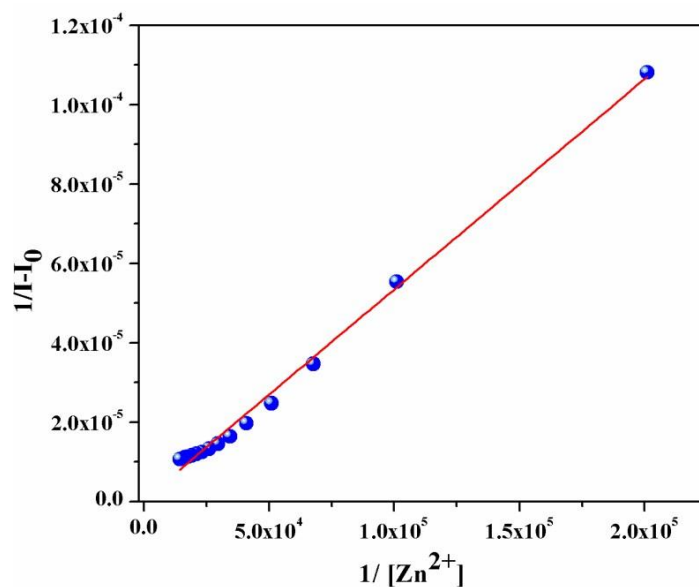
Fig. V.A.9. Benesi−Hilderbrand plot for H$_2$L^7 and Zn(II) complex formation.

V.A.3.5. Isolation of the ligand as zinc(II) complexes

The ligand, H_2L^7, has been trapped as zinc(II) complex by reaction with zinc(II) acetate dihydrate and sodium azide/thiocyanate in a 1:1:1 molar ratio. Two mononuclear zinc(II) complexes, $[Zn(H_2L^7)(OCOCH_3)(N_3)]$ (**7**) and $[Zn(H_2L^7)(OCOCH_3)(NCS)]$ (**8**) have been produced. The synthetic route to complexes has been shown in Scheme **V.A.2**.
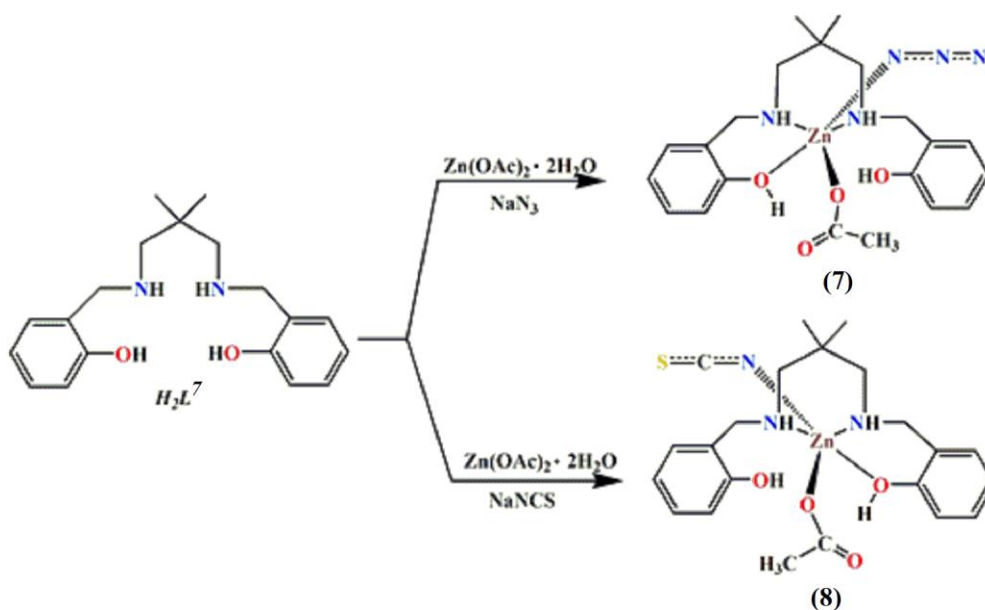
Scheme V.A.2.Synthetic route complexes **7** and **8**.

V.A.3.6. Structure Description

X-ray crystal structure determinations reveal that both complexes consist of discrete mononuclear units $[Zn(H_2L^7)(OCOCH_3)(X)]$, X=azide for **7** and thiocyanate for **8**. Each complex crystallizes in the monoclinic space group, $P2_1/n$. The perspective views of the zinc(II) complexes **7** and **8** with the selecting atom numbering scheme are shown in Figs. **V.A.10.** and **V.A.11.** respectively. In each complex, the zinc(II) center, Zn(1), is pentacoordinated being coordinated by two amine nitrogen atoms, N(1) and N(2) and one phenoxo oxygen atom, O(3), of the reduced Schiff base and one oxygen atom, O(3), from acetate group. The fifth coordination position is occupied by one nitrogen atom, N(3), from

pseudo halide {azide for complex **7** and thiocyanate for complex **8**}. The geometry of any

pentacoordinated metal centre may conveniently be measured by the Addison parameter $(\eta)^{11}$

[η = (x−y)/60, where x and y are the two largest ligand–metal–ligand angles in the

coordination sphere]. In both complexes **7** and **8**, the Addison parameter (η) values are 0.692

and 0.695, respectively. These η values indicate that the geometry around the zinc(II) centers,

Zn(1), is lying in between the square pyramidal and trigonal bipyramidal geometry. Important

bond lengths and bond angles are gathered in Tables **V.A.2** and **V.A.3** respectively. The

saturated six membered chelate ring, Zn(1)-N(1)-C(8)-C(9)-C(12)-N(2) represents a chair

conformation with puckering parameters[12] q(2) = 0.634(2) Å, θ = 4.45(18)° and θ = 54(3)°

for complex **7** and q(2) = 0.638(3) Å, θ = 175.4(3)° and θ = 237(4)° for complex **8**.
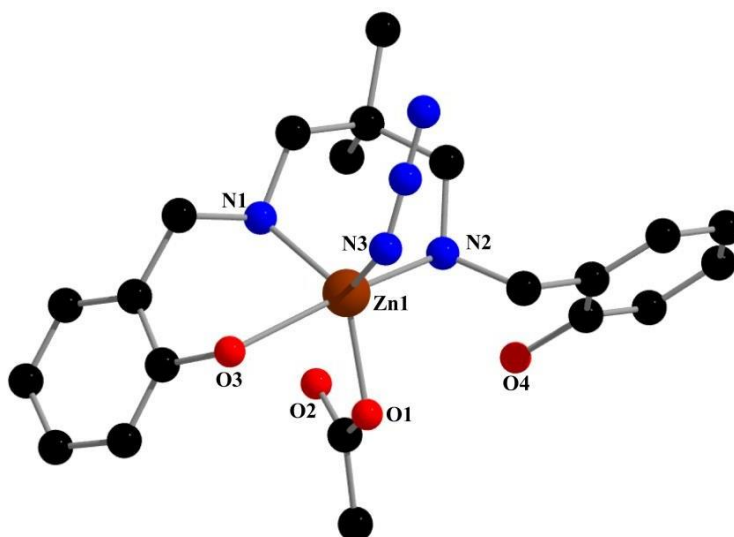

Fig. V.A.10. Perspective view of complex **7** with selective atom numbering scheme.

Hydrogen atoms have been omitted for clarity.

V.A.3.7. Supramolecular Interactions present in the solid state structures of zinc(II) complexes

      Supramolecular non-covalent interaction, i.e. hydrogen bonding, is responsible for the

solid state stability of crystal structures of both complexes. A hydrogen atom, H(2A),

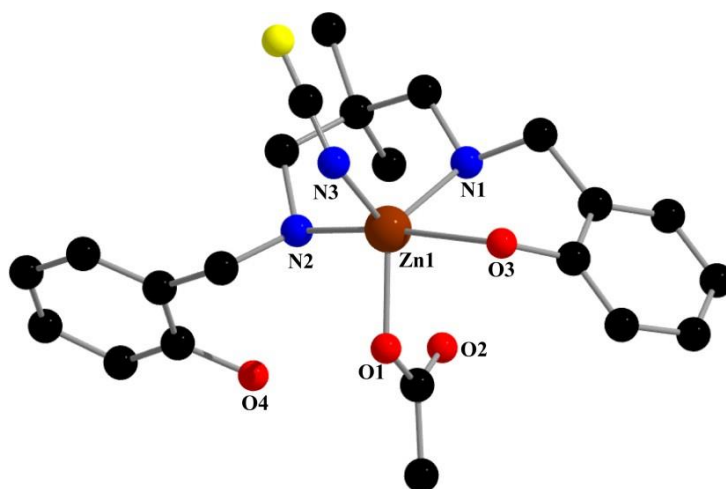attached to an amine nitrogen atom, N(2), in each complex is involved in intramolecular

Fig. V.A.11. Perspective view of complex **8** with selective atom numbering scheme.

Hydrogen atoms have been omitted for clarity.

Table V.A.2: Selected bond lengths (Å) of complexes **7** and **8**.

Complex	7	8
Zn(1)-O(1)	2.0082(18)	2.008(3)
Zn(1)-O(2)	2.691(2)	2.694(3)
Zn(1)-O(3)	2.432(2)	2.431(4)
Zn(1)-N(1)	2.0555(19)	2.058(3)
Zn(1)-N(2)	2.117(2)	2.120(4)
Zn(1)-N(3)	1.984(2)	1.989(4)

Table V.A.3: Selected bond angles (°) of complexes **7** and **8**.

Complex	7	8
O(1)-Zn(1)-O(2)	53.35(7)	53.22(9)
O(1)-Zn(1)-O(3)	78.69(8)	78.69(11)
O(1)-Zn(1)-N(1)	130.09(8)	129.89(10)
O(1)-Zn(1)-N(2)	96.07(8)	96.04(11)
O(1)-Zn(1)-N(3)	113.51(9)	113.91(12)
O(2)-Zn(1)-O(3)	92.65(7)	92.72(10)
O(2)-Zn(1)-N(1)	81.08(7)	81.09(9)

O(2)-Zn(1)-N(2)	79.00(7)	78.92(11)
O(2)-Zn(1)-N(3)	166.31(8)	166.50(12)
O(3)-Zn(1)-N(1)	85.02(8)	84.90(10)
O(3)-Zn(1)-N(2)	171.65(8)	171.64(12)
O(3)-Zn(1)-N(3)	87.71(9)	87.96(13)
N(1)-Zn(1)-N(2)	93.61(9)	93.75(11)
N(1)-Zn(1)-N(3)	112.57(9)	112.39(12)
N(2)-Zn(1)-N(3)	100.40(9)	100.17(14)

hydrogen bonding with a phenoxy oxygen atom, O(4) of the reduced Schiff base. Another hydrogen atom, H(4A), attached to phenoxy oxygen atom, O(4), is involved in intermolecular hydrogen bonding interaction with oxygen atom, O(2) of the acetate group of the adjacent moiety. Similarly hydrogen atom, H(3A), attached to phenoxy oxygen atom, O(3), is involved in intermolecular hydrogen bonding interaction with oxygen atom, O(1) of the acetate group of the adjacent moiety. Due to this hydrogen bonding interactions 1D zigzag hydrogen bonded structure is formed for both complexes (Figs. **V.A.12.** and **V.A.13.**).The details of hydrogen bonding interactions have been given in Table **V.A.4**.
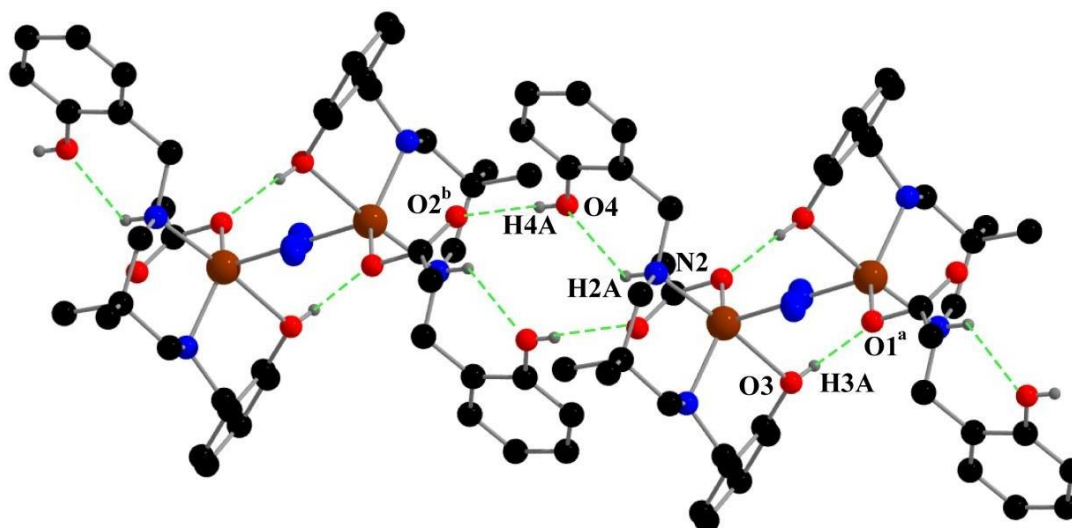

Fig. V.A.12. One dimensional chain of complex **7** formed by hydrogen bonding interactions. Only the relevant hydrogen atoms are shown for clarity. Symmetry transformation
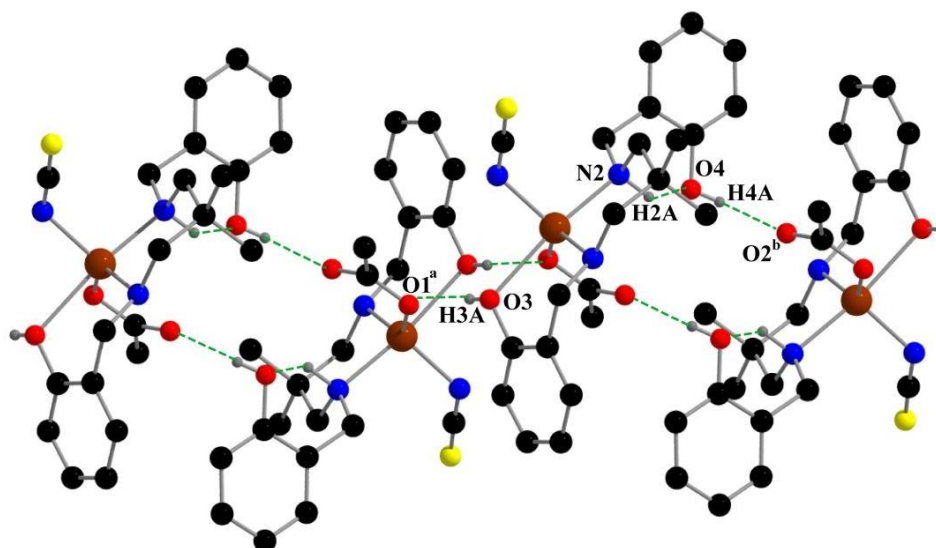
ᵃ=1−x,1−y,1−z, ᵇ= 2−x,1−y,1−z.

Fig. V.A.13. One dimensional chain structure formed by hydrogen bonding interactions in complex **8**. Only the relevant hydrogen atoms are shown for clarity. Symmetry transformation ^{a}= 1−x,1−y,1−z, ^{c}= −x,1−y,1−z .

Table V.A.4: Hydrogen bond distances (Å) and angles (◦) for complex **7** and **8**.

Complex	D–H···A	D-H	H···A	D···A	∠D-H···A
	N(2)-H(2A)···O(4)	0.86(3)	2.30(3)	2.925(3)	131(2)
7	O(3)-H(3A)···O(1)^a	0.76(4)	1.93(4)	2.682(3)	179(5)
	O(4)-H(4A)···O(2)^b	0.70(4)	1.99(4)	2.682(3)	173(4)
	N(2)-H(2A)···O(4)	0.9800	2.2300	2.925(5)	126.00
8	O(3)-H(3A)···O(1)^a	0.73(6)	1.96(6)	2.683(4)	171(6)
	O(4)-H(4A)···O(2)^c	0.78(6)	1.90(6)	2.674(5)	174(6)

D = donor; H = hydrogen; A = acceptor, Symmetry transformation: ^{a} = 1-x,1-y,1-z, ^{b} = 2-x,1-y,1-z , ^{c}= -x,1-y,1-z

V.A.3.8. DFT study on Non-Covalent interactions

We characterized two types of H-bodings in the investigated complex as shown in Figs. **V.A.14a** and **V.A.14b.** The first type of H-bonding, HB1, is characterized by AIM analysis which gives an orange sphere as BCP (Fig. **V.A.15**) between nitrogen atom of NCS and amine hydrogen atom of reduced Schiff base. The second type of hydrogen bonding, HB2, is formed between acetate oxygen and phenolic hydrogen atoms. The existence of both types of hydrogen bonding is well supported by the RDG plots and NCI surfaces as shown in Fig. **V.A.14**.

The reduced density gradient (RDG) was calculated to represent the deviation from a homogeneous electron distribution.[13] As presented in the following eqn. (1), ∇ is the gradient operator and $|\nabla\rho|$ is the electronic density gradient mode. Now, it is a useful approach to explore and visualize different kinds of noncovalent interactions (NCIs) in real space such as both intra- and intermolecular weak interactions like hydrogen bonds and Van der Waals forces. Therefore, the NCI index is used to investigate NCIs in the investigated complex.

$$s = \frac{1}{2(3\pi^2)^{\frac{1}{3}}} \frac{|\nabla\rho|}{\rho^{\frac{4}{3}}} \qquad (1)$$

The color mapped isosurfaces and corresponding scatter diagrams of RDG versus sign $(\lambda_2)\rho$ for the investigated complex in the monomer and dimers are shown in Fig. **V.A.14c,d**. As stated, the results are used to characterize two types of H-bonds via colored isosurfaces according to the values of sign $(\lambda_2)\rho$. The sign of λ_2 is used to distinguish bonded $(\lambda_2 < 0)$ and nonbonded $(\lambda_2 > 0)$ interactions, whereas the electron density is an indicator of the bonding strength. Large negative values of sign $(\lambda_2)\rho$ are indicative of attractive interactions (such as hydrogen bonding),whereas, if sign $(\lambda_2)\rho$ is large and positive, the interaction is nonbonding (usually steric effect). Values near zero indicate weak vdW interactions. The color of RDG

(s) vs. sign (λ_2)ρ and the isosurfaces have the same meaning; blue color represents hydrogen bonds; green, van der Waals forces; and red, steric hindrance. The darker the corresponding color, the stronger is the interaction.

The green region in Fig. **V.A.14a,b** clearly characterizes the HB1 and HB2 hydrogen bonding in the solid-state. Importantly, in HB1, the scatter RDG plot shows some additional blue dots at the left side to identify the stronger intermolecular H-bonding (Fig. **V.A.14c,d**).This is also supported from interaction energy. The BSSE corrected interaction energy for calculated from HB1 is −7.6 kcal/mol whereas this is −3.4 for the HB2.

V.A.3.9. IR, UV and NMR spectra of both complexes

In the IR spectrum of complex **7**, one intense peak at 2058 cm^{-1} indicates the presence of terminal azide.[14] Similarly, an intense peak at 2086 cm^{-1} in the IR spectrum of complex **8** indicates the presence of terminal thiocyanate group.[15] Bands within 3288−3218 cm^{-1} in the IR spectrum of the complexes **7** and **8** are customarily noticed due to amine N–H bond stretching.[16] Broad band within the range from 2949–2853 cm^{-1} due to alkyl C–H stretching vibrations are observed in the IR spectra of the complexes **7** and **8**.[17] IR spectra of both the complexes have been shown in Fig. **V.A.16**.

The electronic spectra of both complexes are quite comparable to each other in methanol medium at room temperature (**Fig. V.A.17**). In each complex, two absorption bands are observed around 235 nm and 284 nm which are due to the $\pi \rightarrow \pi^*$ and n$\rightarrow \pi^*$ electron transfer, respectively.[18] In NMR spectra of both complexes**,** aromatic protons are noticed in the range of 6.76-7.14 ppm. The methylene and benzyl protons appear as singlet at 2.11 ppm and 3.92 ppm, respectively. Methyl protons of 2,2-dimethyl-1,3-diaminopropane appear as singlet at 0.96 ppm. Amine protons are observed as multiplet at 2.04 ppm. The phenolic hydrogen is

observed as a broad singlet at 5.5 ppm. ^{1}H NMR Spectra of complexes **7** and **8** are shown in Fig. **V.A.18.** and **V.A.19.** respectively.
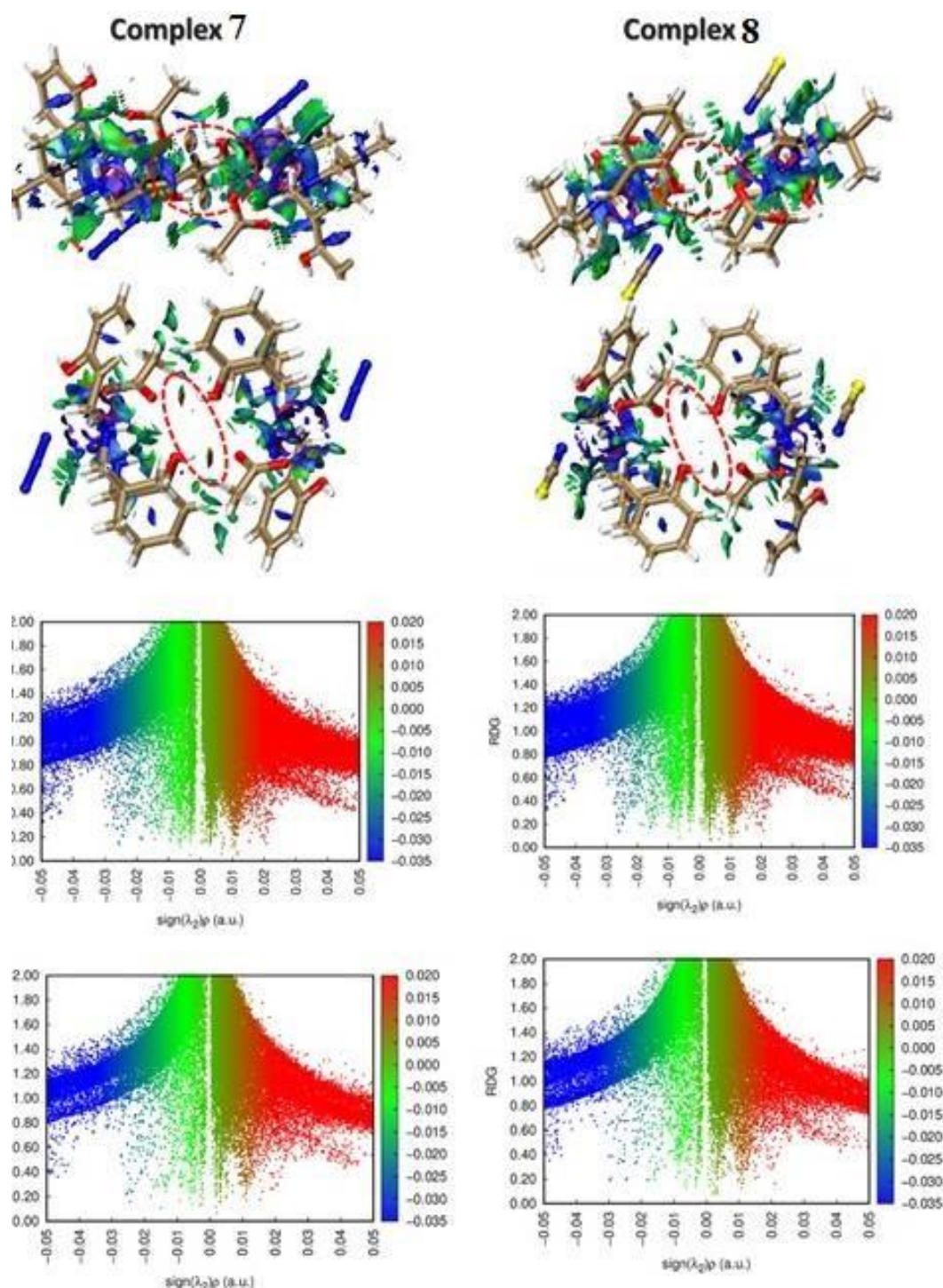

Fig. V.A.14. Noncovalent interaction (NCI) analysis for the hydrogen bonding of the investigated complexes computed at B3LYP/Lanl2DZ/6-31G(d) level showing for HB1 type bonding (a) and (c); and HB2 type bonding (b) and (d).

V.A.3.10. Fluorescence

Upon excitation of both complexes at 284 nm in methanol solution, the emission occurs around 320 nm. The emission spectra **7** and **8** confirm that the fluorescence intensities are very much higher compared to ligand, H_2L^7 (Fig.**V.A.20.**).
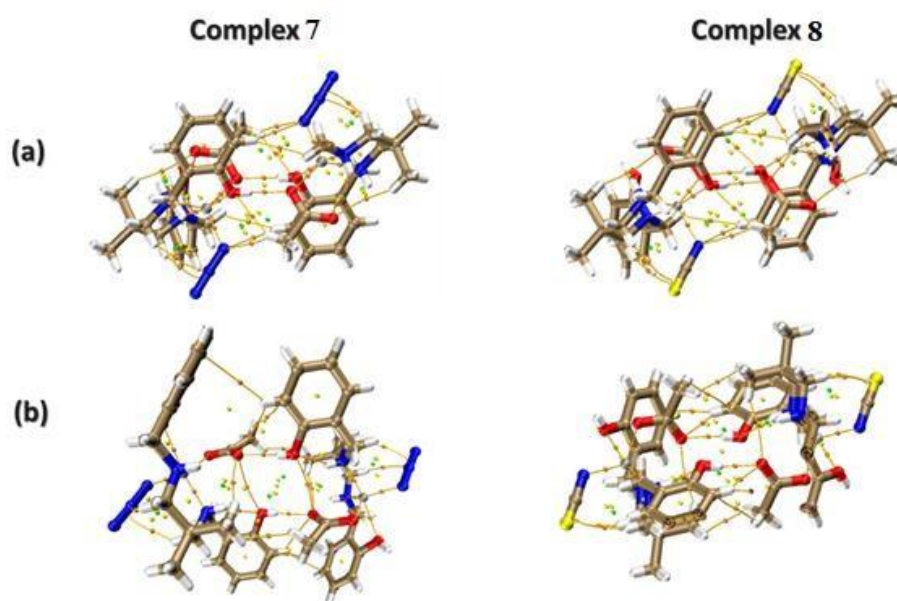
Fig.V.A.15. AIM analyses of the dimers of investigated complex showing intermolecular hydrogen bonding of the type (a) HB1 and (b) HB2 bonds, ring and cage critical points are represented by orange, yellow and green spheres, respectively.
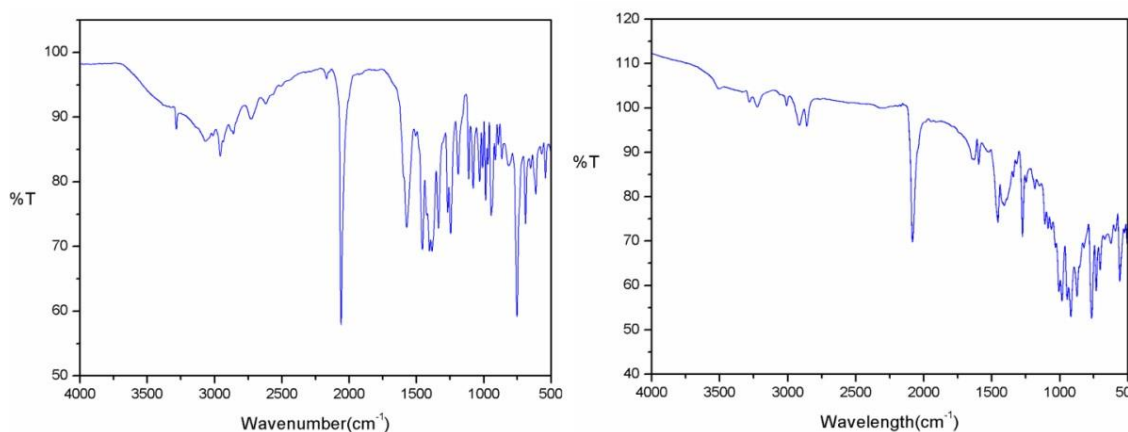
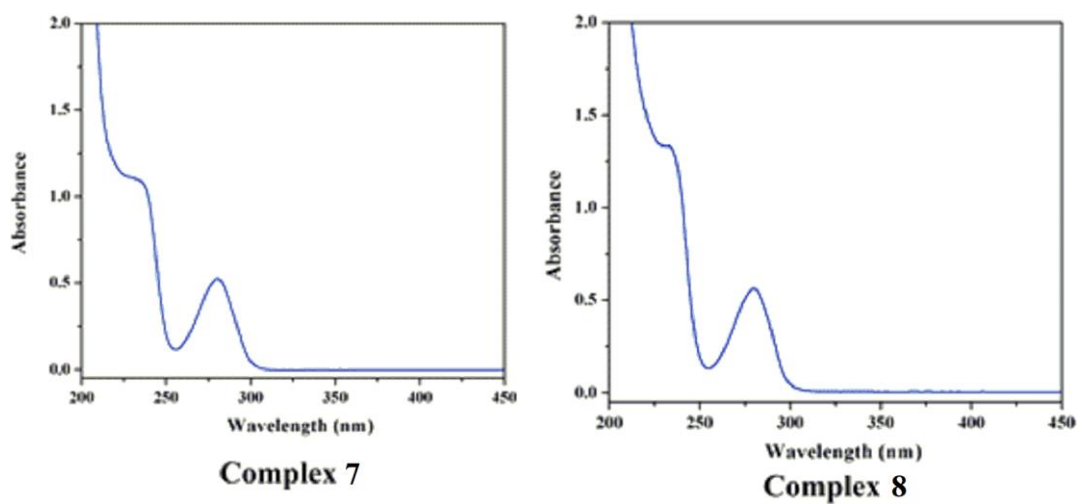**Fig. V.A.16.** IR spectra for both complexes **7** and **8**.

Fig. V.A.17. UV-Vis absorption spectra of both complexes **7** and **8.**

NMR (300 MHz, acetonitrile-d3) δ 7.12 (t, *J* = 7.3 Hz), 7.04 (d, *J* = 7.2 Hz), 6.76 (s), 3.92 (s), 2.11 (s), 1.86 (s), 0.96 (s).
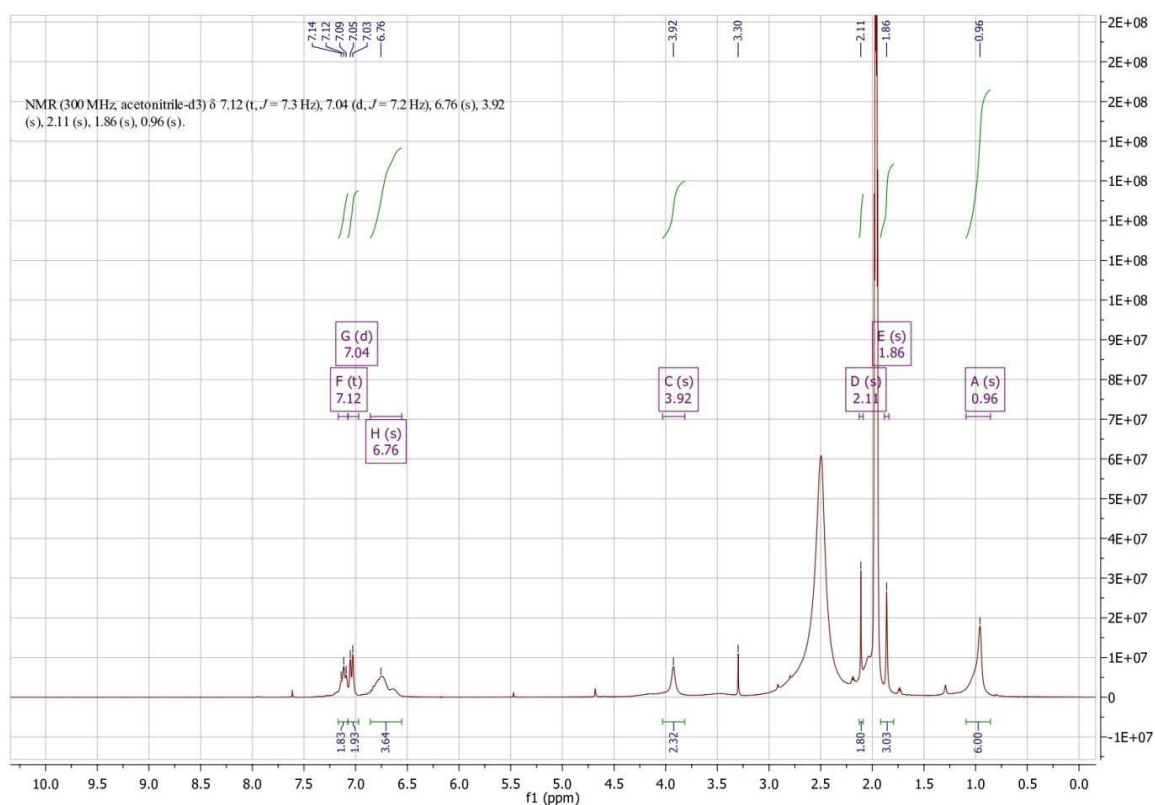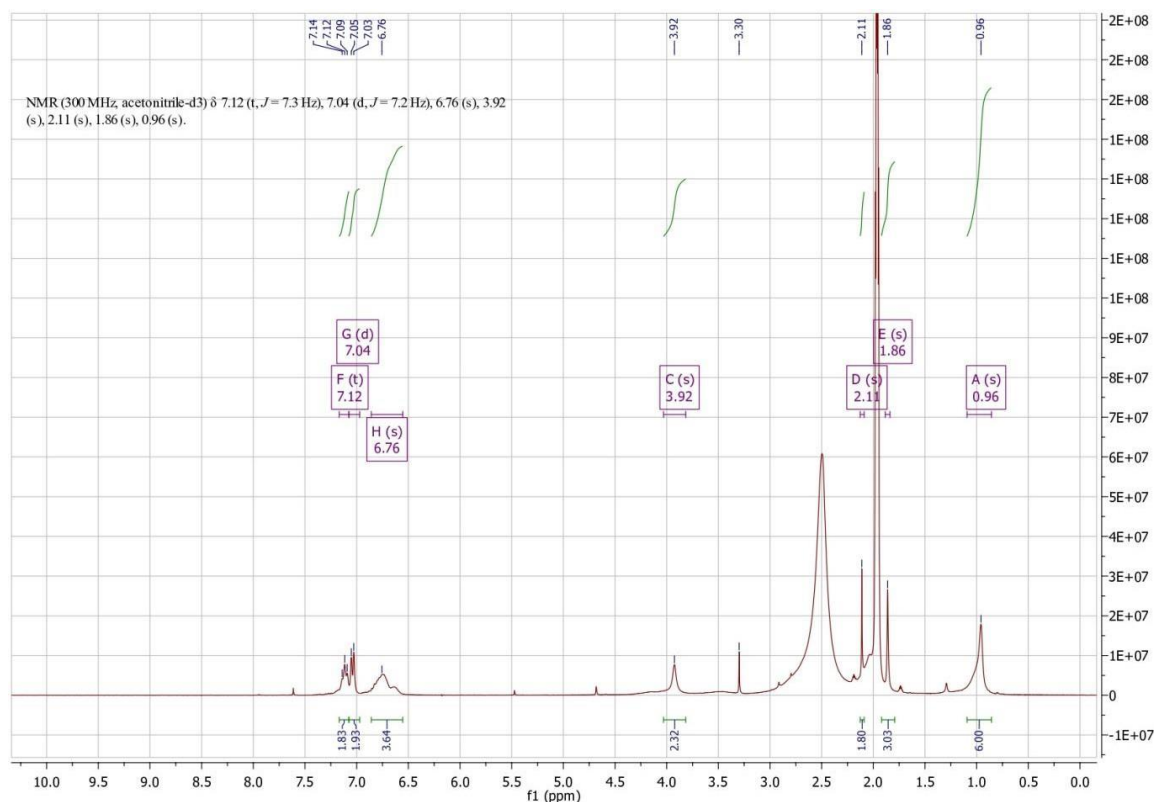
Fig. V.A.18. NMR spectrum of complex **7**.

Fig. V.A.19. NMR spectrum of complex **8.**

The enhancement of fluorescence intensity of zinc(II) complexes (**7** and **8**) compared to the reduced Schiff base ligand (H_2L^7) may be due to chelation enhancement of fluorescence emission (CHEF). In the free ligand, the lone pair electrons are present on two nitrogen atoms and are responsible for the quenching of the fluorescence due to photoinduced electron transfer (PET). On complex formation, the binding of ligand to the metal ions causes an increase in rigidity in structure and blocks the PET process and fluorescence intensity increases.

Emissions for both complexes are tentatively attributed to the intra-ligand transitions modified by metal coordination. Fluorescence lifetimes of both complexes are investigated at room temperature. Lifetimes of complexes **7** and **8** are around 3.62 and 5.20 ns (Table **V.A.5**) respectively.
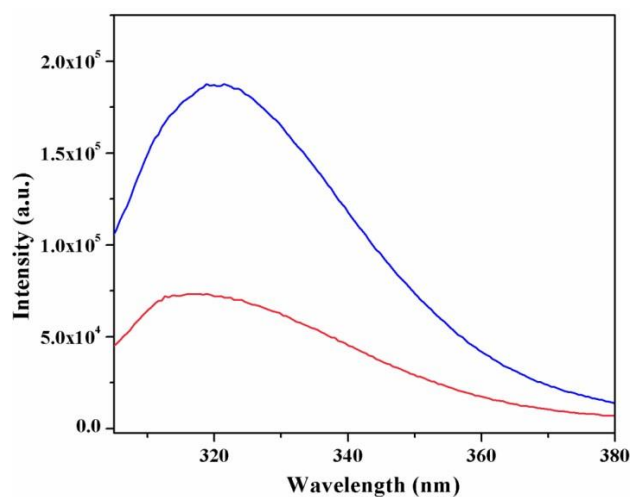
Fig. V.A.20. Fluorescence spectra of complexes **7** and **8**.

Decay profiles (**Fig. V.A.21**) are fitted to a multi-exponential model:

$$I(t) = \sum_i a_i \exp \frac{-t}{c_i}$$

Where, bi-exponential functions are used to fit the emission of both complexes with and obtaining χ^2 close to 1. The intensity-averaged life times (η_{av}) are determined using the following equation:

$$r_{av} = \frac{\sum \alpha_i c_i^2}{\sum \alpha_i c_i}$$

where, α_i and η_i are the pre-exponential factor and excited state luminescence decay time associated with the *i*-th component, respectively.

Table V.A.5: The data of photoluminescence decays of complexes **7** and **8**.

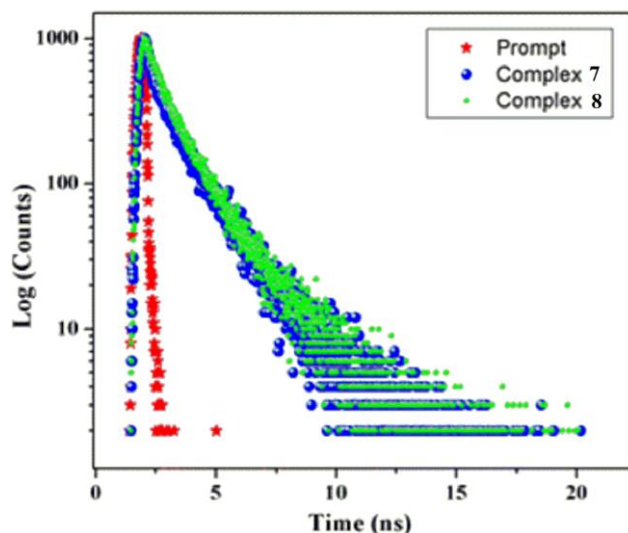| Complex	λ_{ex} (nm)	λ_{em} (nm)	η (ns)	χ^2
7	284	320	3.62	0.9889
8	284	320	5.20	1.1199

Fig. V.A.21. The excited-state decay profiles for complexes **7** and **8** following pulsed excitation at 284 nm in methanol.

V.A.3.11. Structural analysis

The ground state optimized geometries (S_0) were shown in Table **V.A.6** and Fig. **V.A.22**. To verify the reliabilities of the DFT functional, B3LYP and M06-2X results were tested together with available X-ray data for both complexes. The results indicate that B3LYP and M06-2X functional provide similar accuracy. Therefore, from a geometrical view point, the B3LYP level is sufficient and reliable for the complexes under study. The results show that both complexes studies here have distorted trigonal-bipyramidal geometry where two donor atoms of the reduced Schiff base and one donor atom of N_3/ NCS form the equatorial plane. The axial bonds, $Zn-N_{ax1}$ and $Zn-O_{ax2}$, are formed by donor atoms of the reduced Schiff base.

In the ground state geometry in gas phase, for complexes **7/8**, the typical bond distances $Zn-N_{eq1}$, $Zn-N_{eq2}$ and $Zn-O_{eq3}$ are *ca.* 2.188/2.189, 2.034/2.032 and 2.113/2.098 Å, respectively, while the axial bond distances $Zn-N_{ax1}$ and $Zn-O_{ax2}$ are *ca.* 2.206/2.192 and 2.352/2.346 Å, respectively. Upon the change of N_3 by NCS ligand the bond distance

Zn–N(N₃/NCS) remain practically unchanged. Solvent has very little effect on the geometrical parameters.

Notably, the results show that (Table **V.A.6**), in the S_1 geometry, the changes of structural parameters are very similar to that of ground state. This minor structural changes illustrated that a high rigidity of the chromophores.

Table. V.A.6: Selected optimized parameters for complexes **7** and **8** in the ground state (S_0), lowest-lying singlet state (S_1) calculated at B3LYP/Lanl2dZ/6-31G(d).

Complex	7			8		
	S_0	S_0(expt)[a]	S_1	S_0	S_0(expt)[a]	S_1
Zn–N$_{eq1}$	2.188	1.984	2.183	2.186	1.989	2.180
Zn–N$_{eq2}$	2.034	2.055	2.037	2.032	2.057	2.032
Zn–O$_{eq3}$	2.098	2.008	2.106	2.113	2.007	2.121
Zn–N$_{ax1}$	2.206	2.117	2.198	2.192	2.119	2.186
Zn–O$_{ax2}$	2.352	2.431	2.404	2.346	2.430	2.428

V.A.3.12. Orbital analysis

The electronic structures of S_0 and S_1 structures of **7** and **8** were calculated. Detail analysis of frontier molecular orbital (FMO) analysis in terms of energies along with HOMO-LUMO (H-L) gaps and percent composition of ligand, metal orbitals, and the contribution of different ligands to the FMOs were shown in Tables **V.A.7- V.A.10**. The investigated complexes display similar FMO and orbital energy diagram. For comparison, the calculated HOMO and LUMO energy levels of the studied complexes are shown in Fig. **V.A.22**.

The FMOs and H–L energy differences of both the complexes are very similar. The H–L energy difference of both complexes was *ca.* 4.69 eV in S_0 states, the energy gap reduced to *ca.* 4.3 eV in S_1 facilitating the easier electronic transition. In both complexes,

HOMO and H-1are localized on $\pi_{N_3/NCS}$ and H−3 and H−5 are localized on π_{SB}, whereas, LUMO is located on the π^* orbital of reduced Schiff base (Fig. **V.A.23-26**).

Notably, for both **7** and **8**, the composition of HOMO and LUMO in the excited state are very similar to that of the ground states. Thus, the LUMO is localized (99%) on the π^* orbital of reduced Schiff base and HOMO is entirely localized (> 97%) on the π orbital of NCS/N_3.
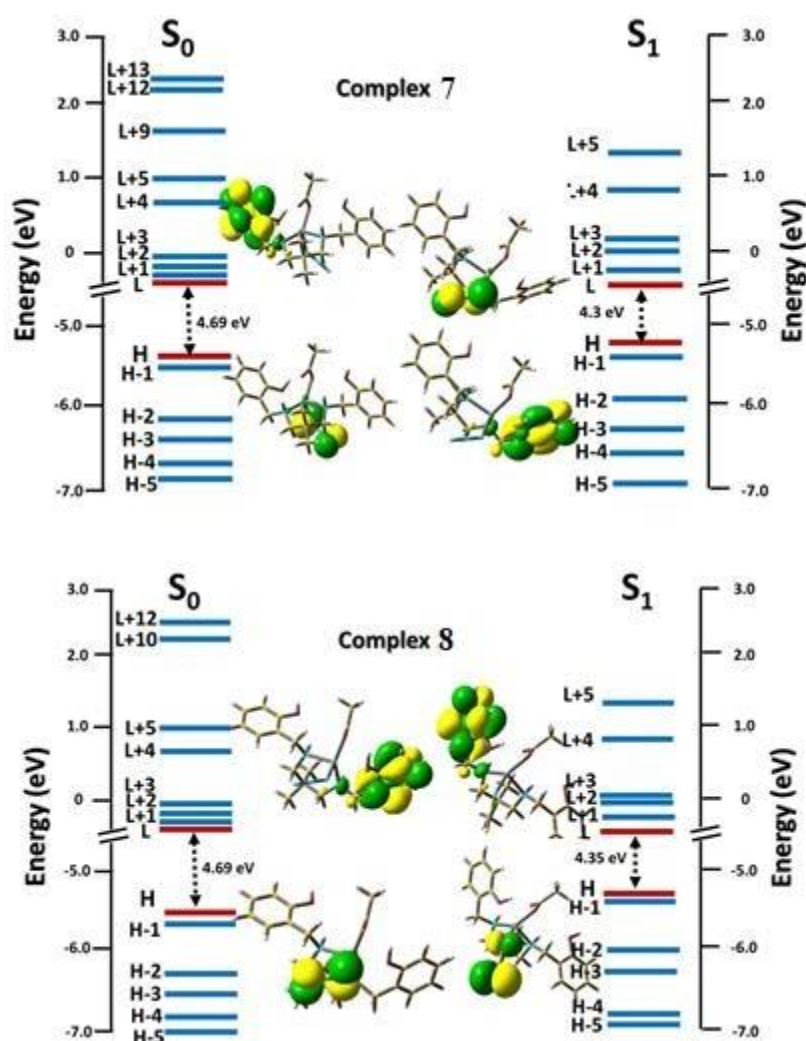

Fig. **V.A.22.** Electron density plots (isovalue= 0.03) of FMOs for the Zn-complexes at their S_0 and S_1 geometries calculated at B3LYP/Lanl2DZ/6-31G(d) level in dichloromethane media.
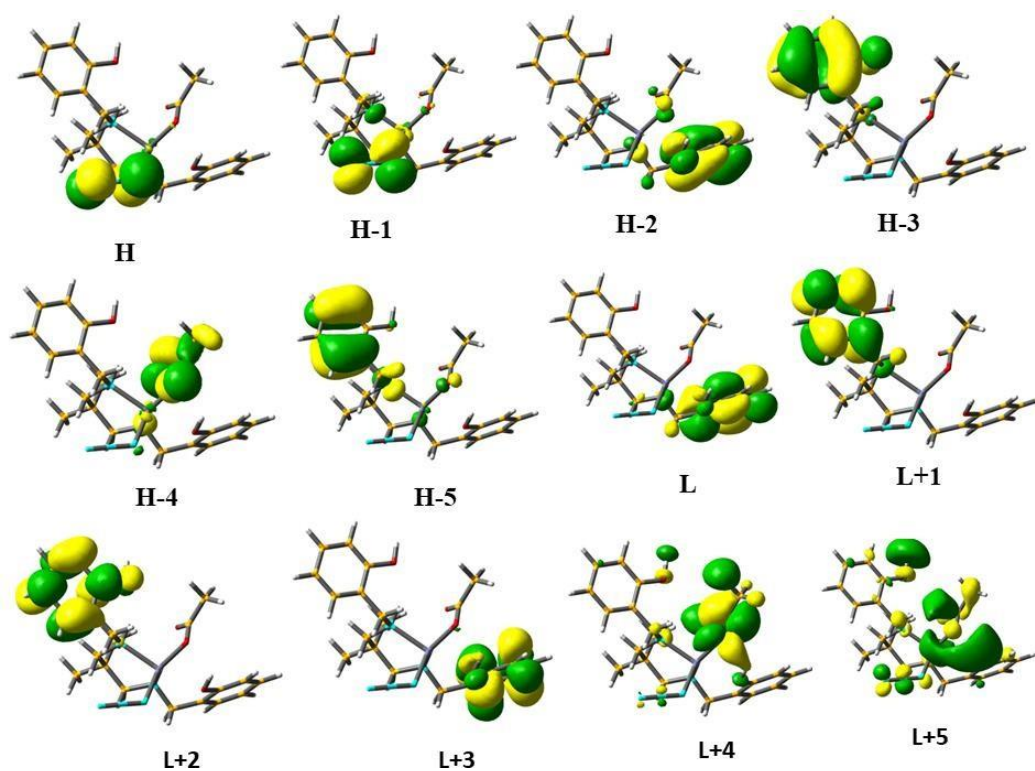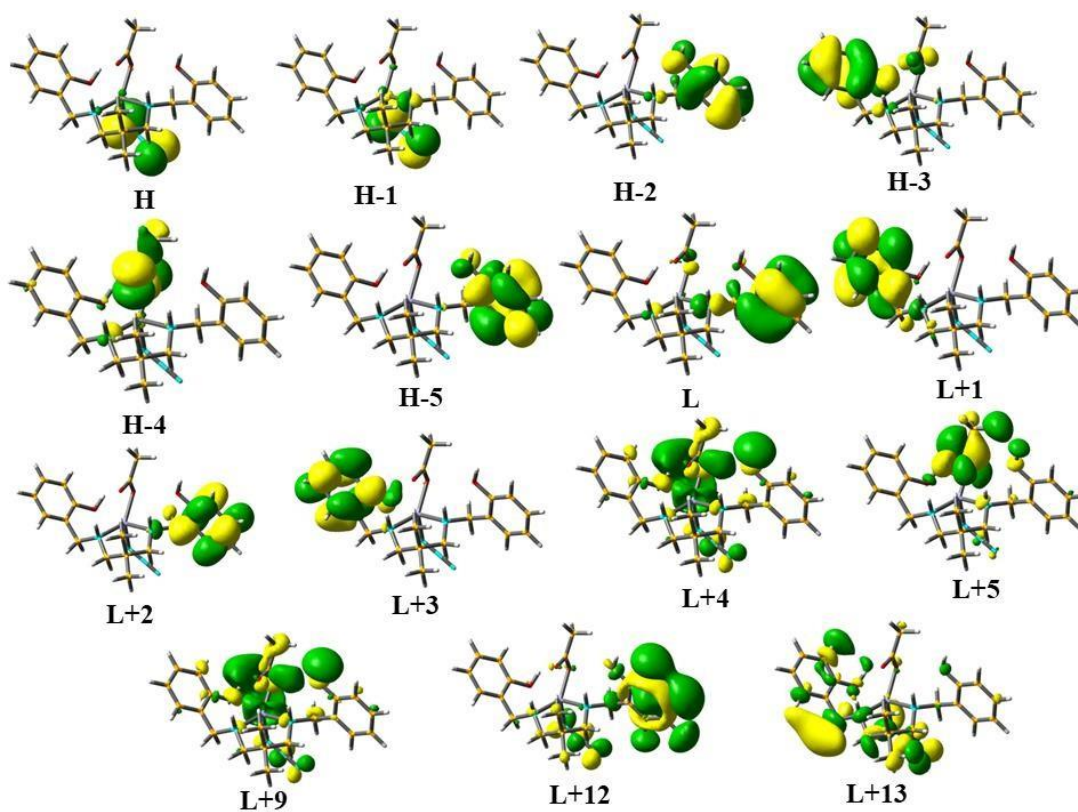
Fig. V.A.23. Excited states of the complex 7
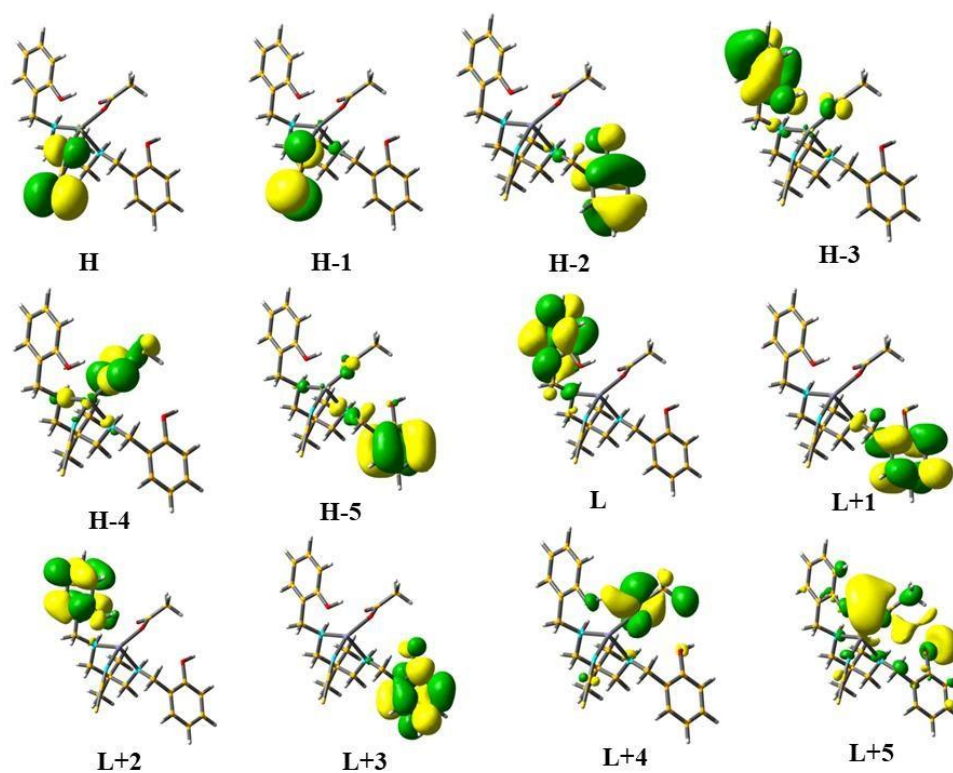

Fig. V.A.24. Ground states of the complex 7.

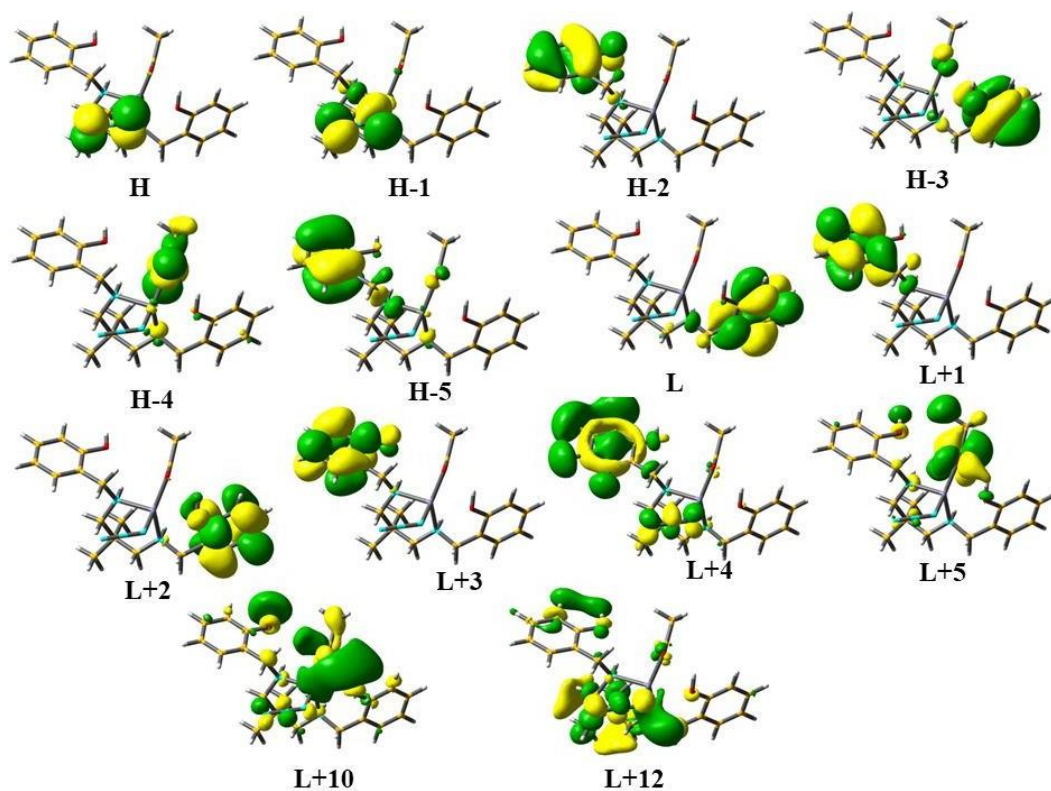**Fig. V.A.25. Excited states of the complex 8**

Fig. V.A.26. Ground states of the complex **8**

Table V.A.7. Selected Frontier molecular orbital energies (eV) and compositions (%) in the ground state for complex 7.

MO	energy	contribution				assignment (major)
		SB	N_3	Ac	Zn	
L+13	2.41	94	1	1	4	$\pi^*(SB)$
L+12	2.29	83	7	2	8	$\pi^*(SB)$
L+9	1.71	23	20	3	54	$\pi^*(SB)+$ $\pi^*(N_3)+d^*(Zn)$
L+5	1.03	33	6	8	53	$\pi^*(SB)+d^*(Zn)$
L+4	0.81	11	1	77	11	$\pi^*(SB)+\pi^*(Ac)+d^*(Zn)$
L+3	0.07	100	0	0	0	$\pi^*(SB)$
L+2	-0.09	99	0	0	1	$\pi^*(SB)$
L+1	-0.33	98	0	0	2	$\pi^*(SB)$
LUMO	-0.46	99	0	0	1	$\pi^*(SB)$

energy gap = 4.69 eV

MO	energy	contribution				assignment (major)
HOMO	-5.15	1	97	0	2	$\pi(N_3)$
H-1	-5.35	5	91	1	4	$\pi(N_3)$
H-2	-6.29	99	0	0	0	$\pi(SB)$

H-3	-6.41	92	0	7	0	π(SB)
H-4	-6.73	6	1	91	2	π(Ac)
H-5	-6.96	97	0	2	0	π(SB)

Ac = CH₃COO

Table V.A.8. Selected Frontier molecular orbital energies (eV) and compositions (%) in the ground state for complex 8.

MO	energy	contribution				assignment (major)
		SB	NCS	Ac	Zn	
L+12	2.4	79	16	1	3	π*(SB)+ π*(NCS)
L+10	2.16	59	18	2	21	π*(SB)+ π*(NCS)+d*(Zn)
L+5	0.96	38	1	6	55	π*(SB)+d*(Zn)
L+4	0.67	9	1	78	12	π*(Ac)+d*(Zn)
L+3	0.01	100	0	0	0	π*(SB)
L+2	-0.18	99	0	0	1	π*(SB)
L+1	-0.39	98	0	0	2	π*(SB)
LUMO	-0.56	99	0	0	1	π*(SB)

energy gap = 4.69 eV

HOMO	-5.25	1	99	0	1	π(NCS)
H-1	-5.28	1	98	0	1	π(NCS)
H-2	-6.35	100	0	0	0	π(SB)
H-3	-6.51	94	0	6	0	π(SB)
H-4	-6.88	8	1	90	2	π(Ac)
H-5	-7.02	97	0	3	0	π(SB)

Ac = CH_3COO

Table V.A.9. Frontier molecular orbital energies (eV) and compositions (%) in the lowest singlet excited state (S_1) for complex 7.

MO	energy	contribution				assignment (major)
		SB	N_3	Ac	Zn	
L+5	1.04	35	6	50	10	π*(SB)+π*(Ac)+d*(Zn)
L+4	0.78	11	1	10	78	π*(SB)+π*(Ac)+d*(Zn)
L+3	0.12	99	0	1	0	π*(SB)
L+2	0.05	100	0	0	0	π*(SB)
L+1	-0.35	98	0	2	0	π*(SB)
LUMO	-0.84	99	0	1	0	π*(SB)

energy gap = 4.3 eV

MO	energy					assignment (major)
HOMO	-5.14	1	97	2	0	$\pi(N_3)$
H-1	-5.34	5	91	4	1	$\pi(N_3)$
H-2	-5.99	97	0	0	3	$\pi(SB)$
H-3	-6.31	99	0	0	0	$\pi(SB)$
H-4	-6.76	5	1	2	93	$d(Ir)$
H-5	-6.98	98	0	0	2	$\pi(SB)$

Ac = $CH_3CO\overline{O}$

Table V.A.10. Frontier molecular orbital energies (eV) and compositions (%) in the lowest singlet excited state (S_1) for complex 8.

MO	energy	contribution				assignment (major)
		SB	NCS	Ac	Zn	
L+5	1.01	37	2	5	55	$\pi^*(SB)+d^*(Zn)$
L+4	0.62	7	1	82	10	$\pi^*(Ac)+d^*(Zn)$
L+3	0.04	99	0	0	1	$\pi^*(SB)$
L+2	0.01	100	0	0	0	$\pi^*(SB)$
L+1	-0.4	98	0	0	2	$\pi^*(SB)$
LUMO	-0.92	99	0	0	1	$\pi^*(SB)$

energy gap = 4.35 eV

HOMO	-5.27	1	99	0	1	π(NCS)
H-1	-5.29	1	98	0	1	π(NCS)
H-2	-6.06	97	0	2	0	π(SB)
H-3	-6.35	100	0	0	0	π(SB)
H-4	-6.93	8	1	89	2	π(Ac)
H-5	-7.03	96	0	4	0	π(SB)

Ac = CH$_3$COO

V.A.3.13. Absorption and Emission energies

On the basis of optimized ground state geometry (S$_0$), the TDDFT/B3LYP method combined with SMD solvation model in methanol media was used to calculate the absorption properties of the investigated complexes. The most important excited state (with larger CI coefficient) and their oscillator strengths, dominant orbital excitations and their assignments are shown in Table **V.A.11**. The theoretically obtained absorption spectra along with the experimental data are shown in **Fig. V.A.27.**

Surprisingly, in complex **7**, the weak lowest energy absorption (population of S$_1$) at 281 nm predominantly contributed by the transition from HOMO and H-1 to L+9, L+10 and L+13. Therefore, the lowest energy absorption can be assigned as the ligand to ligand charge
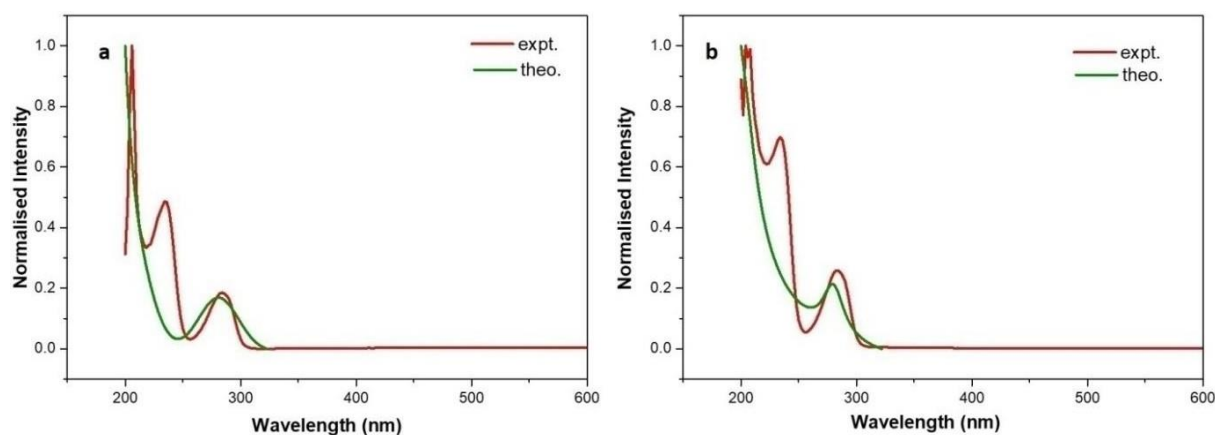
Fig. V.A.27. Absorption spectra obtained by theoretical and experimental studies.

transfer (LLCT) and intra-ligand (ILCT). The theoretical band agrees well with the experimentally observed band at 284 nm. For complex **8**, the lowest energy band found at 279 nm is also very close to the experimentally observed result at 280nm. This band arises due to the transition from H and H-1 to L+10 and L+12. The composition of L+10 and L+12 shows that they delocalized on π*of NCS and reduced Schiff base. Interestingly, both complexes show a strong absorption band at 160 nm (*f*= 1.753) from H-3 and H-5 to LUMO and L+2. The results show that H-3 and H-5 are located on π*of reduced Schiff base and LUMO and L+2 are entirely localized on π of reduced Schiff base. Thus, this strong band appeared in both complexes is due to a high ILCT. The emission involved transition from HOMO to LUMO (100%) for both complexes. As stated previously, this is a charge transfer from π orbital of NCS/N_3 to $π^*$ orbital of reduced Schiff base. The TDDFT calculated emission wavelengths agree well with the experimental value 311 nm.

V.A.3.14. NTO Study

Additionally, analysis on the electronic structure of the excited states employing NTO representation showed that the S_1 state can be mainly characterized by an inter-ligand charge-

Table V.A.11. Lowest-lying and strongest absorption band and lowest-lying emission band calculated wavelength (nm)/energies (eV), oscillator strength (*f*), major contribution, transition characters, and the experimental wavelength (nm) for **7** and **8** complexes in methanol media. H indicates HOMO, L indicates LUMO.

	Excited state	λ	f	Configuration	assignment	Expt. (nm)
Absorption						
1				H-1→L+9 (16%), HOMO→L+12 (13%), HOMO→L+13	MLCT/LLCT/ILCT	275
	S_1	281	0.054	(24%)		
		160	1.7706	H-5→LUMO (38%), H-3→L+2		
	S_{11}			(32%)		
2				H-1→L+12 (19%), HOMO→L+10	MLCT/LLCT/ILCT	280
	S_1	279	0.051	(33%)		
		160	1.7534	H-5→LUMO (39%), H-3→L+2		
	S_9			(32%)		
Emission						
1		325	0.0045	HOMO→LUMO		311
	S_1			(100%)		
2		316	0.0031	HOMO→LUMO		320
	S_1			(100%)		

transfer (ILCT) transition, populating highest-occupied (HO)NTO and lowest-unoccupied (LU)NTO which describe the *hole* and the excited *electron* state, respectively. The charge transfer index (Δr) between HONTO and LUNTO, and hole-electron overlapping indices (ϕ_S) were calculated to identify the charge transition in the excited-states. The Δr value is a quantitative indicator of charge-transfer (CT) length of electron excitation, larger Δr indices and smaller ϕ_S indices imply longer CT distance, whereas, smaller Δr value and larger ϕ_S value are indicator of local-excitation. As shown in Fig. **V.A.28**, the HONTOs and LUNTOs for both complexes show that they are mainly localized on the ligand N_3/NCS and the reduced Schiff base, respectively. The high value of Δr *ca.* 4.5 Å and low value of ϕ_S *ca.* 0.3 indicates the flurophore originated from the charge transfer from N_3/NCS to reduced Schiff base.
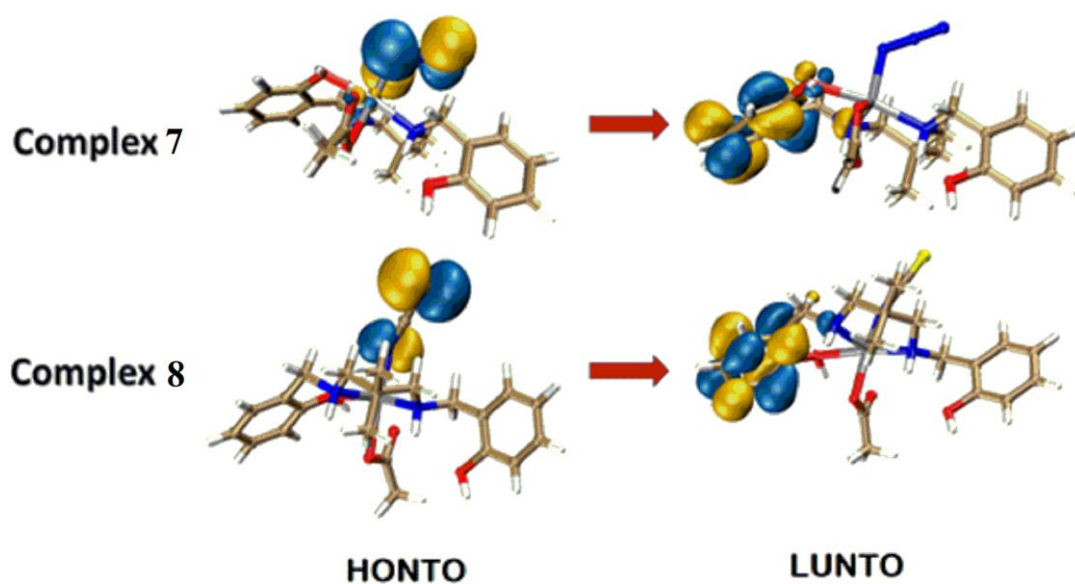
Fig. V.A.28. NTO plots of the studied complexes at their optimized S_1 geometries.

V.A.4. Conclusion

In this present work, a potential tetradentate reduced Schiff base ligand has been synthesized and characterized. The reduced Schiff base has been treated as a fluorescence chemosensor for the detection of zinc(II) via turn-on fluorescence response. The binding

constant for the ligand is 1.056×10^6 M^{-1}. The binding stoichiometry has also been evaluated by Job‟s plot and found 1:1 adduct for ligand and zinc(II). Two mononuclear zinc(II) complexes have also been prepared by reacting zinc(II) acetate with this ligand along with azide/thiocyanate as co-ligands.

We have used a DFT/TDDFT approach to understand the fluorescence behavior of two zinc(II) complexes. The geometric and electronic structures at the S_0 and S_1 states, absorption and emission spectra and phosphorescence efficiencies for both complexes **7** and **8** were calculated and compared. As they have similar geometry, photo-physical behaviors are also very similar. The main origin of fluorescence is assigned to $\pi_{N3/NCS} \rightarrow \pi^*_{SB}$ for both complexes from HOMO$\rightarrow$LUMO charge transfer. The NTO analyses are performed to find the exact location of the fluorophore. This analysis also supports the charge transfer from the π electrons of the N_3/ NCS to π^* of reduced Schiff base. The strong fluorescence behaviors are due to the presence of a rigid hydrogen-bonded network as found in the solid-state. The two types of intermolecular hydrogen bonding, namely, HB1 and HB2 are noticed in the dimeric form of the complexes. The nature of the hydrogen bonding well supported qualitatively and quantitatively with the help of NCI-RDG and QTAIM.

References

1 (a) K. Zhang, L. Zhang, S. Zhang, Y. Hu, Y. Zheng and W. Huang, *Inorg. Chem.*, 2015, **54**, 5295; (b) N. Ahmed, C. Das, S. Vaidya, A. K. Srivastava, S. K. Langley, K. S. Murray and M. Shanmugam, *Dalton Trans.,* 2014, **43**, 17375; (c) X. Yang, D. Schipper, R. A. Jones, L. A. Lytwak, B. J. Holliday and S. Huang, *J. Am. Chem. Soc.*, 2013, **135**, 8468; (d) S. Sarkar and K. A. Dey, *Spectrochim. Acta Part A.*, 2010, **77**, 740; (e) B. H. Koo, K. S. Lim, D. W. Ryu, W. R. Lee, E. K. Kohb and C. S. Hong, *Dalton Trans.*, 2013, **42**, 7204.

2 (a) X. Liu and J.-R Hamon, *Coord. Chem. Rev.*, 2019, **389,** 94; (b) N. Cao, R. Jiang, L. Hao, L. Tian, R. Moc, Y. Fan, J. Zhao and L. Ren, *Materials Letters.*, 2019, **250,** 182; (c) S.-H. Lee, S.-R. Shin and D.-S. Lee, *Materials and Design.,* 2019, **172,** 107774; (d) A. Panja and K. Ghosh, *Mater. Chem. Front.*, 2018, **2**, 1866-1875; (e) S. Kr. Saha and P. Banerjee, *Mater. Chem. Front.*, 2018, **2,** 1674.

3 (a) A. Hazari, L. K. Das, R. M. Kadam, A. Bauzá, A. Frontera and A. Ghosh, *Dalton Trans.*, 2015, **44**, 3862; (b) A. Hazari, A. Das, P. Mahapatra and A. Ghosh, *Polyhedron*, 2017, **134,** 99–106; (c) K. Sundaravel, E. Suresh, K. Saminathan and M. Palaniandavar, *Dalton Trans.*, 2011, **40,** 8092.

4 (a) R. Ganguly, B. Sreenivasulu and J. J. Vittal, *Coord. Chem. Rev.*, 2008, **252,** 1027; (b) B. Sreenivasulu, M. Vetrichelvan, F. Zhao, S. Gao and J. J. Vittal, *Eur. J. Inorg. Chem.*, 2005, 4635.

5 (a) A. Biswas, L. K. Das, M. G. B. Drew, G. Aromí, P. Gamez and A. Ghosh, *Inorg. Chem.*, 2012, **51,** 7993; (b) S. Panda, S. S. Zade, H. B. Singh and R. J. Butcher, *Eur. J. Inorg. Chem.*, **2006**, 172.

6 (a) M. Karmakar, T. Basak and S. Chattopadhyay, *New J. Chem.*, 2019, **43,** 4432; (b) C.-T. Yang, M. Vetrichelvan, X. Yang, B. Moubaraki, K. S. Murray and J. J. Vittal, *Dalton Trans.*, **2004**, 113.

7 G.M. Sheldrick, *Acta Cryst.*, 2008, **A 64,** 112.

8 G.M. Sheldrick, SADABS, V2014/5. Software for Empirical Absorption Correction, University of Göttingen, Institute fur Anorganische Chemieder Universitat, Gottingen, Germany, 1999–2003.

9 K. Sundaravel, E. Suresh, K. Saminathan and M. Palaniandavar, *Dalton Trans.*, 2011, **40,** 8092.

10 S. Mirdya, S. Roy, S. Chatterjee, A. Bauza, A. Frontera and S. Chattopadhyay, *Cryst. Growth Des.*, 10.1021/acs.cgd.9b00881.

11 A. W. Addison, T. N. Rao, J. Reedijk, J. van Rijn and G. C. Verschoor, *J. Chem. Soc., Dalton Trans.* **1984**, 1349.

12 (a) D. Cremer and J. A. Pople, *J. Am. Chem. Soc.*, 1975, **97,** 1354–1358; (b) D. Cremer, *Acta Cryst.*, 1984, **B40**, 498.

13 J. Contreras-García, W. Yang and E. R. Johnson, *J. Phys. Chem. A*, 2011, **115,** 12983.

14 (a) A. Panja, M. Shyamal, A. Saha and T. K. Mandal, *Dalton Trans.*, 2014, **43,** 5443; (b) P. Bhowmik, S. Biswas, S. Chattopadhyay, C. Diaz, C. J. G. García and A. Ghosh, *Dalton Trans.*, 2014, **43**, 12414.

15 (a) S. Purkait, G. Aullón, E. Zangrando and P. Chakraborty, *Dalton Trans.*, 2017, **46,** 2184; (b) S. Sen, P. Talukder, S. K. Dey, S. Mitra, G. Rosair; D. L. Hughes, G. P. A. Yap, G. Pilet, V. Gramlich and T. Matsushita, *Dalton Trans.*, **2006**, 1758.

16 T. Basak, K. Ghosh and S. Chattopadhyay, *Polyhedron,* 2018, **146,** 81.

17 T. Basak, M. G. B. Drew and S. Chattopadhyay, *Inorg. Chem. Commun.*, 2018, **98,** 92.

18 A. Banerjee, A. Frontera and S. Chattopadhyay, *Dalton Trans.,* 2019, **48,** 11433.

Section: V.B

A mononuclear zinc complex with a diamine: Synthesis, characterization, selfassembly, luminescence property and DFT calculations

V.B.1. Introduction

The ability of zinc to attain different coordination numbers and versatile geometries renders it a good candidate for the synthesis of complexes with various diamines.[1-8] Most of the complexes of zinc are showing strong fluorescence.[9-10] Electroluminescence properties of zinc complexes were also explored.[11-12] Chelating Schiff bases have widely been used for the synthesis of zinc complexes.[13-14] The role of Schiff bases to act as fluorescence chemosensor for the detection of zinc by PET on/off mechanism is also well investigated.[15-16] Photoinduced electron transfer (PET) is a term reserved to describe the transfer of an electron between photoexcited and ground-state molecules. Chelation enhanced fluorescence (CHEF) may be observed in some cases.[17-18] On the other hand, the strong fluorescence of many zinc Schiff base complexes may be quenched in presence of different nitroaromatics and this property is exploited by many material scientists to sense these explosives.[13,19]

Salen type Schiff bases constitute a special class of ligands, as they can be synthesised very easily; simply by refluxing (or even stirring) an 1:2 mixture of a diamine and a salicylaldehyde-derivative in appropriate solvent.[20-28] They are also stable over a wide range of solvent and temperature. Reduction of the imine bonds of Schiff bases (preferably with sodium borohydride) may produce secondary amines,[29-30] which are sometimes referred to as reduced analogues of Schiff bases.[31] These reduced analogues of Schiff bases are eventually much more flexible compared to their Schiff base precursors, and therefore they may produce

varieties of complexes having different shapes and geometries.[32-34] It has been observed that they may also be used in different catalysis and sensing.[6, 17, 35]

In this paper, we would like to report the synthesis and characterization of a zinc complex (**9**) with such a secondary diamine, prepared by the reduction of a salen type di-Schiff base ligand (and hence may be considered as a reduced analogue of a di-Schiff base ligand). Its fluorescence property and solid state non-covalent interactions are studied in detail with the help of DFT calculations.

V.B.2. Experimental

V.B.2.1. Synthesis

V.B.2.1.1. **Synthesis of *2,2'-[(cyclohexane-1,2-diyl)bis(iminomethylene)]bis[phenol] (H₂L⁸)***

A methanol solution (20 mL) of cyclohexane-1,2-diamine (mixture of *cis* and *trans*) (1 mmol, 0.1 mL) was refluxed with salicylaldehyde (2 mmol, 0.208 mL) for ca. 2h to produce *N,N'-bis(salicylidene)-cyclohexane-1,2-diamine*. It was then reduced with $NaBH_4$ following the literature method [23] to obtain the colourless diamine, H_2L^8.

Yield: ~0.241 g, ~74% (based on cyclohexane,1.2-diamine). Anal. Calc. for $C_{20}H_{26}N_2O_2$ (F.W. 326.43): C, 73.59; H, 8.03; N, 8.58 %. Found: C, 73.40; H, 7.85; N, 8.75 %, UV-Vis, λ_{max} (nm), [ε_{max} (dm^3 mol^{-1} cm^{-1})] (CH$_3$CN), 276(5.8x10^2); δ ^{1}H NMR (CD$_3$CN) (ppm): 6.70-6.74 (m, $J = 7.7$ Hz, 4H, aromatic CH), 7.04-7.16 (m, $J = 7.7$ Hz, 4H, aromatic CH), 3.72-3.86 (m, 4H, methylene CH$_2$), 2.51 (s, 4H, methylene CH$_2$), 2.05-2.13 (m, 8H, methylene CH$_2$), 2.32 (m, 1H, amine NH).

V.B.2.1.2. **Synthesis of *[Zn(H₂L⁸)(OCOCH₃)₂] (9)***

Zinc acetate dihydrate (1 mmol, 1.095 g) was dissolved in 2mL methanol. 1 mmol (10 mL) H_2L^8 was then added to it with stirring. The stirring is continued for 2 hrs. A small

amount of precipitate was then filtered off. Crystalline compounds separated from the mother liquor after few days. X-ray quality single crystals were collected from the product.

Yield: ~0.360 g, 71%. Anal. Calc. for $C_{24}H_{32}N_2O_6Zn$(F.W. 509.91): C, 57.75; H, 5.82; N, 5.39 %. Found: C, 57.51; H, 5.49; N, 5.59 %;FT-IR (KBr, cm^{-1}): 3300 (ν_{N-H} and ν_{O-H}); 2929 (ν_{C-H}). λ_{max} (nm) [ε_{max}(lit mol^{-1} cm^{-1})] (acetonitrile): 289 (1.026x10^4).^{1}H NMR (CD$_3$CN) (ppm) δ: 6.97, 6.88, 6.67 and 6.41 (m, 2H, aromatic CH), 3.76 (s, 4H, methylene CH$_2$), 2.51 (s, 4H, methylene CH$_2$), 1.7-1.9 (m, 8H, methylene CH$_2$), 2.26 (m, 1H, amine NH), 1.702 (s, 6H, methyl CH$_3$).

Table V.B.1. Crystal data and refinement details of the complex **9**.

Formula	$C_{24}H_{32}N_2O_6Zn$
Formula Weight	509.91
Temperature (K)	273
Crystal System	Triclinic
Space group	*P-1*
a (Å)	8.9866(10)
b (Å)	10.2187(11)
c (Å)	14.8777(17)
V(Å^3)	1287.1(2)
Z	2
d_{cal} (g cm^{-3})	1.316
μ(mm^{-1})	0.993
F(000)	536
Total reflection	37303
Unique Reflections	5673
Observe data[I>2ζ(I)]	4977
R(int)	0.0845

R1, wR2 (all data)	0.1061, 0.3149
R1, wR2 [I>2σ(I)]	0.0962, 0.3042
Residual Electron Density (eÅ^{-3})	3.189, -0.841

CCDC reference no is 1968984

V.B.3. Results and discussion

V.B.3.1. Synthesis

Salicylaldehyde and cyclohexane-1,2-diammine were used to synthesize a Schiff base following the literature method.[14] It was then reduced with borohydride to a secondary diamine, H_2L^8. It was purified by solvent extraction in dichloromethane at least five times. The diamine, H_2L^8, forms a zinc complex, *[Zn(H₂L⁸)(OCOCH₃)₂]* (9) when reacted with zinc acetate in 1:1 molar ratio (Scheme **V.B.1.**).

V.B.3.2. Description of the structure of *[Zn(H₂L⁸)(OCOCH₃)₂]* (9)

A perspective view of the complex together with the selected atom-numbering scheme is shown in Fig. **V.B.1**. The structure consists of a discrete mononuclear unit, *[Zn(H₂L⁸)(OCOCH₃)₂]*, where the zinc center is tetra-coordinated, being bonded to two amine nitrogen atoms (N1 and N2) from the chelating diamine and the two oxygen atoms (O1 and O2) from two acetates. Zn–N and Zn–O bond lengths are ~2.04 Å and ~1.93 Å respectively, as were also observed in other complexes.[36]

In the present complex, the geometry around the zinc center, Zn(1), is distorted tetrahedral with angular index, $\eta_4 = 0.89$, following Houser and co-workers.[37] η_4 values of some zinc complexes have been given in Table **V.B.2.** The saturated five-membered chelate

ring, Zn(1)-N(1)-C(8)-C(13)-N(2) represents a half chair conformation with puckering parameters[38] $q(2) = 0.442(6)$ Å and $\theta = 271.3(6)°$ (Fig. **V.B.2.**).
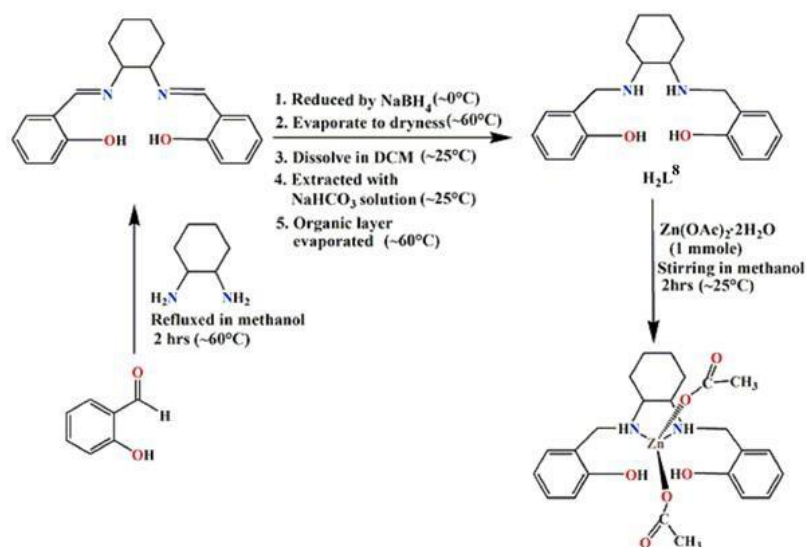
Scheme V.B.1. Synthetic route to the mononuclear zinc(II) complex using the reduced schiff base ligand, H_2L^8.

V.B.3.2. Supramolecular Interactions present in zinc complex

The complex has significant hydrogen bonding interactions. The hydrogen atoms, H(1B) and H(2B), attached to an amine nitrogen atoms, N(1) and N(2) respectively, are involved in intramolecular hydrogen bonding with phenoxy oxygen atom, O(5) of the diamine and carboxy oxygen atom, O(4) of an acetate moiety.

The hydrogen atom, H(5A), attached to phenoxy oxygen atom, O(5), is involved in intermolecular hydrogen bonding interaction with an adjacent symmetry related {symmetry transformation [a]= -x, 1- y, 2-z} oxygen atom, O(3)[a] of the acetate group. The O(4) of the acetate group is linked with a symmetry related hydrogen atom H(6A)[b], attached to phenoxy oxygen atom, O(6)[b] {symmetry transformation [b]= 1−x,1−y,1−z}. Due to these hydrogen bonding interactions, a zigzag chain are formed (Fig**. V.B.3).**
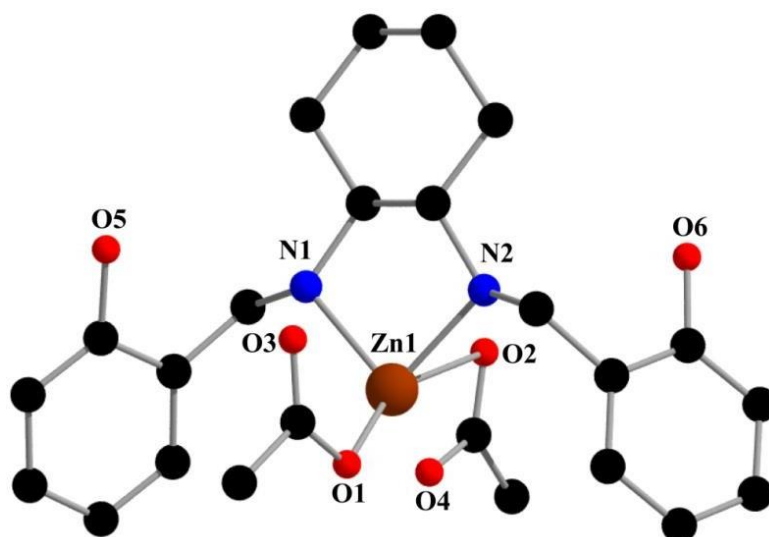
Fig. V.B.1. Perspective view of complex with selective atom numbering scheme. Hydrogen atoms are omitted for clarity. Selected bond lengths (Å) and angles (°): Zn(1)-O(1) 1.938(5), Zn(1)-O(2) 1.929(6), Zn(1)-N(1) 2.044(4), Zn(1)-N(2) 2.039(5),∠O(1)-Zn(1)-O(2) 106.7(2), ∠O(1)-Zn(1)-N(1) 115.0(2), ∠O(1)-Zn(1)-N(2) 116.9(2), ∠O(2)-Zn(1)-N(1) 117.6(2), ∠O(2)-Zn(1)-N(2) 113.6(2), ∠N(1)-Zn(1)-N(2) 86.64(18).
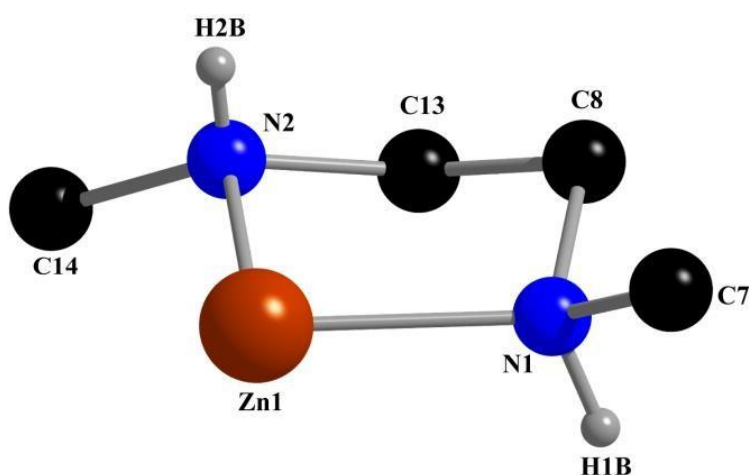
Fig. V.B.2. Half Chair conformation of a saturated five-membered chelate ring.

The details of hydrogen bonding interactions are given in Table **V.B.3**. The complex also shows one inter-molecular C-H⋯π interaction, which may be noteworthy. The symmetry related hydrogen atom, H(9B), attached to carbon atom, C(9)ᶜ, shows a inter-molecular C-

H···π interaction with the symmetry related {symmetry transformation ^{c} = 1-x, 1- y, 2-z} phenyl ring [C(1)–C(2)–C(3)–C(4)–C(5)–C6)] as shown in Fig. **V.B.4**.

Table V.B.2. η values of some zinc complexes

Complex	τ value	Structure of the complex	Reference
[Zn(H$_2$L^8)(OCOCH$_3$)$_2$]	0.7	distorted tetrahedral	This paper
[Zn(H$_2$L^7)(OCOCH$_3$)(N$_3$)]	0.692	between the square pyramidal and trigonal bipyramidal geometry	33
[Zn(H$_2$L^7)(OCOCH$_3$)(NCS)]	0.695	between the square pyramidal and trigonal bipyramidal geometry	33
[Zn{Zn(N$_3$)L^9}$_2$]	0.54 [Zn(1)], 0.63[Zn(3)]	between the square pyramidal and trigonal bipyramidal geometry	39
[{(N$_3$)Zn (L^{10})}$_2$Zn]	~0.5	between the square pyramidal and trigonal bipyramidal geometry	6
[{(SCN)Zn (L^{10})}$_2$Zn]	~0.5	between the square pyramidal and trigonal bipyramidal geometry	6

[{(SCN)Zn (L^{11})}$_2$Zn]	~0.5	between the square pyramidal and trigonal bipyramidal geometry	6

H$_2$L^8 = 2,2'-[(cyclohexane-1,2-diyl)bis(iminomethylene)]bis[phenol], H$_2$L^7= 1,3-bis(2-hydroxybenzylamino)-2,2-dimethylpropane, H$_2$L^9 = 2,2''-[(1-ethyl-1,3-propanediyl)bis(iminomethylene)]bis(6-ethoxyphenol), H$_2$L^{10} = 2,2''-[(1,3-propanediyl)bis(iminomethylene)]bis(6-ethoxyphenol), H$_2$L^{11} = 2,2''-[(2,2-dimethyl-1,3-propanediyl)bis(iminomethylene)]bis(6-methoxyphenol),
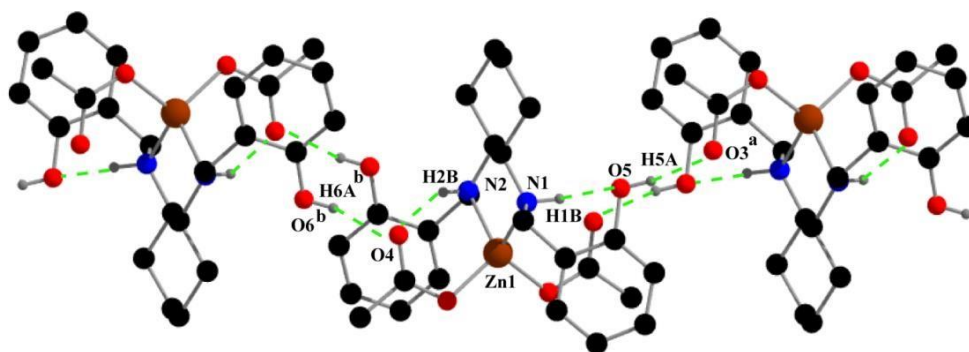
Fig. V.B.3. Hydrogen bonding interactions in complex. Only relevant hydrogen atoms are shown for better clarity. Symmetry transformations ^{a} = -x, 1-y, 2-z and ^{b} = 1−x, 1−y,1−z.

Table V.B.3. Hydrogen bond distances (Å) and angles (∘) for complex.

D–H⋯A	D-H	H⋯A	D⋯A	∠D-H⋯A
N(1)-H(1B)⋯O(5)	0.86(7)	2.41(6)	3.034(7)	129(6)
N(2)-H(2B)⋯O(4)	0.70(4)	2.46(4)	3.007(8)	137(5)
O(5)-H(5A)⋯O(3)^a	0.8200	1.8200	2.622(8)	166.00
O(6)-H(6A)⋯O(4)^b	0.8200	1.8600	2.653(8)	162.00

D = donor; H = hydrogen; A = acceptor, Symmetry transformation: [a] = -x,1-y,2-z, [b] = 1-x, 1-y, 1-z.
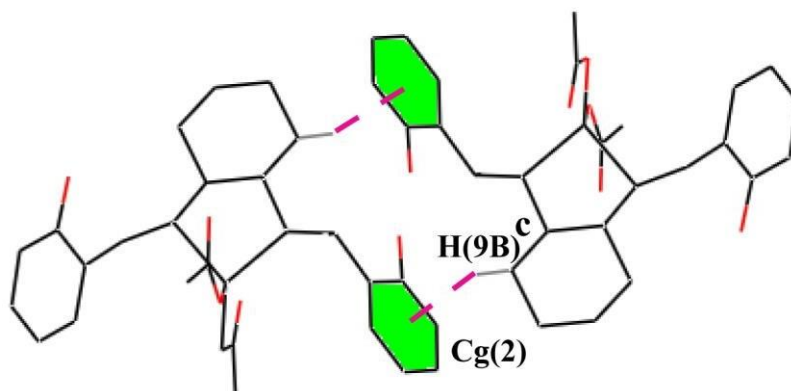
Fig. V.B.4. Perspective view of inter-molecular C-H···π interactions with selective atom numbering scheme. Only relevant atoms are shown for clarity. Symmetry transformations [c] = 1-x, 1-y, 2-z

V.B.3.3. IR, electronic, ^{1}H NMR and fluorescence spectra

The IR and UV-Vis spectra of the complex are shown in Fig. **V.B.5**. A broad band at 2929 cm^{-1} in the IR spectrum of the complex (Fig. **V.B.5a**) indicates the presence of alkyl C–H bonds.[40] The broad band in the region of ~3300 cm^{-1} indicates the presence of hydrogen-bonded OH groups and N–H bonds.[41] The asymmetric and symmetric stretching vibrations of the acetate groups appear at 1557 and 1454 cm^{-1}, respectively.[42] The electronic spectrum of the complex (Fig. **V.B.5b**) recorded in acetonitrile solution at room temperature shows one prominent absorption band at 290 nm, originated from intra-ligand charge transfer transition.[43]

The IR and UV-Vis spectra of the diamine, H$_2$L are shown in Fig. **V.B.6**. Absence of any band around 1600 cm^{-1} (characteristic of azomethine (>C=N) stretching vibrations) in the IR spectrum of the ligand (Fig. **V.B.6a**) confirms the reduction of the Schiff base moiety. The

UV-Vis spectrum of the diamine in acetonitrile solution (Fig. **V.B.6b**) at room temperature shows one prominent absorption band at 276 nm due to intra-ligand charge transfer transition.[44]
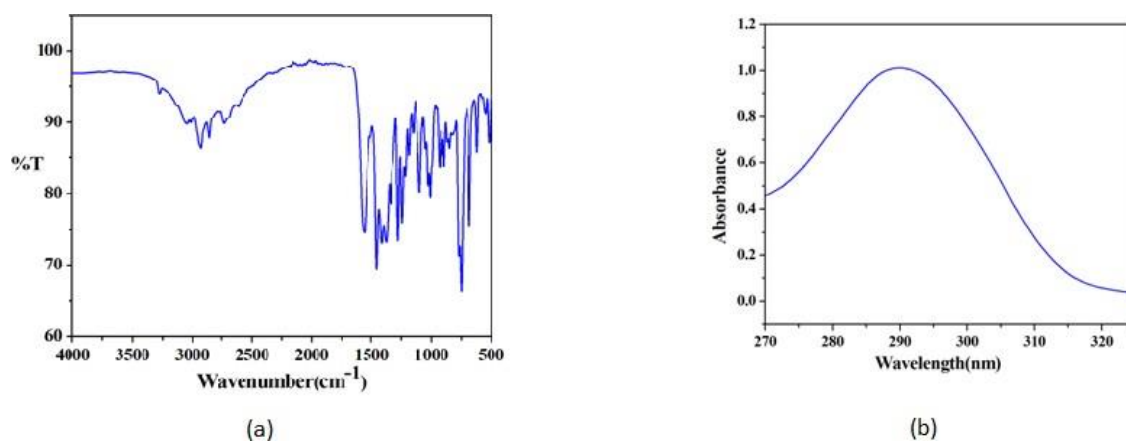

Fig. V.B.5. IR (a) and UV-VIS (b) spectra of the complex **9**.
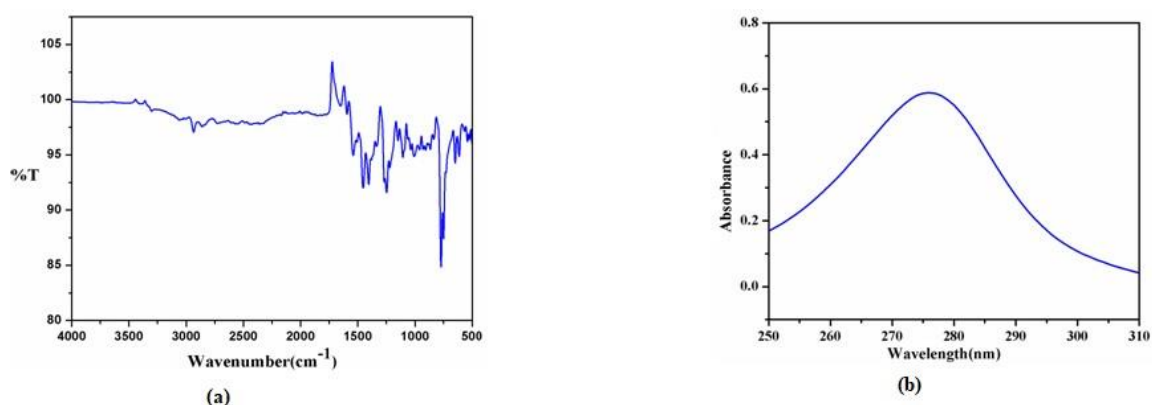

Fig. V.B.6. IR (a) and UV-VIS (b) spectra of the ligand, H_2L^8.

The emission of the ligand is observed at 435 nm (upon excitation at 276 nm) and the intensity of this emission is considerably increased on adding zinc (Fig. **V.B.7a**). When the acetonitrile solution of the complex is excited with light of 290 nm, the complex shows fluorescence at 446 nm (Fig. **V.B.7b**). This is assigned as intra-ligand $\pi \rightarrow \pi^*$ fluorescence.[6]

The fluorescence lifetime of the diamine is 3.16 ns at room temperature. The decay profile is given in Fig. **V.B.8a**.
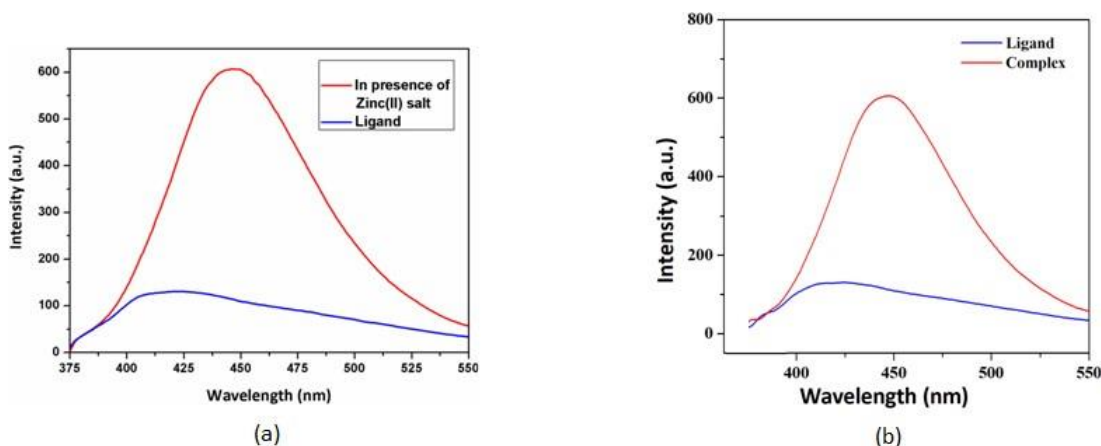
Fig. V.B.7. (a) Fluorescent spectra of the diamine in the absence and presence of zinc salt (500µL); (b) Fluorescence spectra of the complex and the diamine.

On the other hand, on exciting at 290 nm, the complex shows emission at 446 nm. Emission for the complex may be attributed to the intra-ligand transitions modified by metal coordination. The lifetime of the excited state of the complex is around 7.53 ns. The decay profile is given in Fig. **V.B.8b**. A rough mechanism towards the increase/decrease in fluorescence intensity of diamine upon ligation with the metal is given below.

The increase in fluorescence intensity of the diamine on forming the zinc complex indicates chelation enhancement of fluorescence emission (CHEFF).[33] However, the nonbonding electron pairs on the nitrogen atoms in the free diamine may participate in photo-induced electron transfer (PET)[33] and thereby may reduce the intensity of fluorescence. When this diamine forms stable complex with metal, this PET is blocked due to increased rigidity in structure and increase in fluorescence intensity has been observed.

The fluorescence intensities of the mixture (1:1) of diamine, H_2L^8, and M^{2+} (M=Zn, Cd, Pb, Cu, Mn, Co, Cd, Ni) are measured to check the sensing property of H_2L^8. A notable

change in fluorescence intensity is observed only for Zn(OAc)$_2$ and Cd(OAc)$_2$ as shown in Fig. **V.B.9**. As in the presence of zinc, fluorescence intensity is maximum, so it can be said that H$_2$L^8 acts as a fluorescence sensor for zinc. The binding stoichiometry of diamine with zinc can be defined from the Job's plot (Fig. **V.B.10**).
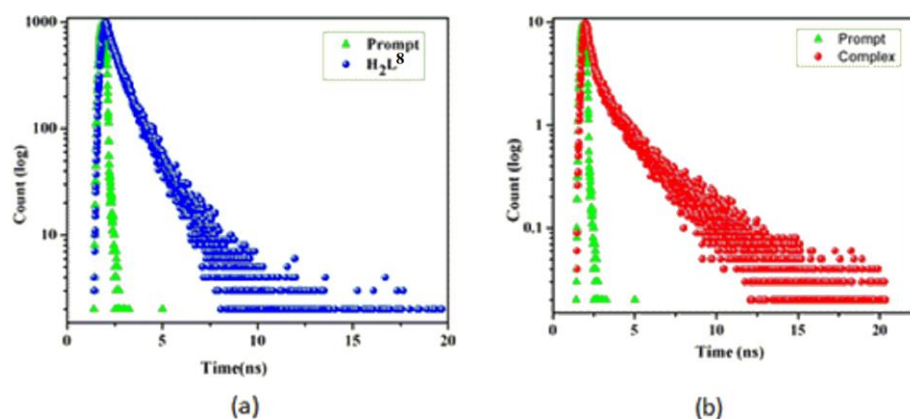

Fig. V.B.8. (a) The decay profile for the excited state (of *H$_2$L^8* in acetonitrile), produced by pulsed excitation at 276 nm; (b) The decay profiles of the excited state of the complex **9**.

^{1}H NMR spectrum of the ligand, H$_2$L8, is shown in Fig. **V.B.11**. Aromatic protons are noticed in the range of 6.70-6.74 ppm and 7.04-7.16 ppm. The methylene protons of cyclohexane ring are observed in the range of 2.05-2.13 ppm. Amine protons appear at 2.32 ppm. ^{1}H NMR spectrum of the complex is shown in Fig. **V.B.12**. The aromatic protons are found in the range of 6.41-6.97 ppm. The methylene protons of cyclohexane ring are observed in the range of 1.8-1.9 ppm. Amine protons appear at 2.26 ppm. Methyl protons of acetate moiety are noticed at 1.702 ppm.[45-46]

Room temperature magnetic susceptibility measurement shows that this complex is diamagnetic with a magnetic moment value close to 0 BM.

V.B.3.4. Comparison of the zinc sensing ability of the ligand with previously reported diamines

A rough comparison based on fluorescence property can be made between the investigated diamine, H_2L^8 with our previously reported diamines, H_2L^7 and H_2L^9.
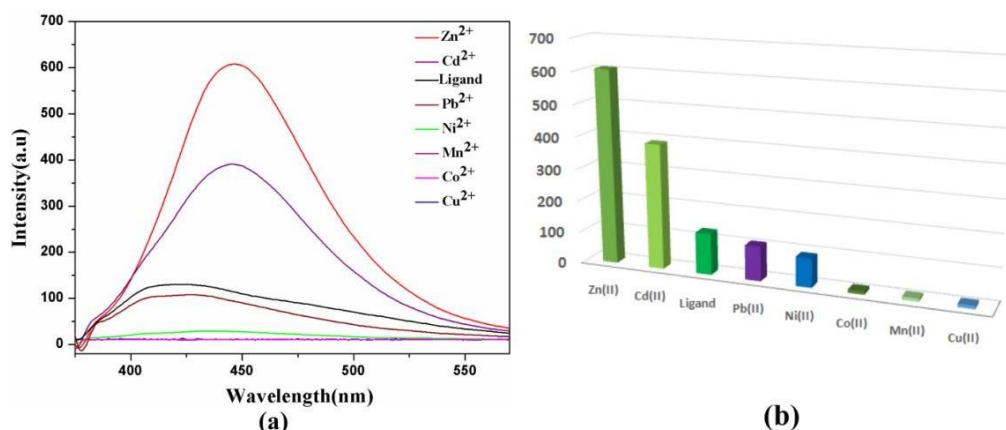

Fig. V.B.9. (a) Fluorescence spectra of the diamine, *H_2L^8* (excitation wavelength 276 nm) in the presence of various metal ions. (b) Fluorescence intensity of the diamine H_2L^8 (excitation wavelength 276 nm) in the presence of various metal ions.
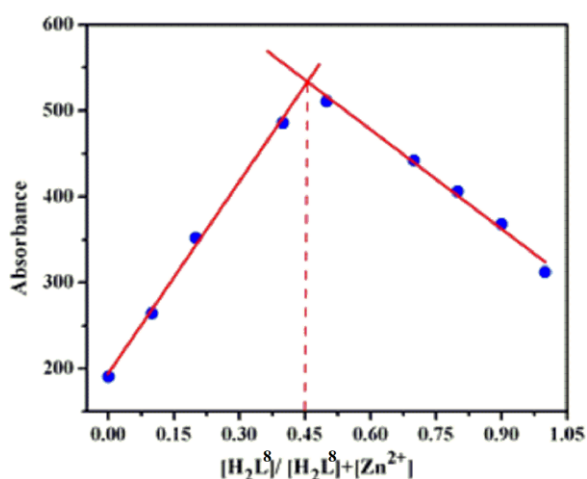
Fig. V.B.10. Indication of 1:1 complex formation between zinc ion and *H_2L^8* (Job's plot).

{H_2L^7= 1,3-bis(2-hydroxybenzylamino)-2,2-dimethylpropane, H_2L^9 = 2,2''-[(1-ethyl-1,3-propanediyl)bis(iminomethylene)]bis(6-ethoxyphenol)}.[33,39] Maximum fluorescence intensity

of H_2L^8 and also some structurally related diamines[33, 39] on adding excess zinc is shown in Fig. **V.B.13**. It indicates that the efficiency of the current diamine is not the best, rather the diamine may be considered as a medium chemo-sensor for the detection of zinc via turn-off fluorescence response.
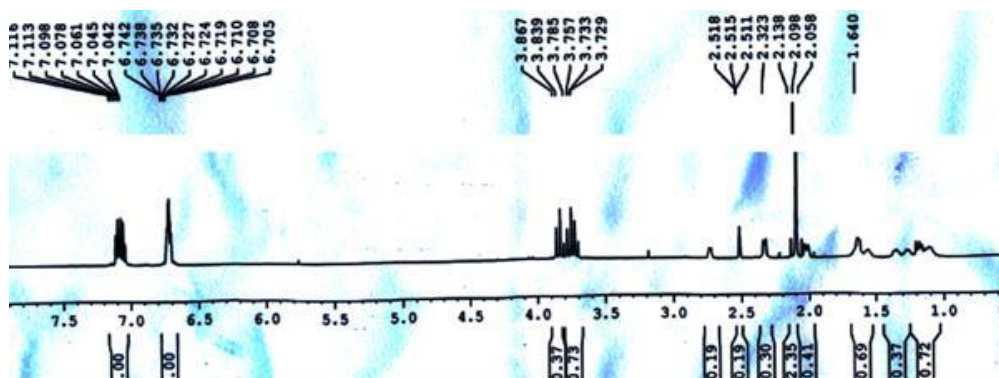
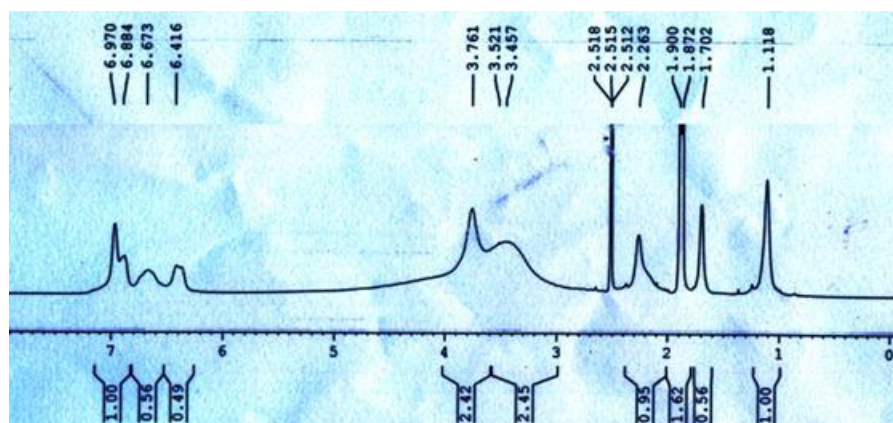

Fig. V.B.11. ^{1}HNMR spectrum of the diamine, H_2L^8.

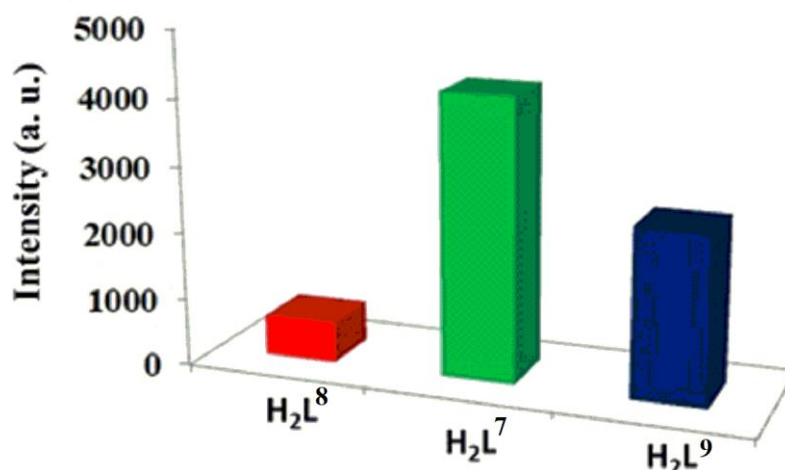**Fig. V.B.12.** ^{1}HNMR spectrum of the complex **9**.

Fig. V.B.13. Maximum fluorescence intensity of some structurally related secondary diamines on adding excess zinc [Ligand Concentration= 10^{-4} (M) in each case]; H_2L^8= 2,2'-[(cyclohexane-1,2-diyl)bis(iminomethylene)]bis[phenol], H_2L^7= 1,3-bis(2-hydroxybenzylamino)-2,2-dimethylpropane, H_2L^9= 2,2'-[(1-ethyl-1,3-propanediyl)bis(iminomethylene)]bis[6-ethoxyphenol]

V.B.3.5. Comparison of the fluorescence property of the studied complex with some previously reported complexes

The fluorescence property of the investigated mononuclear zinc(II) complex has been compared with some previously reported complexes, $[Zn(H_2L^7)(OCOCH_3)(N_3)]$ (**7**), $[Zn(H_2L^7)(OCOCH_3)(NCS)]$ (**8**) and $[Zn\{Zn(N_3)L^9\}_2]$ (**10**), $\{H_2L^7$= 1,3-bis(2-hydroxybenzylamino)-2,2-dimethylpropane, H_2L^9 = 2,2''-[(1-ethyl-1,3-propanediyl)bis(iminomethylene)]bis(6-ethoxyphenol)$\}$.[33, 39] All three reported complexes have been treated as a fluorescence chemosensor for the detection of zinc(II) via turn-on fluorescence response.[33] Maximum fluorescence intensity of complex and also some structurally related complexes.[33, 39] is shown in Fig. **V.B.14**. From Fig. **V.B.14**., it is clear that

the studied complex may act as a medium chemo-sensor for the detection of zinc via turn-on fluorescence response.

The synthesized complex is soluble in acetonitrile, DMSO and DMF. The complex is stable in these solvents. On the other hand, the complex is not soluble in water and methanol. The solubility of the complex in different solvents is shown in **Chart V.B.1**.

Chart V.B.1. Solubility of the complex in different solvents.

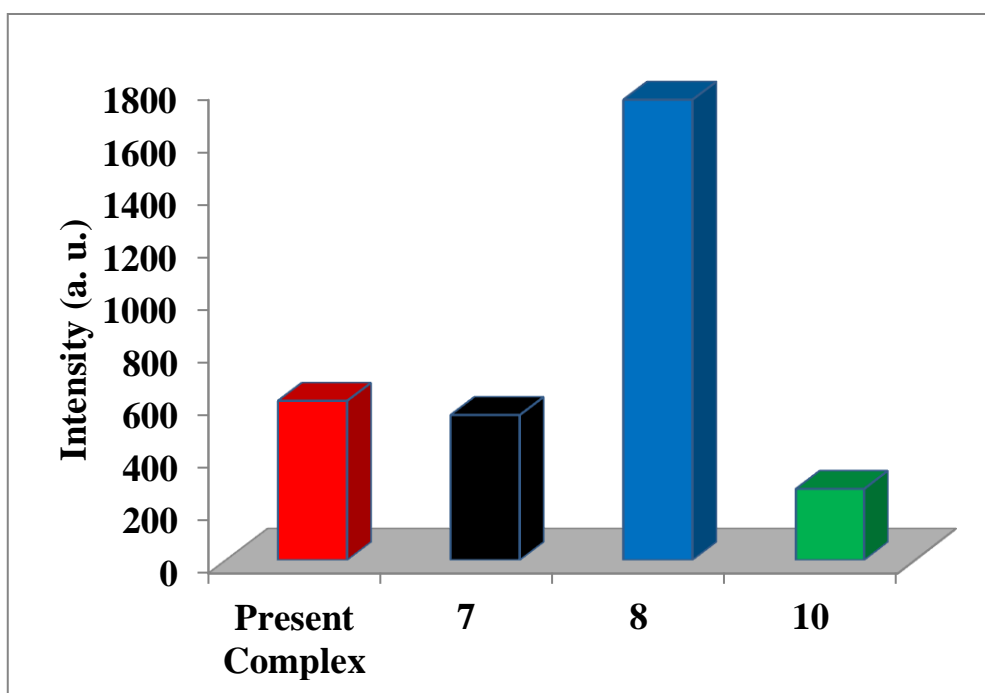| Solvent	Water	Methanol	Acetonitrile	DMSO	DMF
Solubility	Insoluble	Insoluble	soluble	soluble	soluble

Fig. V.B.14. Maximum fluorescence intensity of the studied complex with some previously reported complexes, **7** {[Zn(H$_2$L^7)(OCOCH$_3$)(N$_3$)]}; **8** {[Zn(H$_2$L^7)(OCOCH$_3$)(NCS)]} and **10**{[Zn{Zn(N$_3$)L^9}$_2$]} [Metal Concentration= 10^{-4} (M)]

V.B.3.6. Hirshfeld surface analysis

In order to understand the different intermolecular interactions the Hirshfeld surface study.[47-49]was carried out for the synthesized zinc diamine complex with the help of Crystal Explorer software.[50] The corresponding two dimensional fingerprint plots.[51-53] were achieved during such study. In case of such analysis two types of distances (d_e and d_i) are obtained for each point on the Hirshfeld isosurface. d_e is defined as the distance between the surface and the nearest nucleus external to the surface whereas d_i is just the opposite of d_e i.e. the distance between the surface and the nearest nucleus internal to the surface. Another term (d_{norm}) is also important as far as Hirshfeld surface analysis is concerned. It is nothing but a normalized contact distance. d_e and d_i are normalised by the van der Waals radius of the atom (r_i^{vdW} and r_e^{vdW}) and the summation of these two quantities result in normalized contact distance (d_{norm}) according to the following equation.

$$d_{norm} = \{ (d_i - r_i^{vdw}) / r_i^{vdW} \} + \{ (d_e - r_e^{vdW}) / r_e^{vdW} \}$$

Three types of Hirshfeld surfaces of the complex were achieved on mapping over d_{norm}, curvedness and shape index (Fig. **V.B.15.**). Curvedness is actually a function of the root mean square of the curvature of the surface and thus defining the shape of the crystal. On the other hand shape index is a qualitative measurement of the shape and very sensitive to a slight change in the shape of the surface, particularly in a region where the curvedness is very low. Fig. **V.B.15.** clearly depicts three types of regions i.e. red, blue and white which are defined by d_{norm} values. The value may be positive or negative depending on intermolecular contacts, being longer or shorter than the van der Waals separations. The red regions have negative d_{norm} values, representing shorter contacts or closer contacts. The blue regions have positive d_{norm} values, representing longer contacts. On the other hand the white regions have d_{norm} values equal to zero meaning contact distances are exactly the same as that of the van

der Waals separations. It has been predicted earlier that the the Hirshfeld surface is unique for a set of spherical atomic electron densities in a crystal structure[54] and this property pointed out the possibility of gaining additional insight into the intermolecular interaction of molecular crystals. In our complex the surfaces made transparent in order to visualize the molecular structure clearly. Red spots on the d_{norm} surface indicate the dominant interaction between oxygen and hydrogen atoms. Additional visible spots of light colour correspond to weaker interactions; e.g. $C\cdots H$ and $H\cdots H$ contacts. Besides, the 2D-fingerprint plots (Fig. **V.B.16.**) depict the difference between the intermolecular interaction patterns and the relative contributions (in %) for the major intermolecular interactions associated with the complex.

On analyzing the 2D Fingerprint plots it is found that the proportion of $H\cdots H$ interaction is about 68.7% of the Hirshfeld surface of the complex (Fig. **V.B.16.**). The interaction is represented by a spike ($d_i = 1.125$, $d_e = 1.137$ Å). The $O\cdots H/H\cdots O$ interaction is around 17.2% of the Hirshfeld surface (Fig. **V.B.16.**). The $O\cdots H$ interaction is represented by a spike ($d_i = 1.053$, $d_e = 0.651$ Å) in the bottom right region and the $H\cdots O$ interaction is represented by another spike ($d_e = 1.067$, $d_i = 0.715$ Å) in the bottom left region of the fingerprint plot. The $C\cdots H/H\cdots C$ interaction is around 14% of the Hirshfeld surface (Fig. **V.B.16.**). The $C\cdots H$ interaction is represented by a spike ($d_i = 1.618$, $d_e = 1.056$ Å) in the bottom right region and the $H\cdots C$ interaction is represented by another spike ($d_i = 1.206$, $d_e = 1.518$ Å) in the bottom left region of the fingerprint plot.
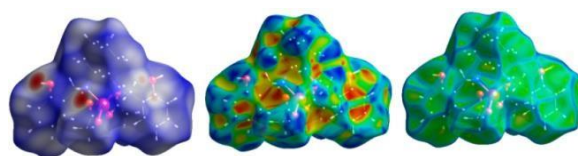

Fig. V.B.15. Hirshfeld surfaces mapped with shape index (left), d_{norm} (middle) and curvedness (right) of the complex.
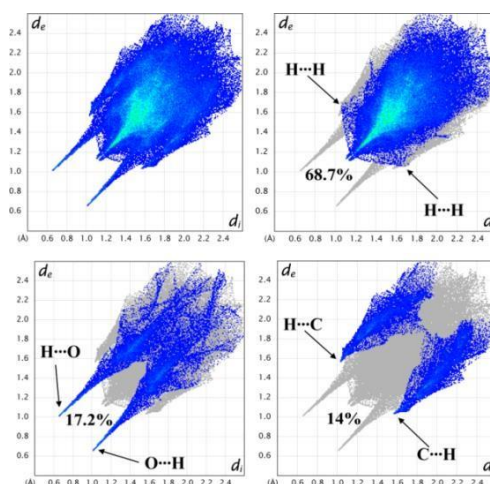
Fig. V.B.16. Fingerprint plot: Full (top left), resolved into H···H/H···H (top right), H···O/O···H (bottom left) and H···C/C···H (bottom right) contacts contributed to the total Hirshfeld Surface area of the complex.

V.B.3.7. Theoretical study

The optimized geometries of the ground and excited states are shown in Fig. **V.B.17.** The results show that the computed main parameters are in agreement with the crystallographic data. For example, Zn–O bonds are 1.94 and 1.96 Å, are in close agreement with the crystallographic result 1.93 and 1.94 Å. However, the Zn–N bonds are overestimated, for example, *ca.* 2.13 Å relative to the crystallographic result of 2.04 Å. The computed results show that the geometry around Zn is distorted-tetrahedral. In the excited state geometry, Zn–O bonds are slightly elongated *ca.* 1.94 and 1.99 Å. Similarly, the Zn–N bonds are elongated to 2.13 and 2.15 Å. The overall rigidity is maintained as shown in Fig. **V.B.17**.

The HOMO-LUMO (H-L) energy difference of the complex was *ca.* 5.75 eV in S_0 states, the energy gap decreased to *ca.* 3.88 eV in S_1 assisting the easier electronic transition. In S_0, the HOMO is localized on one of the CH_3COO group, whereas, LUMO is located on the π^* orbital of the ligand (Fig. **V.B.18.**). However, in S_1, the LUMO is localized (97%) on the π^* orbital of the ligand, while the HOMO is shifted to π orbital of the ligand. Notably, the zinc

center has no contribution to the frontier molecular orbitals (FMOs). The results are shown in Table **V.B.4-5**.
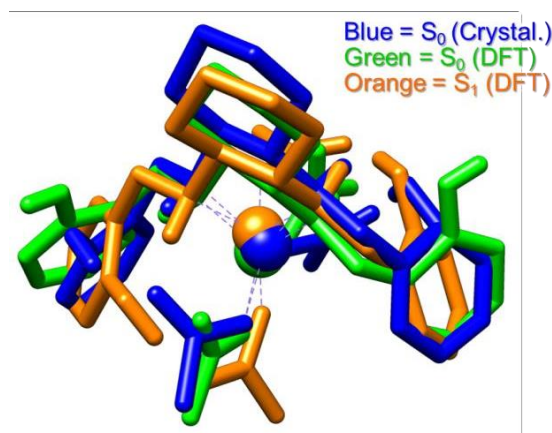

Fig. V.B.17. The optimized geometries of S_0 and S_1 along with the ground state crystalline structure to show overall deformation.

Based on the optimized ground state geometry (S_0), the TDDFT/B3LYP method combined with the solvation model based on density (SMD) in acetonitrile media was used to calculate the absorption properties of the investigated complex (Table **V.B.6.**). The theoretically obtained absorption spectra along with the experimental data are shown in Fig. **V.B.19.** The results show that the lowest energy absorption or the first excited state (population of S1) at 241 nm is predominantly contributed by the transition from HOMO to LUMO. Here, the HOMO of the excited state means the highest occupied molecular orbital at the S_0 geometry. Therefore, the lowest energy absorption can be assigned as the ligand to ligand charge transfer (LLCT) from $n_{AcO} \rightarrow \pi^*_{RSB}$
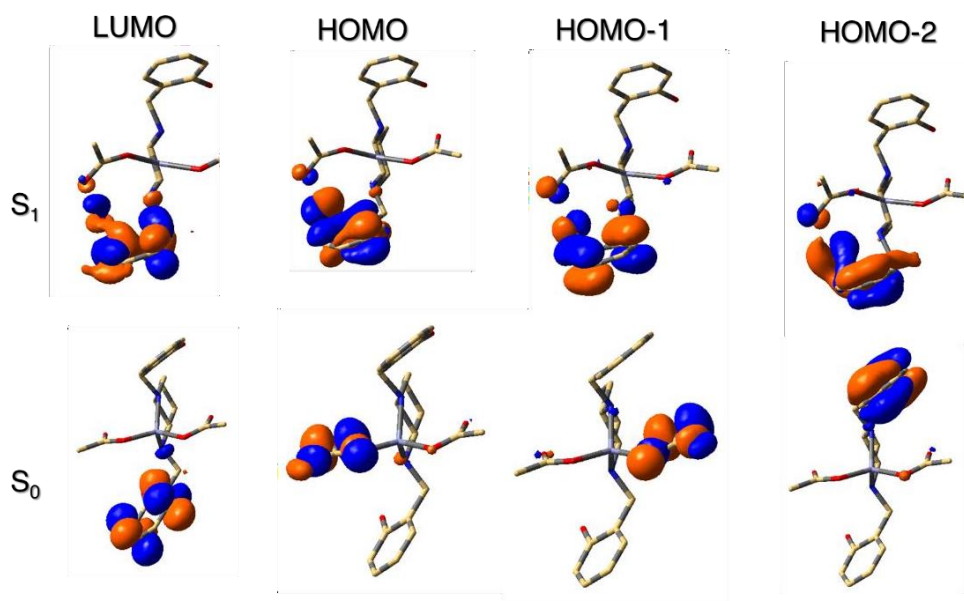
Fig. V.B.18. Iso-surface plot (iso-value = 0.04 a.u.) of the relevant FMOs of the investigated complex

The theoretical band is slightly underestimated from the experimentally observed band at 290 nm. Interestingly, the investigated complex shows a strong absorption band at 233 nm (f = 0.036) originated mainly from H-2 to L+1 (54%) and H-1 to L+1 (19%). The results show that H−1 and H−2 are located on π orbital of diamine and n orbital of CH_3COO groups, respectively. Therefore, this strong band may be assigned as ILCT and LLCT.
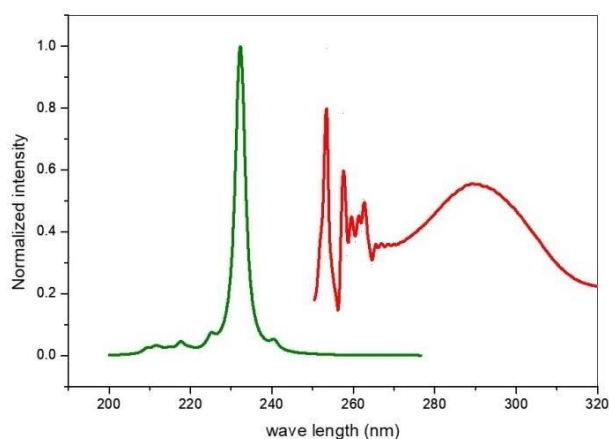

Fig. V.B.19. Experimental (red) and simulated (green) absorption spectra of the investigated complex.
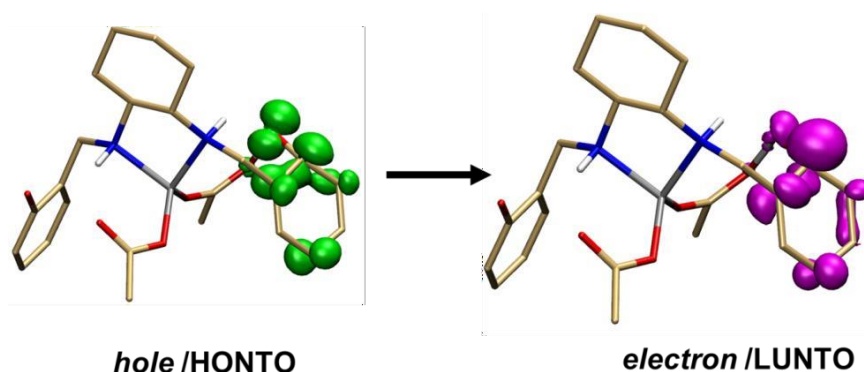
Fig. V.B.20. NTO plots of the complex at its optimized S_1 geometries.

The emission involved a transition from LUMO to HOMO (97%). As shown in FMO analysis, charge transfer occurs from π to π^* orbital of the diamine. However, for the emission, the computed emission wavelength, ca. 364 nm, is a bit underestimated from the experimental value of 446 nm.

The first excited singlet state (S_1) may be characterized by intra-ligand charge-transfer (ILCT) transitions, which is illustrated by the electron-density shift from the HONTO to the LUNTO. As shown in Fig. **V.B.20.**, both HONTOs and LUNTOs are mainly localized on the diamine. The fluorophore is, therefore, originated from the charge transfer within the diamine moiety. The computed values of charge transfer index (Δr) and hole-electron overlapping indices (ϕ_S) are 1.47 Å and 0.52, respectively.

The existence of H-bonds and CH$\cdots\pi$ interactions in the solid-state structure of the complex are well supported by the RDG plots and NCI surfaces in the dimers of the complex, as shown in Fig. **V.B.21**. The H-bonds are well characterized by using AIM analysis. H-bond energy associated with the bond critical points has also been calculated.[33] The calculated the H−bond energy is −6.64 kcal/mol. All these intermolecular interactions indicate a fairly rigid structure. This rigidity enhances the fluorescence quantum yields of the investigated complex.
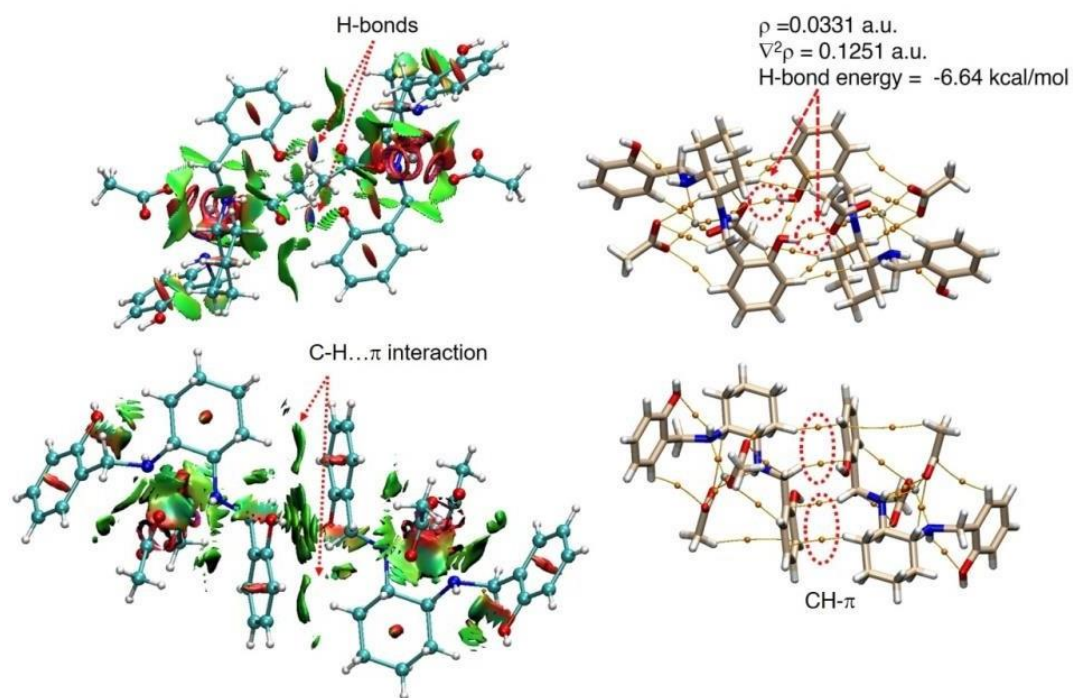
Fig. V.B.21. Non-covalent interaction (NCI) analysis for the hydrogen bonding in the dimers of the complex computed at B3LYP/Lanl2DZ/6-31G(d) level showing for H-bond and CH···π interactions.

Table V.B.4. Selected Frontier molecular orbital energies (eV) and compositions (%) in the ground state for the investigated complex

MO	energy	contribution				assignment (major)
		SB	AcO1	AcO2	Zn	
L+3	0.34	98	0	0	1	π^*(SB)
L+2	0.29	99	0	0	1	π^*(SB)
L+1	-0.02	100	0	0	0	π^*(SB)
LUMO	-0.07	99	0	0	1	π^*(SB)
energy gap = 5.75 eV						
HOMO	-5.82	2	96	1	0	n(AcO)
H-1	-5.99	3	1	96	0	π(AcO)
H-2	-6.17	98	0	2	0	π(SB)
H-3	-6.24	98	2	0	0	π(SB)

AcO = CH$_3$COO

Table V.B.5. Selected Frontier molecular orbital energies (eV) and compositions (%) in the excited state for the investigated complex

MO	energy	SB	AcO1	AcO2	Zn	assignment (major)
L+3	0.24	69	8	18	6	$\pi^*(SB)$
L+2	0.05	73	22	1	3	$\pi^*(SB)$
L+1	-0.16	93	5	0	2	$\pi^*(SB)$
LUMO	-1.34	97	0	1	2	$\pi^*(SB)$
energy gap = 3.88 eV						
HOMO	-5.22	98	0	2	0	n(SB)
H-1	-6.33	98	2	0	0	$\pi(SB)$
H-2	-6.76	90	4	6	0	$\pi(SB)$
H-3	-6.79	94	1	4	0	$\pi(SB)$

AcO = CH_3COO

Table V.B.6. Lowest-lying and strongest absorption band and lowest-lying emission band calculated wavelength (nm)/energies (eV), oscillator strength (f), major contribution, transition characters, and the experimental wavelength (nm) for the investigated complex in acetonitrile media. H indicates HOMO, L indicates LUMO.

	Excited state	λ	f	configuration	assignment	Expt. (nm)
Absorption				HOMO→LUMO (99%)	LLCT	
	S_1	241	0.0018			247, 253, 258, 262, 290
	S_2	233	0.0361	H-2→L+1 (54%), H-1→L+1 (20%)	ILCT and LLCT	
Emission	S_1	365	0.0443	LUMO→HOMO (97%)		360

4. Conclusions

In this work, one secondary diamine, H_2L^8 [2,2'-[(cyclohexane-1,2-diyl)bis(iminomethylene)]]bis[phenol] is prepared by reducing a di-Schiff base ligand, H_2L' [N,N'-bis(salicylidene)-cyclohexane-1,2-diamine] with sodium borohydride. A mononuclear zinc complex, $[Zn(H_2L)(OCOCH_3)_2]$, is then synthesized and characterized. The complex shows strong luminescence and the diamine, H_2L^8 is used as a selective chemosensor for zinc. A DFT/TDDFT approach is employed to understand the absorption and emission behaviour of the complex. The geometrical and electronic structures at the S0 and S1 states, absorption and emission spectra are calculated for the complex. The NTO analysis helps to locate the fluorophore.

References

1. T. Dudev, C. Lim, *J. Am. Chem. Soc.*, 2000, **122**, 11146.

2. L. Taghizadeh, M. Montazerozohori, A. Masoudiasl, S. Joohari, J. M. White, *Mater Sci. Eng C.*, 2017, **77**, 229.

3. T. Chu, L. Belding, P. K. Poddutoori, A. v. d. Est, T. Dudding, I. Korobkov, G. I. Nikonov, *Dalton Trans.*, 2016, **45**, 13440.

4. J. C. M. Rivas, E. Salvagni, R. T. M. d. Rosales, S. Parsons, *Dalton Trans.*, 2003, 3339.

5. T. Basak, A. Bhattacharyya, K. Harms, S. Chattopadhyay, *Polyhedron*, 2019, **157**, 449.

6. M. Karmakar, S. Roy, S. Chattopadhyay, *New J. Chem.*, 2019, **43**, 10093.

7. A. Bhattacharyya, S. Sen, K. Harms, S. Chattopadhyay, *Polyhedron.*, 2015, **88**, 156.

8. I. Mondal, S. Chatterjee, S, Chattopadhyay, *Polyhedron.*, 2020, **190**, 114735.

9. S. Ullmann, R. Schnorr, C. Laube, B. Abel, B. Kersting, *Dalton Trans.*, 2018, **47**, 5801.

10. F. Zeng, J. Ni, Q. Wang, Y. Ding, S. W. Ng, W. Zhu, Y. Xie, *Cryst. Growth Des.*, 2010, **10**, 1611.

11. T. Yu, K. Zhang, Y. Zhao, C. Yang, H. Zhang, D. Fan, W. Dong, *Inorg. Chem. Commun.*, 2007, 10, 401.

12. T. Sano, Y. Nishio, Y. Hamada, H. Takahashi, T. Usiki, K. Shibata, *J. Mater. Chem.*, 2000, **10**, 157.

13. M. E. Germain, M. J. Knapp, *Chem. Soc.*, 2008, **130**, 5422.

14. T. Basak, M. G. B. Drew, S. Chattopadhyay, *Inorg. Chem. Commun.*, 2018, **98**, 92.

15. J. Fan, X. Peng, Y. Wu, E. Lu, J. Hou, H. Zhang, R. Zhang, X. Fu, *J. Lumin.*, 2005, **114**, 125.

16. J. Guan, P. Zhang, T-b.Wei, Q. Lin, H. Yao, Y-m. Zhang, *RSC Adv.*, 2014, **4**, 35797.

17. V. Venkatesan, S. K. R, S. K. A. Kumar, S. K. Sahoo, *Inorg. Chem. Commun.*, 2019, **102**, 171.

18. N. C. Lim, J. V. Schuster, M. C. Porto, M. A. Tanudra,L.Yao, H. C. Freake, C. Bruckner, *Inorg. Chem.*, 2005, **44**, 2018.

19. S. Dasgupta, E. Zangrando, I. Majumder, *ChemistrySelect*, 2017, **2**, 7073.

20. S. Chattopadhyay, G. Bocelli, A. Musatti, A. Ghosh, *Inorg. Chem. Commun.*, 2006, **9**, 1053.

21. S. Chattopadhyay, M. G. B. Drew, A. Ghosh, *Eur. J. Inorg. Chem.*, 2008, 1693.

22. M. Das, S. Chattopadhyay, *Inorg. Chim. Acta*, 2011, **378**, 303.

23. P. Bhowmik, S. Jana, P. P. Jana, K. Harms, S. Chattopadhyay, *Inorg. Chim. Acta*, 2012, **390**, 53.

24. M. Das, S. Chatterjee, S. Chattopadhyay, *Inorg. Chem. Commun.*, 2011, **14**, 1337.

25. S. Jana, S. Chatterjee, S. Chattopadhyay, *Polyhedron*, 2012, **48**, 189.

26. S. Roy, A. Bhattacharyya, S. Purkait, A. Bauzá, A. Frontera, S. Chattopadhyay, *Dalton Trans.*, 2016, **45**, 15048.

27. S. Roy, M. G. B. Drew, A. Bauzá, A. Frontera, S. Chattopadhyay, *Dalton Trans.*, 2017, **46**, 5384.

28. N. Sarkar, M. G. B. Drew, K. Harms, A. Bauzá, A. Frontera, S, Chattopadhyay, *CrystEngComm*, 2018, **20**, 1077.

29. S. Mirdya, M. G. B. Drew, A. K. Chandra, A. Banerjee, A. Frontera, S. Chattopadhyay, *Polyhedron*, 2020, **179**, 114374.

30. A. Banerjee, A. Frontera, S. Chattopadhyay, *Dalton Trans.*, 2019, **48**, 11433.

31. P. K . Bhaumik, S. Chattopadhyay, *Polyhedron*, 2021, **199**, 115086.

32. M. Karmakar, S. Chattopadhyay, *Polyhedron*, 2020, **184**, 114527.

33. I. Mondal, T. Basak, S. Banerjee, S. Chattopadhyay, *CrystEngComm*, 2020, **22**, 3005.

34. M. Karmakar, T. Basak, S. Chattopadhyay, *New J. Chem.*, 2019, **43**,7 .

35. T. Basak, A. Bhattacharyya, K. Harms, S. Chattopadhyay, *Polyhedron*, 2019, **157**, 449.

36. S. Roy, I. Mondal, K. Harms, S. Chattopadhyay, *Polyhedron,* 2019, **159**, 265.

37. L. Yang, D. R. Powell, R. P. Houser, *Dalton Trans.*, 2007, 955.

38. D. Cremer, J. A. Pople, *J. Am. Chem. Soc.*, 1975, **97**, 1354.

39. M. Karmakar, S. Chattopadhyay, *Polyhedron,* 2020, **187**, 114639.

40. D. Dey, G. Kaur, M. Patra, A. R. Choudhury, N. Kole, B. Biswas, *Inorg. Chim. Acta*, 2014, **421**, 335.

41. S. Chattopadhyay, M. S. Ray, S. Chaudhuri, G. Mukhopadhyay, G. Bocelli, A. Cantoni, A. Ghosh, *Inorg. Chim. Acta*, 2006, **359**, 1367.

42. A. Majumder, G. M. Rosair, A. Mallick, N. Chattopadhyay, S. Mitra, *Polyhedron*, 2006, **25**, 1753.

43. S. Mirdya, T. Basak, S. Chattopadhyay, *Polyhedron*, 2019, **170**, 253.

44. M. Karmakar, S. Chattopadhyay, *Polyhedron*, 2020, **187**, 114374.

45. M. Se. Shin, B. J. Oh, J. Y. Ryu, M. H. Park, M. Kim, J. Lee, Y. Kim, *Polyhedron*, 2017, **125**, 101.

46. P. d. Hoog, L. D. Pachón, P. Gamez, M. Lutz, A. L. Spek, J. Reedijk, *Dalton Trans*, 2004, 2614.

47. M. A. Spackman, D. Jayatilaka, *CrystEngComm*, 2009, **11**, 19.

48. F. L. Hirshfeld, *Theor. Chim. Acta*, 1977, **44**, 129.

49. H. F. Clausen, M. S. Chevallier, M. A. Spackman, B. B. Iversen, *New J. Chem.*, 2010, **34**, 193.

50. S. K. Wolff, D. J. Grimwood, J. J. McKinnon, D. Jayatilaka, M. A. Spackman, Crystal Explorer 2.1, University of Western Australia, 2005-2007, http://hirshfeldsurfacenet/CrystalExplorer/crystal_explorer@theochem.uwa.edu.au.

51. A. L. Rohl, M. Moret, W. Kaminsky, K. Claborn, J. J. McKinnon and B. Kahr, *Cryst. Growth Des.*, 2008, **8**, 4517.

52. A. Parkin, G. Barr, W. Dong, C. J. Gilmore, D. Jayatilaka, J. J. McKinnon, M. A. Spackman, C. C. Wilson, *CrystEngComm.*, 2007, **9**, 648.

53. M. A. Spackman, J. J. McKinnon, *CrystEngComm*, 2002, **4**, 378.

54. J. J. McKinnon, M. A. Spackman, A. S. Mitchell, *Acta Crystallogr., Sect. B: Struct. Crystallogr. Cryst. Chem.*, 2004, **B60**, 627.

Section: V.C

An acetate bridged centrosymmetric zinc(II) complex with a tetradentate reduced Schiff base ligand: Synthesis, characterization and ability to sense nitroaromatics by turn off fluorescence response

V.C.1. Introduction

Synthetic inorganic chemists prepared and structurally characterized a large number of zinc(II) complexes with various ligands.[1-3] The geometry of these complexes may vary widely.[1-11] Common geometries include tetrahedral,[4-5] square planar,[6] trigonal bipyramidal,[7-8] square pyramidal[9-10] and octahedral[11] etc. The electronic ground states of zinc(II) (always singlet and always totally symmetric does not experience any ligand field stabilization as a result of d^{10} electronic configuration and therefore there is no ligand field restriction to attain any coordination number or any structure of zinc(II) complexes.[12-13] Zinc(II) may thus adopt different coordination geometry depending only upon steric requirements of the ligands.

Zinc(II) is an important metal in biology.[14-16] Zinc(II) is present in the active site structure of many hydrolytic enzymes, e.g. carbonic anhydrase, carboxy peptidase A, phosphatase etc. Many zinc(II) complexes are shown to have the ability to mimic these metalloenzymes.[17-18] Zinc(II) complexes are also shown to act as photo-catalyst to degradation of synthetic dyes.[19] Zinc(II) complexes have also been reported to show photoluminescence as well as electroluminescence.[20]

The strong fluorescence of zinc(II) complexes may, however, be quenched in presence of electron deficient species.[21] Nitroaromatics are electron-deficient aromatics and can quench the fluorescence of zinc(II) complexes, and therefore, nitroaromatic explosives may be detected by monitoring the quenching of the fluorescence intensity of zinc(II) complexes.[11, 21-22] In the present work, a zinc(II) complex has been prepared and characterized. Single crystal X-ray diffraction has confirmed its structure. The complex shows strong luminescence in visible region. The ability of the complex to act as fluorescence chemosensor for the detection of nitroaromatic explosives has also been investigated.

Herein, we report the synthesis, characterization, structure and fluorescence of a trinuclear zinc(II) complex with a reduced Schiff base ligand and its nitroaromatic sensing ability.

V.C.2. Experimental

V.C.2.2. Synthesis

V.C.2.2.1. Synthesis of the reduced Schiff base ligand, *1,3-bis(2-hydroxybenzylamino)2,2-dimethylpropane (H₂L⁷)*

A Schiff base ligand, *N,N'-bis(salicylidene)-2,2-dimethylpropane-1,3-diamine*, was synthesized by refluxing 2,2-dimethylpropane-1,3-diamine (1 mmol, 0.1 mL) with salicylaldehyde (2 mmol, 0.2 mL) in methanol (20 mL) solution for ca. 2 h. The Schiff base ligand was not purified but used directly for the preparation of the reduced Schiff base ligand (H_2L^7). After that, the solution (10 mL) was cooled to 0°C and solid sodium borohydride (4 mmol, ~150 mg) was added to it with constant stirring. Then the resulting solution was acidified with glacial acetic acid (2 mL) and stirred for 10 minutes. The methanol was evaporated to dryness under reduced pressure in a rotary evaporator (~60°C). The white

residue was then dissolved in water (15 mL) and extracted with the mixture of dichloromethane (15 mL) and saturated solution of sodium bicarbonate. The organic phase was dried over anhydrous sodium acetate and the solvent (i.e. dichloromethane) was evaporated under reduced pressure using a rotary evaporator to get the white color reduced Schiff base ligand (H_2L^7).

V.C.2.2.2. Synthesis of the complex $[Zn_3L^7{}_2(CH_3CO_2)_2(DMSO)_2]$ (10)

The methanol solution (10 mL) of zinc(II) acetate dihydrate (1 mmol, 1.095 g) was added to the methanol solution (20 mL) of the reduced Schiff base ligand, H_2L^7 and the resulting solution was stirred for 1 hour to give a colourless solution. Then few drops of triethylammine were added to the solution. The solution was cooled and DMSO was added in the mixture as solvent. It was kept in open atmosphere at room temperature for 3 days. White crystalline product was obtained by slow evaporation of the filtrate. X-ray quality single crystals were collected from this crystalline product.

Yield: 340 g, 71% (based on zinc). Anal. Calc. for $C_{46}H_{66}N_4O_{10}S_2Zn_3$[+ solvent] (F.W. 1095.32): C, 51.23; H, 6.45; N, 4.98 %. Found: C, 51.18; H, 6.39; N, 5.04 %. FT-IR (KBr, cm^{-1}): 3297 (ν_{N-H}); 2961–2859 (ν_{C-H}). λ_{max} (nm) [ε_{max}(lit mol^{-1} cm^{-1})] (acetonitrile): 280 (1.1x10^4).

The details of crystallographic data and refinements are given in **Table V.C.1**.

Table V.C.1. Crystal data and refinement details of the complex **10**.

Formula	$C_{46}H_{66}N_4O_{10}S_2Zn_3$[+ solvent]
Formula Weight	1095.32
Temperature (K)	273

Crystal System	Monoclinic
Space group	$C2/c$
a (Å)	22.329(2)
b (Å)	12.3058(13)
c (Å)	19.706(2)
β (°)	92.839(3)
V(Å^3)	5408.2(10)
Z	4
d_{cal} (g cm^{-3})	1.345
μ(mm^{-1})	1.451
F(000)	2288
Total reflection	30918
Unique Reflections	4794
Observe data[I>2ζ(I)]	3814
R(int)	0.0420
R1, wR2 (all data)	0.1117, 0.2831
R1, wR2 [I>2σ(I)]	0.0927, 0.2646
Residual Electron Density (eÅ^{-3})	1.553, -1.449

CCDC reference number is 2017336

V.C.3. Results and discussion

V.C.3.1. Synthesis

Salicylaldehyde and 2, 2-dimethylpropane-1,3-diamine have been used to prepare a Schiff base ligand, following the reported method.[25] It was then reduced with borohydride following literature procedure.[26] It was extracted with dichloromethane several times to eliminate impurities. The ligand is then trapped as a zinc(II) complex, *[Zn₃L⁷₂(CH₃CO₂)₂(DMSO)₂]* by

reacting with zinc(II) acetate in 1:1 molar ratio followed by addition of few drops of triethylammine and DMSO. Addition of triethylamine helps to deprotonate the reduced Schiff base and this, in turn, triggers the formation of the trinuclear complex. When trimethylamine is not added, the reduced Schiff base is not deprotonated. This results in the formation of mononuclear complexes in presence of azide or thiocyanate.[2] Single crystals of the trinuclear complex could not be grown in methanol medium. So, DMSO was added to grow the single crystals, suitable for X-ray diffraction. DMSO actually coordinates zinc centre to form stable complex (vide infra). Formation of the complex has been shown in **Scheme V.C.1**.
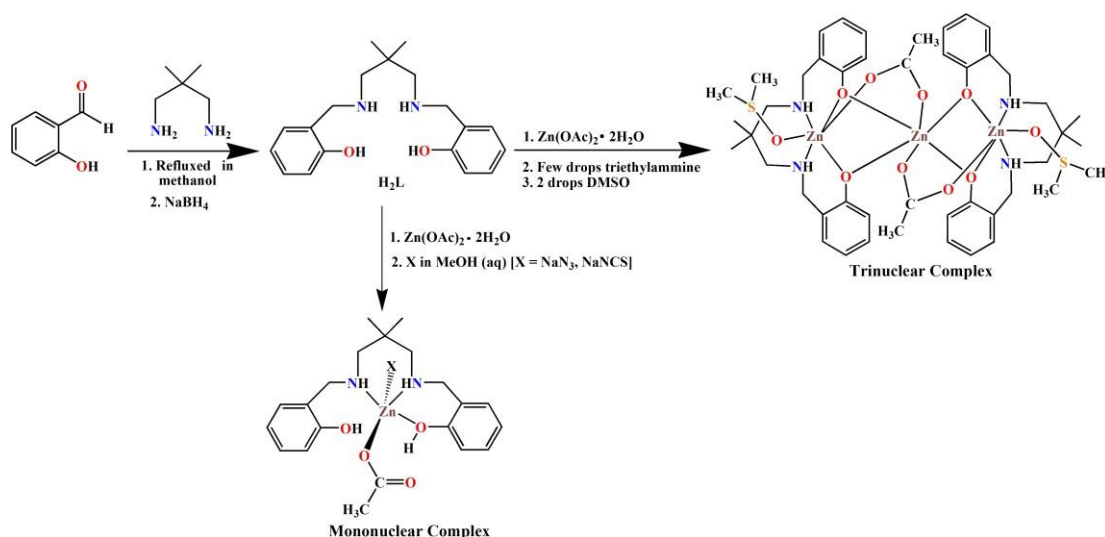
Scheme V.C.1. Synthetic route to the trinuclear complex related to mononuclear complexes using the reduced schiff base ligand, H_2L^7.

V.C.3.2. Description of structure

The X-ray crystal structure determination revealed that this complex crystallizes in the monoclinic space group *C2*/c. A perspective view of the complex along with selective atom-numbering scheme is shown in Fig. **V.C.1**. Important bond lengths and bond angles have been gathered in Tables **V.C.2**. and **V.C.3**. respectively. The zinc(II) centre, Zn(1) has six-coordinated distorted octahedral geometry in which two amine nitrogen atoms N(1) and N(2) and two phenoxo oxygen atoms O(1) and O(2) of a reduced Schiff base ligand, L^{2-}, constitute

the equatorial plane. On the other hand, the axial positions are coordinated by an oxygen atom, O(3) of DMSO and an acetate oxygen atom, O(5), furnishing a distorted octahedral coordination sphere around itself. The deviation of all the coordinating atoms, N(1), N(2), O(1) and O(2), in the basal plane from the mean plane passing through them are −0.002(7), 0.002(7), 0.002(7) and −0.002(6)Å. Similarly Zn(2) is six-coordinated by O(1), O(2), O(1)', O(2)' (' = 0.5-x, 0.5-y, 1-z) of two symmetry related reduced Schiff base ligands and O(4) from acetate ion and O(4)' one symmetry related Zn(2)' atom (' = 0.5-x, 0.5-y, 1-z). In the Zn_2O_2 core the bridging angles, Zn(1)–O(1)–Zn(2) and Zn(1)–O(2)–Zn(2), are 98.6(3)° and 98.4(2)°respectively. The distance between two zinc(II) centres in Zn_2O_2 core are 3.094(2) Å. The saturated five membered chelate ring, Zn(1)-N(2)-C(12)-C(8)-N(1) represents a chair conformation with puckering parameters[27, 28] q(2) = 0.631(7) Å and θ = 137(20)°, θ = 2.3(6)°.

V.C.3.3. Supramolecular Interactions

The hydrogen atom, H(22B), attached to carbon atom, C(22), is involved in intramolecular C–H⋯π interaction with the phenyl rings, Cg25, [C(1)–C(2)–C(3)–C(4)–C(5)–C(6)].
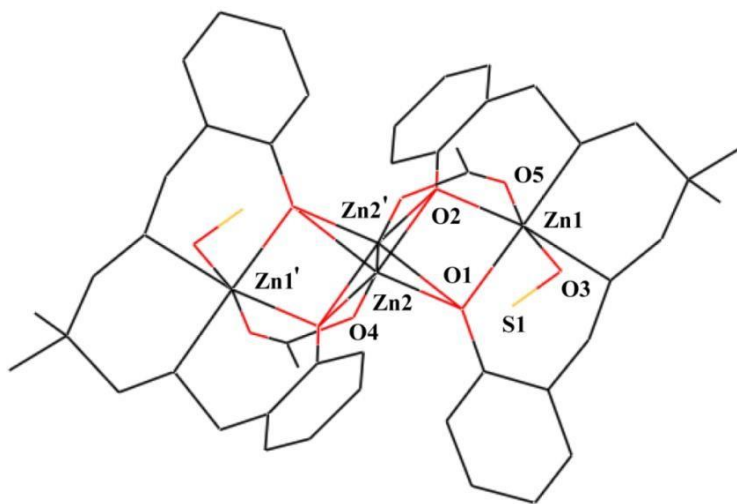

Fig. V.C.1. Perspective view of the complex with selective atom numbering scheme. Both positions of central zinc(II) are shown in figure. Central zinc(II) atom (Zn2) is disordered over two positions (Zn2 and Zn2'). The carbon atom attached to sulphur atom of DMSO is omitted for clarity. All the hydrogen atoms have been omitted for clarity. Symmetry transformation ' = 0.5-x, 0.5-y, 1-z.

Table V.C.2: Selected bond lengths (Å) of the complex **10**.

Zn(1)-O(1)	2.053(6)	Zn(2)-O(1)	2.029(6)
Zn(1)-O(2)	2.046(5)	Zn(2)-O(2)	2.042(5)
Zn(1)-O(3)	2.481(7)	Zn(2)-O(4)	1.971(14)
Zn(1)-N(1)	2.105(6)	Zn(2)-O(1a)	2.055(7)
Zn(1)-N(2)	2.106(6)	Zn(2)-O(2a)	2.112(5)
Zn(1)-O(5a)	2.110(9)		

Table V.C.3: Selected bond angles (°) of the complex **10**.

O(1)-Zn(1)-O(2)	81.2(2)	O(5a) -Zn(1)-N(1)	95.1(3)
O(1)-Zn(1)-O(3)	90.1(2)	O(5a) -Zn(1)-N(2)	96.1(3)
O(1)-Zn(1)-N(1)	91.8(2)	O(1)-Zn(2)-O(2)	81.8(2)
O(1)-Zn(1)-N(2)	166.9(3)	O(1)-Zn(2)-O(4)	114.2(5)
O(1)-Zn(1)-O(5a)	95.9(3)	O(1)-Zn(2)-O(1a)	144.3(3)
O(2)-Zn(1)-O(3)	89.9(2)	O(1)-Zn(2)-O(2a)	88.1(2)
O(2)-Zn(1)-N(1)	166.9(2)	O(2)-Zn(2)-O(4)	114.6(4)
O(2)-Zn(1)-N(2)	92.3(2)	O(1a)-Zn(2)-O(2)	89.3(2)
O(2)-Zn(1)-O(5a)	96.7(3)	O(2)-Zn(2)-O(2a)	144.9(3)

O(3)-Zn(1)-N(1)	79.0(2)	O(1a)-Zn(2)-O(4)	101.1(5)
O(3)-Zn(1)-N(2)	78.5(2)	O(2a)-Zn(2)-O(4)	100.2(4)
O(3)-Zn(1)-O(5a)	171.7(3)	O(1a)-Zn(2)-O(2a)	79.5(2)
N(1)-Zn(1)-N(2)	92.3(2)		
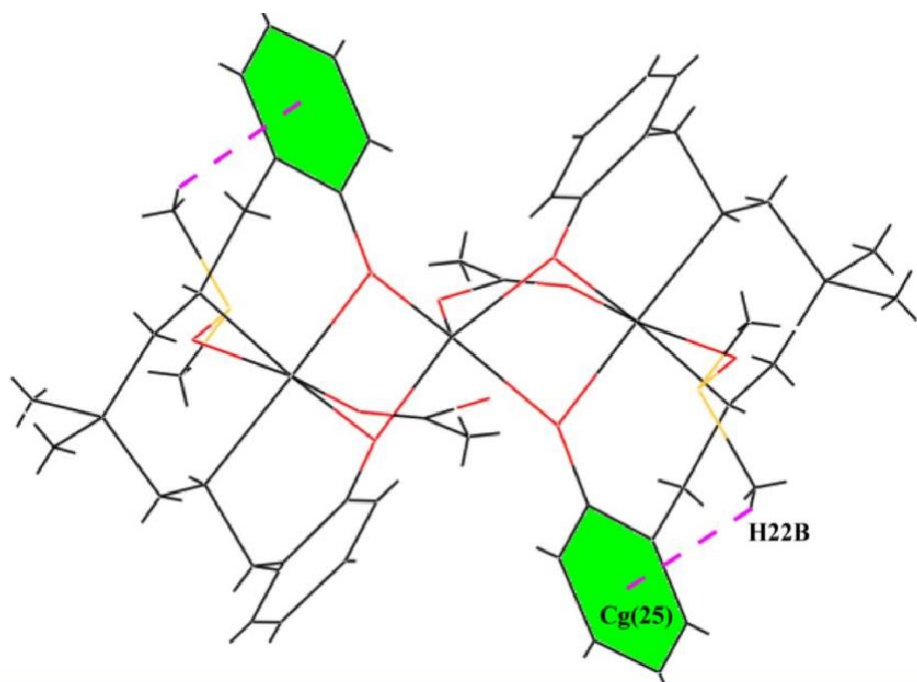
Fig. V.C.2. Intramolecular C-H⋯π interactions in the complex. Only the relevant atoms have been shown for clarity.

V.C.3.4. IR, UV and fluorescence spectra of the complex

A band at 3297 cm^{-1} in the IR spectrum of the complex (Fig. **V.C.3.**) is customarily noticed due to amine N–H bond stretching.[29-30] The bands within the range from 2961–2859 cm^{-1} due to alkyl C–H stretching vibrations are routinely observed also.[31] The UV-Visible spectrum of the complex consists of only one band at 280 nm, which may be assigned as intra-ligand charge transfer transition.[19] The complex shows strong fluorescence at 408 nm when excited at 280 nm (**Fig. V.C.4.**).

V.C.3.5. Sensing Property

This trinuclear zinc(II) complex has been used for sensing harmful organic analytes. The fluorescence spectra of this complex have been recorded in presence of organic analytes such as benzaldehyde and different nitroaromatics (4-nitrotoluene, 4-nitrophenol, 3-methyl-4-nitrobenzoic acid). Quenching of fluorescence intensity has been observed significantly upon
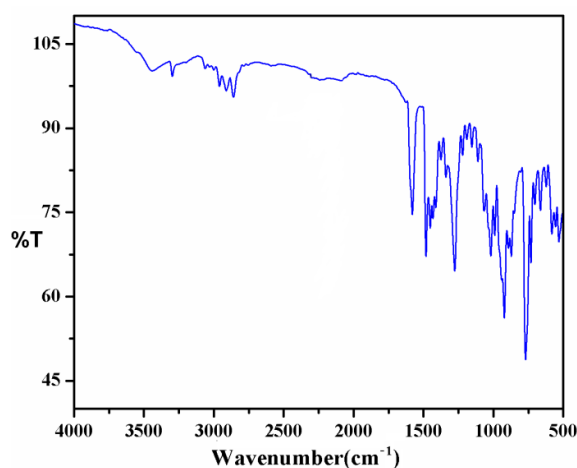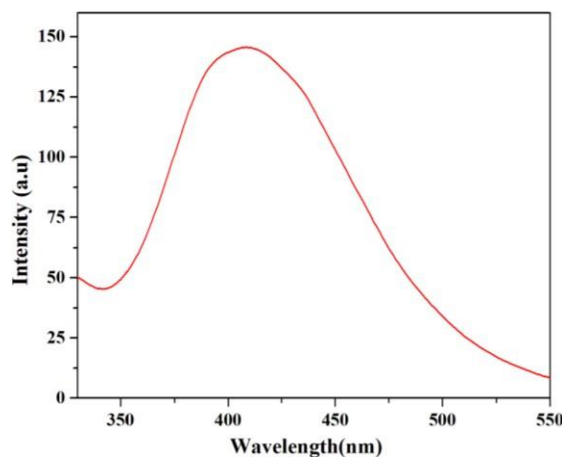

Fig. V.C.3. IR spectrum of the complex **10**.

Fig. V.C.4. Fluorescence spectrum of the complex **10**.

addition of different nitroaromatics but no quenching of fluorescence intensity has been observed upon addition of benzaldehyde (Fig. **V.C.5.**). So this can be concluded that this complex can be used as sensor for the selective sensing of nitroaromatics.

The fluorescence titrations of the complex (10^{-5} M) have been performed in DMF solutions by gradually adding (20 µL) different nitroaromatics (4-nitrotoluene, 4-nitrophenol, 3-methyl-4-nitrobenzoic acid,) (10^{-2} M) separately with a increase in concentration. The fluorescence intensity of the complex kept on decreasing with an increase in the concentration of different nitroaromatics.
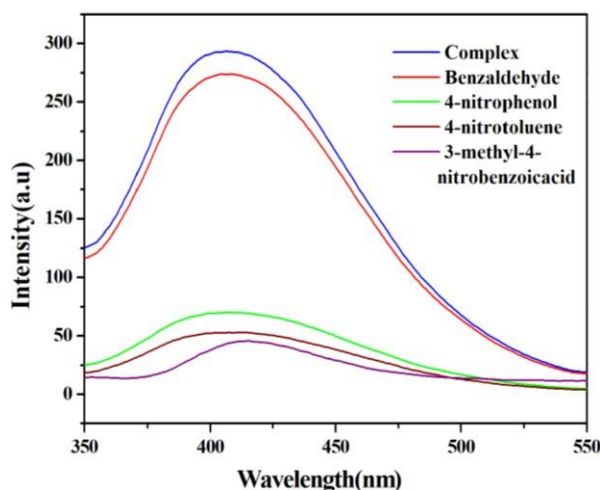

Fig. V.C.5. Fluorescence spectra of the complex in DMF (excitation wavelength 280 nm and conc. 10^{-5} M) upon the addition of various organic analytes.
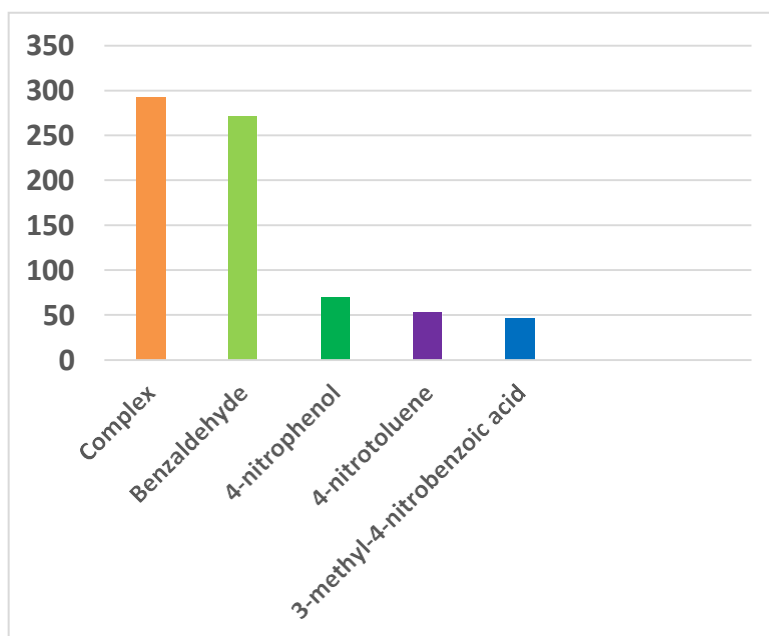
Fig. V.C.6. Relative changes in the fluorescent intensity of the complex in presence of various organic analytes.

The quenching of the fluorescence intensity of this complex with the addition of benzaldehyde, 4-nitrotoluene, 4-nitrophenol and 3-methyl-4-nitrobenzoicacid has been shown in Fig. **V.C.7**.
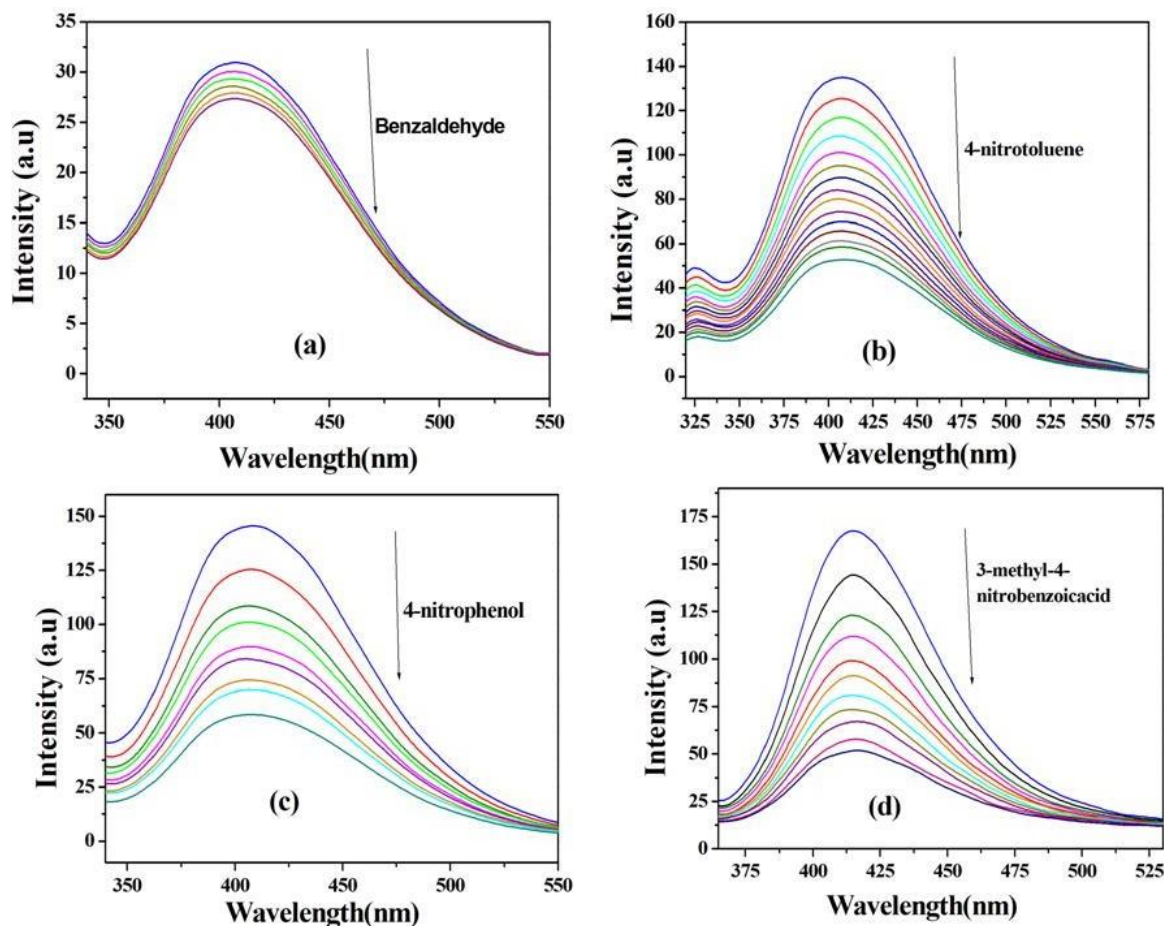

Fig. V.C.7. Fluorescence spectra of the complex in DMF (excitation wavelength 280 nm and conc 10^{-5} M) upon increasing concentration of benzaldehyde (a), 4-nitrotoluene (b), 4.-nitrophenol (c) and 3-methyl-4-nitrobenzoicacid (d).

Quenching of fluorescence intensity by nitroaromatics is mostly due to their more electron deficient nature is shown in Fig. **V.C.6.** The efficient quenching by nitroaromatics can be explained considering the possibility of $\pi \cdots \pi$ interactions between nitroaromatics and the reduced Schiff base complex, inducing electron transfer from the excited state of metal complex to the ground state of electron-deficient nitroaromatics. A schematic representation

of electron transfer from the complex to nitrobenzene has been shown in Fig.**V.C.8.** Nitroaromatics with electron-deficient property can acquire an electron from excited ligand,[29-30] which can be confirmed by molecular orbital theory.[31-32]
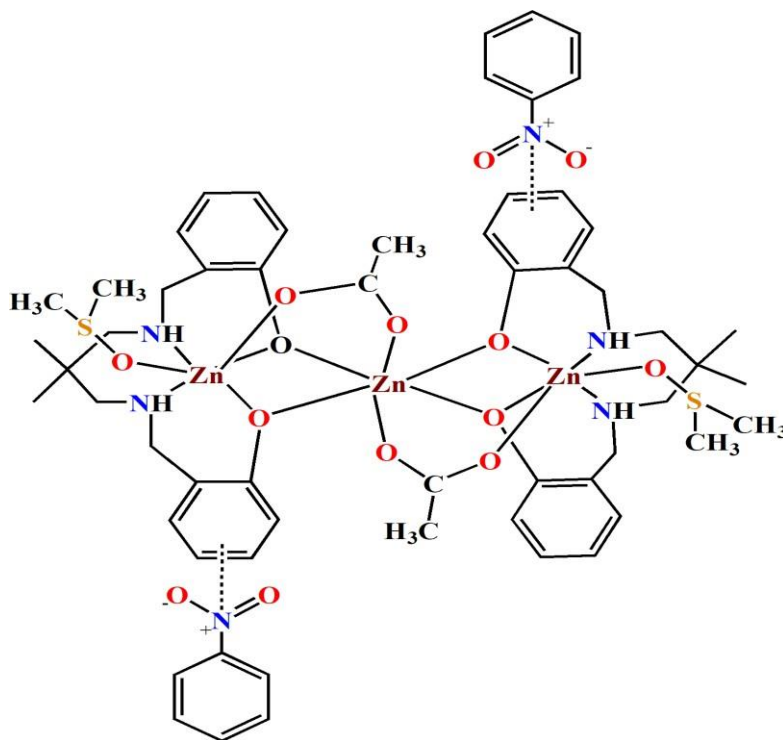

Fig. V.C.8. Schematic representation of electron transfer from the complex to nitrobenzene.

The quenching efficiency of nitroaromatics may be determined by the Stern-Volmer equation given below,

$$\frac{I_0}{I} = 1 + K_{sv}\,[Q]$$

Where, K_{SV} is the quenching constant (M^{-1}), [Q] is the molar concentration of the quencher, I_0 and I are luminescence intensities before and after adding the quencher, respectively. At low concentrations, the Stern-Volmer plot of nitroaromatics is linear whereas at higher concentrations, consequently deviate from linearity and turn upward (Fig. **V.C.9.**), which may be due to self-absorption.[33] The Stern-Volmer quenching constants (Ksv) have been calculated from the slope of the linearly fitted curves (insets in Fig. **V.C.9.**) and gathered in

Table **V.C.4**. Data indicates that 3-methyl-4-nitrobzoicacid is more responsive to quench the intensity of fluorescence of the synthesized complex.
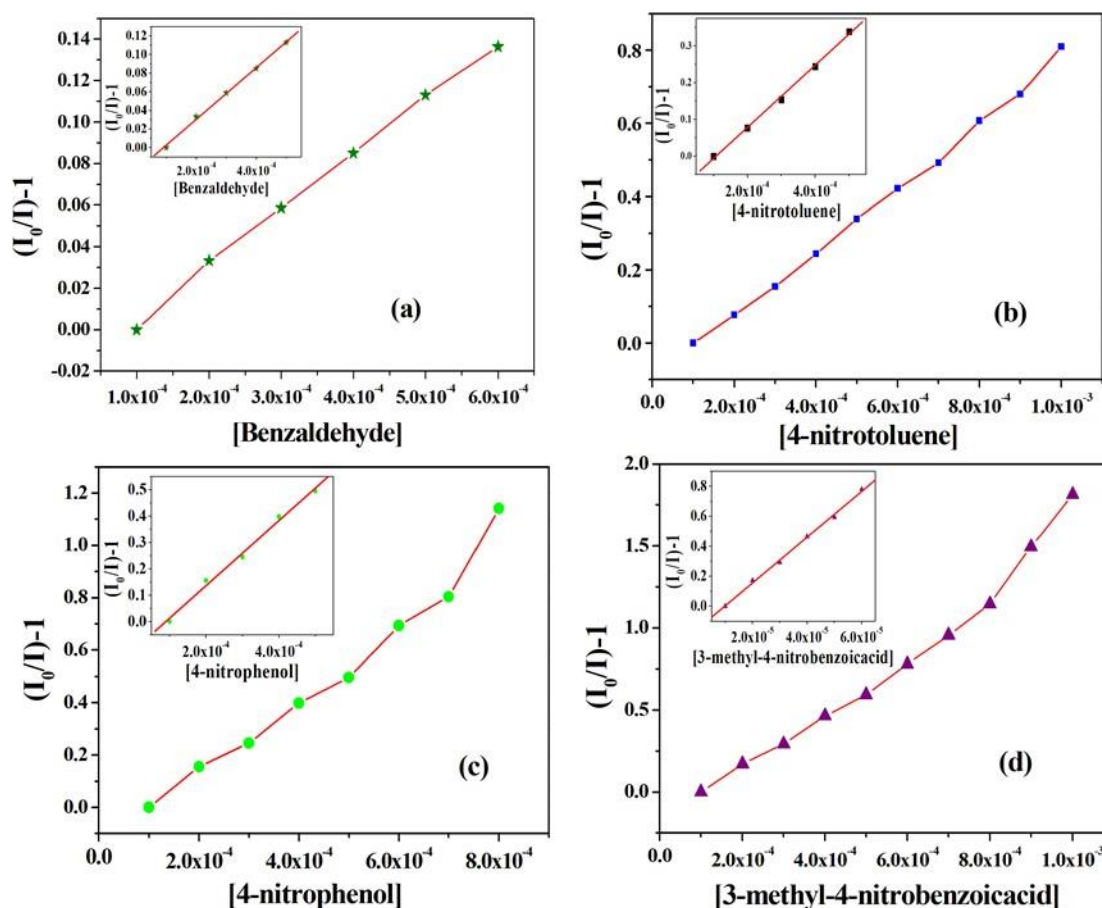

Fig. V.C.9. Stern-Volmer plot of the complex with benzaldehyde (a), 4-nitrotoluene (b), 4-nitrophenol (c) and 3-methyl-4-nitrobenzoicacid (d) in DMF.

The limit of detection (LOD) of the complex with different nitroaromatics have also been gathered in Table **V.C.4.** The detection limit of nitroaromatics towards complex is calculated using the equation, LOD = $3\zeta/k$, where ζ is the standard deviation in blank measurements.[34] The slope of the plot of fluorescence intensity versus concentration of the complex gives k. The LOD (limit of detection) values of the complex with different nitroaromatics in DMF have been shown in Fig. **V.C.10**.

The nitroaromatic sensing activity of the present complex may be compared with some of the other reported zinc(II) based complexes[11, 18-19, 21] based on the Ksv values (Table **V.C.5**). Higher Ksv value usually indicates that the complex is more effective for sensing a probe.

Table **V.C.5** may therefore suggest that the present complex is a mediocre sensor for the detection of nitroaromatics via turn-off fluorescence response.
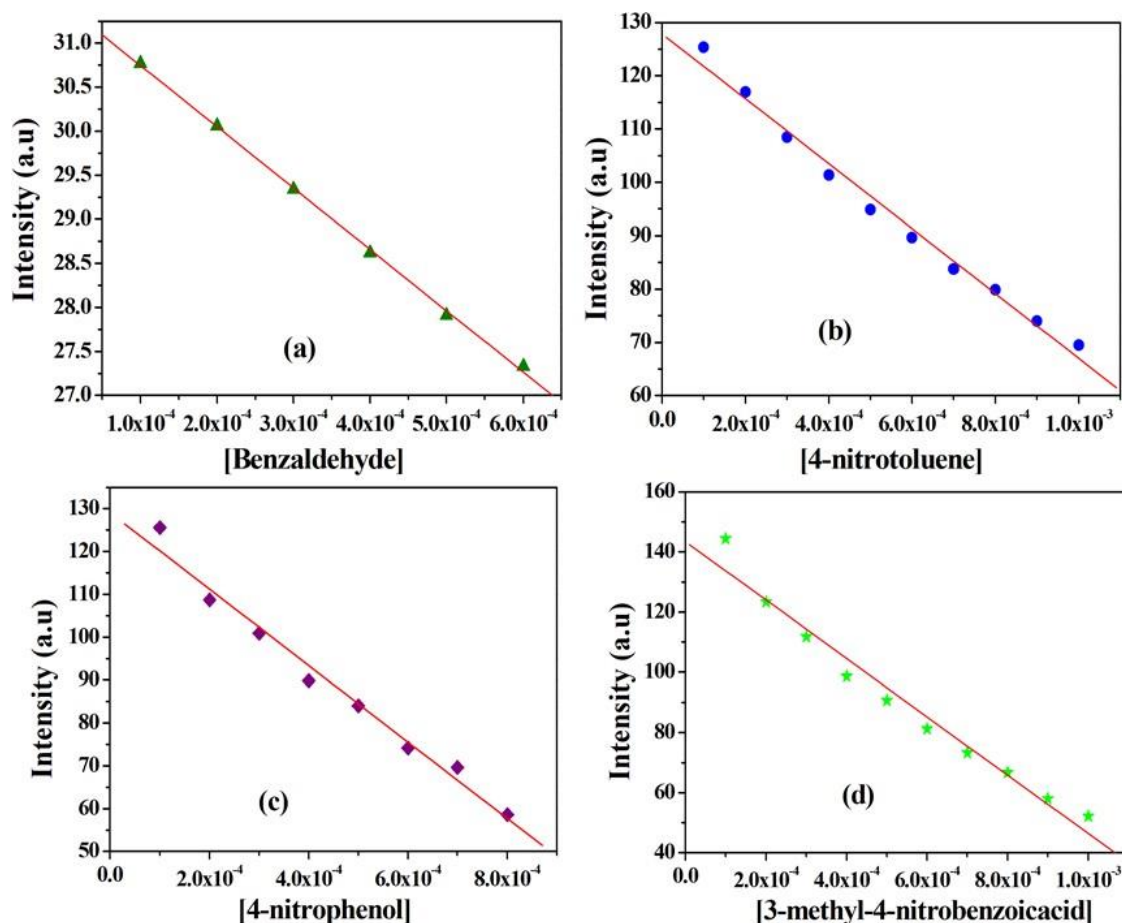

Fig. V.C.10. Plot of limit of detection of the complex towards benzaldehyde (a) 4-nitrotoluene (b), 4-nitrophenol (c) and 3-methyl-4-nitrobenzoicacid (d) in DMF.

Table V.C.4: Stern-Volmer constants (Ksv) and LOD values of the complex **10** with different nitroaromatics in DMF

	Ksv	LOD
Benzaldehyde	2.78×10^2	6.11×10^{-6}
4-nitrotoluene	8.85×10^2	4.18×10^{-6}
4-nitrophenol	9.34×10^2	2.25×10^{-6}
3-methyl-4-nitrobenzoicacid	1.03×10^3	2.34×10^{-6}

Table V.C.5: Comparison of nitroaromatic sensing ability.

Complex	Nitro Aromatic Compound	Solvent	Ksv	Ref
[Zn$_3$(L)$_2$(CH$_3$CO$_2$)$_2$(DMSO)$_2$]	3-methyl-4-nitrobenzoicacid	DMF	1.03×10^3	Present Work
[{(N$_3$)Zn(L^1)}$_2$Zn]	2-Chloro-4-nitrobenzoicacid	DMF	9.16×10^4	11
[{(SCN)Zn(L^1)}$_2$Zn]	2-Chloro-4-nitrobenzoicacid	DMF	7.15×10^4	11
[{(SCN)Zn(L^2)}$_2$Zn]	2-Chloro-4-nitrobenzoicacid	DMF	8.49×10^4	11
[{(N$_3$)Zn(L^2)}$_2$Zn]	2-Chloro-4-nitrobenzoicacid	DMF	8.12×10^4	11
[{(N$_3$)Zn(L^3)}$_2$Zn]CH$_2$Cl$_2$	2-Chloro-4-nitrobenzoicacid	DMF	9.30×10^4	11
[($\mu_{1,1}$-N$_3$)$_2${(N$_3$)Zn(L^4)Zn}$_2$Zn(L^4)]	3-methyl-4-nitrobenzoicacid	DMF	6.49×10^4	18
[Zn{Zn(N$_3$)L^5}$_2$]	2-Chloro-4-nitrobenzoicacid	CH$_3$CN	1.38×10^5	19
Cd{L^{6}Zn(NCS)]$_2$	1,3-dinitrobenzene	DMF	8.6×10^4	21

{H$_2$L = 1,3-bis(2-hydroxybenzylamino)2,2-dimethylpropane; H$_2$L^1 = 2,2'-[(1,3-propanediyl)bis-(iminomethylene))]bis[6-ethoxyphenol]; H$_2$L^2 = 2,2'-[(2,2-dimethyl-1,3-

propanediyl)bis(iminomethylene)]-bis[6-methoxyphenol]; H₂L³ = 2,2'-[(2,2-dimethyl-1,3-propanediyl)bis(iminomethylene)]bis[6-ethoxyphenol]; H₂L⁴ = 2,2'-[(1-Methyl-1,2-ethanediyl)bis(iminomethylene)]bis[6-methoxyphenol]; H₂L⁵ = 2,2'-[(1-ethyl-1,3-propanediyl)bis(iminomethylene)] bis[6-ethoxyphenol]; H₂L⁶ = N,N'-bis(3-ethoxysalicylidene)-2,2-dimethylpropane-1,3-diamine}

V.C.4. Concluding remarks

The synthesis and characterization of a new trinuclear zinc(II) complex with a reduced Schiff base ligand is depicted in this paper. X-ray crystal structure determination confirmed its structure. The complex shows strong luminescence property. The fluorescence intensity decreases in presence of nitroaromatic compounds, but remains practically same on adding benzaldehyde. The decrease in fluorescence intensity is maximum on adding 3-methyl-4-nitrobenzoicacid. The efficient quenching by nitroaromatics can be explained considering the possibility of $\pi \cdots \pi$ interactions between nitroaromatics and the complex, inducing electron transfer from the excited state of metal complex to the ground state of nitroaromatics. The quenching efficiency of nitroaromatics is determined by the Stern-Volmer equation. The limit of detection (LOD) of the complex 10 with different nitroaromatics has also been calculated. The Ksv

values of this complex for the detection of different nitrpoaromatics are not very high. The results indicate that the synthesized complex may act only as a moderate fluorosensor for the detection of nitroaromatic substances. However, this complex is stable in water, which is not the case for many other complexes with higher Ksv values. Solubility in water makes the complex more useful.

References

1. N. Ahmed, C. Das, S. Vaidya, A. K. Srivastava, S. K. Langley, K. S. Murray and M. Shanmugam, *Dalton Trans*., 2014, **43**, 17375.

2. I. Mondal, T. Basak, S. Banerjee, S. Chattopadhyay, *CrystEngComm*., 2020, **22**, 3005.

3. A. Das, S. Jana, A. Ghosh, *Cryst. Growth Des*., 2018, **18**, 2335.

4. A.-C. Chamayou, S. Ludeke, V. Brecht, T.B. Freedman, L.A. Nafie, C. Janiak, *Inorg. Chem*., 2011, **50**, 11363.

5. L. Taghizadeh, M. Montazerozohori, A. Masoudiasl, S. Joohari, J. M. White, *Mater Sci Eng C*., 2017, **77**, 229.

6. G. Parkin, *Chem. Rev*., 2004, **104**, 699.

7. J. C. M. Rivas, E. Salvagni, R. T. M. d. Rosales, S. Parsons, *Dalton Trans*., 2003, 3339.

8. A. Bhattacharyya, S. Sen, K. Harms, S. Chattopadhyay, *Polyhedron*, 2015, **88**, 156.

9. D. Majumdar, S. Das, R. Thomas, Z. Ullah, S. S. Sreejith, D. Das, P. Shukla, K. Bankura, D. Mishra, *Inorg. Chim. Acta*, 2019, **492**, 221.

10. A. Majumder, G.M. Rosair, A. Mallick, N. Chattopadhyay, S. Mitra, *Polyhedron*, 2006, **25**, 1753.

11. M. Karmakar, S. Roy, S. Chattopadhyay, *New J. Chem*., 2019, **43**, 10093.

12. A. L. Johnson, N. Hollingsworth, G. Kociok-Köhn, K. C. Molloy, *Inorg. Chem*, 2008. **47**, 12040.

13. D. J. D. Wilson, C. M. Beavers, A. F. Richards, *Eur. J. Inorg. Chem.*, 2012, 1130.

14. S. Mandal, Y. Sikdar, D. K. Maiti, G. P. Maiti, S. K. Mandal, J. K. Biswas, S.Goswami, *RSC Adv.*, 2015, **5**, 72659.

15. C. Patra, A. K. Bhanja, A. Mahapatra, S. Mishra, K. D. Saha, C. Sinha, *RSC Adv.*, 2016, **6**, 76505.

16. K. E. Dalle, F. Meyer, *Eur. J. Inorg. Chem.*, 2015, 3391.

17. R. Sanyal, A. Guha, T, Ghosh, T. K. Mondal, E. Zangrando, D. Das, *Inorg. Chem.*, 2014, **53**, 85.

18. M. Karmakar, T. Basak, S. Chattopadhyay, *New J. Chem.*, 2019, **43**, 4432.

19. M. Karmakar, S. Chattopadhyay, *Polyhedron*, 2020, **187**, 114639.

20. P. Wang, Z. Hong, Z. Xie, S. Tong, O. Wong, C.-S. Lee, N. Wong, L. Hung, S. Lee, *Chem. Commun.* 2003, 1664.

21. S. Roy, I. Mondal, K. Harms, S. Chattopadhyay, *Polyhedron*, 2019, **159**, 265.

22. S. Dasgupta, E. Zangrando, I. Majumder, *ChemistrySelect*, 2017, **2**, 7073.

23. G. M. Sheldrick, *Acta Crystallogr., Sect. A: Found. Crystallogr.*, 2008, 64, 112.

24. G. M. Sheldrick, SADABS, V2014/5, Software for Empirical Absorption Correction, University of Go¨ttingen, Institute fur Anorganische Chemieder Universitat, Gottingen, Germany, 1999–2003.

25. T. Basak, M. G. B. Drew, S. Chattopadhyay, *Inorg. Chem.Comm.*, 2018, **8**, 92.

26. A. Hazari, L. K. Das, R. M. Kadam, A. Bauza´, A. Frontera, A. Ghosh, *Dalton Trans*, 2015, **44**, 3862.

27. D. Cremer, J.A. Pople, *J. Am. Chem. Soc.*, 1975, **97**, 1354.

28. D. Cremer, *Acta Crystallogr. Sect. B: Struct. Sci*., 1984, **40**, 498.

29. S. Chattopadhyay, M. S. Ray, S. Chaudhuri, G. Mukhopadhyay, G. Bocelli, A. Cantoni, A. Ghosh, *Inorg. Chim. Acta*., 2006, **359**, 982.

30. S. Roy, A. Dey, P. P. Ray, J. Ortega-Castro, A. Frontera, S. Chattopadhyay, *Chem.Commun*., 2015, **51**, 12974.

31. K. Ghosh, K. Harms, A. Bauzá, A. Frontera, S. Chattopadhyay, *Dalton Trans*., 2018, **47**, 331.

32. D. Tian, Y. Li, R.-Y. Chen, Z. Chang, G.-Y. Wang, X.-H. Bu, *J. Mater. Chem*., 2014, **2**, 1465.

33. Z.-J. Wang, L. Qin, J.-X. Chen, H.-G. Zheng, *Inorg. Chem*., 2016, **55**, 10999.

34. A. Kumar, A. Kumar and D. S. Pandey, *Dalton Trans,* 2016, **45**, 8475.

Chapter VI

Highlights of the thesis

The total research work discussed in this thesis primarily focuses on synthesis, characterization and applications of a series of manganese(III) and zinc(II) complexes with the N_2O_2 donor salicylidene Schiff base ligands and zinc(II) complexes with the reduced analogues of N_2O_2 donor salicylidene Schiff base ligands. A few complexes of manganese(III) and zinc(II) are among the weak supramolecular interactions that have been studied in the solid state. To comprehend and quantify the energetic contribution of each interaction in the development of supra-molecular assemblies, density (DFT) calculations and NCI plots have been used on a number of occasions. A few manganese(III) and zinc(II) compounds have shown excellent performance in the areas of catalysis and nitroaromic sensing. The exciting observations have been gathered below.

- ❖ Excellent catalase mimicking activity of three mononuclear manganese(III) Schiff base complexes have been described in Section A of chapter II.

- ❖ Section B of chapter II reported the efficiency of a mononuclear manganese(III) Schiff base complex towards catalytic decomposition of hydrogen peroxide. The energetic features of significant supramolecular interactions present in the complex, have been calculated using DFT calculations and further corroborated with NCI plot index computational tool.

- ❖ In chapter III, a compartmental Schiff base ligand has been used to prepare a hetero-trimetallic, zinc(II)-cadmium(II)-zinc(II) complex. This complex acts as turn-off fluorescence chemosensor for detection of various nitroaromatics.

- ❖ The synthesis and X-ray characterization of a new dinuclear zinc(II) complex using a tetradentate N_2O_2 donor Schiff base and azide as anionic co-ligand has been described in chapter IV. This complex forms self-assembled dimers in the solid state governed by ζ-hole tetrel bonding interactions involving the zinc(II) methoxy group. The

energy of π-stacking interaction has been estimated using DFT calculations and several computational tools.

❖ Section A of chapter V reported the synthesis and characterization of a reduced Schiff base ligand. This ligand used as a fluorescence chemo-sensor for the selective detection of zinc(II). Two mononuclear zinc(II) complexes have also been synthesized with the ligand and DFT/TDDFT approach has been used to understand the fluorescence behavior of two zinc(II) complexes.

❖ Synthesis and characterization of a zinc(II) complex with a reduced schiff base ligand has been described in Section B of chapter V. Its fluorescence property and solid state non-covalent interactions have been studied in detail with the help of DFT calculations.

❖ Section C of chapter V highlights synthesis, characterization, structure and fluorescence of a trinuclear zinc(II) complex with a reduced Schiff base ligand and its nitroaromatic sensing ability.

Appendix

List of publications

1. "Synthesis and structural characterization of three manganese(III) complexes with N₂O₂ donor tetradentate Schiff base ligands: Exploration of their catalase mimicking activity"

I. Mondal, K. Ghosh and S. Chattopadhyay, *Inorg. Chim. Acta.,* 2019, **494**, 123.

2. "Synthesis and characterization of a manganese(III) schiff base complex and exploration of Br···Br interaction in the solid state structure of the complex"

I. Mondal, K. Ghosh, A. Franconetti, A. Frontera, S. Chatterjee and S.Chattopadhyay, *J. Coord. Chem.,* 2019, **72**, 3237.

3. "A trigonal dodecahedral cadmium(II) complex with zinc(II)–salen type metalloligand: Synthesis, structure, self-assembly and application in the detection of various nitroaromatics via turn-off fluorescence response"

S. Roy, **I. Mondal**, K. Harms and S. Chattopadhyay, *Polyhedron*, 2019, **159**, 265.

4. "On the importance of RH₃C···N tetrel bonding interactions in the solid state of a dinuclear zinc complex with a tetradentate Schiff base ligand"

I. Mondal, A. Frontera and S. Chattopadhyay, *CrystEngComm*, 2021, **23**, 3391.

5. "A theoretical insight on the rigid hydrogenbonded network in the solid state structure of two zinc(II) complexes and their strong fluorescence behaviors"

I. Mondal, T. Basak, S. Banerjee and S. Chattopadhyay, *CrystEngComm*, 2020, **22**, 3005

6. "An acetate bridged centrosymmetric zinc(II) complex with a tetradentate reduced Schiff base ligand: Synthesis, characterization and ability to sense nitroaromatics by turn off fluorescence response"

I. Mondal, S. Chatterjee and S.Chattopadhyay, *Polyhedron*, 2019, **159**, 265.

7. "A mononuclear zinc complex with a diamine: Synthesis, characterization, self assembly, luminescence property and DFT calculations"

I. Mondal, S. Banerjee and S. Chattopadhyay, *J. Mol. Struct*., 2022, **1249**, 131598.

8. "Development of multi-metallic complexes using metal-salen complexes as building blocks"

I. Mondal and S.Chattopadhyay, *J. Coord. Chem.,* 2019, **72**, 3183.*

[* = Not included in the thesis]

Research paper

Synthesis and structural characterization of three manganese(III) complexes with N$_2$O$_2$ donor tetradentate Schiff base ligands: Exploration of their catalase mimicking activity

Ipsita Mondal, Kousik Ghosh, Shouvik Chattopadhyay[*]

Department of Chemistry, Inorganic Section, Jadavpur University, Kolkata 700 032, India

ABSTRACT

Three manganese(III) complexes, *[Mn(L¹)(N₃)(H₂O)]·CH₃OH·H₂O (1)*, *[Mn(L²)(N₃)(H₂O)] (2)* and *[Mn(L³)(H₂O)₂]ClO₄ (3)* {where *H₂L¹ = N,N'-bis(3-methoxysalicylidene)1,2-ethanediamine*, *H₂L² = N,N'-bis(3-methoxysalicylidene)1,2-diamino-1-propene* and *H₂L³ = N,N'-bis(3-methoxysalicylidene)1,2-propanediamine*}, have been synthesized and characterized. Single crystal x-ray diffraction analysis confirmed their structures. Weak non-covalent interactions generate extended supra-molecular assemblies in all three complexes. Catalase mimicking activities (catalytic decomposition of hydrogen peroxide into oxygen and water) of the complexes have been investigated. Complex 3 catalyzes the decomposition of hydrogen peroxide most effectively. The higher catalase mimicking efficiency of complex 3 has been related to its structure.

1. Introduction

Manganese(III) complexes have attracted a lot of attention because of their interesting magnetic properties (with four unpaired electrons in high spin and two unpaired electrons in low spin complexes) and structural diversities [1–5]. SOD (superoxide dismutase) and catalase are two important enzymes that help to defend the cell structure against various reactive oxygen species, e.g. hydrogen peroxide, hydrogen superoxide etc (capable of damaging different cellular components), produced naturally during oxygen metabolism [10–12]. If not destructed, these reactive oxygen species can cause oxidative stress leading to a number of human diseases [13–15]. SOD destroys hydrogen superoxide reducing it into hydrogen peroxide [16,17]. Catalase is responsible for the catalytic decomposition of hydrogen peroxide by means of its disproportionation reaction into nontoxic dioxygen and water [18–20]. Many manganese(III) complexes have also been used to mimic several enzymes, e. g. superoxide dismutase, catalase etc [6–9]. Signorella et al. reported a manganese(III) complex that can exhibit both superoxide dismutase and catalase-like activity [21]. Two manganese(II) complexes were also synthesised by the same group and both of these complexes show superoxide dismutase and catalase-like activity [22]. Britovsek et al. synthesized a bio-inspired manganese(II) complex with a linear pentadentate ligand framework containing soft sulfur donors and an alternating NSNSN binding motif which can display excellent dual catalase/SOD-like antioxidant activity [23].

Párkányi et al. have reported a manganese(II) complex exhibiting similar type activity [24]. Synthesis, structural characterization and catalase-like activity of a number of manganese(II) complexes were reported by Devereux et al. [25]. A novel single site manganese(II) complex was successfully synthesized and tested in the aqueous disproportionation of hydrogen peroxide by Barszcz et al. [26]. Li et al. synthesized two new manganese(II) complexes which can decompose hydrogen peroxide catalytically, and possess the combined functions of SOD and catalase in basic or weakly basic solutions [27].

With the specific aim to mimic catalase enzyme, we have synthesized and characterized three octahedral manganese complexes, each having [MnLXY] core, where H₂L is tetradentate Schiff base ligand occupying the equatorial positions; X and Y are monodentate ligands occupy the axial positions, as expected from considering the structures of similar Mn(III) complexes [9,28]. These monodentate ligands could be substituted by hydrogen peroxide to initiate catalase activity of the complexes (Manganese(III) is d⁴ and labile). This special characteristic feature makes them good catalysts towards decomposition of hydrogen peroxide into dioxygen and water.

2. Experimental section

2.1. Materials

All starting materials were available from commercial suppliers and

---

* Corresponding author.
E-mail address: shouvik.chem@gmail.com (S. Chattopadhyay).

Taylor & Francis
Taylor & Francis Group

Check for updates

Synthesis and characterization of a manganese(III) schiff base complex and exploration of Br···Br interaction in the solid state structure of the complex

Ipsita Mondal[a], Kousik Ghosh[a], Antonio Franconetti[b], Antonio Frontera[b], Sudipta Chatterjee[c] and Shouvik Chattopadhyay[a]

[a]Department of Chemistry, Inorganic Section, Jadavpur University, Kolkata, India; [b]Departamento de Química, Universitat de les Illes Balears, Palma (Baleares), Spain; [c]Department of Chemistry, Serampore College, Serampore, Hooghly, India

ABSTRACT

A mononuclear manganese(III) complex, $[MnL(CH_3OH)(H_2O)]ClO_4$, has been synthesized and structurally characterized {H_2L ¼ N,N'-bis(5-bromo-3-methoxysalicylidene)2,2-dimethyl-1,3-propanediamine}. The energetic features of significant supramolecular interactions present in the complex, i.e. Br···Br, hydrogen-bonding and p–p stacking interactions, have been calculated using DFT calculations and further corroborated with NCI plot index computational tool. Catalase mimicking activity (catalytic decomposition of hydrogen peroxide into oxygen and water) of the complex has been investigated. The complex catalyzes the decomposition of hydrogen peroxide effectively in solution. The efficiency of the complex toward catalytic decomposition of hydrogen peroxide is related to its structure.
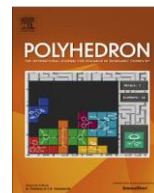
Noncovalent interactions are by far the most effective means for the formation of molecular aggregates and assemblies [1–3]. Among these interactions, conventional ones, i.e. hydrogen bonding, C–H···p, p–p stacking, etc. are the most frequently

---

Contents lists available at ScienceDirect

Polyhedron

A trigonal dodecahedral cadmium(II) complex with zinc(II)–salen type metalloligand: Synthesis, structure, self-assembly and application in the detection of various nitroaromatics via turn-off fluorescence response

Sourav Roy [a], [⇑], Ipsita Mondal [a], Klaus Harms [b], Shouvik Chattopadhyay [a], [⇑]

[a] Department of Chemistry, Inorganic Section, Jadavpur University, Kolkata 700032, India
[b] Fachbereich Chemie, Philipps-Universität Marburg, Hans-Meerwein-Strasse, D-35032 Marburg, Germany

ARTICLE INFO

ABSTRACT

A compartmental Schiff base ligand, N,N'-bis(3-ethoxysalicylidene)-2,2-dimethylpropane-1,3-diamine (H_2L) has been used to prepare a hetero-trimetallic cadmium(II)/zinc(II) complex, Cd{LZn(NCS)}$_2$. Single crystal X-ray diffraction analysis has confirmed the structure of the complex. The complex behaves as a sensor for the detection of various nitroaromatics via turn-off fluorescence response.

© 2018 Elsevier Ltd. All rights reserved.

1. Introduction

Although crown ethers, cryptands and related ligands are particularly good classes of complexing agents for alkali and 3d metal ions [1], there are many other simpler and certainly more affordable ligands that are also extremely effective in this respect [2]. One such ligand is N,N'-bis(3-methoxysalicylidene) propane-1,3-diamine [3], produced by the condensation of 3-methoxysalicaldehyde and 1,3-diaminopropane. This compartmental Schiff base has already been used exhaustively to prepare varieties of hetero-bimetallic 3d/4f complexes [4]. Structure determination showed that the 3d metals were placed in the N_2O_2 compartment of the ligand whereas lanthanide ions were placed in the O_4 compartment in all the complexes without exception [5]. The metal centres in many such complexes were found to be ferromagnetically coupled [6]. The ligand has also been used to prepare linear trinuclear complexes [7]. Many such complexes were found to show SMM behaviour [8]. Many other compartmental Schiff bases, e.g., N,N'-bis(3-ethoxysalicylidene) propane-1,3-diamine, N,N'-bis(3-methoxysalicylidene)ethane-1,2-diamine, N,N'-bis(3-methoxysalicylidene)-2,2-dimethylpropane-

1,3-diamine, etc., have also been used to prepare many such homo and heteronuclear complexes [9]. Nitroaromatic compounds are potential explosive, highly toxic in nature and are serious pollution sources of environment [10]. So, the detection of nitroaromatic compounds is an important area of current research. Moreover, fluorescence based detection has recently been considered as one of the most promising techniques for explosive detection [11].

In the present work, a compartmental Schiff base ligand, N,N'-bis(3-ethoxysalicylidene)-2,2-dimethylpropane-1,3-diamine (H_2L) has been used to prepare a hetero-trimetallic complex, Cd{LZn (NCS)}$_2$, where cadmium(II) is exhibiting octa-coordinate trigonal dodecahedral geometry. Although several trinuclear cadmium(II) complexes having similar formula were reported in literature [12], there is only two crystal structures reported of any trinuclear zinc(II)–cadmium(II)–zinc(II) complex with compartmental Schiff bases [13]. The complex acts as turn-off fluorescence chemosensor for detection of various nitroaromatics.

2. Experimental

All materials were commercially available, reagent grade and used as purchased from Sigma-Aldrich without further purification.

* Corresponding authors.
E-mail addresses: souravscott@gmail.com (S. Roy), shouvik.chem@gmail.com (S. Chattopadhyay).

On the importance of RH₃C···N tetrel bonding interactions in the solid state of a dinuclear zinc complex with a tetradentate Schiff base ligand†

Ipsita Mondal,[a] Antonio Frontera 🅓 *[b] and Shouvik Chattopadhyay 🅓 *[a]

The synthesis and X-ray characterization of a new dinuclear Zn complex using a tetradentate N_2O_2 donor Schiff base and azide as an anionic co-ligand of formula [(DMSO)₂ZnL(μ₁,₁-N₃)Zn(N₃)₂] (1) are reported herein. This complex forms self-assembled dimers in the solid state governed by σ-hole tetrel bonding interactions (C···N) involving the Zn-coordinated methoxy group. The σ-hole tetrel bonding interaction has been differentiated from a trifurcated CH₃···N H-bonding interaction using the NBO analysis and the inspection of the donor–acceptor orbital interactions. Other interactions (like π-stacking) are also important governing the solid state architecture of the dinuclear Zn-complex. The energy of π-stacking interaction has also been estimated using DFT calculations and several computational tools (MEP surfaces, QTAIM and NCI plot analyses).

Introduction

Over the last five years, σ-hole interactions,[1] involving elements of groups 12−18 of the periodic table[2] have emerged as key players in supramolecular chemistry. For instance, they have been used in substitution of the ubiquitous H-bonding in several fields like molecular recognition, catalysis and crystal engineering.[2b] The position, size and number of the depleted areas of electron density on the surface of covalently bonded atoms depend on the type (single or double/delocalized bonds) and number of covalent bonds formed by the atom. In particular, σ-holes are located approximately along the vector of a single σ-bond. In the case of group 14, the σ-holes are large and accessible for interacting with electron rich atoms in the heavier tetrel atoms (Ge, Sn and Pb).[3] For Si and especially C, the σ-hole is usually very small, thus leading to σ-hole interactions with a marked directionality. The linearity of this type of bonding has been confirmed by multitude CSD analyses[4] combined with computational studies.[5] It is well known that the σ-hole intensity increases as the electron withdrawing ability of its substituents increases. Therefore, the σ-hole opposite to C−Y bonds, where Y = fluorine, cyano, or nitro or a charged atom/group is favoured over other substituents.[6]

2 : 1 condensation of salicylaldehyde and ethylenediamine produces a N_2O_2 donor tetradentate Schiff base, which is commonly known as 'salen' [sal(from salicylaldehyde) + en (ethylenediamine) = salen]. Use of other diamines and different salicylaldehyde derivatives produced many other 'salen type' Schiff bases.[7] These salen type N_2O_2 donor Schiff bases have been widely used to synthesize many dinuclear and polynuclear zinc complexes exploiting the bridging ability of phenoxo oxygen atoms.[8a,b] Tridentate N_2O donor Schiff bases have also been used by many research groups to prepare such complexes.[8c,d] In the present work, we have used a tetradentate N_2O_2 donor Schiff base to prepare a new dinuclear zinc complex. It forms in the solid state self-assembled supramolecular dimers, where the coordinated methoxy group of one monomer interacts *via* tetrel bonding interaction with the azido group of the other monomer and *vice versa*. Although other interactions like π-stacking are also important governing the solid state architecture of the dinuclear Zn-complex reported herein, we have focused our work mainly on the more unconventional tetrel bonding interactions, which have been investigated using DFT calculations combined with molecular electrostatic potential (MEP) surfaces, the quantum theory of "atoms-in-molecules" and the non-covalent interaction index (NCI plot). The σ-hole nature of the interaction has been confirmed by using the natural bond orbital (NBO) method.

Experimental section

All chemicals were of reagent grade and used as purchased from Sigma-Aldrich without further purification.

[a] *Department of Chemistry, Inorganic Section, Jadavpur University, Kolkata - 700032, India. E-mail: shouvik.chem@gmail.com*

[b] *Departament de Quimica, Universitat de les Illes Balears, Crta de valldemossa km 7.5, 07122 Palma de Mallorca, Baleares, Spain. E-mail: toni.frontera@uib.es*

A theoretical insight on the rigid hydrogen-bonded network in the solid state structure of two zinc(II) complexes and their strong fluorescence behaviors†

Ipsita Mondal,[a] Tanmoy Basak,[a] Snehasis Banerjee [iD] *[b] and Shouvik Chattopadhyay [iD] *[a]

A reduced Schiff base has been synthesized and characterized and used as a fluorescence chemo-sensor for the selective detection of zinc(II). Fluorescence titrations have also been conducted for the ligand and the binding constant for the ligand ($K = 1.056 \times 10^6$ M^{-1}) has been evaluated using the Benesi–Hildebrand equation. Two mononuclear zinc(II) complexes have also been synthesized with the ligand and S_0 and S_1 of their electronic structures were calculated. The HOMO–LUMO energy difference in each complex is *ca.* 4.69 eV in S_0 states and the energy gap is reduced to *ca.* 4.3 eV in S_1 facilitating easier electronic transition. Their strong fluorescence behaviors may be correlated with the presence of a rigid hydrogen-bonded network in their solid state structure. Two types of intermolecular hydrogen bonding are noticed in the dimeric form of the complexes. The hydrogen bonding environment is well supported qualitatively and quantitatively with the help of NCI-RDG (noncovalent interaction reduced density gradient) and QTAIM. The physical nature of other weak non-covalent interactions in both complexes was also examined. Based on the optimized ground state geometry (S_0), the TDDFT/B3LYP method combined with the SMD solvation model in methanol media was used to calculate the absorption properties of the investigated complexes. Additionally, analysis on the electronic structure of the excited states employing NTO (natural transition orbital) representation showed that the S_1 state can be mainly characterized by an inter-ligand charge-transfer (ILCT) transition, populating the highest-occupied (HO) NTO and lowest-unoccupied (LU) NTO, which describe the hole and the excited electron state, respectively. The calculation indicates that the fluorescence originates from the charge transfer from N$_3$/NCS to the reduced Schiff base.

Introduction

Schiff base ligands have been used by chemists for many years.[1] They have been widely used to prepare several transition and non-transition metal complexes.[1h–j] Many complexes of Schiff bases were found to have interesting applications in materials science.[2] They are also linked with the development of inorganic biochemistry,[1b] catalysis,[1c] medical imaging,[1d] optical materials and thin films.[1e] Inorganic chemists extensively utilized these Schiff bases to synthesize molecular ferromagnets[1f,g] and catalysts.[1h] Among various Schiff bases, salen type ligands deserve a special mention for their easy synthetic route, stability and complexing ability.[1i] They have outstanding potential as molecular building blocks (similar to porphyrins) for the development of new materials. They were also widely used in biological modeling applications and as liquid crystals.[1j] Sodium borohydride is a mild reducing agent and it could easily be used to reduce these salen type N$_2$O$_2$ donor Schiff bases.[3] These reduced Schiff bases may also be used to form transition and non-transition metal complexes.[4] Due to the reduced Schiff bases being more flexible (as a result of reduction of the imine linkage), the molecular architectures of their complexes are more versatile.[5] They have also been shown to have different applications in catalysis and magnetism.[5a,6] However, compared with the huge number of reports on the complexes of salen type Schiff bases, their reduced counterparts are relatively less explored. In the

[a] Department of Chemistry, Inorganic Section, Jadavpur University, Kolkata-700032, India. E-mail: shouvik.chem@gmail.com

[b] Govt. College of Engineering and Leather Technology, Salt Lake Sector-III, Block-LB, Kolkata 700106, India. E-mail: sbanchem@gmail.com

Contents lists available at ScienceDirect

Polyhedron
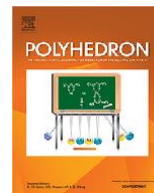
An acetate bridged centrosymmetric zinc(II) complex with a tetradentate reduced Schiff base ligand: Synthesis, characterization and ability to sense nitroaromatics by turn off fluorescence response

Ipsita Mondal [a], Sudipta Chatterjee [b], Shouvik Chattopadhyay [a],⇑

[a] *Department of Chemistry, Inorganic Section, Jadavpur University, Kolkata 700032, India*
[b] *Department of Chemistry, Serampore College, Serampore, Hooghly, 712201, India*

ABSTRACT

A unique trinuclear centrosymmetric zinc(II) complex, $[Zn_3L_2(CH_3CO_2)_2(DMSO)_2]$ has been synthesized and characterized by using a reduced Schiff base ligand H_2L {H_2L = 1,3-bis(2-hydroxybenzylamino)2,2-dimethylpropane}. The complex has been characterized by spectral and elemental analysis. Single crystal X-ray diffraction analysis has confirmed the structure of the complex. The complex has showed strong fluorescence, which may be quenched in presence of different nitroaromatic substances. The complex thus used as a sensor for the detection of nitroaromatics in DMF via turn-off fluorescence response.

© 2020 Elsevier Ltd. All rights reserved.

1. Introduction

Synthetic inorganic chemists prepared and structurally characterized a large number of zinc(II) complexes with various ligands [1–3]. The geometry of these complexes may vary widely [1–11]. Common geometries include tetrahedral [4,5], square planar [6], trigonal bipyramidal [7,8], square pyramidal [9,10] and octahedral [11] etc. The electronic ground states of zinc(II) (always singlet and always totally symmetric) does not experience any ligand field stabilization as a result of d^{10} electronic configuration and therefore there is no ligand field restriction to attain any coordination number or any structure of zinc(II) complexes [12,13]. Zinc(II) may thus adopt different coordination geometry depending only upon steric requirements of the ligands.

Zinc(II) is an important metal in biology [14–16]. Zinc(II) is present in the active site structure of many hydrolytic enzymes, e.g. carbonic anhydrase, carboxy peptidase A, phosphatase etc. Many zinc(II) complexes are shown to have the ability to mimic these metalloenzymes [17,18]. Zinc(II) complexes are also shown to act as photo-catalyst to degradation of synthetic dyes [19]. Zinc(II) complexes have also been reported to show photoluminescence as well as electroluminescence [20].

The strong fluorescence of zinc(II) complexes may, however, be quenched in presence of electron deficient species [21]. Nitroaromatics are electron-deficient aromatics and can quench the fluorescence of zinc(II) complexes, and therefore, nitroaromatic explosives may be detected by monitoring the quenching of the fluorescence intensity of zinc(II) complexes [11,21,22]. In the present work, a zinc(II) complex has been prepared and characterized. Single crystal X-ray diffraction has confirmed its structure. The complex shows strong luminescence in visible region. The ability of the complex to act as fluorescence chemosensor for the detection of nitroaromatic explosives has also been investigated.

Herein, we report the synthesis, characterization, structure and fluorescence of a trinuclear zinc(II) complex with a reduced Schiff base ligand and its nitroaromatic sensing ability.

2. Experimental

2.1. Materials

All chemicals were of reagent grade and used as purchased from Sigma-Aldrich without further purification.
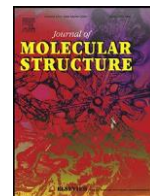
2.2. Preparation

2.2.1. Preparation of the reduced Schiff base ligand, 1,3-bis(2-hydroxybenzylamino)2,2-dimethylpropane (H₂L)

A Schiff base ligand, H_2L^0 {H_2L^0 = *N,N'-bis(salicylidene)-2,2-dimethylpropane-1,3-diamine*}, was synthesized by refluxing 2,2-dimethylpropane-1,3-diamine (1 mmol, 0.1 mL) with

---

A mononuclear zinc complex with a diamine: Synthesis, characterization, self assembly, luminescence property and DFT calculations

Ipsita Mondal[a], Snehasis Banerjee[b],*, Shouvik Chattopadhyay[a],*

[a] Department of Chemistry, Inorganic Section, Jadavpur University, Kolkata 700032, India
[b] Govt. College of Engineering and Leather Technology, Salt Lake Sector-III, Block-LB, Kolkata 700106, India

abstract

A zinc complex with a N_2O_2 donor diamine is synthesized and its fluorescence property is explored. The hydrogen bonding environment in its solid state structure is well supported qualitatively and quantitatively with the help of Reduced Density Gradient (RDG) based NCI (non-covalent interactions) index calculation and AIM analyses. Also, the physical nature of other weak non-covalent interactions in the complex is examined. The absorption and emission properties of the complex are explained using density functional theory (DFT) calculations. Analysis of the natural transition orbitals (NTO) shows that the excited state can be mainly characterized by an intra-ligand charge transfer (ILCT) transition within a diamine from the highest-occupied NTO (*hole*) to the lowest-unoccupied NTO (*electron*).

© 2021 Elsevier B.V. All rights reserved.

1. Introduction

The ability of zinc to attain different coordination numbers and versatile geometries renders it a good candidate for the synthesis of complexes with various diamines [1–8]. Most of the complexes of zinc are showing strong fluorescence [9,10]. Electroluminescence properties of zinc complexes were also explored [11,12]. Chelating Schiff bases have widely been used for the synthesis of zinc complexes [13,14]. The role of Schiff bases to act as fluorescence chemosensor for the detection of zinc by PET on/off mechanism is also well investigated [15,16]. Photoinduced electron transfer (PET) is a term reserved to describe the transfer of an electron between photoexcited and ground-state molecules. Chelation enhanced fluorescence (CHEF) may be observed in some cases [17,18]. On the other hand, the strong fluorescence of many zinc Schiff base complexes may be quenched in presence of different nitroaromatics and this property is exploited by many material scientists to sense these explosives [13,19].

Salen type Schiff bases constitute a special class of ligands, as they can be synthesised very easily; simply by refluxing (or even stirring) an 1:2 mixture of a diamine and a salicylaldehyde-derivative in appropriate solvent [20–28]. They are also stable over

a wide range of solvent and temperature. Reduction of the imine bonds of Schiff bases (preferably with sodium borohydride) may produce secondary amines [29,30], which are sometimes referred to as reduced analogues of Schiff bases [31]. These reduced analogues of Schiff bases are eventually much more flexible compared to their Schiff base precursors, and therefore they may produce varieties of complexes having different shapes and geometries [32–34]. It has been observed that they may also be used in different catalysis and sensing [6,17,35].

In this paper, we would like to report the synthesis and characterization of a zinc complex with such a secondary diamine, prepared by the reduction of a salen type di-Schiff base ligand (and hence may be considered as a reduced analogue of a di-Schiff base ligand). Its fluorescence property and solid state non-covalent interactions are studied in detail with the help of DFT calculations.

2. Experimental

2.1. Preparation

2.1.1. Preparation of 2,2'-[(cyclohexane-1,2-diyl)bis(iminomethylene)]bis[phenol] (H₂L)

A methanol solution (20 mL) of cyclohexane-1,2-diamine (mixture of *cis* and *trans*) (1 mmol, 0.1 mL) was refluxed with salicylaldehyde (2 mmol, 0.208 mL) for *ca*. 2 h to produce *N,N'-bis(salicylidene)-cyclohexane-1,2-diamine.* It was then reduced with

---

* Corresponding author.
E-mail addresses: sbanchem@gmail.com (S. Banerjee), shouvik.chem@gmail.com (S. Chattopadhyay).

Taylor & Francis
Taylor & Francis Group

REVIEW

Check for updates

Development of multi-metallic complexes using metal-salen complexes as building blocks

Ipsita Mondal and Shouvik Chattopadhyay

Department of Chemistry, Jadavpur University, Kolkata, India

ABSTRACT

Metal-salen complexes have been widely used in inorganic chemistry to synthesize polynuclear complexes. This review highlights the synthetic strategy of multi-metallic complexes using metal-salen complexes as building blocks and structures of the resulting complexes. Three different processes have been used to prepare multi-metallic complexes using metal-salen complexes: (i) use of metal-salen complexes as metalloligands, (ii) self-assembly processes involving [M(salen)] complexes and various cyanaometallates and (iii) use of salen-type compartmental ligands. Complexes formed by these methods are included in the review. X-ray single crystal diffraction analysis confirmed the structures of these complexes. The properties of these complexes are also briefly discussed. This review will be of interest to researchers and synthetic chemists for synthetic strategy of homo- and heterometallic polynuclear complexes using salen-type Schiff bases.

Synthetic Strategy

CONTACT Shouvik Chattopadhyay ✉ shouvik.chem@Gmail.com ✉ Department of Chemistry, Jadavpur University, Kolkata, 700032, India